

Silverwood, Robert Keith (2020) *An assessment of mesenchymal stromal cell function from patients with neck of femur fractures and the development of a three-dimensional culture model*. PhD thesis.

<http://theses.gla.ac.uk/81602/>

Copyright and moral rights for this work are retained by the author

A copy can be downloaded for personal non-commercial research or study, without prior permission or charge

This work cannot be reproduced or quoted extensively from without first obtaining permission in writing from the author

The content must not be changed in any way or sold commercially in any format or medium without the formal permission of the author

When referring to this work, full bibliographic details including the author, title, awarding institution and date of the thesis must be given

Enlighten: Theses

<https://theses.gla.ac.uk/>
research-enlighten@glasgow.ac.uk

An assessment of mesenchymal stromal cell function from patients with neck of femur fractures and the development of a three-dimensional culture model

Mr Robert Keith Silverwood

BMedSci, MBChB, MSc, MRCS (Ed)



Submitted in fulfilment of requirements for the degree of Doctor of Philosophy (PhD)

**The Centre for the Cellular Microenvironment
Institute of Molecular, Cell and Systems Biology
School of Medical, Veterinary and Life Sciences
University of Glasgow
Glasgow
G12 8QQ**

December 2019

Abstract

Osteoporosis represents an ever increasing burden to health care services world-wide. Within the UK alone, over 500 000 fragility fractures secondary to osteoporosis occur each year, resulting in significant morbidity and mortality. Furthermore, the management of these injuries cost health care services billions of pounds. A revolution in the diagnosis and treatment of the disease is required to prevent significant suffering of future generations.

MicroRNAs are known to regulate many key physiological processes, including mesenchymal stromal cell (MSC) differentiation. They have been demonstrated to be abnormally expressed in many musculoskeletal conditions, including osteoporosis. Patients who have suffered a neck of femur fracture are known to be at risk of, or have undiagnosed, osteoporosis. Dysregulated microRNAs have been identified in bone and serum samples of patients with this injury type. Great hope has been placed on the development of targeted therapies to manipulate microRNA expression and improve bone quality.

This study has focussed on rigorously assessing the functionality of MSCs from patients who have suffered a neck of femur fracture. Extracellular MSC markers and differentiation capacity were shown to be significantly altered within this patient group. MicroRNA expression was analysed, and key microRNAs, microRNA-143 and microRNA-31, were manipulated using functionalised gold nanoparticles to further understand their role in MSC differentiation. Furthermore, the metabolomic effect of inhibiting microRNA-31 was explored to further understand its role in osteogenesis. To reduce the gap between *in vitro* and clinical research an optimal 3D, scaffold free, culture model was identified for bone marrow derived MSCs.

These results provide further insight to the impaired MSC function of patients who have suffered a fragility fracture. Furthermore, the potential of microRNAs to be utilised as a biomarker or therapeutic target for osteoporosis has been reinforced.

Table of Contents

An assessment of mesenchymal stromal cell function from patients with neck of femur fractures and the development of a three-dimensional culture model.....	1
Abstract.....	i
Table of Contents	ii
List of Tables	vii
List of Figures.....	viii
Fellowships, grants and awards	x
Publications	x
Conference proceedings	x
Acknowledgement	xii
Author's Declaration	xiii
Definitions & Abbreviations	xiv
Chapter 1	1
1.1 Osteoporosis	2
1.1.1 Disease mechanism of action.....	2
1.1.2 Bone in health	3
1.1.3 Cellular mechanisms of bone homeostasis and osteoporosis	6
1.1.4 Diagnosis, monitoring and fracture risk assessment	7
1.1.5 Prevalence.....	8
1.1.6 Morbidity and mortality	9
1.1.7 Economic impact	9
1.1.8 Current therapies	10
1.1.9 Duration and monitoring of Osteoporosis therapy.....	14
1.1.10 Future osteoporosis therapies.....	15
1.1.11 Mesenchymal Stromal Cells in Osteoporosis and the effect of ageing	17
1.1.12 Mesenchymal stromal cell functionality in osteoporosis	19
1.2 MicroRNAs in regenerative medicine	20
1.2.1 MicroRNAs mechanism of action.....	20
1.2.2 MicroRNAs in Osteoporosis.....	23
1.3 MicroCT	25
1.3.1 MicroCT in orthopaedic research	25
1.3.2 Observed bony characteristics of Osteoporotic bone via MicroCT scanning	28
1.4 Three-Dimensional cell culture.....	30
1.4.1 Techniques of three-dimensional culture.....	31

1.5	Aims	34
Chapter 2	35
2	Materials and Methods.....	36
2.1	Materials and reagents.....	36
2.1.1	Cell culture reagents	36
2.1.2	Immunostaining reagents	37
2.2	Preparation of cell culture solutions	38
2.3	Cell type.....	39
2.3.1	Ethical Approval	40
2.4	Cell Culture	40
2.4.1	Bone Marrow Extraction.....	40
2.4.2	General Protocol	41
2.4.3	Cell Culture Media	42
2.4.4	Freezing cells for storage	42
2.4.5	Thawing cells from storage	42
2.5	Cell Culturing Methods.....	43
2.5.1	Differentiation culture	43
2.5.2	MicroRNA Culture.....	43
2.6	Spheroid formation	45
2.6.1	Hanging drop spheroid formation	45
2.6.2	Ultra-low attachment spheroid formation	46
2.6.3	Magnetic Nanoparticle Uptake into Cells	46
2.6.4	MNP Spheroid culture in media	47
2.7	Flow cytometry.....	47
2.7.1	Flow cytometry staining.....	47
2.7.2	Flow cytometry compensation	48
2.7.3	Flow cytometry gating strategy and analysis.....	49
2.8	Histochemical staining	50
2.8.1	Oil Red O staining	50
2.8.2	Von Kossa staining.....	50
2.9	MicroRNA extraction.....	50
2.10	MicroRNA analysis.....	51
2.11	Immunostaining for In Cell Western™	51
2.12	RNA extraction	52
2.13	Reverse Transcription	53
2.14	Analysis of quantitative real-time-PCR (qRT-PCR)	53
2.15	Electron Microscopy	55
2.16	Cell Viability Staining	55
2.17	MicroCT scanning of femoral head samples	55

2.18	Metabolomic analysis.....	56
2.19	Statistical Analysis.....	56
2.20	Research Colleagues.....	57
Chapter 3		58
3	An analysis of microRNA expression and functional capacity of mesenchymal stromal cells from patients with neck of femur fractures.....	59
3.1	Introduction.....	59
3.2	Objectives.....	61
	Materials and Methods.....	62
3.2.1	Patient samples.....	62
3.2.2	Cell Culture.....	62
3.2.3	Flow Cytometry.....	62
3.2.4	Differentiation media.....	62
3.2.5	Histochemical staining and imaging.....	62
3.2.6	MicroRNA expression.....	64
3.2.7	MicroCT scanning.....	65
3.3	Results	66
3.3.1	Flow Cytometry.....	66
3.3.2	Differentiation Potential of Bone Marrow Mesenchymal Stromal Cells from NOF and OA patients	70
3.3.3	microRNA expression in NOF and OA.....	74
3.3.4	MicroCT Characteristics of femoral head samples from NOF and OA 82	
3.4	Discussion	88
3.4.1	Flow cytometry confirms cell populations contain MSCs.....	88
3.4.2	MSCs from neck of femur fracture patients show reduced stemness 89	
3.4.3	Mesenchymal stem cells from NOF patients have impaired functionality.....	90
3.4.4	MicroRNA expression in NOF patients shows significant dysregulation.....	92
	Conclusion	102
Chapter 4		103
4	An assessment of mesenchymal stromal cell differentiation following microRNA manipulation.....	104
4.1	Introduction.....	104
4.2	Objectives.....	105
4.3	Materials and Methods	106
4.3.1	Cell Culture.....	106
4.3.2	Nanoparticles	106
4.3.3	Differentiation Media	106

4.3.4	Quantitative real-time (qRT)-PCR	106
4.3.5	In Cell Western™ (ICW).....	106
4.3.6	Metabolomic analysis	107
4.4	Results	108
4.4.1	MicroRNA-143 mimic culture	108
4.4.2	AntagomiR-31 culture	110
4.5	Discussion	137
4.5.1	MicroRNA manipulation influences differentiation.....	137
4.5.2	Metabolomic analysis displays manipulation of differentiation...	139
4.6	Conclusion.....	143
Chapter 5	144
5	Optimising Bone Marrow Derived MSC Spheroid Formation	145
5.1	Introduction.....	145
5.2	Objectives.....	147
	Materials and Methods.....	148
5.2.1	Cells and Spheroid forming techniques.....	148
5.2.2	Light microscopy	149
5.2.3	Viability staining.....	149
5.2.4	Electron Microscopy.....	149
5.2.5	Statistical analysis	149
	Results	150
5.2.6	Hanging Drop (HD) Technique.....	150
5.2.7	Ultra-Low Attachment Technique	153
5.2.8	Magnetic Nanoparticle Technique	157
5.3	Discussion	162
5.3.1	Hanging Drop technique generates stable spheroids over 72 hours 162	
5.3.2	Ultra-Low Attachment technique rapidly produces spheroids with consistent morphology and viability	164
5.3.3	Magnetic Nanoparticle technique generates spheroids of varied size with compromised viability.....	164
5.4	Conclusion.....	166
Chapter 6	167
6	Discussion	168
6.1	Relevance of results.....	168
6.1.1	The functionality of mesenchymal stromal cells from patients with neck of femur fractures is impaired	168
6.1.2	microRNA expression of mesenchymal stromal cells is dysregulated post neck of femur fracture	169

6.1.3	microRNA manipulation represents an important method of differentiation control.....	170
6.1.4	ULA technique identified as optimal method for spheroid formation in bone marrow derived MSCs	172
6.2	Limitations	173
6.3	Future work	174
6.3.1	Further interrogation of mesenchymal stromal cell biology in patients who have suffered fragility fractures.....	174
6.3.2	Longer culture and assessment of effect of microRNA-31 in mesenchymal stromal cells	174
6.3.3	Assessing the impact of current osteoporosis therapies on microRNA expression	175
6.3.4	Application of three-dimensional culture method to osteoporotic mesenchymal stromal cells	175
6.4	Thesis conclusion	177
	Bibliography.....	178

List of Tables

Table 1-1 Factors associated with an increased risk of developing OP.....	3
Table 1-2 Common microarchitectural indices measured via microCT.....	28
Table 2-1 Constituents of medias used for cell culture.	42
Table 2-2 The physical properties of the functionalised GNPs used in miRNA manipulation studies..	44
Table 2-3 Details of culture conditions for miRNA manipulation studies.	44
Table 2-4 Details of antibodies used in flow cytometric analysis experiments. ..	48
Table 2-5 Details of primary and secondary antibodies utilised in In Cell Western experiments.	52
Table 2-6 Constituents of wells for qRT-PCR analysis.	54
Table 2-7 Details of primers utilised in qRT-PCR experiments.....	54
Table 3-1 Phenotyping demonstrates positive and negative expressive expression of MSC markers on flow cytometric analysis.	66
Table 3-2 Top 20 microRNAs with increased expression in NOF group vs OA group, with log 2-fold change.	77
Table 3-3 Top 20 microRNAs with decreased expression in NOF group vs OA group, with log 2-fold change.	78
Table 3-4 Table showing previously identified abnormally regulated microRNAs related to OP	95
Table 5-1 Summary of results for 3 spheroid forming techniques.....	162

List of Figures

Figure 1-0-1 Femoral head and neck imaged via microCT	5
Figure 1-0-2 Anatomy of an adult femur.....	4
Figure 1-0-3 Depiction of bone homeostasis	6
Figure 1-0-4 X-ray of a right neck of femur fracture	11
Figure 1-0-5 MicroRNA biogenesis and action.	21
Figure 1-0-6 Radiographs of common musculoskeletal diseases and commonly reported dysregulated miRNAs.	23
Figure 1-0-7 MiRNA regulation sites related to osteoblastogenesis	24
Figure 1-0-8 Coronal and axial examples of microCT imaging of femoral heads.	27
Figure 1-0-9 Imaging of human MSC spheroids.....	31
Figure 1-0-10 Four commonly utilised spheroid forming techniques.	32
Figure 2-1 Hanging drop technique.	45
Figure 2-2 Ultra-low attachment.	46
Figure 2-3 Magnetic nanoparticle spheroid formation technique.	47
Figure 2-4 Flow cytometry gating strategy	49
Figure 3-1 Histochemical analysis example	64
Figure 3-2 MicroCT images of femoral heads demonstrating the 7 VOIs.	65
Figure 3-3 Flow cytometric assessment of antibody expression	67
Figure 3-4 Flow cytometric assessment of antibody expression	68
Figure 3-5 Brightfield microscopy of Oil Red O staining basal media.....	71
Figure 3-6 Brightfield microscopy of Oil Red O staining adipogenic media.....	71
Figure 3-7 Level of Oil Red O staining.....	72
Figure 3-8 Brightfield microscopy of von Kossa in basal medium.	73
Figure 3-9 Brightfield microscopy of von Kossa staining in osteogenic medium ..	73
Figure 3-10 Level of von Kossa staining	74
Figure 3-11 Volcano plot of microRNA expression in the NOF group in comparison to the OA group.	75
Figure 3-12 PCA plot of log transformed microRNA expression in NOF and OA groups.	76
Figure 3-13 MicroRNA Network 1	79
Figure 3-14 MicroRNA Network 2.	80
Figure 3-15 MicroRNA Network 3	81
Figure 3-16 MicroRNA Network 4.....	82
Figure 3-17 Mean BV/TV % observed in each VOI.....	83
Figure 3-18 Range of BV/TV (%) observed in patient samples from OA group	83
Figure 3-19 Range of BV/TV (%) observed in patient samples from NOF group...	84
Figure 3-20 Mean trabecular thickness.....	84
Figure 3-21 Mean trabecular separation/mm in each VOI	85
Figure 3-22 Mean trabecular number in each VOI.....	85
Figure 3-23 Mean structural model index.....	86
Figure 3-24 Mean degree of anisotropy in each VOI	86
Figure 3-25 Mean Connectivity density in each VOI,.....	87
Figure 4-1 qRT-PCR analysis of PPAR γ at day 7 culture of OA and NOF MSCs in miR-143 experimentation.....	108
Figure 4-2 qRT-PCR analysis of FABP at day 7 culture of OA and NOF MSCs in miR-143 experimentation	109
Figure 4-3 In Cell Western TM analysis of PPAR γ protein expression of OA and NOF MSCs in miR-143 experimentation.	110
Figure 4-4 qRT-PCR analysis of Osterix at day 7 culture of OA and NOF MSCs in AntagomiR-31 experimentation.	111

Figure 4-5 qRT-PCR analysis of RUNX2 expression at day 7 culture of OA and NOF MSCs in AntagomiR-31 experimentation.	111
Figure 4-6 In Cell Western™ analysis of Osterix protein expression of OA and NOF MSCs in AntagomiR-31 experimentation.	112
Figure 4-7 Amino Acid metabolite profile of OA MSCs at day 7 of culture in AntagomiR-31 experimentation.	114
Figure 4-8 Amino Acid metabolite profile of NOF MSCs at day 7 of culture in AntagomiR-31 experimentation.	115
Figure 4-9 PCA plot of amino acid metabolites detected at day 7 of MSC culture in the OA group AntagomiR-31 experimentation.	116
Figure 4-10 PCA plot of amino acid metabolites detected at day 7 of MSC culture in the NOF group AntagomiR-31 experimentation.	117
Figure 4-11 PCA plot of carbohydrate metabolites detected at day 7 of MSC culture in the OA group AntagomiR-31 experimentation.	118
Figure 4-12 PCA plot of carbohydrate metabolites detected at day 7 of MSC culture in the NOF group AntagomiR-31 experimentation.	119
Figure 4-13 Carbohydrate metabolite profile of OA group MSCs at day 7 of culture in AntagomiR-31 experimentation.	120
Figure 4-14 Carbohydrate metabolite profile of NOF MSCs at day 7 of culture in AntagomiR-31 experimentation.	121
Figure 4-15 PCA plot of lipid metabolites detected at day 7 of MSC culture in the OA group AntagomiR-31 experimentation.	122
Figure 4-16 PCA plot of lipid metabolites detected at day 7 of MSC culture in the NOF group AntagomiR-31 experimentation.	123
Figure 4-17 Lipid metabolite profile of OA MSCs at day 7 of culture in AntagomiR-31 experimentation.	124
Figure 4-18 Lipid metabolite profile of NOF MSCs at day 7 of culture in AntagomiR-31 experimentation.	125
Figure 4-19 Predicted altered canonical pathways in the NOF group culture conditions in comparison to basal media.	126
Figure 4-20 Predicted altered canonical pathways in the OA group in comparison to basal media.	127
Figure 4-21 Metabolomic Network 1 at day 7 of culture in osteogenic media in comparison to basal media.	128
Figure 4-22 Metabolomic pathway Network 1 at day 7 of culture in basal media and AmiR-31 in comparison to basal media.	130
Figure 4-23 Metabolomic pathway Network 2 at day 7 of culture in basal media and AmiR-31 in comparison to basal media.	132
Figure 4-24 Metabolomic pathway Network 2 at day 7 of culture in osteogenic media in comparison to basal media.	134
Figure 4-25 Metabolomic pathway Network 4 at day 7 of culture in basal media and AmiR-31 in comparison to basal media.	136
Figure 5-1 Mean spheroid diameter measured at day 3 and day 21 by the HD technique with different cell seeding densities.	150
Figure 5-2. Day 7 viability staining in HD spheroids.	151
Figure 5-3 Day 21 viability staining in HD spheroids.	151
Figure 5-4 Scanning electron microscopy of spheroids formed by the HD technique.	152
Figure 5-5 Transmission electron micrographs of HD spheroids.	153
Figure 5-6 Mean spheroid diameter measured at day 3 and day 21 by the ULA technique.	154
Figure 5-7 Day 7 viability staining in ULA spheroids.	154

Figure 5-8 Day 21 viability staining in ULA spheroids.....	155
Figure 5-9 Scanning electron microscopy of spheroids formed by the ULA technique.....	156
Figure 5-10 Transmission electron micrographs of ULA spheroids at 24 hours..	157
Figure 5-11 Mean spheroid diameter at day 3 and 21 by the MNP technique ...	158
Figure 5-12 Day 7 viability staining in MNP spheroids	159
Figure 5-13 Day 21 viability staining in MNP spheroids.....	159
Figure 5-14 Scanning electron microscopy of spheroids formed by the MNP technique.....	160
Figure 5-15 Transmission electron micrographs of MNP spheroids	161
Figure 5-16 The three stages of multicellular spheroid formation.	163

Fellowships, grants and awards

Funding and awards received for research relating to this thesis.

The Robertson Trust Research Fellowship from the Royal College of Surgeons of Edinburgh. Project Number RTRF/17/008. August 2017- August 2018.

Small Pump Priming Grant from the Royal College of Surgeons of Edinburgh. Project Number SRG/17/105. February 2017.

Wellcome Trust Institutional Strategic Support Fund- Consolidator Funding, October 2016

Glasgow Meeting of Orthopaedic Research, 1st Poster Prize, March 2019

Publications

Authored by the candidate on research relating to this thesis.

Silverwood RK, Shields DW, Young PS. “Swapping a drill for a microscope”.
Published in The Journal of Trauma & Orthopaedics March 2018

Conference proceedings

Silverwood RK, Ross EA, Meek RMD, Dalby MJ, Berry CC. “An Analysis of
MicroRNA Expression and Functional Capacity of Mesenchymal Stromal Cells from

Patients with Neck of Femur Fractures” **Podium Presentation** Glasgow Meeting of Orthopaedic Research 2019

Silverwood RK, M Mullin, Meek RMD, Dalby MJ, Berry CC. “The development of a 3D Osteoprogenitor culture model for investigating future osteoporosis therapies” **Poster Presentation** European Society of Biomaterials, Maastricht 2018 & Glasgow Meeting of Orthopaedic Research 2019

Silverwood RK, M Mullin, Meek RMD, Dalby MJ, Berry CC. “The development of a 3D Osteoprogenitor culture model for investigating future osteoporosis therapies” **Podium Presentation** Glasgow Orthopaedic Research Initiative, 23/02/2018

Silverwood RK, Berry CC, Ahmed F, Meek RMD, Dalby MJ. “Development of 3D Osteoporotic Model for MicroRNA Assessment and Manipulation.” **Poster Presentation** European Orthopaedic Research Society Annual Meeting 2016, Bologna (14-16/09/2016)

Silverwood RK, Berry CC, Ahmed F, Meek RMD, Dalby MJ. “Development of 3D Osteoporotic Model for MicroRNA Assessment and Manipulation.” **Podium Presentation** British Orthopaedic Research Society Annual Meeting 2016, Glasgow (6/09/2016)

Acknowledgement

To Wai-Yan, Reuben and Luca, without your support and inspiration I would never have completed this thesis. I wish to dedicate it to my family, whom I love most in the world, don't worry I don't expect you to read it all.

I would like to thank Professor Matthew Dalby and Dr Catherine Berry for their guidance during this research. They allowed my project to explore many avenues, and gave me a wonderful experience of postgraduate research. I am extremely grateful for Professor Meek's supervision as I moved to Glasgow and started a career in Orthopaedics. Without hesitation he encouraged and facilitated my journey into postgraduate research, and I aim to inspire others the way he has inspired me.

Several people within the CCE, now CeMi, taught me numerous, essential skills for laboratory research, and provided incredible support and humour during this long process! I would particularly like to thank Dr Monica Tsimbouri, Carol-Ann Smith, Dr Ewan Ross, Dr Virginia Llopis-Hernandez and Margaret Mullin.

To anyone currently struggling to finish their PhD, persevere, every word typed is one closer to the end.

Author's Declaration

I hereby declare that, unless otherwise stated, the research reported within this thesis is my own work and at the time of submission is not being considered for any other academic qualification.

Robert Silverwood

The 16th of December 2019

Definitions & Abbreviations

2D	Two-dimensional
3D	Three-dimensional
AGO2	Argonaute-2
AKT	Protein Kinase B
AmiR	AntagomiR
ANOVA	Analysis of variance
BCL2	B-cell lymphoma 2
BM	Bone marrow
BMD	Bone mineral density
BMI	Body mass index
BMP-2	Bone morphogenic protein-2
BSA	Bovine serum albumin
BV/TV	Percentage bone volume
cDNA	complementary deoxyribonucleic acid
CO ₂	Carbon dioxide
Conn.D	Connectivity density
CT	Computed tomography
DA	Degree of anisotropy
Dkk-1	Dickkopf-1
DMEM	Dulbecco's modified Eagle's medium
DMSO	Dimethyl sulfoxide
DNA	Deoxyribonucleic acid
DXA	Dual energy x-ray absorptimotry
EDTA	Ethylenediaminetetraacetic acid
ERK	Extracellular signal-signal regulated kinases
FABP4	Fatty acid binding protein 4
FACS	Fluorescence-activated cell sorting
FBS	Foetal bovine serum
FITC	Fluorescein isothiocyanate
FRAX	Fracture risk
Fx	Fracture
GAPDH	Glyceraldehyde 3-phosphate dehydrogenase
GNP	Gold nanoparticle
H ₂ O	Water
HD	Hanging drop
HEPES	4-(2-hydroxyethyl)-1-piperazineethanesulfonic acid
HRT	Hormone replacement therapy
HSC	Haematopoietc stem cell
IBMX	Isobutylmethylxanthine
ICW	In Cell Western

IDEOM	Identification and Evaluation of Metabolomics
IL1B	Interleukin 1 beta
IPA	Ingenuity pathway analysis
KEGG	Kyoto encyclopaedia of genes and genomes
LCMS	Liquid chromatography mass spectrometry
LTFx	Low traum fracture
MFI	Median fluorescence intensity
miRNA	microRNA
MNP	Magnetic nanoparticle
mRNA	messenger RNA
MSC	Mesenchymal stromal cell
MSK	Musculoskeletal
NICE	National institute for health and care excellence
NOF	Neck of femur fracture
OA	Osteoarthritis
OCN	Osteocalcin
OP	Osteoporosis
OPN	Osteopontin
OSX	Osterix
PBS	Phosphate buffered saline
PC	Product code
PCA	Principal component analysis
PCR	Polymerase chain reaction
PEG	Polyethylene glycol
PPARG	Peroxisome proliferator activated receptor gamma
qRT-PCR	quantitative real-time polymerase chain reaction
RA	Rheumatoid arthritis
RANK	Receptor activator of nuclear factor kappa B
RANKL	Receptor activator of nuclear factor kappa B ligand
RISC	RNA induced silencing complex
RNA	Ribonucleic acid
RPM	Revolutions per minute
RUNX1/2	Runt- related transcription factor 1 or 2
SC	Sodium cacodylate
SD	Standard deviation
SEM	Scanning electron microscopy
SMI	Structural model index
SPR	Surface plasmon resonance
TAGLN	Transgelin
Tb.N	Trabecular number
Tb.Sp	Trabecular separation
Tb.Th	Trabecular thickness
TEM	Transmission electron microscopy
Thy-1	Thymocyte antigen

TRITC	Tetramethylrhodamine	
ULA	Ultra-low attachment	
UV	Ultraviolet	
VDAC	Outer mitochondrial membrane channel	
VOI	Volume of interest	
Wnt	Wingless-related integration site	

Chapter 1

1.1 Osteoporosis

Osteoporosis (OP) is a systemic skeletal disease, which is characterised by low bone mass and microarchitectural deterioration of bone tissue, resulting in an increase in bone fragility with susceptibility to fracture. The disease has become vastly more prevalent, and health care services and current therapies have failed to cope with the increasing demands (Khosla and Hofbauer, 2017). A revolution is required for the management of this disease, to prevent significant morbidity and mortality to future generations.

1.1.1 Disease mechanism of action

The World Health Organization utilises T scores for its diagnostic criteria of OP. The T score is derived by calculating the bone mineral density (BMD), via dual-energy X-ray absorptiometry (DXA) applied to the femoral neck of a patient. OP is defined as a bone mineral density (BMD) of 2.5 standard deviations or more below the average value for a young, healthy control, with low bone mass, osteopaenia, defined as a T score of between -1 and -2.5 (World Health Organization, 2007). The disease itself is asymptomatic and it commonly remains undiagnosed until a fragility fracture occurs.

As bone mass, and its loss, are intrinsic to the definition of OP, factors which affect the attainment of peak bone mass and the rate of its loss are therefore precipitators of the disease (Miller and Thompson, 2016). Peak bone mass occurs in the third decade of life. Bone mass is then lost faster in women, with an acceleration occurring after the menopause. Both sexes suffer a net decline in bone mass and this natural decline can result in OP. However, there are many other contributors which can result in OP, see Table 1-1.

Table 1-1 List of BMD dependent and independent factors associated with an increased risk of developing OP (Miller and Thompson, 2016; Ramachandran and Nunn, 2018).

Risk Factors for Osteoporosis	
Gender	Female
Ageing	With each decade there is a 1.4-1.8-fold increased risk of the disease
Ethnicity	Increased risk if northern European or Asian
Sex hormone deficiency	Oestrogen and testosterone
Low Body Mass Index (kg/m²)	<19 kg/m ²
Lifestyle	excessive exercise, immobilisation, smoking, alcohol
Chronic Disease	osteogenesis imperfecta, rheumatoid arthritis, chronic obstructive pulmonary disease, chronic kidney disease, liver disease
Drugs	Glucocorticoids, corticosteroids, thyroxine, heparin, phenytoin, antiandrogens, chemotherapy,
Gastrointestinal	Malabsorption, vitamin D and Calcium insufficiency, anorexia nervosa
Genetic	Collagen Type 1 A1, vitamin D receptor and oestrogen receptor genes
Clinical	previous fragility fracture, loss of height, strong family history of OP

As disease management has improved, along with life expectancy, a greater number of people will be taking regular medication and secondary OP due to the above causes will be more frequently encountered (McClung, Baron and Bouxsein, 2017). Thus, its recognition and appropriate management is crucial to preventing fragility fractures.

1.1.2 Bone in health

Bone is a highly specialized connective tissue which serves several functions:

- **Reservoir of calcium and phosphate:** Bone is the primary reservoir of calcium and phosphate in the body.
- **Haematopoiesis:** Within cancellous bone the haematopoietic bone marrow supplies the body's cells, tissues and organs with erythrocytes, leukocytes and platelets.
- **Protective and mechanical:** Bone has protective and mechanical roles, protecting soft internal viscera and permitting movement and locomotion through attachment of muscles (Ramachandran and Nunn, 2018).

Long bones, such as the femur, tibia, radius and ulna have three anatomical regions, the epiphysis, metaphysis and diaphysis, Figure 1-0-1. Diaphyseal regions of long bones have thick cortices surrounding the intra-medullary canal.

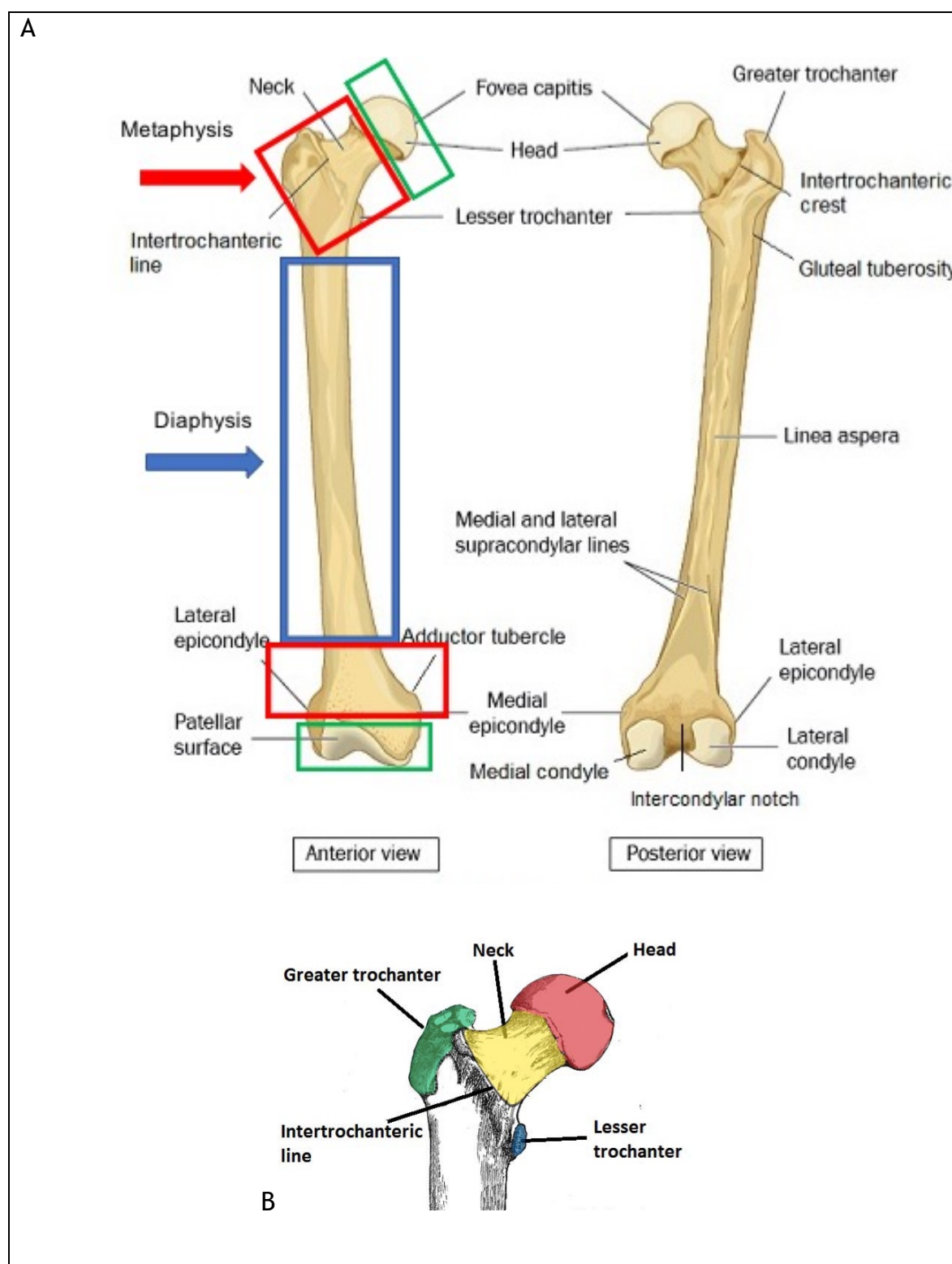


Figure 1-0-1 Anatomy of an adult femur. Image A shows common anatomical points of a femur and demonstrates key regions, namely diaphyseal- blue box, metaphyseal- red boxes and epiphyseal- green boxes. Image B depicts the proximal femur in closer detail and the areas within it. Image adapted from (Jones, 2019).

Contrastingly metaphyseal regions of bone have thin cortical bone and a denser network of cancellous bone, Figure 1-0-2. Epiphyseal regions are located at the ends of long bones, contain the physis, also known as the growth plate, and the articular surface (Ramachandran and Nunn, 2018).

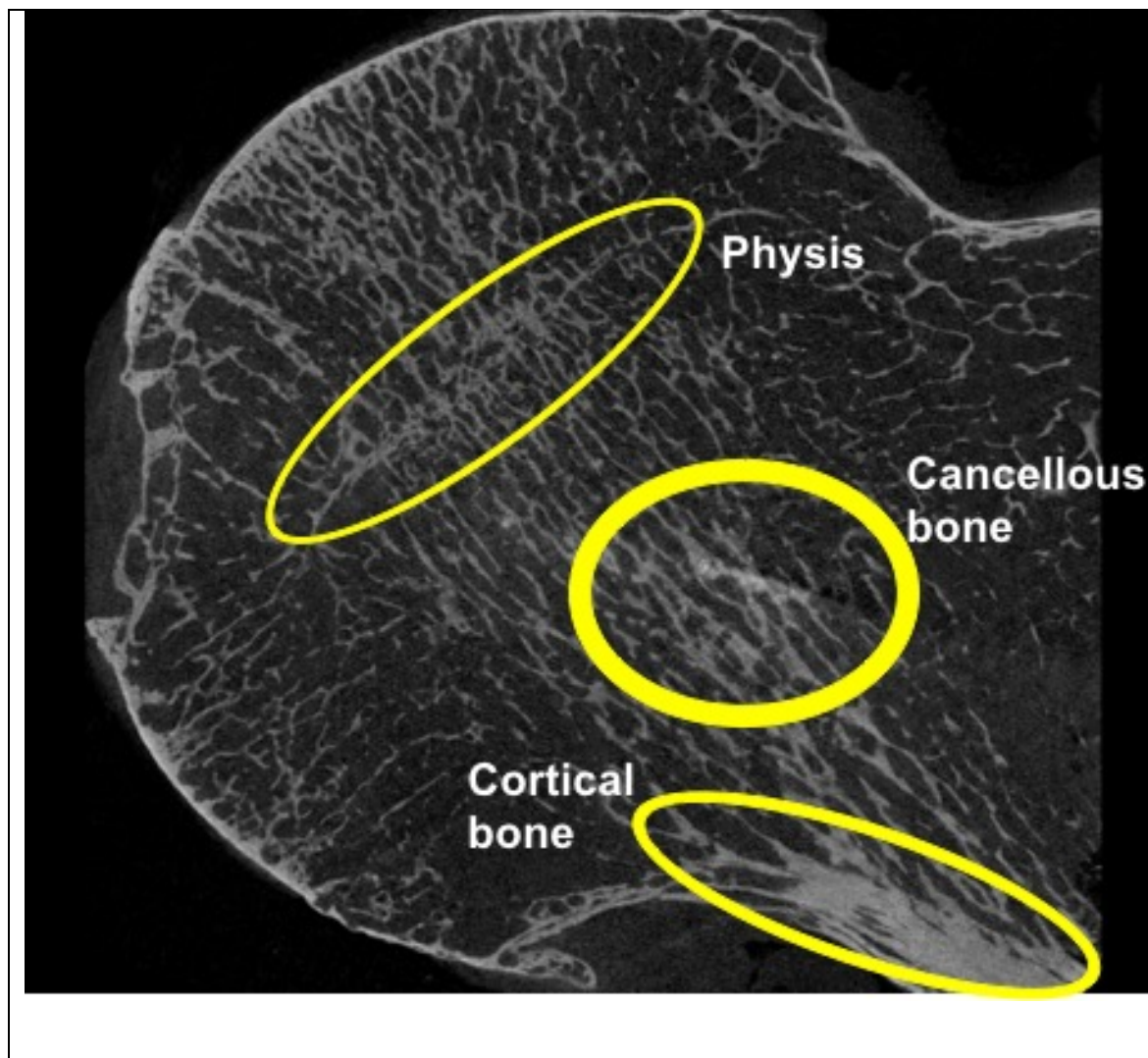


Figure 1-0-2 Femoral head and neck from patient with osteoarthritis excised during hip arthroplasty, imaged during microCT experiment of research project. Coronal microCT imaging of the specimen, thick cortical bone in the inferior neck and inter-connected central cancellous bone are visible. The physis of the proximal femur is also highlighted, where some of the increasing limb length occurs during skeletal growth.

1.1.2.1 Cortical and cancellous bone

Cortical bone is a subtype of lamellar (mature) bone, it forms the envelope of cuboid bones and the diaphysis of long bones, and thus comprises approximately 80% of the human skeleton. In comparison to cancellous bone cortical bone characteristically has a slower rate of turnover and is more resistant to compressive and tensile forces. Cortical bone has a Young's modulus, a measure of a materials elasticity, of 20 Newton's per square metre (GPa).

In contrast to cortical bone cancellous bone has a higher rate of remodelling and a lower Young's modulus, approximately 1 GPa, resulting in more elastic property. Cancellous bone is formed as a loose network, and within the porous areas bone marrow resides (Ramachandran and Nunn, 2018).

1.1.3 Cellular mechanisms of bone homeostasis and osteoporosis

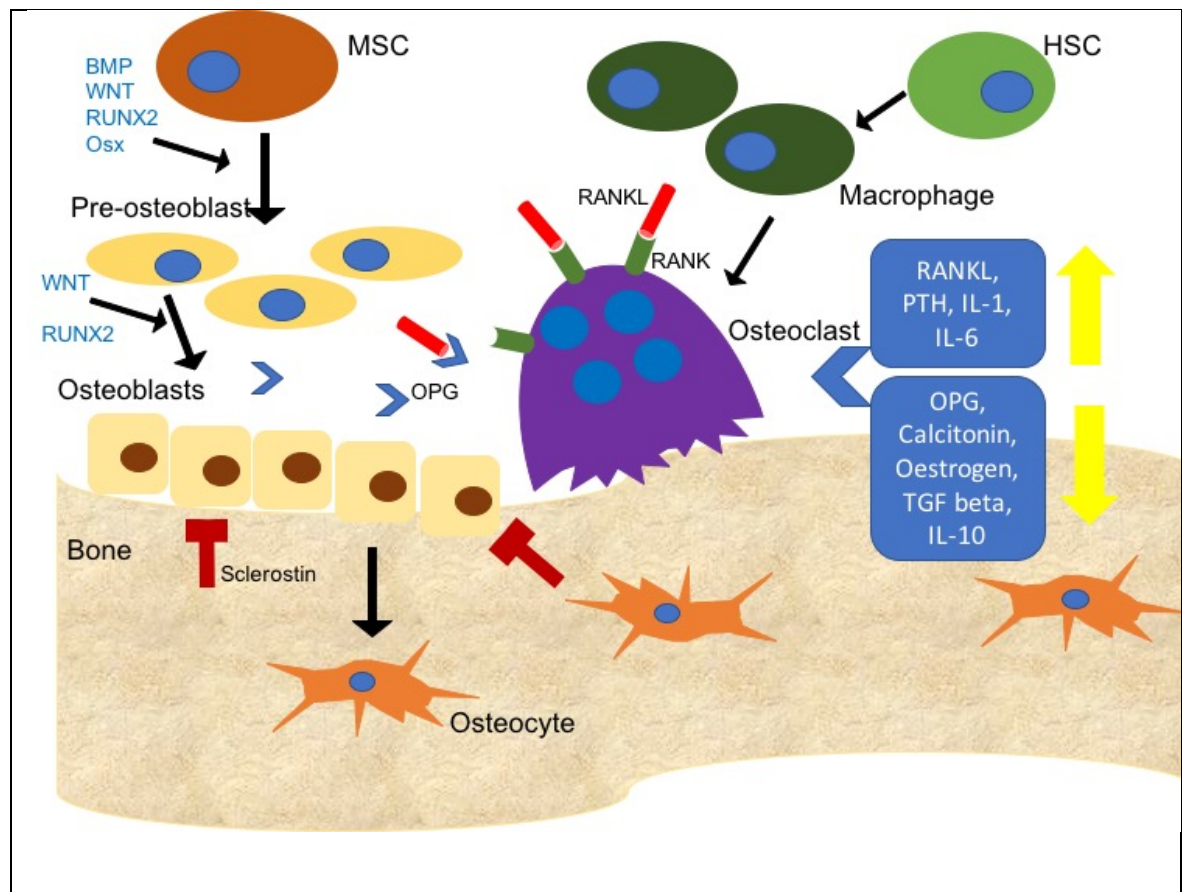


Figure 1 0-3 Depiction of bone homeostasis with key cells and their regulators demonstrated. Osteoblasts are derived from mesenchymal stromal cells (MSC), and once buried within the newly formed matrix become osteocytes. Sclerostin is expressed by osteocytes and acts to inhibit osteoblast activity. Osteoblasts express Osteoprotegrin (OPG) which inhibits osteoclast activity and receptor activator of nuclear factor kappa B ligand (RANKL) which stimulates osteoclast activity and bone remodelling, both of which bind to receptor activator of nuclear factor kappa B (RANK) present on osteoclasts. An osteoclast, derived from haematopoietic stem cells (HSC), is demonstrated on the bone surface with its ruffled border and known regulators are shown in the blue boxes with their effects indicated by the yellow arrows. Image adapted from (Qin and Hu, 2014).

Osteoblasts are bone forming cells, derived from mesenchymal stromal cells (MSCs), which secrete matrix and can be mineralised. Osteoclasts are responsible for bone resorption and play a key role in tandem with osteoblasts in

bone remodelling, Figure 1 0-3. The change in the dynamic between these two cell types is key to the development of OP.

Osteoclasts originate from haematopoietic stem cells (HSC) and are closely related to other HSC lineage cells such as monocytes and macrophages. The formation of activated multinucleated osteoclasts depends on receptor activator of nuclear factor kappa B-ligand (RANKL) and macrophage-colony stimulating factor (M-CSF). RANKL is produced by osteoblasts, bone marrow MSCs, T and B lymphocytes and leads to the activation of RANK, present on osteoclasts. Once RANKL-RANK stimulation occurs the differentiation, proliferation, multinucleation activation and survival of osteoclasts occurs through the action of regulatory transcription factors and enzymes. Resorption of bone then occurs (Rachner, Khosla and Hofbauer, 2011).

During OP trabeculae within cancellous bone are thinned and decreased in number, with some lost entirely, leaving that bone vulnerable to injury. Decreased osteon size and enlarged marrow spaces are observed in osteoporotic cortical bone, leading to thinner cortices (Miller and Thompson, 2016; Ramachandran and Nunn, 2018). Microarchitectural changes result from increased osteoclast activity and reduced osteoblast function and thus result in a predisposition to fragility fractures (Brandi, 2009).

1.1.4 Diagnosis, monitoring and fracture risk assessment

The World Health Organization and the International Osteoporosis Foundation recommend DXA imaging of the femoral neck for the diagnosis of OP. This is due to the higher predictive value for risk of fracture at this site in comparison to other skeletal sites. The lumbar spine is subsequently used for monitoring response to initiated treatment (National Institute for Health and Care Excellence, 2016). Although DXA has a high specificity as a diagnostic investigation for OP, the majority of patients will suffer a fragility fracture with a T score in a non-diagnostic range for OP.

Further tools used to help diagnosis the disease include the Fracture Risk Assessment Tool (FRAX). FRAX is widely used and included in multiple clinical guidelines. It estimates a 10-year probability of major OP fracture or hip

fracture alone. FRAX has been utilised clinically with and without DXA to identify patients requiring preventative therapy or who require further investigation (Compston, McClung and Leslie, 2019).

Quantitative computed tomography can also be utilised for calculating femoral neck T scores and are noted to be the equivalent of DXA-derived scores (Cann *et al.*, 2014).

However, the mainstay of diagnosis and disease monitoring of OP is via DXA scanning, and it has its inherent limitations. BMD only partly explains bone strength, with bone microarchitecture increasingly becoming understood to be key to strength, and its insensitivity impairs the monitoring of response to therapy (Delmas and Seeman, 2004; Watts *et al.*, 2005).

1.1.5 Prevalence

Osteoporosis represents a global burden of ever-increasing proportions. Due to ageing populations in societies across the world the prevalence of the disease is rising dramatically. The disease most commonly affects the elderly, and with populations ageing throughout the world the incidence of the disease and its complications are set to significantly rise. 300,000 OP related fractures occur annually in the UK alone, and this is expected to double by the year 2050. In addition to the detrimental effects on quality of life, the disease and its associated fragility fractures will cripple many healthcare budgets (National Institute for Health and Care Excellence, 2016; Compston *et al.*, 2017; Compston, McClung and Leslie, 2019).

The prevalence of OP increases markedly in post-menopausal women. At the age of 50 approximately 2% of women suffer from the disease, this rises to 50% at 80 years of age (NICE 2011b). In the UK more than 500 000 new fragility fractures occur each year (Svedbom *et al.*, 2013). Although much more common in women, men also suffer from the disease, and it is estimated that 1 in 5 men will sustain one or more OP related fractures during their lifetime ('NOGG 2017: Clinical guideline for the prevention and treatment of osteoporosis', 2017).

1.1.6 Morbidity and mortality

The morbidity of the disease is caused by fragility fractures. Due to the weakened status, patients' bones are more susceptible to fracture from low energy trauma. A fragility fractures is defined as a fracture occurring from a fall from standing height or less. The most commonly occurring osteoporotic fractures are of the vertebrae, neck of femur and distal radius. Vertebral fractures may occur without a fall, or in association with bending and lifting (Compston *et al.*, 2017).

These fractures are of great importance as patients who suffer hip fractures or vertebral fractures have a decreased life expectancy compared with population-based controls. Approximately 25% of the deaths that occur following a hip fracture are related to the fracture, and the 1 year mortality rate post hip fracture is 20% (Kanis *et al.*, 2003).

Recent research has shown that despite an increasing prevalence of these injuries improved post fracture outcomes have been achieved (Tucker *et al.*, 2017). Mortality rates after hip fracture have decreased, and this is important as an increasing complexity of patient is being encountered, with patients living longer and presenting with more comorbidities (Hannah *et al.*, 2017).

In addition to the high mortality rate, neck of femur fractures are also associated with significant morbidity. 53% of patients do not regain their previous level of mobility post injury and can no longer return to living independently (Compston *et al.*, 2017).

Vertebral fractures can present with acute severe back pain; however, greater than 50% of these pathological fractures are asymptomatic. Vertebral fractures cause loss of height, impaired mobility and reduced respiratory function. Once a patient has suffered one vertebral fracture they are at great risk of suffering multiple (Compston *et al.*, 2017).

1.1.7 Economic impact

The cost of managing fragility fractures is enormous. In the UK in 2010 it was estimated to have cost the NHS over £4.4 billion. These injuries are not just

costly, but also resource intensive with the average length of stay after a hip fracture in Scotland being 17 days (Scottish Hip Fracture Audit, 2019). In the UK alone fragility fractures are estimated to double in incidence during the next 50 years, thus these injuries will represent a significant proportion of a healthcare services budget (Compston *et al.*, 2017).

1.1.8 Current therapies

The primary objective of treating OP is to reduce the incidence of future fragility fractures. This can be achieved by reducing fall frequency, strengthening the skeleton, or both. All patients at risk of OP should be advised on good nutrition, regular physical activity, smoking cessation and appropriate levels of alcohol consumption (National Institute for Health and Care Excellence, 2016; 'NOGG 2017 : Clinical guideline for the prevention and treatment of osteoporosis', 2017).

The evidence of the efficacy of reducing fracture risk via the supplementation of calcium and vitamin D is inconsistent. A benefit can be seen, but for patients who are replete in these nutrients there appears to be little or no benefit (Jackson *et al.*, 2006; Zhao *et al.*, 2017).

Figure 1-0-4 demonstrates the mechanism of action of the most commonly used class of drugs for OP currently prescribed.

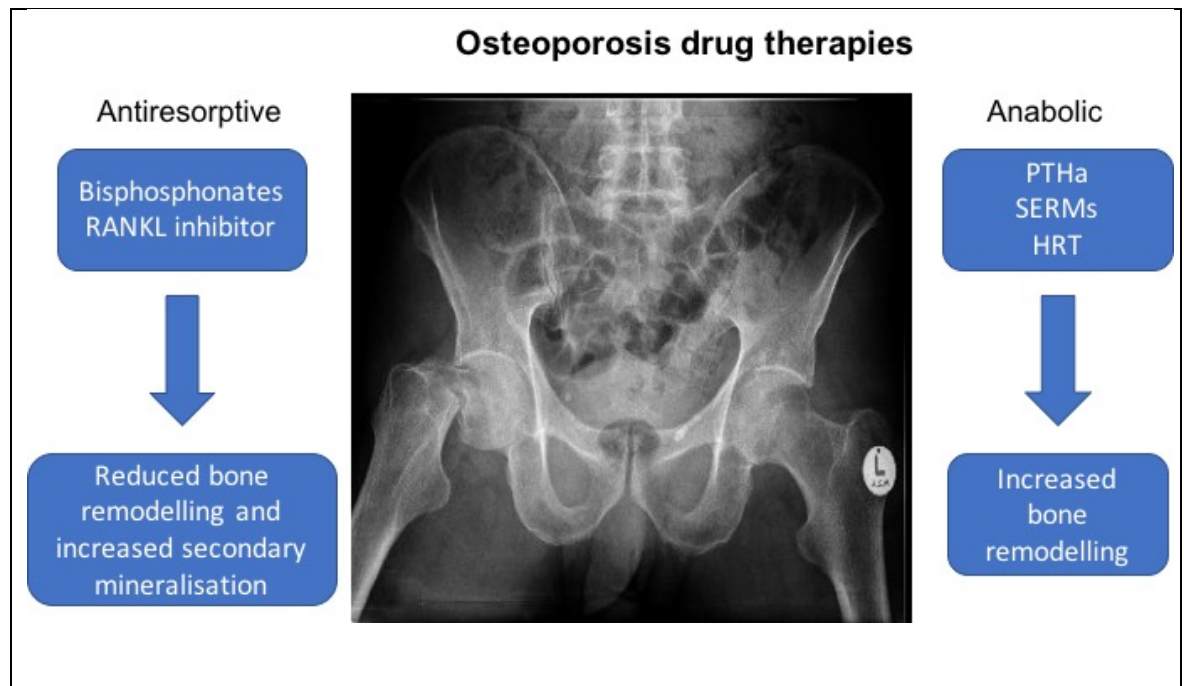


Figure 1-0-4 X-ray of a right neck of femur fracture, a common injury in patients with osteoporosis. The diagrams describe the two main classes of Osteoporosis therapies and their effect on bone homeostasis. A negative remodelling balance is evident in age related bone loss due to an increase remodelling. Antiresorptive agents act to reduce the remodelling rate and anabolics aim to create a positive remodelling balance by increasing osteogenic activity. HRT- hormone replacement therapy, PTHa- parathyroid hormone agonist, SERM- selective oestrogen receptor modulator. Adapted from Compston et al 2019.

1.1.8.1 Bisphosphonates

Bisphosphonates are antiresorptive agents and are currently the first line of therapy. Following fracture risk assessment, if a patient is deemed at high risk of an OP fracture an oral bisphosphonate is offered. Bisphosphonates have been shown to reduce the risk of vertebral fracture by 40-70%, and hip fractures by 40-50% (Scottish Intercollegiate Guidelines Network, 2009; Khosla and Hofbauer, 2017). The mechanism of action for bisphosphonates was discovered long after their introduction to clinical use; osteoclast viability and function is impaired by inhibiting the enzyme, farnesyl pyrophosphate synthase, which generates isoprenoid lipids used in post-translational modifications of small guanosine triphosphate (GTP)-binding proteins (Khosla and Hofbauer, 2017).

In clinical practice, initially alendronate or risedronate are trialled. Alendronate is approved for use in men and women and has specific requirements in its delivery. Patients are required to fast overnight prior to taking the medication, tablets should be swallowed whole with approximately 200 ml of water. The

patient should take the medication standing or sitting and is then required not to lie down for 30 minutes. If oral therapy is not tolerated an intravenous bisphosphonate, zoledronic acid, can be utilised (Compston *et al.*, 2017).

In addition to this difficult mode of taking the oral bisphosphonates, their side effects can be severe. They include upper gastrointestinal symptoms with oral therapy and flu-like symptoms with intravenous (National Institute for Health and Care Excellence, 2016). Osteonecrosis of the jaw is a rare, but devastating complication. Most concerning is the occurrence of an atypical femoral shaft fracture, which frequently impairs a patient's mobility and requires surgery. The risk of an atypical femoral shaft fracture increases with duration of therapy, affecting 1 in a 1000 patients after 8 years of therapy; and they are associated with significant morbidity ((Shane *et al.*, 2014; Compston, McClung and Leslie, 2019).

1.1.8.2 RANK ligand inhibitor

Denosumab is a human monoclonal antibody which can be delivered by subcutaneous injection every 6 months to reduce the risk of vertebral, non-vertebral and hip fractures. It causes a marked inhibition of bone remodelling, due to its binding and inhibition of the RANK ligand. Denosumab results in an increase in BMD. However, upon stopping treatment bone remodelling occurs at an accelerated rate before returning to the patient's baseline level. This leads to an initial rapid decrease in BMD and an increased risk of vertebral fractures, with reports of multiple fractures occurring 3-18 months following treatment cessation. Thus, on stopping denosumab, a substitute antiresorptive agent should be prescribed (Compston, McClung and Leslie, 2019).

Denosumab is associated with skin rashes and an increased risk of infections. Like bisphosphonates, denosumab is also associated with atypical femoral fractures (Compston, McClung and Leslie, 2019).

1.1.8.3 Teriparatide

A further subcutaneous injection, which is given for a course limited to 2 years, Teriparatide is a Parathyroid hormone receptor agonist. It has been shown to significantly reduce the risk of vertebral and non-vertebral fractures.

Teriparatide course duration is limited due to the risk of osteosarcoma and is also contraindicated in patients with skeletal malignancies, previous ionising radiation to bone or hypercalcaemia. Furthermore, its cost is prohibitive for regular use (Khosla and Hofbauer, 2017).

1.1.8.4 Abaloparatide

Abaloparatide, a synthetic analogue of parathyroid hormone-related protein, is not licensed for use in the UK, but similarly positive skeletal effects are seen in Teriparatide use. It is available in the US but due to unconvincing reduction in non-vertebral fractures, and increases in cardiovascular side effects, it has not been approved in Europe (Compston, McClung and Leslie, 2019).

1.1.8.5 Hormone replacement therapy

Hormone replacement therapy (HRT), in the form of oestrogen, with or without progesterone, has been shown to be an effective method in reducing fracture risk in post-menopausal women. HRT was seen to reduce the risk of vertebral and hip fractures by 34% in the Women's Health Initiative study (Cauley *et al.*, 2003). If a patient has failed first line therapy and is early menopausal, HRT can be an effective therapy. Due to the risk of cardiovascular side effects this recommendation is limited to within 10 years of the menopause (Compston, McClung and Leslie, 2019).

1.1.8.6 Selective oestrogen receptor modulators

Raloxifene is a weak antiresorptive agent and is both an agonist and antagonist of oestrogen. It is observed to reduce the risk of vertebral fractures only. It is further limited by its side effect profile, which includes an increased risk of venous thrombosis, death from stroke and vasomotor menopausal symptoms (Compston, McClung and Leslie, 2019).

1.1.8.7 Strontium ranelate

The use of strontium ranelate was limited to the treatment of severe osteoporosis only, and it did not gain approval for use in the USA. The drug reduces bone resorption and increases serum markers of bone formation, resulting in a 41% reduction in vertebral fractures (Khosla and Hofbauer, 2017).

However, it is associated with several limitations, which has led to its use being uncommon. The drug is associated with a rise in the rates of myocardial infarction, heart failure and serious skin reactions, raising questions about its safety (Bolland and Grey, 2016). The production of the drug has been permanently discontinued.

1.1.9 Duration and monitoring of Osteoporosis therapy

There is no current evidence to support therapy for a duration longer than 10 years. Clinicians are advised to prescribe oral bisphosphonates for an initial treatment period of 5 years. If the patients fulfil one of the following criteria they are advised to continue on therapy for a further 3-5 years:

- hip BMD remains persistently low
- or they suffer a further fracture
- previously have had a vertebral or hip fracture
- are prescribed oral glucocorticoid therapy
- aged over 75 years
- persistently high FRAX score

In patients who do not fall into the above categories an assessment of their fracture risk should be performed after they have completed their initial treatment period, with a drug holiday for 2-3 years to be considered concluded by a further fracture assessment. Monitoring of BMD and bone turnover markers during the initial years of therapy remains controversial, and is not routinely recommended (Compston, McClung and Leslie, 2019).

It is evident that current therapies for OP have failed to stem the tide of the disease. The overall aim of osteoporosis therapy is to produce a reduction in fracture risk. Since a patient or clinician will not know when a fracture has been prevented, monitoring of current therapies is not as detailed as for other chronic diseases such as diabetes and hypertension. New therapies which induce

progressive increases in BMD would produce the possibility of accurate monitoring, and a determination of a treatment target. However, bisphosphonates, the most commonly used current therapies do not produce a significant enough amount of BMD to be accurately quantifiable and used to tailor the patient's therapy (Khosla and Hofbauer, 2017).

Alarming, despite the well-known detrimental effects these injuries have on a patient's life, the prescription of secondary prevention has been seen to be falling in several studies (Ström *et al.*, 2011; Svedbom *et al.*, 2013; Solomon *et al.*, 2014). This trend was observed in studies conducted in different countries with different health service modalities. High risk patients are not being managed as per guidelines, with evidence to show that they are at an even higher risk of further fracture (Compston, McClung and Leslie, 2019).

Several factors have been suggested for this under-treatment. This has been associated with the poor education of clinicians and patients, fear of side effects and failings of health care in managing patients with fragility fractures (Khosla and Hofbauer, 2017).

This evidence shows that a revolution in the management of OP is essential. Improvements in diagnosis, disease monitoring and management and further education of clinicians and patients are all required.

1.1.10 Future osteoporosis therapies

It seems evident that current therapies have proven intolerable or unacceptable due to their side effects and associations. In developing targeted therapies, achieving certain criteria is the goal of future therapies. These would include:

- Prolonged anabolic effect
- Efficacy at > 5 years duration
- Improve fracture healing
- Avoid osteonecrosis of the jaw and atypical femoral fractures

- Simple drug delivery method

Multiple different avenues are being explored for the development of targeted therapies for osteoporosis.

1.1.10.1 Sclerostin inhibitors

Sclerostin is a protein expressed by the *SOST* gene in osteocytes, it acts by inhibiting Wingless-related integration site (Wnt) signalling and results in reduced osteoblastogenesis. Sclerosteosis and van Buchem disease result in an increased bone mass and strength due to the absence of functional sclerostin (Hamersma, Gardner and Beighton, 2003; Van Lierop *et al.*, 2013). This insight provided a therapeutic target, and sclerostin inhibition via monoclonal antibodies has resulted in enhanced bone strength and resistance to fractures. Romosozumab is under advanced clinical trials and has shown positive results for reducing vertebral fragility fractures. However, a reduction in non-vertebral fragility fractures was not seen, similar side effects to bisphosphonates were encountered and there was an association with cardiovascular events (Khosla and Hofbauer, 2017).

1.1.10.2 Cathepsin K inhibitors.

Cathepsin K was identified as a therapeutic target, to reduce bone resorption by osteoclasts but enable ongoing paracrine signalling to osteoblasts. Mature osteoclasts secrete cathepsin K, resulting in degradation of bone matrix proteins (Costa *et al.*, 2011).

The development of the cathepsin K inhibitor, odanacatib, was discontinued in 2016. Despite clinical trials showing a reduction in risk of vertebral and hip fracture an unacceptable increase in stroke, atypical femoral fracture and skin reactions were encountered (Khosla and Hofbauer, 2017).

1.1.10.3 Dickkopf-1 antibodies

The inhibition of Dickkopf-1 (Dkk-1) has been investigated in several diseases which suffer from excessive bone resorption, such as multiple myeloma and rheumatoid arthritis and Dkk-1 inhibition has been seen to reduce osteolysis

(Florio *et al.*, 2016). Due to its promise, it is being investigated for clinical use in OP. However, prolonged inhibition of Dkk-1 raises concerns due to the known association of increased Wnt signalling to diseases such as colorectal and hepatocellular cancer (Rachner, Khosla and Hofbauer, 2011; Khosla and Hofbauer, 2017).

1.1.10.4 Stem cell therapies for OP

Cell therapy has long been hailed as holding great potential for regenerative medicine, and this extends to the field of orthopaedics. The use of MSCs has been investigated for the treatment of many pathologies, including OA, non-unions of fractures, tissue regeneration for defects in bone, cartilage and tendon and augmenting the primary healing of muscle, ligament and menisci (Chew, Prakash and Khan, 2017; De Albornoz *et al.*, 2018). However, the current clinical picture has yet to deliver the expected outcomes. Numerous factors are involved in the underwhelming progress made with MSC therapy. Bone marrow and adipose samples to provide autologous therapy result in a low number of MSCs, with 0.005% to 0.01% MSCs present in the sample population respectively (Qadan *et al.*, 2018). This is in stark contrast to laboratory-purified culture-expanded cells. Furthermore great heterogeneity is observed in cell formulations from different patients, reducing the observed efficacy of MSC therapy (Rodeo, 2019).

Currently cell therapies have not proven to be a replacement to the gold standard treatment for many conditions, such as total hip arthroplasty for hip osteoarthritis. The aim must be to initiate the cell therapy after an early tissue diagnosis of disease, to regenerate or delay disease progression. In advanced disease with deformities such as osteophytes, erosions and limb malalignment, it is difficult to envisage cell therapy surpassing the efficacy of surgery.

1.1.11 Mesenchymal Stromal Cells in Osteoporosis and the effect of ageing

MSCs represent a population of progenitor cells with the capability of differentiating to produce cells of various connective tissue lineage. At least 5 *in vivo* roles have been described for MSCs, including bone, cartilage and fat formation and vascular and haematopoietic support (Aggarwal and Pittenger, 2005; Dominici *et al.*, 2006; Ball *et al.*, 2007).

When considering the osteogenic potential of MSCs it is important to consider the donor's age and gender. Bone formation indices peak in late teenage years for men and then begin a steady decline until the age of 50. In females, bone formation and resorption are increased after the menopause, but result in a net reduction in BMD (Szulc, Kaufman and Delmas, 2007).

Due to the association of OP with age it is important to understand the effect aging has on the differentiation capacity of MSCs. Age related changes in MSCs include loss of differentiation potential, loss of proliferation potential, increasing senescent cell numbers and decreased osteogenic activity (Sethe, Scutt and Stolzing, 2006). However, this statement is made less definitive by several papers showing no change in the number of observed colony forming units in samples of donors with differing ages (Stenderup *et al.*, 2001; Oreffo *et al.*, 2002).

A study on the effect of aging on the fitness of MSCs, in donors ranging from 5 to 55 years of age identified significant reduction in colony forming units in donors aged 18 or older. MSCs from donors older than 40 showed an increased expression of tumour suppression protein p53 and cell-cycle regulation p21, and this was accompanied with a significant increase in the levels of apoptosis in comparison to MSC cultures from donors aged less than 18 years. Furthermore a significant reduction in Notch-1 receptor was observed in MSCs from donors aged over 40 (Stolzing *et al.*, 2008).

The research by Stolzing *et al* identified important differences occurring in MSCs during ageing. MSC samples were from a relatively young age group, with the main patient population of OP not assessed. It would be of great interest if this could be extended to include a further group of donors with ages greater than 65 to further analyse these trends and to observe their rate.

It was thought that as patients became elderly their MSCs were more prone to forming adipocytes instead of osteoblasts, and thus contributed to the development of OP, often termed senile OP (Meunier *et al.*, 1971). This theory, of the loss of osteogenic potential, was termed "adipogenic switch" and has been investigated by many studies. Some researchers have reported an increase in adipogenesis in aged MSC, but this is balanced with other experiments

showing no change in the rate of adipocyte formation with age (Stenderup *et al.*, 2003; Moerman *et al.*, 2004; Sethe, Scutt and Stolzing, 2006; Valenti *et al.*, 2011).

Sethe *et al* concluded that no definitive statement regarding age-related effects in differentiation could be made, due to differing results from multiple studies (Sethe, Scutt and Stolzing, 2006). It has become apparent that the cause of OP cannot solely be attributed to the impaired activity of MSCs, however it is likely that some degree of deficiency in differentiation exists.

Thus, the cause of impaired bone formation and density cannot be just a cellular problem, with local and patient environmental factors playing a crucial role also. This has implications for future therapies as well. To effectively treat OP a holistic approach, focusing on more areas than just local bone marrow MSCs will be required.

1.1.12 Mesenchymal stromal cell functionality in osteoporosis

As discussed above, a longstanding hypothesis of the cause of OP was termed the “adipogenic switch”. This was described in 1971 by Meunier *et al* and describes the loss of osteogenic preponderance of MSCs within the BM environment, and a change to pro-adipogenesis. This was thought to account for the reduced osteoblast activity and an increase in marrow adiposity (Meunier *et al.*, 1971).

Many studies have argued against this theory of ageing and osteoporotic MSCs being pro-adipogenic, at the expense of osteogenesis (Stenderup *et al.*, 2001; Veronesi *et al.*, 2014). However an attenuated regenerative competence has been described of bone marrow MSCs in patients at risk of OP (Bidwell *et al.*, 2013). It appears more nuanced than to suggest that with age bone marrow MSCs have a propensity to the adipogenic lineage, and thus the cause of OP MSC dysfunction is not directly in keeping with this simplistic view.

This is supported by Abdallah & Kassem, who disregard the simple notion of an inverse relationship between adipogenesis and osteogenesis in the bone marrow environment (Abdallah and Kassem, 2012). They state that secreted factors from

different MSC populations within the bone marrow exert significant regulatory control of differentiation. Furthermore, with regards to osteogenic differentiation of OP MSCs, Prall *et al* suggest that pre-induction, these cells have a reduced osteogenic state, however they maintain a sufficient upregulation of osteogenic differentiation on BMP-2 induction (Prall *et al.*, 2013). This group further identified reduced cellular migration and invasion of MSCs from OP patients (Haasters *et al.*, 2014).

The development of OP has many causes. However, determining to what extent the MSC or the local environment is responsible has yet to be fully understood. This further identifies the deficiencies of current therapies, which fail to address the potentially impaired functionality of MSCs (Bidwell *et al.*, 2013).

1.2 MicroRNAs in regenerative medicine

1.2.1 MicroRNAs mechanism of action

Mature microRNAs (miRNAs) are a class of naturally occurring, small non-coding ribonucleic acids, 18-23 nucleotides in length. They were discovered by Lee and colleagues and described in 1993 (Lee, Feinbaum and Ambros, 1993). MicroRNAs are partially complementary to one or more messenger RNA (mRNA) molecules, and their main function is to down regulate gene expression. This down regulation can occur through several different mechanisms including translational repression, mRNA cleavage and deadenylation (Dweep, Sticht and Pandey, 2011). Figure 1-0-5 demonstrates the transcription of miRNAs through to their cytoplasmic action.

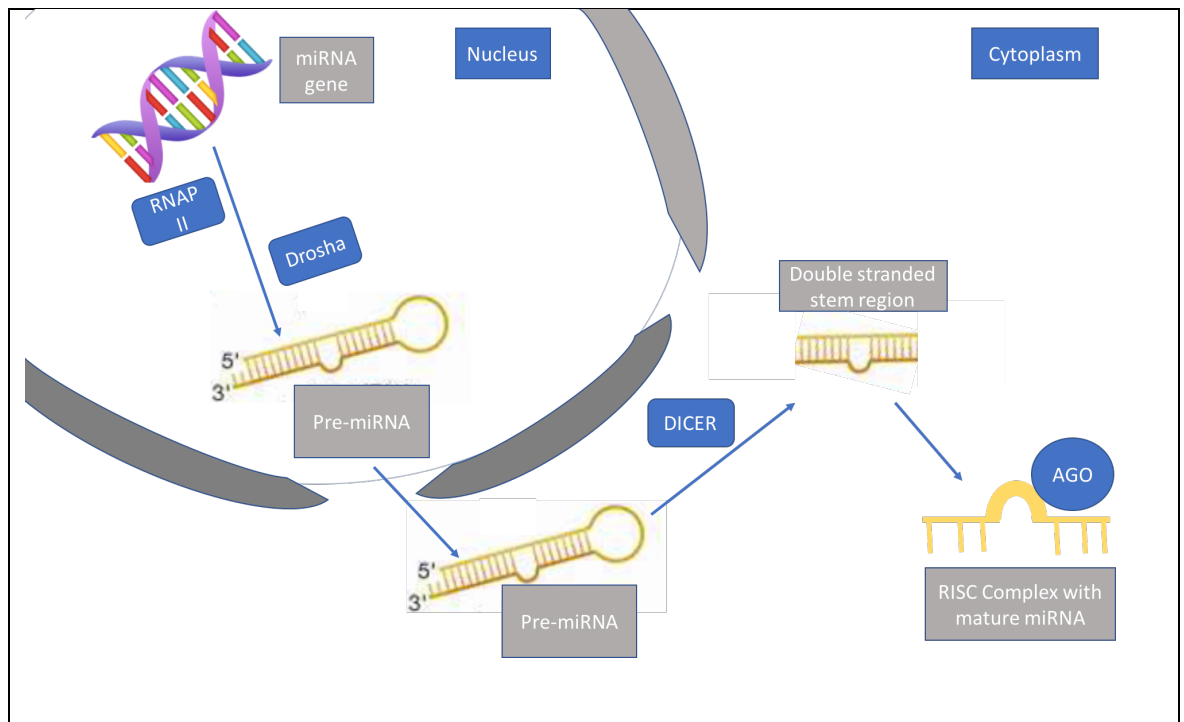


Figure 1-0-5 MicroRNA biogenesis and action. MiRNAs are transcribed in the nucleus from a miRNA gene or intronic regions by RNA polymerase II (RNAPII), yielding the precursor miRNA (pri-miRNA) hairpin structure. Drosha, the endoribonuclease processes, the pri-miRNA resulting in pre-miRNA formation. The pre-miRNA is exported to the cytoplasm, where Dicer binds and cleaves the pre-miRNA loop and end-regions upon an RNA-induced silencing complex (RISC), where double stranded miRNAs are transformed to single stranded mature miRNA bound to an Argonaute protein (AGO). Adapted from (Foessl, Kotzbeck and Obermayer-Pietsch, 2019)

The regulatory effect exhibited by miRNAs does not require perfect base pairing, and one miRNA can bind to, and control the expression of many mRNAs. Thus, miRNA overlap of gene targeting can occur. MiRNAs regulate gene expression by their binding to the 3' UTR (untranslated region) of the target RNA. This results in translational inhibition of the mRNA or destabilization resulting in cleavage and degradation (Lewis *et al.*, 2003; Dweep, Sticht and Pandey, 2011).

Several thousand miRNAs exist in humans, along with their intracellular roles many are detectable systemically, thus leading to great interest in their roles in many different diseases. Over 2500 miRNAs are found in humans. They are known to regulate multiple physiological processes and play an important role in organ development, cell proliferation, apoptosis and bone homeostasis (Kim and Lim, 2014). Furthermore, the dysregulation of miRNA expression has been observed in multiple malignancies and also cardiovascular diseases such as atherosclerosis, hypertension and myocardial infarction (Larrea *et al.*, 2016; Samanta *et al.*, 2016).

Further to this, microRNAs have been shown to be dysregulated in many musculoskeletal diseases,

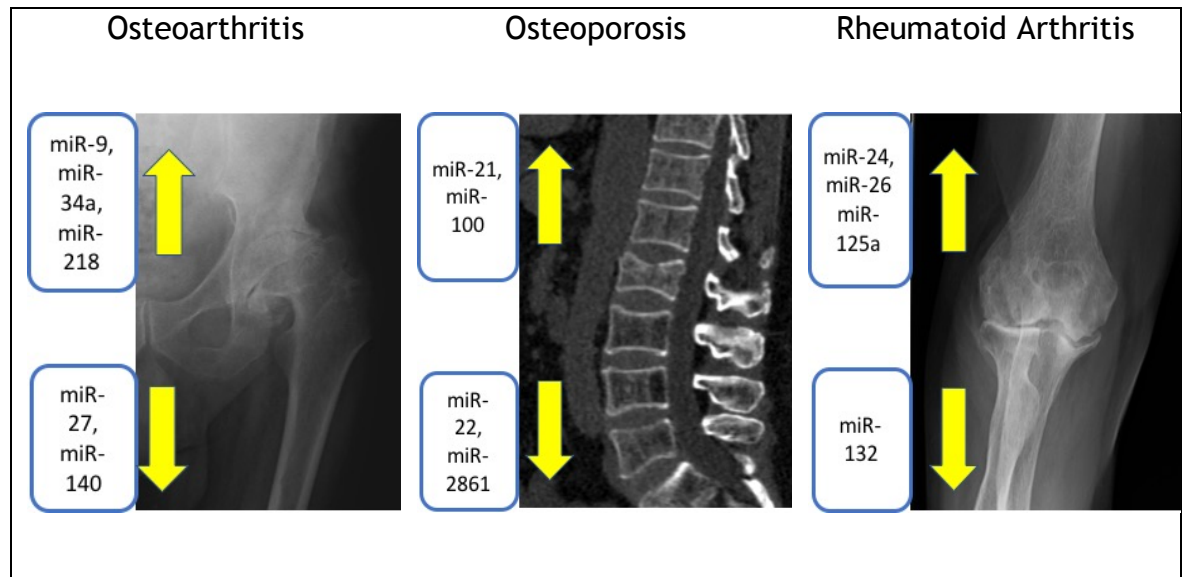


Figure 1-0-6. They have therefore been identified as future biomarkers or molecular targets for many diseases (Kim and Lim, 2014). In osteoarthritis multiple miRNAs, including miR-9, miR-27 and mir-140 have been shown to be dysregulated (Nugent, 2016). Mouse models of the disease have demonstrated improved cartilage protection with the utilisation of a miR-218-5p inhibitor (Lu *et al.*, 2017).

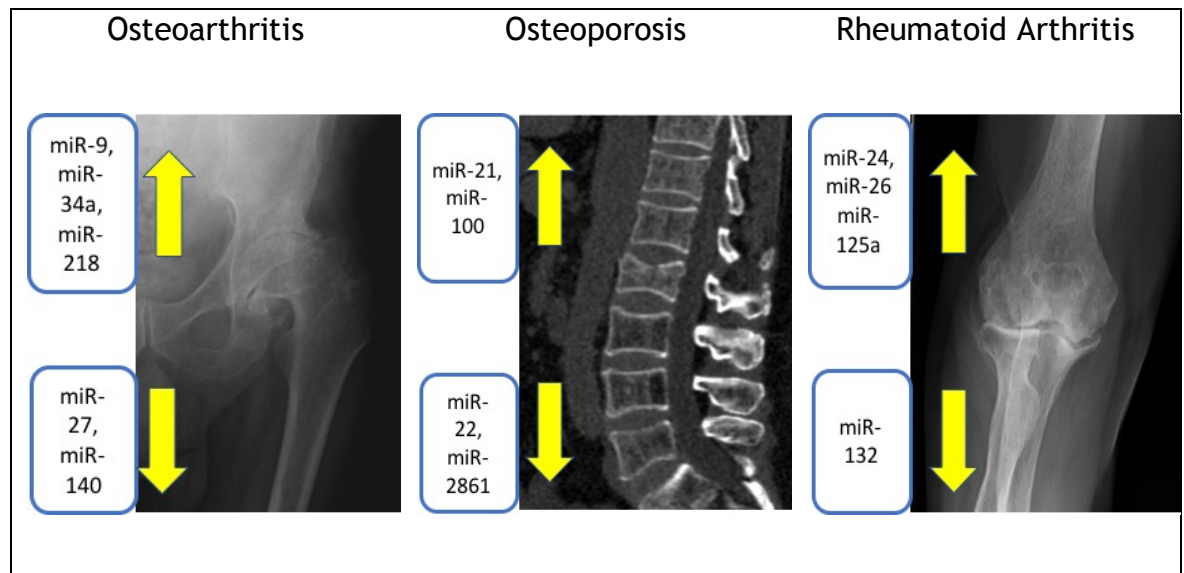


Figure 1-0-6 Radiographs of three common musculoskeletal diseases and some commonly reported dysregulated miRNAs known to be involved in the specific disease pathogenesis. Yellow arrows depict up or downregulation of the expression of the microRNA within the disease (Li *et al.*, 2009; Murata *et al.*, 2013; Kim and Lim, 2014; Nugent, 2016; Liu *et al.*, 2019).

In rheumatoid arthritis, miRNAs are being investigated as both therapeutic targets and biomarkers. Increased miR-23b expression was demonstrated in a human study to represent an accurate method identifying patients with rheumatoid arthritis, and was detectable in both synovial and plasma samples. Furthermore, on treating the disease a reduction in the expression levels of miR-23b was noted (Liu *et al.*, 2019).

Great research focus has been placed on increasing our understanding of their role in physiological and diseased states, with the aim of developing targeted therapies and biomarkers.

1.2.2 MicroRNAs in Osteoporosis

Increasing our knowledge of bone homeostasis, with the interactions between osteoblast and osteoclast activity has highlighted the important role miRNAs play. Specific miRNAs are related to osteoblastogenesis and osteoclastogenesis.

The first miRNA that was associated with OP was miR-2861, and was reported by Li *et al.* MiR-2861 was shown to target histone deacetylase 5, which negatively regulates RUNX2. This was demonstrated in a clinical study of adolescents with a diagnosis of primary OP. They identified that a rare homozygous mutation in the

genomic locus that encodes miR-2861 causes familial OP. *In vitro* and *in vivo* experimentation with a mouse model showed that miR-2861 plays a significant role in bone metabolism, and the use of an intravenous antagomiR-2861 in the mouse model resulted in a reduction in bone mineral density, further highlighting the importance of this dysregulated miRNA (Li *et al.*, 2009).

Many more miRNAs have been identified as regulating osteogenic activity, from the level of the MSC through to osteocyte formation. This is demonstrated in Figure 1-0-7.

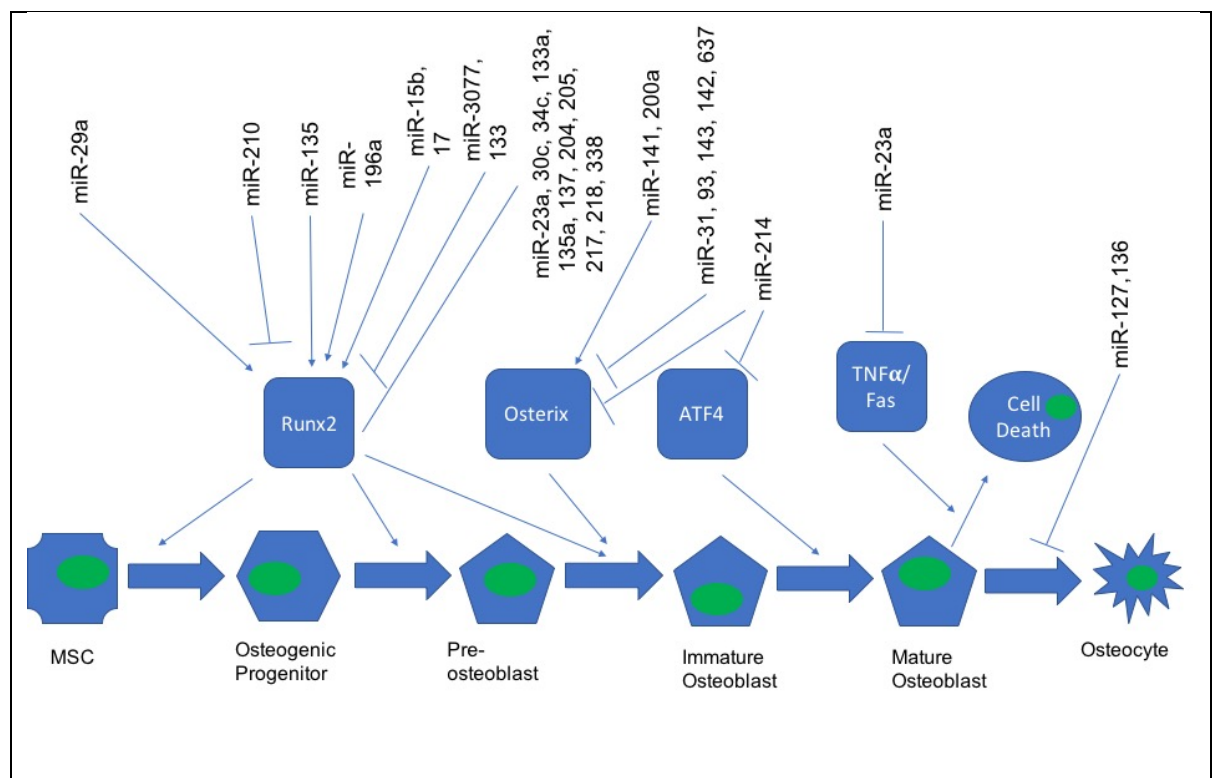


Figure 1-0-7 Demonstration of numerous miRNA regulation sites related to osteoblastogenesis, occurring from MSC through to mature osteoblast and cell death. Adapted from (Kim and Lim, 2014).

Significantly, and clinically relevant, research has focused on identifying miRNAs that are dysregulated in bone and serum, which have a role in disease progression of OP. These miRNAs are likely to be key in developing strategies for monitoring the disease utilising a serum sample, and avoiding ionising radiation (Panach *et al.*, 2015; Weilner *et al.*, 2015).

MiRNAs, including miR-21, miR-23a, miR-24, miR-25 and miR-100 have been identified as dysregulated in serum and bone samples in patients with OP

(Panach *et al.*, 2015). These miRNAs are involved in the regulation of key osteoblast and osteoclast differentiation genes such as osterix, bone morphogenic protein receptor type II, RANKL and runt-related transcription factor 2 (RUNX2) (Hassan *et al.*, 2010; Sun *et al.*, 2016).

Furthermore, manipulating the expression of dysregulated miRNAs has been shown to significantly alter the osteogenic activity of MSCs (Weilner *et al.*, 2015; Heilmeier *et al.*, 2016). This highlights the possibility of developing not only a miRNA biomarker for OP, which could provide a quick, non-ionising and sensitive method of monitoring disease activity, but also targeted therapies.

However, the non-specific nature of miRNA action makes their clinical use as a therapeutic target complex. Significant overlap exists between differing physiological systems, with miRNAs known to be important to osteoblast development also implicated in tumourigenesis in another tissue. Thus, inhibiting or upregulating the expression of a miRNA would require careful investigation to ensure its safety.

This complex picture of miRNAs involved in bone homeostasis and disease clearly demonstrates that although they may represent a potential targeted therapy site for improved bone health, significant further research is required to ensure there is no systemic adverse effect.

1.3 MicroCT

1.3.1 MicroCT in orthopaedic research

Whilst diagnosis and monitoring of OP utilises DXA scanning to assess BMD, further information of bone can be obtained via computed tomography (CT). It is not currently clinically practical to utilise CT techniques for diagnosis or monitoring of OP, due to the levels of ionising radiation and the requirement of high-resolution quantitative CT scanning. However, microCT provides great details of microarchitecture for *in vitro* samples, Figure 1-0-8.

CT images are produced by multiple radiographic projection images taken from multiple different angles; this requires x-rays and relies on the differential

absorption of differing tissues. Transmitted photons are received by a detector and converted into a projection image. In clinical scenarios the emitter and detector are rotated, in microCT the specimen may be rotated. Cross-sectional images are derived via a mathematical conversion of the projections. These cross-sectional images can be assembled into an image stack (Hounsfield, 1973).

MicroCT uses special scanners to achieve a higher spatial resolution. Techniques are utilised to reduce two commonly encountered artefacts in microCT scanning. Performing a scan with no specimen produces a “flat field”, which is then subtracted from the scan with the specimen. This compensates for ring artefact which occurs from variation in the sensing ability of each pixel of the detector. Beam hardening is a common problem of microCT and occurs due to differentially energized photons being emitted from the emitter. The energy of x-rays used increases as an object size increases, which affects the mathematical algorithm required for reconstruction of back projection images (Feldkamp, Davis and Kress, 1984). A secondary process is therefore utilised to remove halo effects from the algorithm; furthermore a filter can be placed between the emitter and the specimen to reduce the spread of the spectrum x-rays.

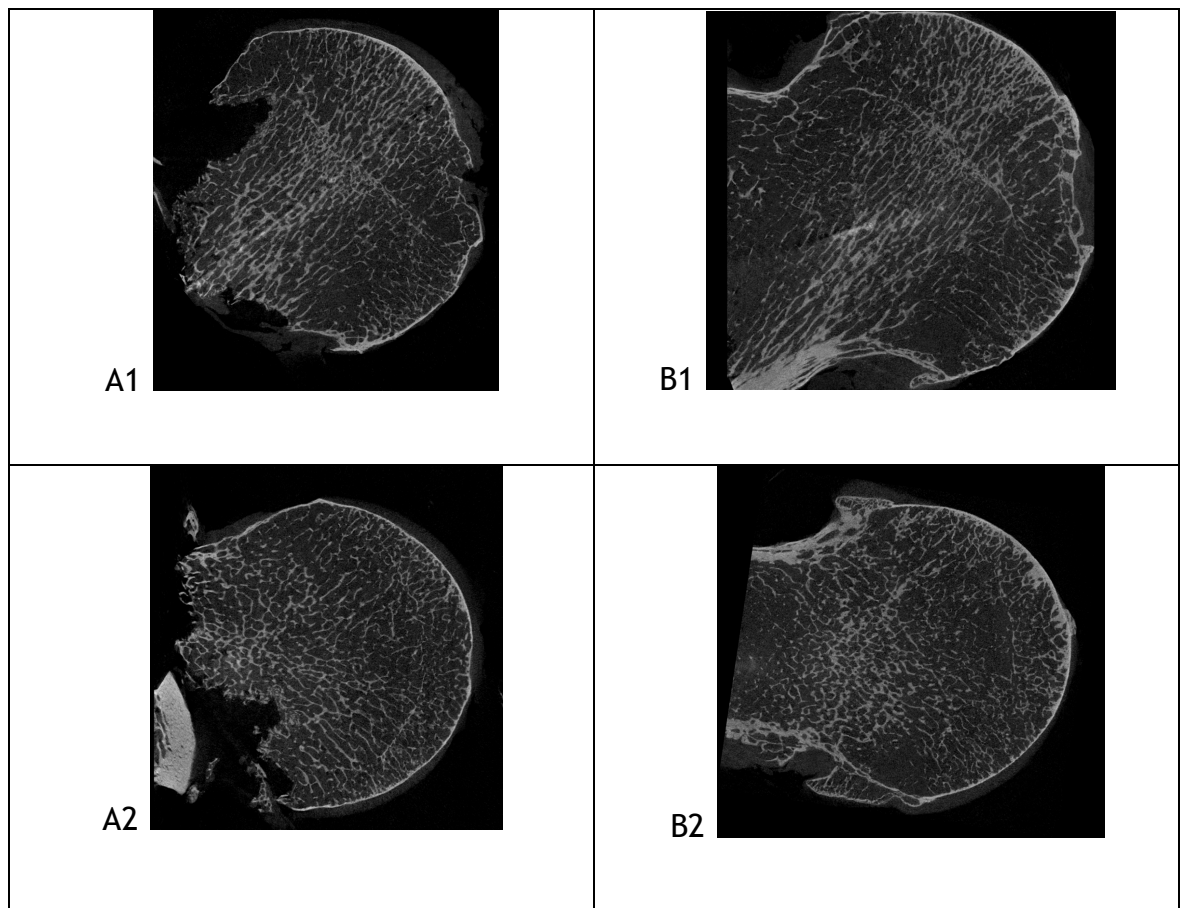


Figure 1-0-8 Coronal and axial examples of microCT imaging of femoral heads. A1/ B1 represent coronal slices and A2/B2 axial. A1/A2 are from a patient who has suffered an intra-capsular neck of femur fracture, B1/B2 from a patient with osteoarthritis.

A balance is required to be struck between object size and resolution when performing microCT scanning. As a specimen size increases the detail can diminish, as resolution diminishes with distance from the centre of axis of rotation of the specimen.

Previously histomorphometry was the gold standard for analysing bone specimens. A quantitative histological technique (Frost, 1958), histomorphometry utilises mathematical formulations to derive three dimensional parameters from specimens.

MicroCT has superseded histomorphometry, allowing immediate measurement of bone microarchitecture without specimen destruction (Hildebrand and Rüegsegger, 1997; Ulrich *et al.*, 1997) . MicroCT measurements have been shown to be reliable at describing trabecular structure, (Chevalier *et al.*, 2007) and were often reported in combination with histomorphometry (Gielkens *et al.*,

2008). Specimens acquired from biopsy, or residual tissue from surgery or post mortem can be imaged by microCT, furthermore *in vivo* scanning is also now available with great utilisation in small animal studies (Freitag *et al.*, 2019).

Many microarchitectural indices are used to assess bone via microCT and are described in Table 1-2.

Table 1-2 Common microarchitectural indices that can be measured via microCT and their definitions.

Micro-Architectural index	Abbreviation	Unit	Description
Percentage bone volume	BV/TV	%	Measure of the ratio of solid to space within a given volume surrogate parameter for bone strength (Legrand <i>et al.</i> , 2000)
Trabecular thickness	Tb.Th	mm	The width of the trabecular- important for determining structural integrity (Hildebrand and Rüegsegger, 1997; Tanck <i>et al.</i> , 2009)
Trabecular separation	Tb.Sp	mm	The thickness of the marrow cavities
Trabecular number	Tb.N		The number of plates per unit length
Structural model index	SMI	None	Indicates relative presence of rods, plates or cylinders in a 3D model(Hildebrand and Rüegsegger, 1997). Plate 0, rod 3, sphere 4.
Degree of Anisotropy	DA	None	Measure of how well orientated a microstructure is within a given volume(Cotter <i>et al.</i> , 2009).
Connectivity density	Conn. D	mm ⁻³	Number of connections between trabecular structures in a given volume- a good measure of bone structure (Fajardo and Müller, 2001).

Overall bone volume fraction (BV/TV) has been seen to be a key index, as trabecular thickness, spacing, connectivity and structural index are all correlated to BV/TV (Goldstein, Goulet and McCubbrey, 1993).

1.3.2 Observed bony characteristics of Osteoporotic bone via MicroCT scanning

Wolff's law states that osseous architecture is dictated by the mechanical stress placed upon it (Wolff and Wolff, 1986). However trabecular structure also changes with age and disease. Peak bone mass occurs at different time points in

male and female populations. Females achieve peak bone mass early in their third decade of life, whereas this occurs late in the same decade for males. Thereafter a gradual decline occurs. Following this there is a gender dependent change in bone mass, with females observed to suffer a faster rate of reduction of bone mass which is then accelerated due to the menopause (Riggs *et al.*, 2004).

Cancellous bone loss occurs earlier, in both men and women, cortical bone loss occurs later, post menopause for women, and is associated with increased porosity (Boskey and Imbert, 2017). Trabecular bone undergoes many changes with age in both sexes, with a reduction in thickness, number and connectivity observed (Seeman, 2002). Men suffer a greater reduction in trabecular thickness, and women a reduction in trabecular number (Farr and Khosla, 2015).

Sex hormone deficiency results in significant architectural change to bone, with decreased trabecular number, increased space and a change in morphology from plates to rods (Ammann and Rizzoli, 2003). It is hypothesised that these architectural changes result in reduced strength of bone, as loss of vertebral bone strength precedes any observable reduction in BMD (Ammann and Rizzoli, 2003).

In postmenopausal women with reduced BMD, lower percentage bone volume (BV/TV) and trabecular thickness (Tb.Th) values are observed in comparison to normal elderly women (Boskey and Imbert, 2017). Furthermore, highlighting the importance of bone quality in OP, glucocorticoid therapy, a common secondary cause of OP, results in an increased fracture risk without significant changes in BMD. Mouse models have shown an increase in osteocyte lacunae, reduced BV/TV, trabecular thickness and increased trabecular separation (Lane *et al.*, 2006). This is also evident in humans. A study assessing key bone indices in premenopausal women who had sustained a distal radius fracture in comparison to healthy controls showed that despite comparable BMD the fracture group had significantly reduced trabecular thickness and number in both radius and tibia (Rozental *et al.*, 2013).

Per decade there is a 7% reduction in ultimate stress of cancellous bone from femur specimens from the ages of 20-100 years (McCalden, McGeough and Court-Brown, 1997).

Key differences are observed in the microarchitecture of bone specimens from patients suffering from OA in comparison to OP. Due to the difficulty in obtaining bone specimens from healthy controls, patients suffering from OA are a common control group, because as they undergo arthroplasty for their disease surplus tissue can be utilised for research. Higher percentage of bone volume and increased trabecular number are common observations in OA specimens, with OP samples having reduced connectivity and more rod-like trabeculae in the place of plate formation (Montoya *et al.*, 2014). This is in agreement with histomorphometric research by Blain *et al.*, which showed multiple differences in micro-architecture of bone from the femoral necks of patients with OP in comparison to OA (Blain *et al.*, 2008). Reduced cortical thickness, bone volume, trabecular number and thickness were all noted in the OP group. MicroCT provides a useful research tool to correlate *in vitro* experiment results to the observed phenotype.

1.4 Three-Dimensional cell culture

Historically the majority of *in vitro* MSC research was performed in monolayer, two-dimensional (2D) culture conditions. However, it is now well known that 2D conditions pose significant limitations in developing a model of close clinical relativity.

Three-dimensional (3D) culture of MSCs results in improved inter-cell interactions, recreation of nutrient and oxygen gradients and generation of extracellular matrix (Cesarz and Tamama, 2016). Compared to 2D culture enhanced differentiation and self-renewal properties of MSCs are noted (Hong *et al.*, 2015). The importance of the above factors has led to an understanding that traditional monolayer cultures do not provide optimal conditions for MSC culture and research (Saleh and Genever, 2011; Saleh *et al.*, 2012).

1.4.1 Techniques of three-dimensional culture

Many different strategies exist to perform 3D culture of MSCs. Broadly this can also be subdivided to cultures with or without a supportive scaffold.

Cells can be grown and then implanted into a supportive scaffold, thus converting their culture to a 3D environment. Many different substrates can be utilised to form the scaffold, such as collagen, hyaluronic acid, synthetic biomaterials made from polymers and biologically derived from decellularized tissues. Scaffolds can then be implanted *in vivo*, to repair defects or assist in functions (Saleh and Genever, 2011). The disadvantage of utilising scaffolds is the variability in their reproduction, the potential for cell adsorption of the scaffold, and compromised analysis of the culture by optimal imaging (Rimann and Graf-Hausner, 2012).

Sphere like *in vitro* aggregation of cells, referred to as spheroids, is an important 3D culture method which can be formed without the use of a substrate or scaffold, Figure 1-0-9. The formation of the spheroid is dependent on intracellular adhesions between homotypic and heterotypic cell types (Duguay, Foty and Steinberg, 2003; Foty and Steinberg, 2005).

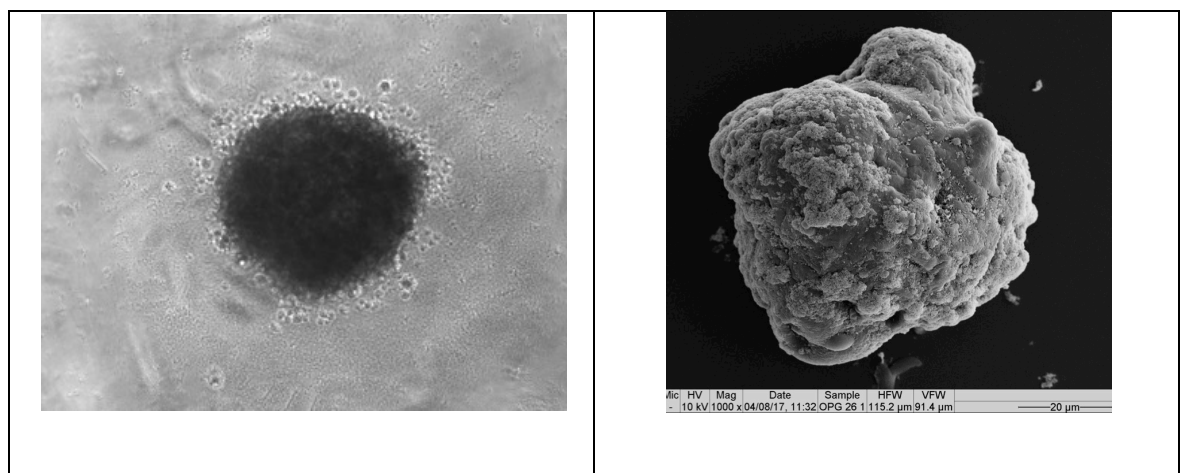


Figure 1-0-9 Imaging of human MSC spheroids from osteoarthritic bone marrow, formed by two different techniques during this research. Image A light microscopy of spheroid formed by ultra low attachment (ULA) technique at 72 hours of culture. Image B scanning electron microscopy of a spheroid formed by magnetic nanoparticle technique at 24 hours post formation.

Multiple and different techniques have been developed to perform 3D *in vitro* cultures. They vary in complexity and in the equipment required to perform. For

spheroids common techniques include the addition of viscous agents to the culture medium, such as methylcellulose referred to as the liquid-overlay method, and the hanging drop method. Dynamic culture techniques are also used to develop spheroids, through rotating cultures, spinner flasks and bioreactors (Saleh *et al.*, 2012). Additionally, culturing cells with magnetic nanoparticles (MNPs), combined with an external magnetic force, has been shown to be a consistent method of spheroid formation, with the benefit of the opportunity of functionalisation of the MNPs (Lewis *et al.*, 2017). Figure 1-0-10 depicts these common spheroid forming techniques.

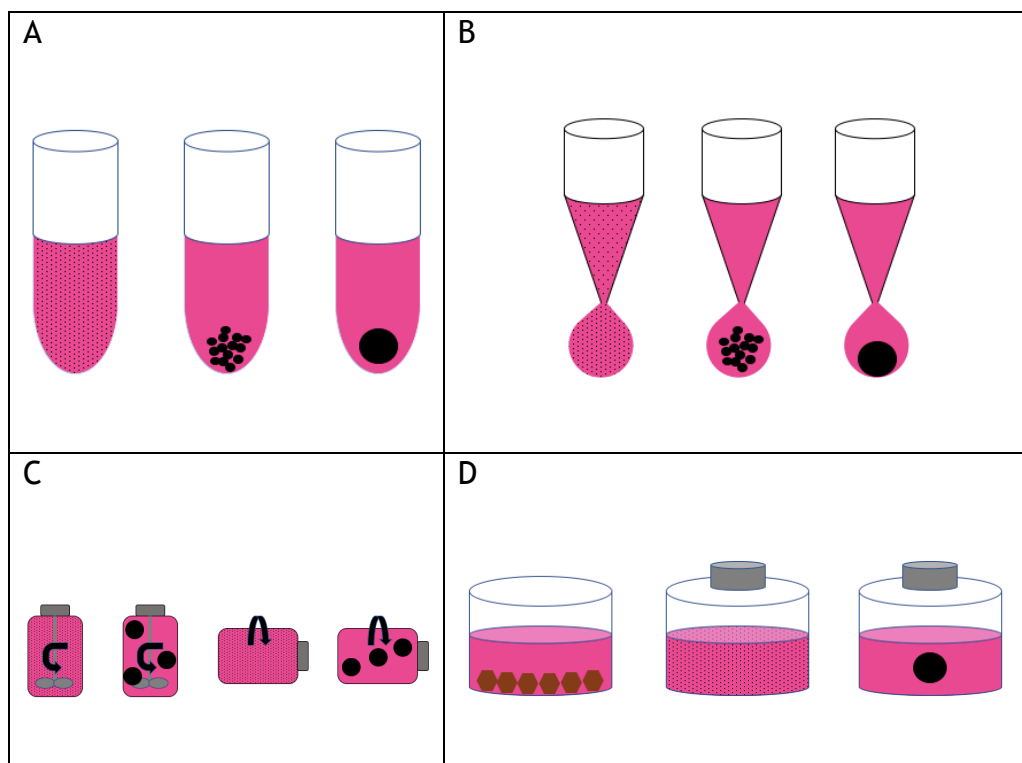


Figure 1-0-10 Schematic representations of four commonly utilised spheroid forming techniques. A- ultra-low attachment- the hydrophilic, neutrally charged coating forces cells into a suspended state, B- hanging drop- cells in suspension sediment at the base of the droplet and form aggregations and later, spheroids. C- spinner + rotational flasks, both techniques maintain cells in suspension, prevent settling and lead to cell aggregation. D- magnetic nanoparticle- cells are cultured with nanoparticles with a magnetic core. Once the nanoparticles are internalised an external magnetic field can be applied to induce aggregation.

Spheroids have been utilised in cancer research for several decades, and provide a model with similarities to the *in vivo* tumour environment. Similar to tumours they have non-proliferating cells within the core and proliferating cells on the periphery of the spheroid and possess oxygen and nutrient gradients which are relevant to a solid tumour with poor blood supply (Yamada and Cukierman,

2007). Their use has been extended to many other areas of research including tissue engineering of solid organs and high-throughput drug screening (Shea *et al.*, 2000; Kunz-Schughart *et al.*, 2004). Heterogenous spheroid cultures are also utilised, with particular importance to recreating *in vivo* microenvironments such as the bone marrow niche, and assessing the interaction of neighbouring cells to the tissue of interest (Lewis *et al.*, 2016).

There are drawbacks to utilising 3D research methods, with increased cost in comparison to monolayer culture and variability in spheroid size produced leading to non-uniform results being common criticisms (Tibbitt and Anseth, 2009; Gurski *et al.*, 2010). Furthermore, rotational methods require non-physiological shearing forces to produce the spheroid.

Little has been published in the literature with regards to developing a 3D OP *in vitro* model. Due to the burden OP poses, and the significant laboratory research required to develop improved therapies, it appears prudent to improve *in vitro* models of the disease.

1.5 Aims

This thesis aims to assess the biological status and bone phenotype encountered in patients with neck of femur fractures. Furthermore, the effect of microRNA manipulation on metabolomic activity and differentiation capacity of MSCs will be investigated. Finally, an optimal 3D culture model will be identified for future *in vitro* research involving bone marrow MSCs.

This will advance the field of fragility fracture research and help in the development of improved therapies.

This will be achieved by assessments of the following experiments:

- microRNA expression in MSCs from bone marrow aspirates
 - It is hypothesised that the neck of femur fracture group will demonstrate abnormal microRNA expression related to key osteoblast and osteoclast pathways in comparison to the osteoarthritic group.
- extracellular MSC markers in NOF and OA patients
 - It is hypothesised that MSC markers will be differentially expressed across the two patient groups.
- metabolomic effect of microRNA manipulation in MSCs
 - It is hypothesised that manipulating key microRNAs in culture of MSCs from neck of femur fracture patients will improve their differentiation potential in osteogenic and adipogenic lineages.
- three spheroid forming techniques with bone marrow derived MSCs
 - It is hypothesised that the magnetic nanoparticle technique will provide a rapid method of forming spheroids with the additional benefits of functionalisation of available.

Chapter 2

2 Materials and Methods

This chapter describes the materials and methods utilised to perform the experiments in subsequent chapters.

2.1 Materials and reagents

2.1.1 Cell culture reagents

Reagent	Supplier
Accutase™	Thermo Fisher Scientific, UK
Ascorbate-2-phosphate (100mM)	Sigma-Aldrich, UK
Bovine Serum Albumin (BSA)	Sigma-Aldrich, UK
Dexamethasone (500ng/ mL)	Sigma-Aldrich, UK
Dulbecco's Modified Eagle's Medium (DMEM), high glucose, glutamine	Sigma-Aldrich, UK (Product Code (PC) D5671)
Ethylenediaminetetraacetic acid (EDTA)	Sigma-Aldrich, UK
Foetal Bovine Serum (FBS)	Sigma-Aldrich, UK (PC F9665)
Fungizone ® Amphotericin B (250 µg/ mL)	Gibco by Life Technologies, UK (PC 15290-026)
Insulin	Sigma-Aldrich, UK
Isobutylmethylxanthine	Sigma-Aldrich, UK

Minimum Essential Medium Non-essential Amino Acids (MEM-NEAA)	Sigma-Aldrich, UK
Penicillin-Streptomycin (10 mg/mL stock)	Sigma-Aldrich, UK (PC 0781)
Phosphate- Buffered Saline (PBS)	Sigma-Aldrich, UK
Sodium hydroxide (0.1 M)	Sigma-Aldrich, UK
Sodium pyruvate (100 mM)	Sigma-Aldrich, UK
Trypsin (10X solution)	Sigma-Aldrich, UK

2.1.2 Immunostaining reagents

Reagent	Supplier
Biotinylated anti-goat IgG produced in donkey	Vector Laboratories, UK
Biotinylated anti-mouse IgG produced in horse	Vector Laboratories, UK
Formaldehyde	Thermo Fisher Scientific, UK
Magnesium Chloride Hexahydrate (MgCl ₂ .6H ₂ O)	Sigma-Aldrich, UK
Sodium Chloride	VWR Chemicals
Sucrose	Thermo Fisher Scientific, UK
Triton X-100	Thermo Fisher Scientific, UK

Tween 20	Sigma-Aldrich, UK
----------	-------------------

2.2 Preparation of cell culture solutions

Reagent	Component	Amount
Trypsin/Versene solution	NaCl	150 mM
	KCl	5 mM
	Glucose	5 mM
	HEPES	10 mM
	Phenol red solution	0.5 % (v/v)
	Trypsin	5 % (v/v)
HEPES saline solution	NaCl	150 mM
	KCl	5 mM
	glucose	5 mM
	HEPES	10 mM
	Phenol red solution	0.5 % (v/v)
Fixative solution	PBS	90 mL
	Formaldehyde	10 mL
	Sucrose	2 g

Permeabilisation buffer	Sucrose	0.1 % (w/v)
	NaCl	50 mM
	MgCl ₂ .6H ₂ O	3 mM
	HEPES	20 mM
	Triton X-100	0.5 % (v/v)
Blocking buffer	PBS	100 mL
	BSA	1 % (w/v)
ICW™ blocking buffer	PBS	100 mL
	Milk powder	1 % (w/v)
FACS buffer	PBS	100 mL
	BSA	0.5 % (w/v)
	EDTA	2 mM

2.3 Cell type

One cell source was used during all experiments. At the time of hip surgery, a bone marrow aspirate was taken and the adherent fraction was cultured. Two patient groups were assessed:

1. Osteoarthritic (OA)- patients undergoing hip arthroplasty for Osteoarthritis
2. Neck of Femur fracture (NOF)- patients undergoing hip arthroplasty after suffering a low energy neck of femur fracture.

The NOF group represented a patient group at risk of developing, or having undiagnosed OP (Compston *et al.*, 2017). For miRNA expression and microCT analysis patient samples were excluded if there was known metabolic bone disease, bone metastases, or if the patient was already using osteoporosis therapy.

2.3.1 Ethical Approval

Ethical approval for this research was obtained from the University of Glasgow and NHS Greater Glasgow and Clyde's Biorepository Management Committee, application number 287. This granted approval for the sampling and investigation of bone marrow and femoral heads which were surplus to requirements during hip arthroplasty for indications of osteoarthritis or neck of femur fracture.

2.4 Cell Culture

2.4.1 Bone Marrow Extraction

Bone marrow samples are taken at time of surgery for total hip replacement or hemiarthroplasty for neck of femur fracture. After exposure of the proximal femur an oscillating saw is used to cut the femoral neck. A rasp is then introduced into the upper third of the femoral shaft, to create space for the femoral component of the replacement. During the rasping of the femur a syringe is used to aspirate bone marrow from the canal. Approximately 15 ml of bone marrow are obtained from each patient.

The bone marrow is processed within 48 hours from surgery. Each bone marrow sample was divided into two and centrifuged for 10 minutes at 1400 rpm. The supernatant was then removed and the pellet was re-suspended in 10ml of fresh media and centrifuged again, at 1400 rpm for 10 minutes. The media was removed and the pellet was re-suspended in 10mL fresh media; the cell suspension was then slowly overlaid onto 7.5 mL of Ficoll-Paque Premium (GE Healthcare, UK), and then centrifuged for 45 minutes at 1513 rpm. The middle layer was then aspirated and resuspended in 10 mL of fresh media, followed by centrifugation at 1400 rpm for 10 minutes. The supernatant was then removed

and the pellet was resuspended in 10 mL of fresh media and then placed in a vented flask and incubated at 37 °C with 5% CO₂.

To expand the number of MSCs from the sample, at day 7 of culture, basal media containing 10% Mesenchymal stem cell growth medium 2 (PromoCell GmbH, Germany) was performed utilised. Subsequent media changes were then with basal media.

2.4.2 General Protocol

The MSCs were cultured in T75 flasks with modified DMEM media at 37°C with 5% CO₂. Upon reaching confluence the cells were washed with HEPES (Fisher Scientific, UK) solution and then detached from the surface using trypsin/versene, 2 minutes at 37 °C, (Sigma-Aldrich, UK). Fresh media was then added to the flask to neutralise the active trypsin, the cell suspension was then centrifuged for 4 minutes at 1400 rpm. After centrifugation the supernatant was removed leaving a cell pellet. The cells were then re-suspended in fresh media and seeded into appropriate wells for experiments. MSCs were used between passage a number of 1-3.

2.4.3 Cell Culture Media

In addition to basal and expansion media, pro-osteogenic and adipogenic media were utilised to induce MSC differentiation. The constituents of the media are detailed in Table 2-1 Constituents of media used for cell culture., with the adipogenic and osteogenic induction media as per Alakpa et al (Alakpa *et al.*, 2018).

Table 2-1 Constituents of media used for cell culture.

Name	Constituents
Basal media	DMEM with 10% FBS with 2% antibiotic mixture, 1% Non essential Amino Acids and 1% sodium pyruvate
Osteogenic media	DMEM, 10% FBS with 2% antibiotic mixture, Ascorbate-2-phosphate 350 μ M, dexamethasone 0.1 μ M
Adipogenic induction media	DMEM, 10% FBS with 2% antibiotic mixture, 1 μ M Dexamethasone, 1.7nM insulin, 200 μ M indomethacin, 500 μ M isobutylmethylxanthine
Adipogenic maintenance media	DMEM, 10% FBS with 2% antibiotic mixture, 1.7nM insulin
Expansion media	DMEM, 10% FBS with 2% antibiotic mixture, 1% Non essential Amino Acids and 1% sodium pyruvate, 10% Mesenchymal stem cell growth medium 2 (Promocell GmbH, Germany)

2.4.4 Freezing cells for storage

MSCs from some patient samples, obtained as described above, were frozen and stored at -80 °C for future experiments. The cells were detached with trypsin/versene and centrifuged. The pellet was then resuspended in dimethyl sulfoxide ((DMSO) Sigma-Aldrich, UK)/foetal bovine serum ((FBS) Sigma-Aldrich, UK) and stored at -80 °C.

2.4.5 Thawing cells from storage

Cells were revived from storage at -80 °C by rapidly thawing in a 37 °C water bath. The cells were then transferred into 10 ml of warmed culture media and centrifuged for 5 minutes at 445 x g. The subsequent cell pellet was re-suspended in basal culture media and transferred to a T75 flask.

2.5 Cell Culturing Methods

2.5.1 Differentiation culture

Growing MSCs were utilised and detached from their flask via trypsin/versene. A cell count was performed and the cells plated on cover slips in basal media at a density of 2000 thousand per cm². After 24 hours the media was exchanged for differentiation media. For osteogenic differentiation osteogenic media was used for all culture exchanges for the remainder of the experiment. For adipogenic differentiation culture media alternated between adipogenic induction media for 7 days and adipogenic maintenance media for 7 days, for the remainder of the experiment. The differentiation medias are described in Table 2-1. The constituents of the adipogenic and osteogenic media were as per (Alakpa *et al.*, 2018).

2.5.2 MicroRNA Culture

Cultures of MSCs with miRNA mimics and inhibitors were performed. The miRNA mimics/inhibitors were delivered via functionalised gold nanoparticles (GNPs). The thiolated sequences were obtained from Dharmacon and functionalised with GNPs at the Universidade NOVA de Lisboa's Life Sciences department. The synthesis is as described by McCully *et al.*'s paper on nanoparticle-antagoMiR based targeting of miR-31 (McCully *et al.*, 2018). Table 2-2 details the GNP physical properties utilised during the miRNA manipulation experiments.

Table 2-2 The physical properties of the functionalised GNPs used in miRNA manipulation studies. Polyethylene glycol (PEG) was used to passivate the NPs (percent saturation indicated); SPR- corresponds to surface plasma resonance, used to determine nanoparticle aggregation.

Name	miR (nM) on GNPs	PEG	Size (nm)	SPR	Acronym- used in chapter
Au-NPs- 30% PEG miR-143	66	857	22.45	522	miR-143 mimic
Au- NPs-30% PEG- AntagomiR-31	90	857	26.4	522	AntagomiR- 31 (AmiR-31)
Non-targeting	NA	857	19.5	520	Non-T

As previously, cultured MSCs were utilised from both patient groups and detached from their flask via trypsin/versene. A cell count was performed and the cells were cultured in 24 well plates in basal media at a density of 2000 thousand per cm². After 24 hours the media was exchanged for the conditions described in Table 2-3. The nanoparticle conditions were cultured at a concentration of 50nM per 500 µl of media.

Table 2-3 Details of culture conditions for miRNA manipulation studies.

No Particles	Non-targeting	miR
Basal media	Basal media and Non-targeting nanoparticles	Basal media and AntagomiR-31/miR-143 nanoparticles
Adipogenic media	Adipogenic media and Non-targeting nanoparticles	Adipogenic media and AntagomiR-31/miR-143 nanoparticles
Osteogenic media	Osteogenic media and Non-targeting nanoparticles	Osteogenic media and AntagomiR-31/miR-143 nanoparticles

After 48 hours of incubation with the above conditions, the media was exchanged, and for the remaining time in culture media without nanoparticle supplementation was used.

2.6 Spheroid formation

2.6.1 Hanging drop spheroid formation

MSCs were detached from a T75 flask. Cell suspensions of MSCs were prepared at concentrations of 5×10^3 , 1×10^4 and 2×10^4 cells per 40 μl . A GravityPLUS™ (Perkin Elmer, Waltham, MA, USA) 96 well plate was used, with 40 μl pipetted into each well. The cells were cultured in the presence of a humidifier pad, to reduce water evaporation from the droplet. After 24 or 72 hours of culture an additional 70 μl of media was added to the cell suspension droplet and the spheroid was transferred to a non-adherent GravityTRAP™ (Perkin Elmer, Waltham, MA, USA) plate placed below, for long term culture.

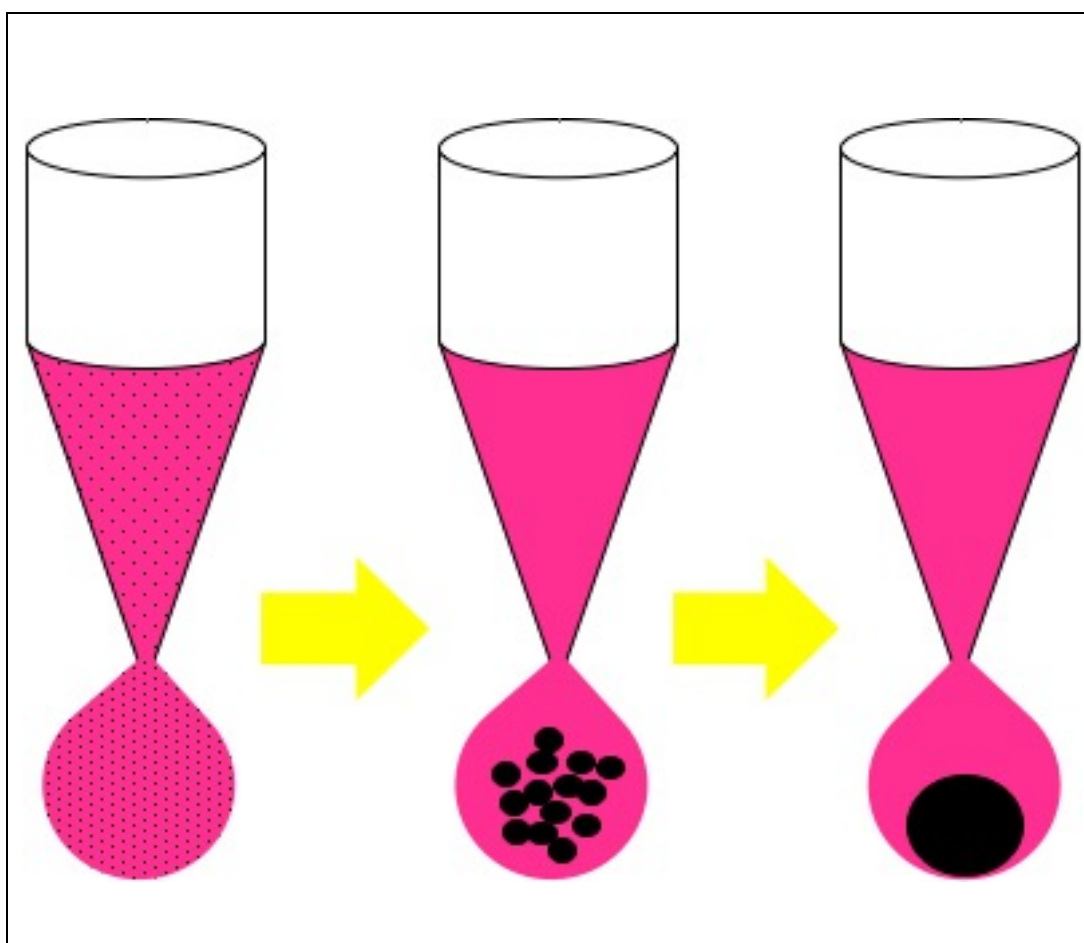


Figure 2-1 Depiction of the Hanging drop technique. A droplet is formed with MSCs in suspension (black dots), with time they are seen to coalesce to aggregates (black circles) and finally a singular spheroid.

2.6.2 Ultra-low attachment spheroid formation

MSCs were detached and cell suspensions of concentrations of 5×10^3 , 1×10^4 and 2×10^4 cells in 200 μ l of media were created. 200 μ l of each cell suspension was then pipetted, per well, into a CellCarrier Spheroid ULA 96-well microplate (Perkin Elmer, Waltham, MA, USA). These plates have round-bottomed wells and a non-adherent coating. 100 μ l of media was exchanged every 72 hours.

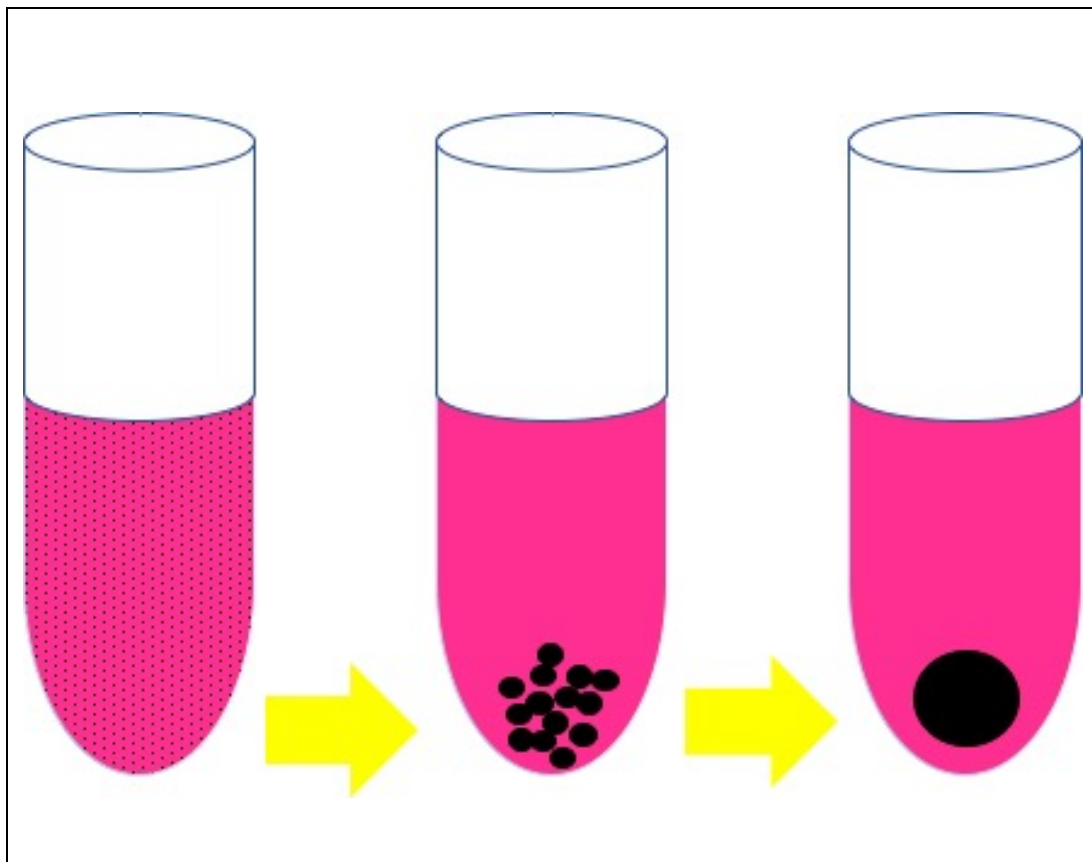


Figure 2-2 Depiction of the Ultra-low attachment. MSCs (black dots) are in suspension, and unable to adhere to the round bottomed, non-adherent well. With progressive time the MSCs form aggregates (black circles) and finally a singular spheroid.

2.6.3 Magnetic Nanoparticle Uptake into Cells

MSCs were seeded at a concentration of 1×10^4 cells/cm in a 24 well plate and left 24 hours to adhere (37 °C/5% CO₂). The media was removed and exchanged for 1mL of magnetic nanoparticles (mNPs) diluted in fresh DMEM media at a concentration of 0.1mg/ml. This was followed by a 30-minute incubation (37

°C/5%CO₂) in the presence of a magnetic field of 350 mT (24 magnet array placed beneath the 24 well plate, Chemicell).

2.6.4 MNP Spheroid culture in media

Following incubation with the MNPs, the cells (1×10^4 cells/cm) were detached with Accutase™ cell detachment solution (Stemcell Technologies, UK), and centrifuged at 1400 rpm for 4 minutes. The cells were then resuspended in fresh media and 0.5 ml of cell suspension was added to 4 ml of fresh media in a 6 well plate. A single magnet (13 mm diameter, 350 mT) was placed on top of the well and the plate was incubated at 37 °C with 5% CO₂ for the remainder of the experimental duration.

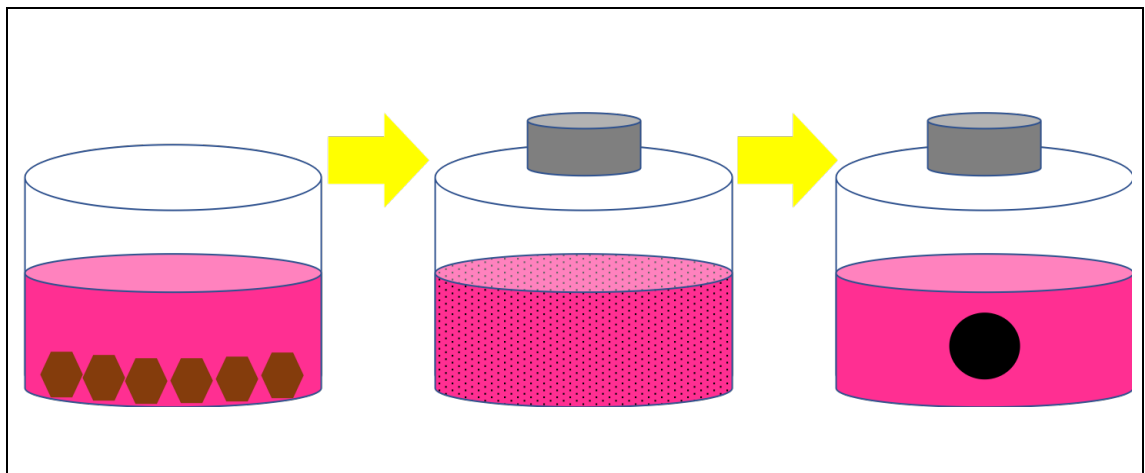


Figure 2-3 Depiction of Magnetic nanoparticle spheroid formation technique. MNPs (brown hexagons) are incubated with adherent MSCs, leading to internalisation of the MNPs. The MSCs are then detached and resuspended in fresh media. The MSCs in suspension (black dots) are then placed in a new well with an external magnetic force applied above. With time the external magnet encourages aggregate and spheroid formation (large black circle).

2.7 Flow cytometry

2.7.1 Flow cytometry staining

Cells for flow cytometric analysis were harvested from passage 2 cultures of patient samples from both groups. Cells were detached from flasks via incubation with Accutase™, and centrifuged at 400 x g for 5 minutes. They were then resuspended in 800 µl 0.5% BSA in phosphate buffered solution ((PBS) Sigma-Aldrich, UK) containing 2 mM EDTA (FACS buffer). They were washed again, following the same protocol. Staining with appropriate antibodies was

then performed in 100 µl volumes, using pre-determined dilutions of antibodies for 30 minutes on ice, protected from light. Details of antibodies utilised in flow cytometric analysis are displayed in Table 2-4. They were washed 2 further times and suspended in 200 µl FACS buffer. They were then run on a ThermoFisher Attune NXT analyser. An unstained control sample was utilised to set the voltage for each channel and an isotype control sample was also used to determine background binding of the antibodies.

Table 2-4 Details of antibodies used in flow cytometric analysis experiments.

Manufacturer	Marker	Clone	Fluorochrome
eBioscience	CD13	WM15	PE
eBioscience	CD29	TS2/16	FITC
eBioscience	CD31	WM59	PE-CY7
eBioscience	CD34	4H11	PE
eBioscience	CD44	IM7	PE-CY7
eBioscience	CD45	H130	FITC
eBioscience	CD73	AD2	FITC
eBioscience	CD105	SN6	PE
eBioscience	CD106	STA	PE-Cy7
Biolegend	CD140b	18A2	PE
Biolegend	CD146	P1H12	PerCP-Cy5.5
eBioscience	CD166	3A6	PerCP-eFluor710
Biolegend	CD271	ME20.4	PE-Vio770
eBioscience	HLA-ABC	W6/32	PE
eBioscience	HLA-DR	L243	FITC

Cells were run using a ThermoFisher Attune NXT flow cytometer. Unstained controls were used to set the voltage for each of the fluorescent channels used. Isotype controls for each channel were used with cells as negative controls, thus allowing the non-specific background signal to be differentiated from the specific antibody signal.

2.7.2 Flow cytometry compensation

UltraComp eBeads™ (ThermoFisher Scientific, UK) were used to perform fluorescence compensation by correcting for spectral overlap. 1 drop of beads was added to a 5 ml conical tube, and 2 µl of fluorescently labelled antibody was added, and incubated for 30 minutes at 4°C. Centrifugation at 600 x g for 5 minutes was then performed. The pellets were resuspended in 500 µl FACS

buffer and the samples were run in the cytometer. Spectral overlap settings were set automatically, by the accompanying software.

2.7.3 Flow cytometry gating strategy and analysis

With assistance from Dr Ewan Ross, University of Glasgow, gating strategy work was conducted using the FlowJo™ software. Forward scatter area (FSC-A) versus side scatter area (SSC-A) was calculated to identify the population of viable cells. This population was then assessed for its expression of specific antibodies, Figure 2-4. Positive expression was determined by a fluorescence signal that was higher than the isotype background control.

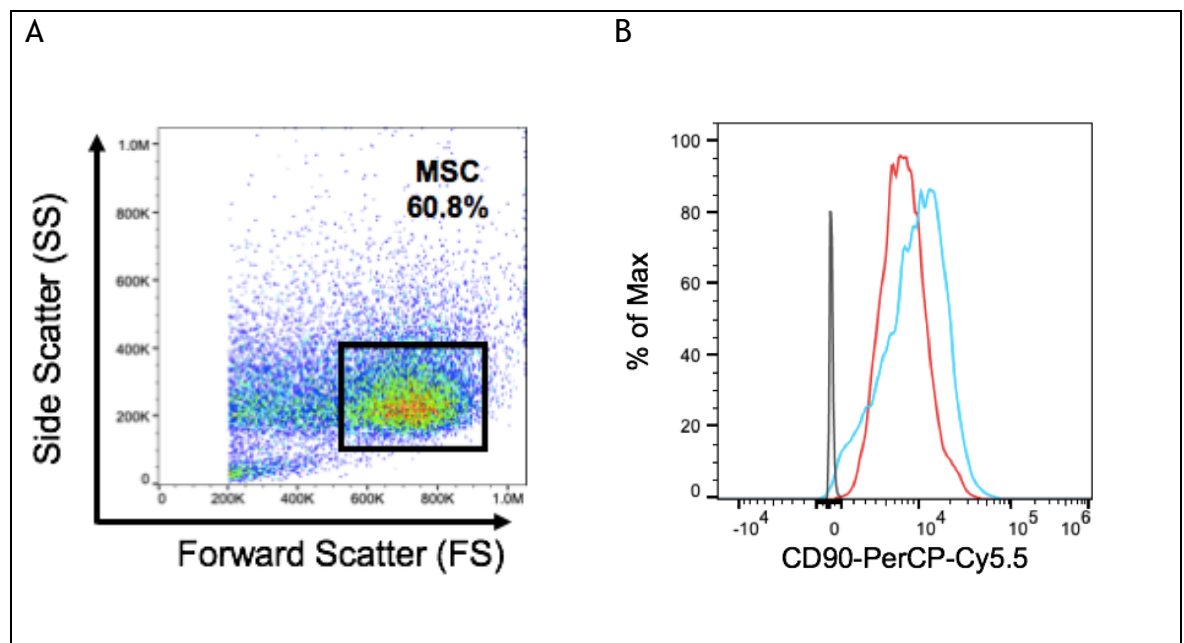


Figure 2-4 Image A demonstrates flow cytometry gating strategy for identification of viable MSCs with a forward scatter versus side scatter plot. The viable, single cell population, with doublet exclusion are highlighted, sample data is from the OA group. Image B demonstrates antibody staining observed, with positive expression of CD90 identified in OA (Red) and NOF (Blue) in comparison to Isotype control (Grey).

The mean fluorescence intensity (MFI) of each sample was calculated and the fold change of antibody expression between the NOF and OA groups was determined. This was assessed for statistical significance by a two-tailed Mann Whitney test.

2.8 Histochemical staining

2.8.1 Oil Red O staining

Oil Red O staining was utilised to assess differentiation of MSCs to mature adipocytes. At the end of culture, cells were washed in PBS and fixed via a 15 minute incubation with 4% formaldehyde, 2% sucrose in PBS at 37 °C. A 0.3% stock solution of Oil Red O (Sigma Aldrich, UK) was prepared and diluted 3:2 in distilled water. The fixative was removed and the samples washed in distilled water. A wash in 60% isopropanol was then performed. The dilute Oil Red O solution was then added to the samples through a syringe filter, and incubated at 15-20 °C for 15 minutes. The solution was removed from the samples and washed twice with water. PBS was then placed on the coverslips and brightfield microscopy was performed.

2.8.2 Von Kossa staining

At the end of culture cells were washed in PBS and fixed, as described previously. The samples were then immersed in 5% silver nitrate and exposed to UV light for 20 minutes. The samples were then rinsed in deionized water. 5% sodium thiosulphate was added to the samples for 10 minutes at 15-20 °C and then washed for 5 minutes in tepid water, followed by a further wash in deionized water. The samples were then counterstained in nuclear fast red for 5 minutes and rinsed three times in deionized water and finally with 70% ethanol. Samples were allowed to dry and then observed by brightfield microscopy was performed.

2.9 MicroRNA extraction

MiRNAs were extracted from MSC cultures of both patient groups for analysis. A TRIzol (ThermoFisher Scientific) extraction method was utilised. Cells were detached from flasks via Trypsin and centrifuged at 1400 rpm for 4 minutes. The cell pellet was resuspended in 1ml of basal media and transferred to an RNase free Eppendorf tube, and centrifuged at 1445 x g for 5 minutes. The supernatant was removed and the pellet was resuspended in 1ml TRIzol. The sample was mixed via vortex for 30 seconds and incubated at 15-20 °C for 5 minutes. 200 µl

chloroform was added and the sample was vortexed again for 30 seconds followed by 2 minutes of incubation at 15-20 °C. The sample was then centrifuged at 14848 x g for 10 minutes. After centrifugation the uppermost clear layer of liquid was transferred to a new RNase free Eppendorf. Isopropanol was then added, 70% of the volume of sample. The sample was mixed and then centrifuged at 14848 x g for 10 minutes. The supernatant was removed, the pellet was washed in 200 µl 80% ethanol, and centrifuged for 5 minutes at 14848 x g. This was repeated and the pellet was then allowed to dry at 15-20 °C. 25 µl RNase free water was added and the sample resuspended. The RNA concentration of the sample was assessed by NanoDrop™ (ThermoFisher Scientific) and the samples were then stored at -80 °C.

2.10 MicroRNA analysis

The miRNA samples were analysed at the University of Glasgow's Polyomics Department. Next Generation sequencing was performed utilising the NextSeq™ 500 platform. 3 patient samples per group were analysed, with 3 technical replicates for each patient sample.

MiRNA expression was tested for differential expression and statistical significance by the DESeq2 package (Bioconductor). P adjusted value of <0.1 was considered statistically significant.

2.11 Immunostaining for In Cell Western™

At set time points cells were fixed for 15 minutes at 37 °C, (with 4% formaldehyde, 2% sucrose in PBS) and incubated in permeabilising buffer (10.3g sucrose, 0.292g NaCl, 0.06g MgCl₂ (hexahydrate), 0.476 HEPES, 0.5 ml Triton X (Sigma-Aldrich, UK) in 100 ml PBS, pH 7.2) for 5 minutes at 4°C. The permeabilising buffer was then removed and 150 µl PBS/1% milk protein was added. The plate was placed on a shaker at 15-20 °C for 90 minutes. The blocking solution was removed and the primary antibody, diluted in 150 µl PBS/1% milk protein, was added and incubated for 2.5 hours at 15-20 °C. The antibody was removed and 5 washes were performed with diluted Tween 20, (1 x PBS + 0.1% Tween 20 solution (Sigma-Aldrich, UK)), with 5 minutes of shaking per wash. Secondary antibody solution was then incubated for 1 hour on a shaker at

15-20 °C protected from light. The secondary antibody solution was made up to 150 µl and contained 1:800 secondary antibody, 1:500 Li-Cor Cell Tag 700 stain (Li-Cor, UK) and 0.2% Tween 20. 5 further washes in diluted Tween 20 were performed, with the samples protected from light throughout. The final wash buffer was removed, the coverslips were transferred to a new 24 well plate, protected from light, and stored at 4°C until dry. Table 2-5 displays the primary and secondary antibodies used during In Cell Western™ (ICW) analysis.

Table 2-5 Details of primary and secondary antibodies utilised in In Cell Western experiments.

Primary Antibody	Manufacturer	Dilution	Secondary Antibody
Osterix	Santa Cruz, Biotechnologies, Dallas TX, USA	1:100	Rabbit
PPAR γ	Santa Cruz, Biotechnologies, Dallas TX, USA	1:100	Donkey

2.12 RNA extraction

RNA extractions from cell pellets were performed utilising Qiagen RNeasy mini kits, according to the manufacturer's protocol. All centrifuge runs were at 8000 x g for 15 seconds unless stated otherwise. Pellets were either used immediately after cell harvest or after storage at -80 °C. Four wells were combined to provide one replicate, with 350 µl of buffer RLT added to each well and the sample homogenised with pipetting. 1400 µl of 70% ethanol was added to the lysate, and mixed via pipetting. Samples were then transferred to an RNeasy MinElute spin column, and centrifuged. The flow through was discarded and 350 µl of buffer RW1 were added to the spin column and centrifuged. 80 µl of DNase I in buffer RDD were added directly to the spin column membrane, and incubated at 20 °C for 15 minutes. 350 µl of buffer RW1 were added, and the column was centrifuged, the collection tube was then replaced. 500 µl of buffer RPE was added and the column was centrifuged. 500 µl of 80% ethanol was then added and the column centrifuged for 2 minutes at 8000 x g. The collection tube was then discarded. The spin column was then placed in a new collection tube and centrifuged at 16,000 x g for 5 minutes to dry the membrane. The column was then placed into a 1.5 ml collection tube, and the previous collection tube

was discarded. 14 µl of RNase-free H₂O were added to the centre of the spin column membrane and the RNA was eluted by a further centrifugation at 16,000 x g for 1 minute.

2.13 Reverse Transcription

Reverse transcription was performed using a QuantiTect Reverse Transcription Kit, according to the manufacturer's protocol. RNA samples were thawed on ice. The kit reagents, gDNA Wipeout Buffer, Quantiscript Reverse Transcriptase, Quantiscript RT Buffer, RT Primer Mix and RNasefree water, were thawed at room temperature (15-25 °C). The solutions were mixed and centrifuged. All subsequent reactions were performed on ice. RNA content was normalised to 500 ng total in each reaction, if possible from the sample. If not achievable, when assessed by Nanodrop quantification, the total volume of RNA elute was used. Genomic DNA elimination reaction was performed with 2 µl of gDNA Wipeout Buffer appropriate volume of RNA sample to yield 500 ng made up to 14 µl with RNase-free water. This reaction was incubated at 42 °C for 2 minutes then placed on ice. Reverse transcription was then performed with 1 µl Quantiscript Reverse Transcriptase, 4 µl Quantiscript RT buffer, 1 µl RT primer mix and 14 µl sample RNA from the genomic DNA elimination reaction. An incubation step at 42 °C for 15 minutes, followed by 3 minutes at 95 °C to inactivate the Quantiscript Reverse Transcriptase was performed. The complete reverse transcription reaction samples were then stored at -20 °C.

2.14 Analysis of quantitative real-time-PCR (qRT-PCR)

Samples were removed from storage and assessed by qRT PCR. A master mix for each gene to be analysed was prepared. Table 2-6 demonstrates the constituents of the master mix. 2 µl of cDNA at a concentration of 2.5 ng/µl was added to each well, with each sample analysed in duplicate. A negative control, was also placed in a known location on the 96 well plate. The wells were then sealed firmly with a thin film of plastic. The primers used to assess the samples are displayed in Table 2-7.

Table 2-6 Constituents of wells for qRT-PCR analysis.

Reagent	Volume required per well (μl)
SYBR-Mix (Qiagen)	10
100 μM Primer Forward (0.1 μl)	0.1
100 μM Primer Backward (0.1 μl)	0.1
H ₂ O	7.8
Total	18

Table 2-7 Details of primers utilised in qRT-PCR experiments

Gene	Forward primer	Reverse primer	Manufacturer
GAPDH	TCAAGGCTGAGAACGGGAA	TGGGTGGCAGTGATGGCA	Eurofins
Osterix	GGCAAAGCAGGCACAAA GAAAG	AATGAGTGGGAAAAGGGAG GG	Eurofins
RUNX2	CAGACCAGCAGCACTCC ATA	CAGCGTCAACACCATCATTC	Eurofins
PPAR _γ	TGTGAAGCCCATTGAAG ACA	CTGCAGTAGCTGCACGTGT T	Eurofins
FABP4	ACAAACCACCGCACAA CA G	CGCCTGCACTTTTGGGTA	Eurofins

The 7500 Real Time PCR system was used to perform the amplification and glyceraldehyde 3-phosphate dehydrogenase (GAPDH) was used as the reference gene. The expression of the target genes was assessed in comparison to GAPDH. For quantification the $2^{-\Delta\Delta C_t}$ method was used to determine gene expression and amplification of the negative control samples was also assessed against the sample conditions.

2.15 Electron Microscopy

On day 3 of spheroid formation spheroid samples were prepared for scanning electron microscopy (SEM) and transmission electron microscopy (TEM). The spheroids were fixed in 2.5% glutaraldehyde in 0.1 M sodium cacodylate (SC) buffer for 1 hour. The spheroids were then washed 3 times in 0.1 M SC and incubated for 1 hour in 1% osmium tetroxide. The spheroids were then rinsed 3 times in distilled water prior to a 1 hour incubation in 0.5% aqueous uranyl acetate in the dark. The spheroids were then washed 2 times further in distilled water and then subjected to dehydration through an alcohol series, prior to being critical point dried. SEM samples were then mounted on to stubs and sputter coated in gold prior to microscopy. TEM samples were embedded in resin and sectioned prior to imaging.

2.16 Cell Viability Staining

Viability of the cells within the spheroid was determined using an ethidium homodimer/calcein AM viability kit (Life Technologies, Carlsbad, CA, USA), which stains live cells green and dead cells red. At time points of 24 hours, 7 days and 28 days after spheroid formation culture media containing 1 μ L/ml of each stain was added to the spheroids. After 1-hour incubation at 37 °C the cells were washed with warmed media and immediately imaged using a fluorescence microscope.

2.17 MicroCT scanning of femoral head samples

Femoral heads were obtained from 3 patients undergoing total hip replacement for osteoarthritis and 3 for hemiarthroplasty for patients who had sustained osteoporotic type intracapsular neck of femur fractures. The sample was stored in formalin at 4 °C until scanning was performed.

MicroCT scanning was undertaken with a Skyscan 1172 microCT scanner (Bruker microCT, Kontich, Belgium). Shadow projection images were taken at 0.34 degree steps for a 180-degree rotation. The pixel resolution was 34 μ m. To reduce signal noise a random motion of 5 was used with 3 frames averaged. Beam energy was 100 kilovolts and an aluminium filter was used to reduce beam

hardening. Acquired images were reconstructed into axial slices using NRecon (version 1.6, Skyscan Ltd, Belgium). Orientation of the images was performed on the DataViewer software and further analysis was performed using the software package CTAn (version 1.11, Bruker-microCT, Belgium).

2.18 Metabolomic analysis

At defined culture time points media was removed from wells, and the cells were washed in chilled PBS. All PBS was then removed from the wells. Chilled extraction solvent (1:3:1 of chloroform, methanol and water) was added to the wells, the plate was sealed by parafilm, and placed on a rotary shaker at 4 °C for 1 hour. The solution was then pipetted from the well and centrifuged for 3 minutes at 13000 x g at 4 °C. The supernatant was transferred to a fresh Eppendorf tube. A control, pooled sample was taken with 10 µl from each well of the experiment per biological replicate. The samples were stored at -80 °C, until they were subjected to liquid chromatography by the Glasgow Polyomics Facility at the University of Glasgow. For each patient sample 1 replicate was used from each condition.

The liquid chromatography mass spectrometry (LCMS) was carried out by staff at the Glasgow Polyomics. LCMS allows the isolation of individual metabolites from the mixture produced in each sample, and separated them relative to their mass:charge (m/z) ratio. An UltiMate 3000 RSCLC featuring a 20 mm x 2.1 mm ZIC-pHILIC analytical column running at 300 µl/minute, coupled to an Orbitrap Q-Exactive (Thermo Fisher) was used. Standards comprising known metabolites were also processed in this manner and their respective retention times in the chromatography column were used to identify sample metabolites.

2.19 Statistical Analysis

Statistical tests were performed using GraphPad Prism 6 software. Data sets were analysed for normality by the Shapiro-Wilk test. If normal distribution of data existed, then analysis of variance (ANOVA) was performed using one-way ANOVA test, followed by a Tukey post-hoc test. If data was not normally distributed then non-parametric tests were used, namely Mann Whitney and Kruskal-Wallis, with multiple comparisons.

The statistical significance of the results was determined by calculating the probability of a null hypothesis being true, using a pre-specified threshold (p-value). The null hypothesis was rejected and the result was classed as being statistically significant if the p-value was ≤ 0.05 .

2.20 Research Colleagues

Dr Ewan Ross assisted with conducting flow cytometry. Dr Robert Wallace, University of Edinburgh, operated the microCT scanner for imaging of the femoral heads. TEM samples were sectioned by Margaret Mullin, Electron Microscopy Facility, University of Glasgow. Next Generation sequencing of RNA samples and metabolomic analysis was performed at the University of Glasgow's Polyomics department.

Chapter 3

3 An analysis of microRNA expression and functional capacity of mesenchymal stromal cells from patients with neck of femur fractures

3.1 Introduction

Decreasing the burden OP poses to future generations is an important goal. To achieve this more must be known of the condition, and its associated fragility fractures to improve the development of biomarkers and therapies.

It is also imperative to improve primary preventative therapies, and their monitoring, to successfully reduce the significant morbidity and economic effect of OP (Compston, McClung and Leslie, 2019).

MSCs have long been heralded for their promise and importance in regenerative medicine (Rodeo, 2019). The ageing effect on MSCs has been explored; however, defining characteristics present in BM MSCs from patients with OP has not been thoroughly investigated (Sethe, Scutt and Stolzing, 2006; Abdallah and Kassem, 2012).

Determining the multipotent potential of MSCs from NOF patients will further elucidate their role in the development of OP. It will also identify their usefulness as a source for *in vitro* research. It is hypothesised that MSCs from the NOF group will have deficient multipotent potential. Improving our understanding of MSCs from patients with, or at risk of OP, will result in more relevant research with the aim of optimising the development of future therapies.

MicroRNAs hold great promise as biomarkers and targets for many diseases. This hope extends to musculoskeletal diseases including OP (Cheng *et al.*, 2019). Studies have shown dysregulated microRNAs in both serum and bone marrow, and it is hoped that microRNA therapies can be developed which can improve bone density (Heilmeyer *et al.*, 2016). Due to their non-specific binding each microRNA can play a variety of roles *in vivo*, and thus rigorous investigation of potential therapeutic candidates is required.

MicroCT scanning of femoral heads provides a means of assessing the phenotype produced in the OA and NOF groups. MicroCT has previously shown significant differences in these patient groups (Jenkins *et al.*, 2013), and will act as a means of corroborating the deficiencies produced by dysregulation of MSC function and microRNA expression.

3.2 Objectives

This chapter aims to rigorously characterise bone and BM MSCs from the two patient groups within the study, namely osteoarthritic and neck of femur fracture. The cell phenotype of BM MSCs from each group will be interrogated and the bone phenotype produced assessed. This will be achieved by the following experiments.

1. Extracellular surface marker analysis by flow cytometry
2. Culture within conditioned media to determine differentiation capacity
3. microRNA expression analysis of BM MSCs
4. Analysing bone micro-architectural indices via microCT scanning of femoral heads

Materials and Methods

3.2.1 Patient samples

Bone marrow and femoral head samples of the same patients were utilised for the microCT and microRNA experiments. All of the patients were of the same gender, with no statistical difference in mean age between the NOF and OA group, $P = 0.9$ (Mann Whitney test).

3.2.2 Cell Culture

In this chapter bone marrow extraction was performed from the OA and NOF groups, and culture of MSCs in monolayer was as described in section 2.4.

3.2.3 Flow Cytometry

To characterise and identify MSC markers in cells extracted from BM from both patient groups, flow cytometric analysis was performed as described in section 2.7. Antibodies used for phenotyping are listed in section 2.7.1.

3.2.4 Differentiation media

Culture of MSCs of both patient groups was performed in conditioned media. This was performed as described in section 2.5.1, to induce adipogenesis and osteogenesis. The cells were seeded from growing flasks at a concentration of 2000 cells per cm^2 and after allowing 24 hours of attachment to the coverslip the media was exchanged for basal, adipogenic or osteogenic media. Every 7 days the adipogenic media was substituted from induction to maintenance or vice versa.

3.2.5 Histochemical staining and imaging

Histological analysis was performed to observe and quantify differentiation of MSCs from both patient groups. MSCs were seeded onto coverslips and after 24 hours differentiation media was applied. The cells were cultured for 21 days, with feeding every 72 hours. The cells were fixed and stained with Oil red O or von Kossa to assess adipogenesis and osteogenesis, respectively. MSCs grown in monolayers were utilised as a control.

3.2.5.1 Oil Red O staining

As described in section 2.8.1, Oil Red O staining was utilised to observe the deposition of lipids and neutral triglycerides as an indication of adipogenic differentiation.

3.2.5.2 Von Kossa staining

Von Kossa staining demonstrates mineralization, and thus evidence of osteogenic differentiation within a culture. Samples were prepared as described in section 2.8.2.

3.2.5.3 Quantification of histochemical staining

After histochemical staining samples were imaged by light microscopy at 10x magnification. For each patient 3 technical replicates were utilised, and 5 images were taken of each coverslip at specified areas, see Figure 3-1.

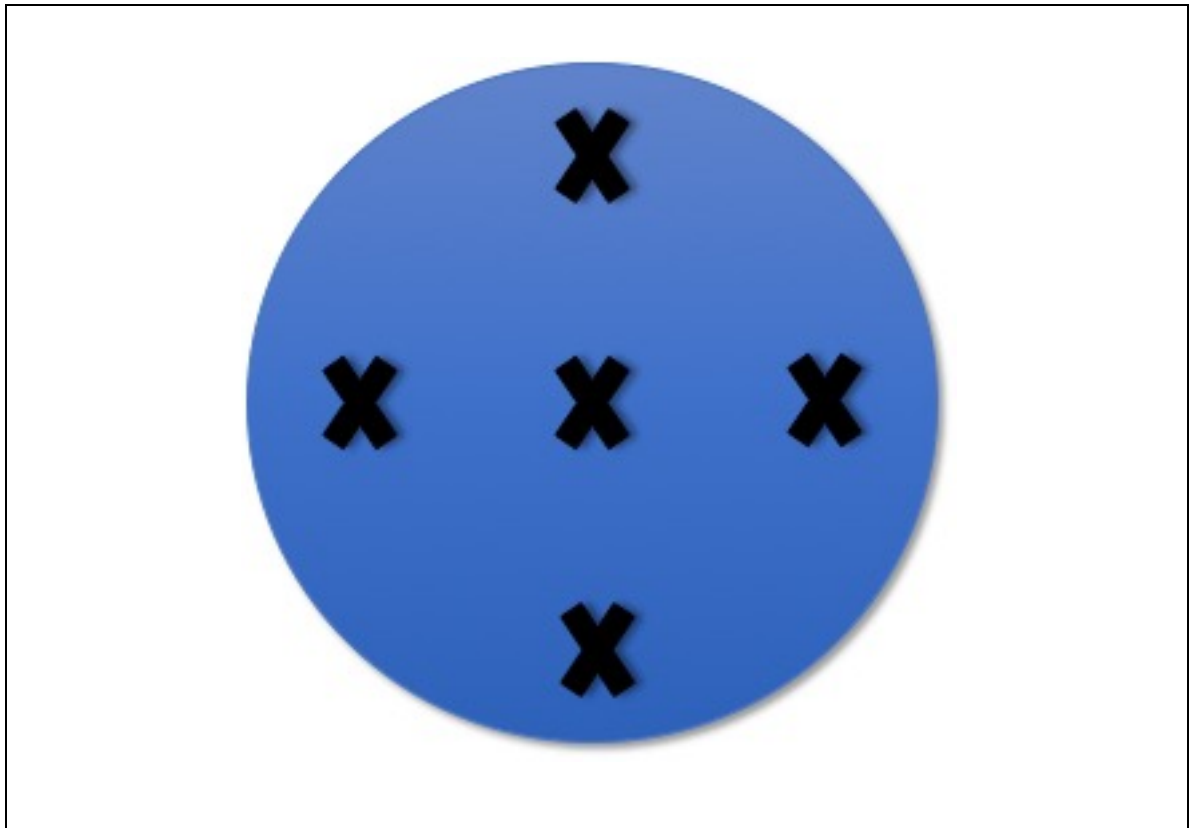


Figure 3-1 Example of areas imaged for analysis during histochemical staining. For both Oil red O and von Kossa staining coverslips were assessed by light microscopy and in 5 pre-determined areas, demonstrated by crosses in the above depiction, images of the observed staining recorded.

The obtained images were then processed in ImageJ and quantified as follows:

Oil Red O quantification: Images were converted to an 8-bit image and thresholding was performed to identify the areas of the cover slip positively stained by Oil Red O. The basal media was used as a control, the mean threshold value was calculated for this condition, and this value was then applied as a threshold for staining to the adipogenic media group, and the area of positive staining calculated, and utilised in statistical analysis.

von Kossa quantification: all images were converted to an 8-bit image. Manual thresholding to identify positive areas of mineralization was performed. The area of positive staining was utilised in statistical analysis.

3.2.6 MicroRNA expression

As described in section 2.9 RNA extraction from MSCs was performed via a TRIzol method for both groups. Next Generation Sequencing was performed on the

extracted RNA, via the University of Glasgow's Polyomics department. Three patient samples from each group were analysed. Three technical replicates were used for each patient.

3.2.7 MicroCT scanning

3 femoral heads from both the NOF and OA group were imaged via microCT scanning with a pixel resolution of 34 μ m. Acquired images were reconstructed into axial slices, and orientated by identification of the calcar and physeal scar.

The mid axial scan image of each femoral head was identified. A virtual sphere was then drawn fitting the diameter of the femoral head. The centre of this sphere was utilised as the location of the first volume of interest (VOI), from which all other VOIs were calculated Figure 3-2. The VOIs were cuboidal, measuring 7.5mm³. Each VOI was separated from VOI 1 by 2mm, in their respective directions. All bone characteristic data analysed was from these VOIs.

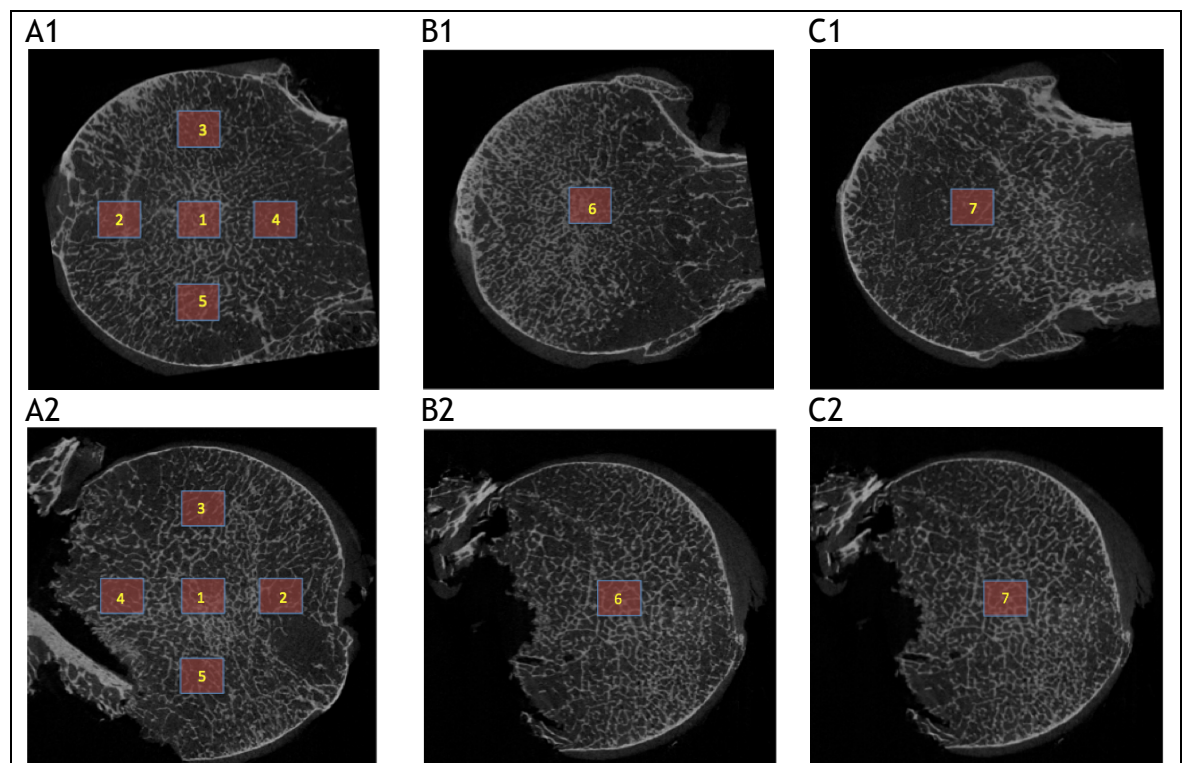


Figure 3-2 MicroCT images of femoral heads demonstrating the 7 VOIs. Images A1/B1/C1 are representative of the OA group, images A2/B2/C2 are representative of the NOF group. Images A1/A2 show centre axial slices where 5 VOIs were analysed. Images B1/B2, C1/C2 show upper and lower slices respectively where 1 central VOI was analysed.

3.3 Results

3.3.1 Flow Cytometry

The phenotype of the NOF and OA patient groups was assessed by flow cytometry. The expression of specific surface antigens used to define MSC populations was assessed. Surface antigens, known to characterise haematopoietic stem cells, were also evaluated, to determine the heterogeneity of the cell population.

Displayed in Table 3-1 both patient groups positively expressed markers of MSCs, namely CD105, CD73 and CD90. Importantly both groups did not express surface antigens known to represent HSC populations, CD45, CD34, CD14, CD79 and HLA-DR, which would have been suggestive of co-culture conditions. Results from the flow cytometric analysis confirmed the adherent fraction of the BM was producing a cell population containing MSCs, which was consistent to both patient groups.

Table 3-1 Phenotyping demonstrates positive and negative expression of MSC markers on flow cytometric analysis.

	OA	NOF
CD 105	+	+
CD 73	+	+
CD 90	+	+
CD45	-	-
CD34	-	-
CD14	-	-
HLA-DR	-	-
CD79	-	-

Differential expression between the two groups was observed, however this only reached statistical significance for three markers, CD90, CD13 and CD166, Figure 3-3. In each case, these markers were reduced in NOF MSCs compared to OA MSCs.

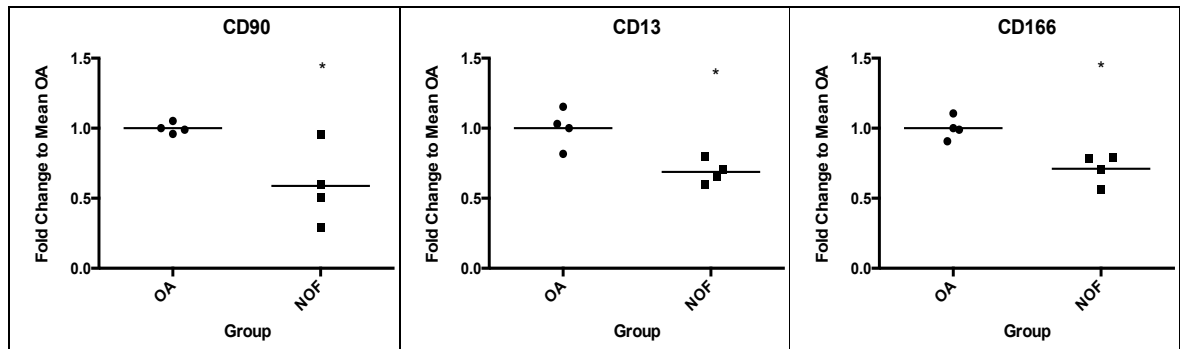


Figure 3-3 Flow cytometric assessment of antibody expression, CD90, CD13 and CD166 with fold change of antibody expression between the NOF and OA groups determined. Statistical significance assessed by a two-tailed Mann Whitney test, $P=0.0286$. $N=4$. These MSC markers were all reduced in NOF MSC cell populations in comparison to the OA group.

No statistically significant difference was observed in the expression of the remaining antibodies, Figure 3-4.

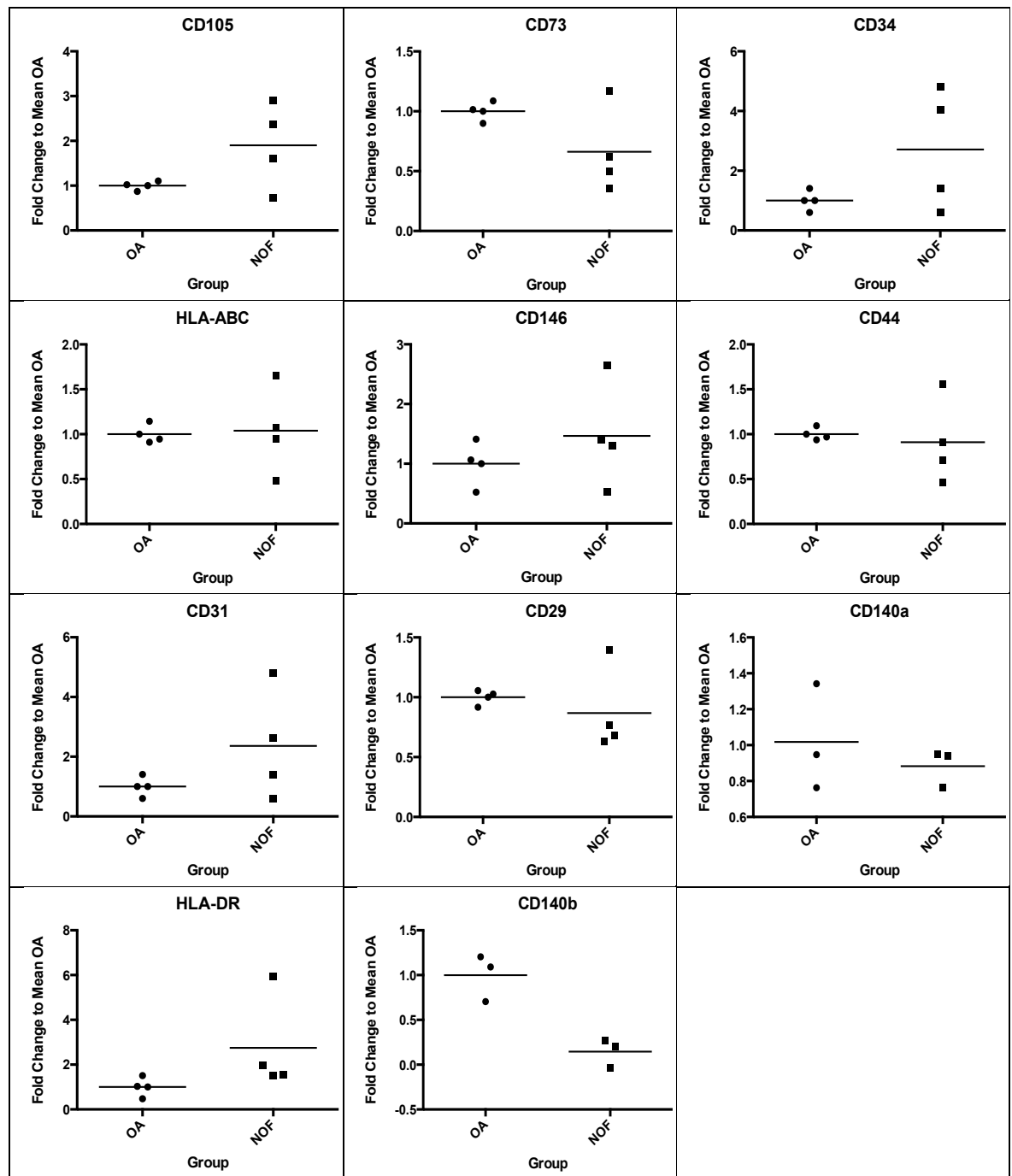


Figure 3-4 Flow cytometric assessment of antibody expression, with fold change of antibody expression between the NOF and OA groups determined. $N=4$ for all antibodies except CD140a and CD140b $N=3$.

Examples of the observed antibody expression is demonstrated in Figure 3-5, with data from one patient of from each group demonstrated.

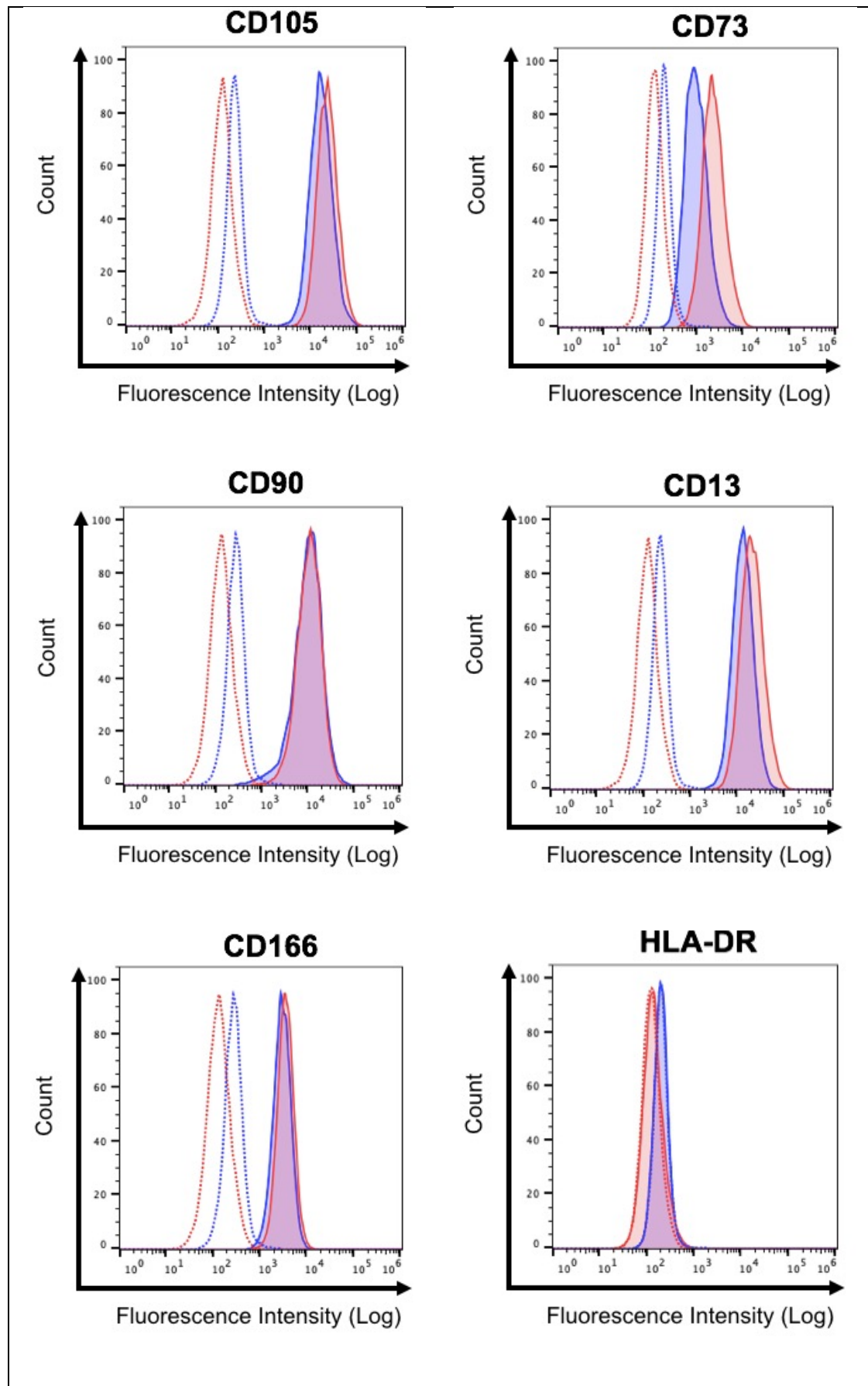


Figure 3-5 Demonstration of histograms antibody expression by flow cytometry. One patient from OA and NOF group with isotype controls as negative controls displayed. Solid blue- NOF patient, Solid red- OA. Dotted red and blue- isotype controls. Data normalised to allow comparison between samples.

3.3.2 Differentiation Potential of Bone Marrow Mesenchymal Stromal Cells from NOF and OA patients

A 21-day culture in differentiation media was performed to assess the multipotency capacity of each group. Two differentiation lineages were selected, adipogenesis and osteogenesis.

3.3.2.1 Adipogenesis

Small areas of positive Oil Red O staining were observed in both patient groups in the basal media condition, Figure 3-6, however by day 21 adipocytes were not observed in this control condition. Both the OA and NOF group were able to form mature adipocytes, see Figure 3-7, when cultured in adipogenic media. Clusters of adipocytes were observed in both patient groups when cultured in adipogenic media.

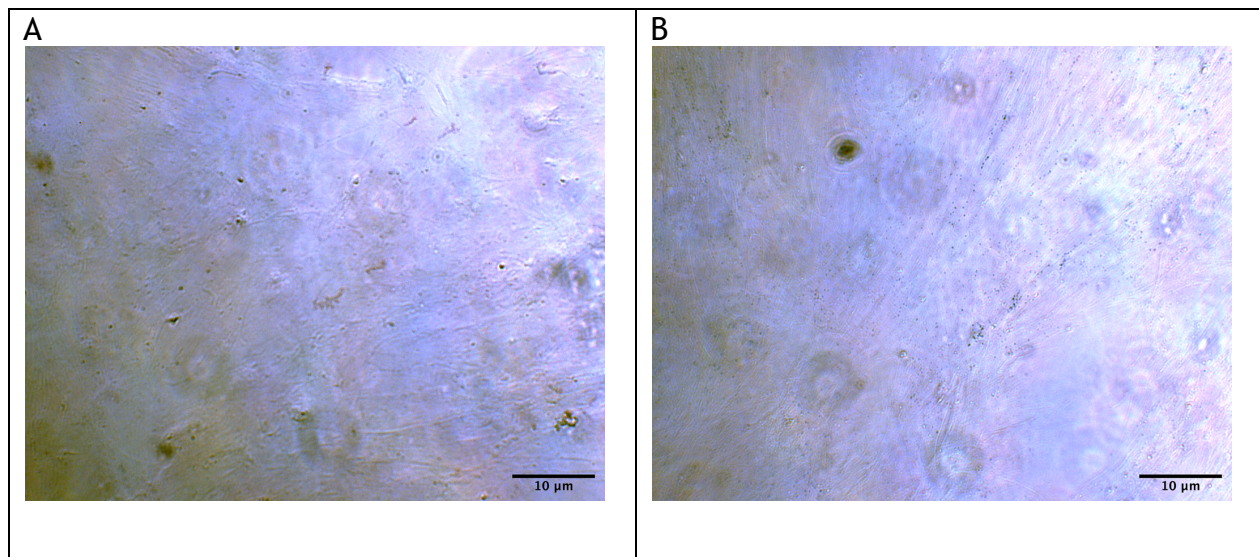


Figure 3-6 Brightfield microscopy of Oil Red O staining at Day 21 of MSC culture in basal medium. Image A represents OA group, B NOF group. Scale bar = 10µm.

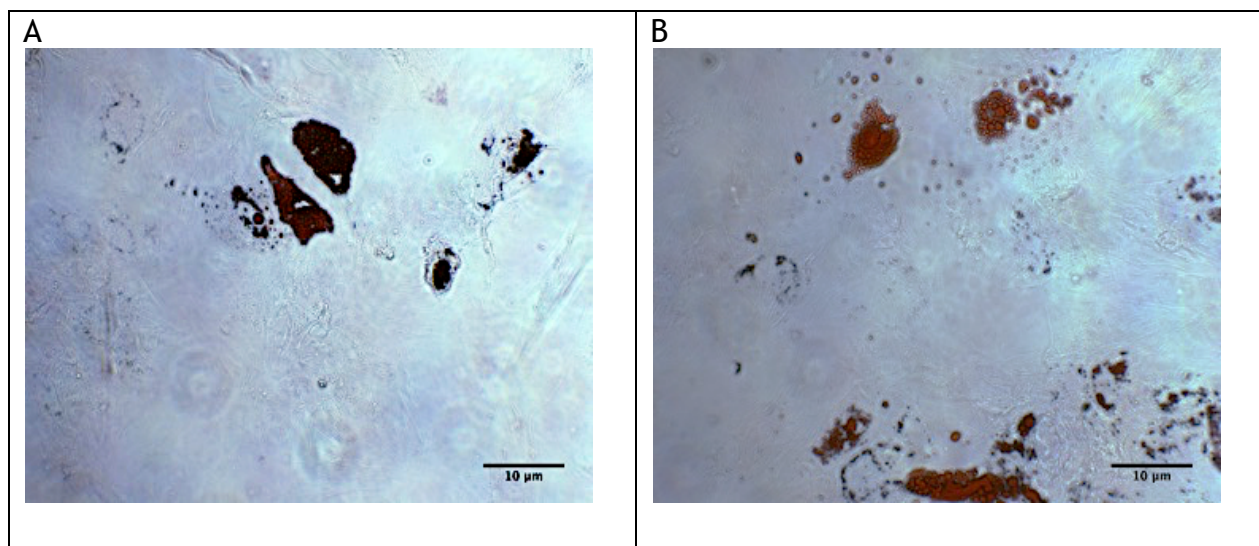


Figure 3-7 Brightfield microscopy of Oil Red O staining at Day 21 of MSC culture in adipogenic medium. Image A represents OA group, B NOF group. Scale bar = 10µm.

An increase in positive Oil Red O staining was seen in both groups in the adipogenic media at day 21. A statistically significant increase in Oil Red O staining was observed in the OA group, however this was not observed in the NOF group, Figure 3-8. The NOF group displayed a trend of increasingly positive Oil Red O staining in the adipogenic media, however this did not reach statistical significance. This may correlate to a more adipogenic state for NOF MSCs in basal media noting that staining revealed no evidence for this, or, perhaps more likely, a reduced capacity of differentiation from MSCs from the NOF group.

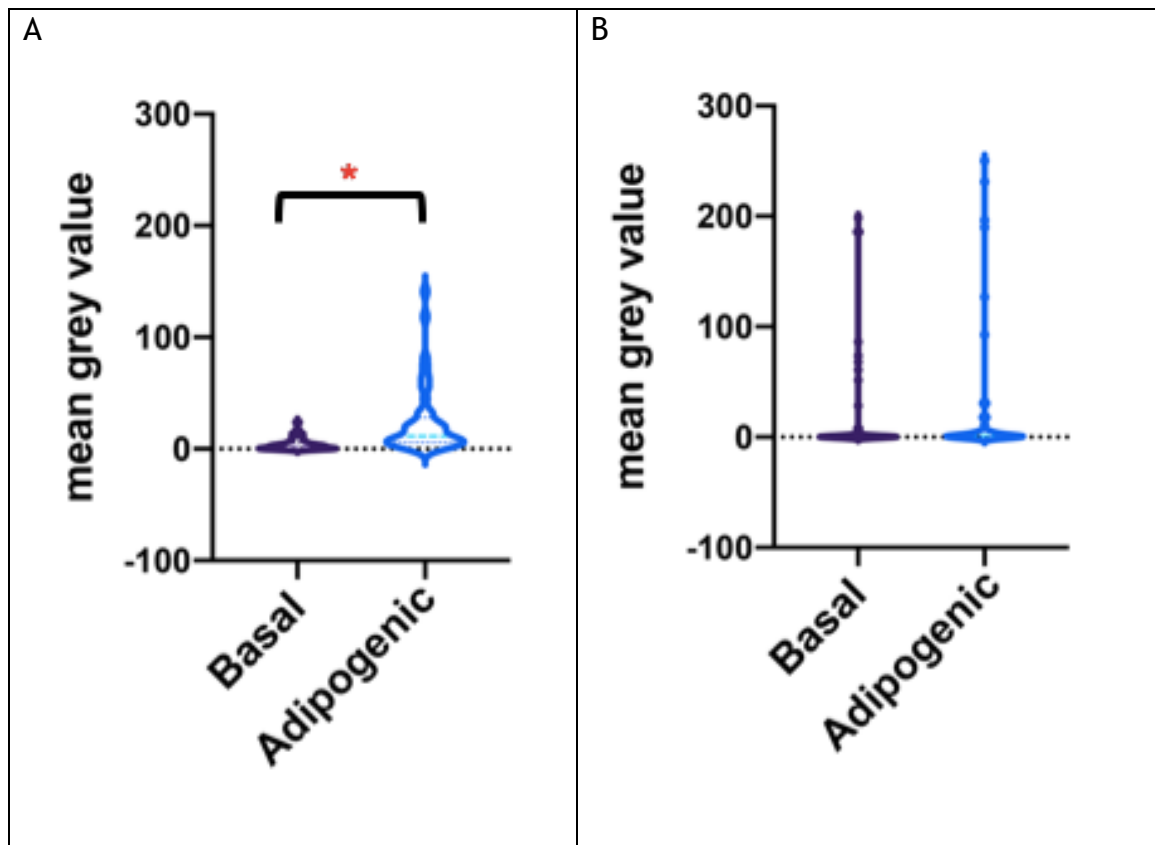


Figure 3-8 Level of Oil Red O staining in OA (A) and NOF (B) MSCs at day 21 in basal and adipogenic culture medium. For each group 3 patient samples were used with 3 cover slips per culture condition analysed. 5 images were taken per coverslip resulting in 45 images per group and condition. Mean grey value with standard deviation is displayed. Statistical analysis by Mann Whitney test, group A, $P < 0.0001$, group B $P = 0.637$.

3.3.2.2 Osteogenesis

Von Kossa staining was performed to assess the presence of mineralization as a marker of osteogenesis. Microscopy revealed the monolayer formation of MSCs with evidence of mineralization in the basal media in both patient groups, Figure 3-9.

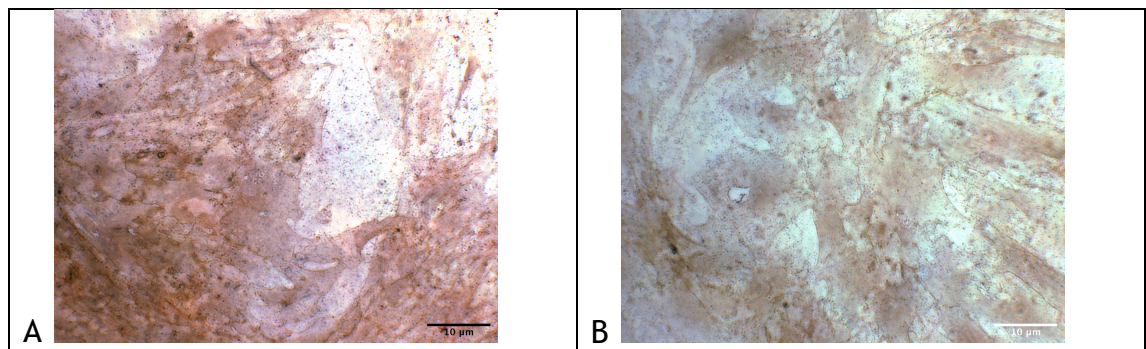


Figure 3-9 Brightfield microscopy of von Kossa staining at Day 21 of MSC culture in basal medium. Image A represents OA group, B NOF group. Scale bar = 10µm.

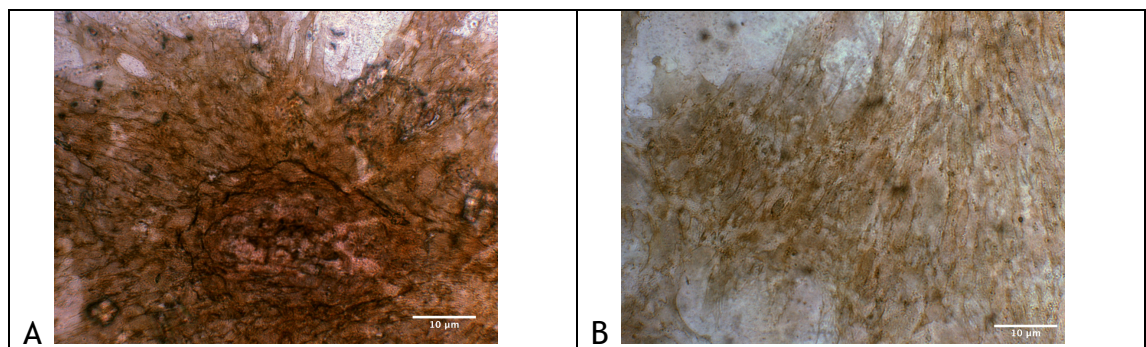


Figure 3-10 Brightfield microscopy of von Kossa staining at Day 21 of MSC culture in osteogenic medium. Image A represents OA group, B NOF group. Scale bar = 10µm.

When cultured in osteogenic media, clustering of cells and larger mineral deposition was evident by microscopy, with positive staining visible in both groups, Figure 3-10. The OA group again appeared to show a greater potential for differentiation.

The overall trend of expression was similar between the two groups, Figure 3-11, with both patient groups showing a statistically significant increase in von Kossa staining when cultured in osteogenic media. Greater variation was observed in the NOF group, with a wider spread of mean gray values. A direct comparison was not made between the groups as staining and imaging was not performed on the same day for all samples.

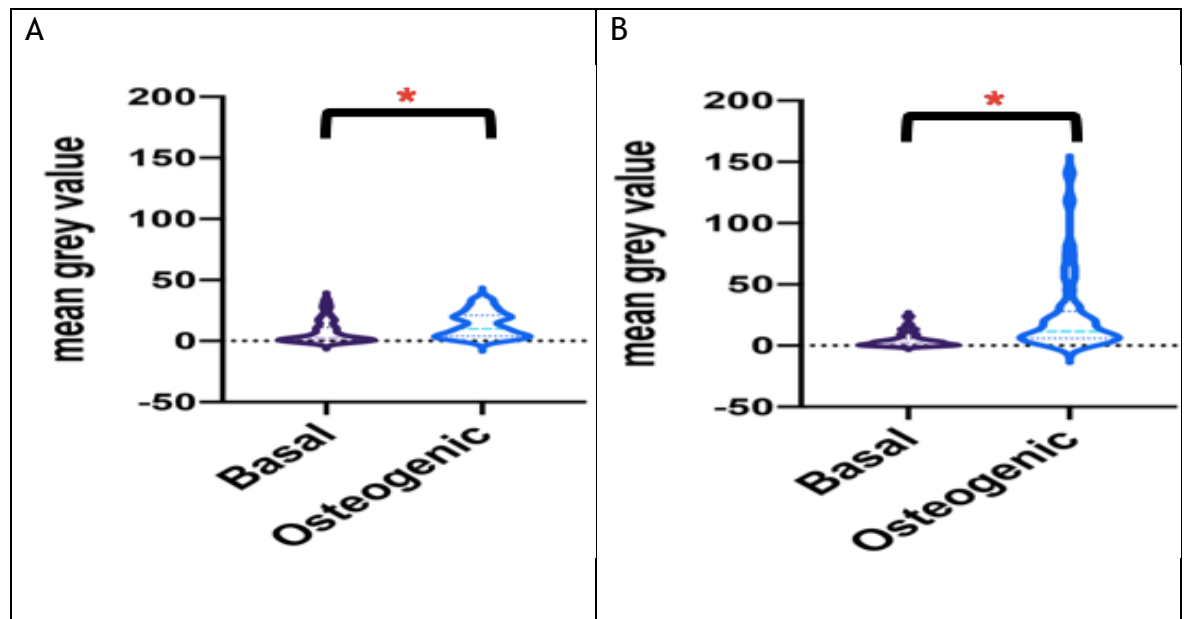


Figure 3-11 Level of von Kossa staining in OA (A) and NOF (B) MSCs at day 21 in basal and osteogenic culture medium. Mean grey value with standard deviation is displayed. Statistical analysis by Mann Whitney test, group A and B $p < 0.0001$.

3.3.3 microRNA expression in NOF and OA

Over 2000 microRNAs were screened in MSCs from both patient groups. This revealed significant variations in expression levels of microRNAs known to be involved in the pathogenic process of OP (Kim and Lim, 2014; Heilmeier *et al.*, 2016; Mäkitie *et al.*, 2018). Figure 3-12 demonstrates the 105 significantly abnormally expressed microRNAs observed in the NOF group in comparison to the OA group. This shows an approximately even distribution of over and under-expressed miRNAs when comparing the NOF patients to the OA group.

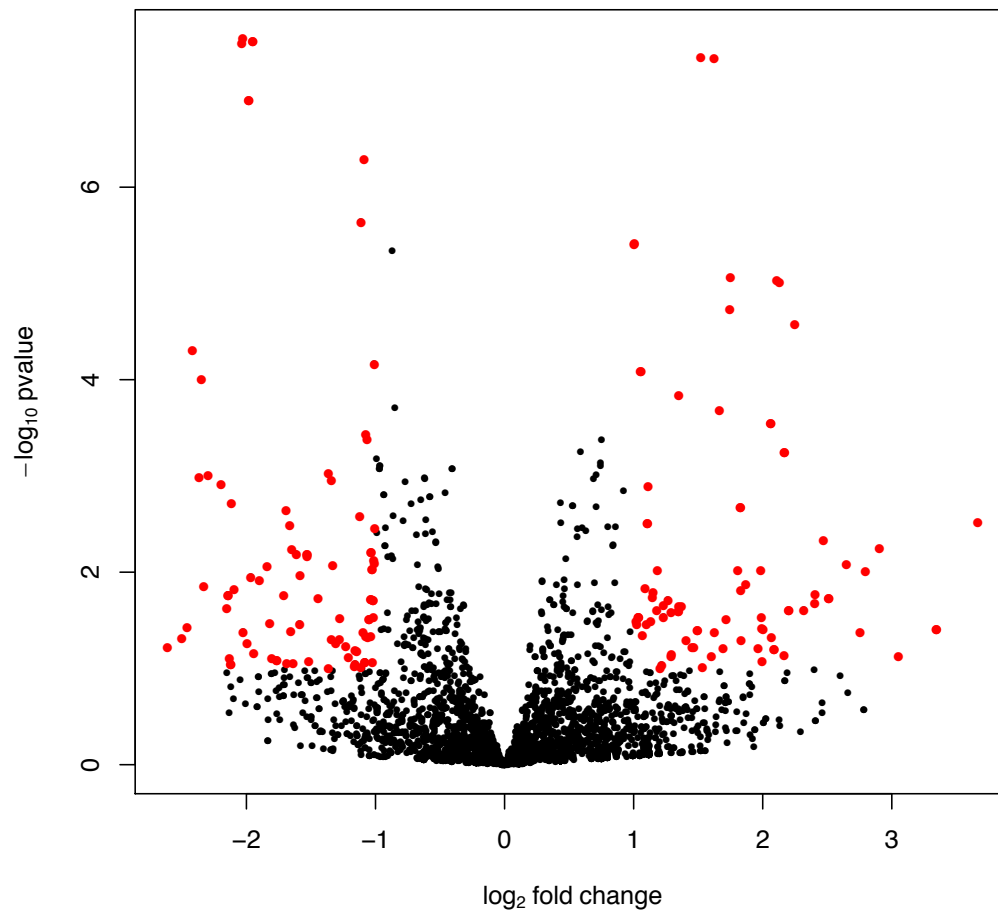


Figure 3-12 Volcano plot of microRNA expression in the NOF group in comparison to the OA group. X axis represents log₂ of the fold change and Y axis represents the p value. Red dots demonstrate miRNAs which are significantly dysregulated with a p adjusted value of <0.1. Statistical analysis by DESeq2.

Principal component analysis (PCA) was performed to assess the clustering of microRNA expression within patient samples and groups, Figure 3-13. A weak pattern of separation was observed between the two patient groups. Replicates of patient samples were seen to cluster better in the OA group with more variance seen in the NOF group.

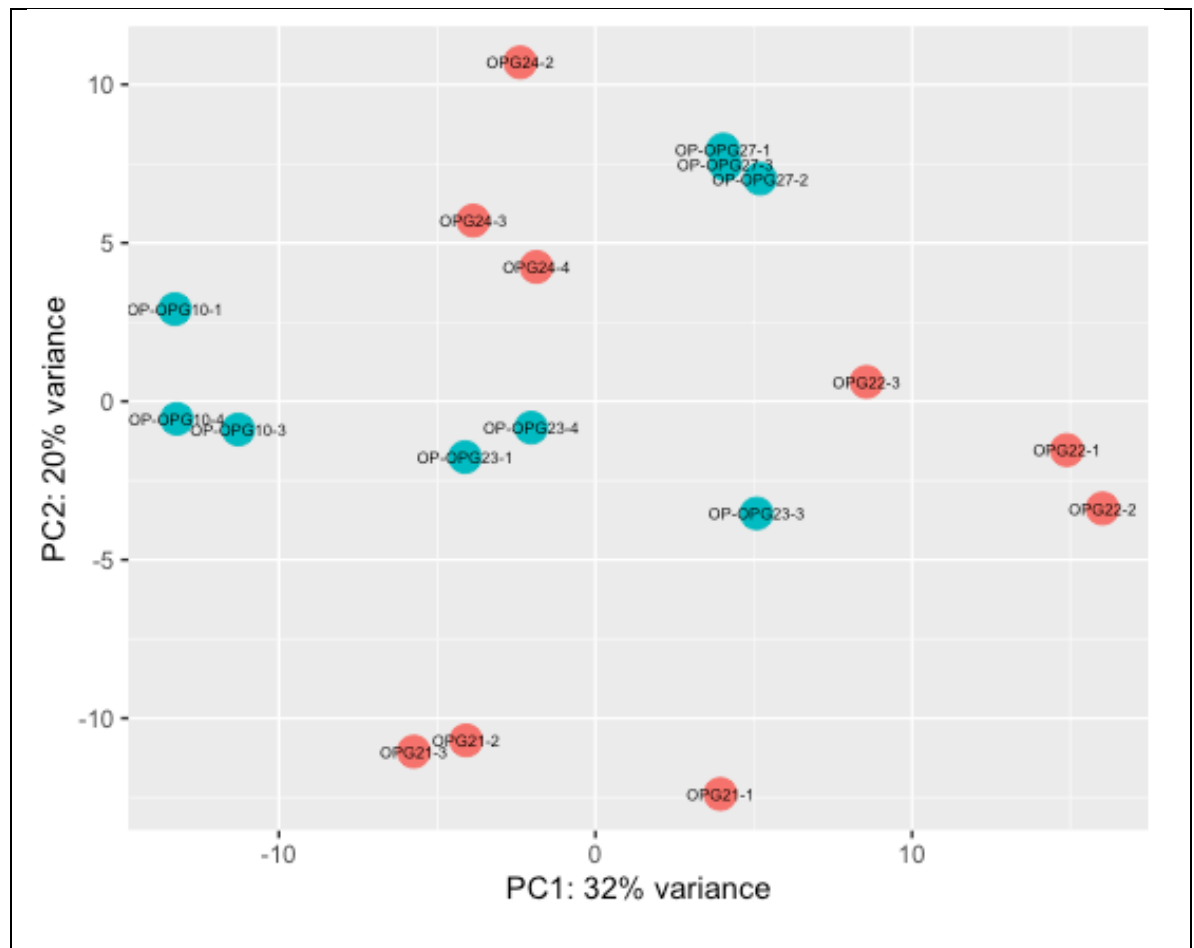


Figure 3-13 PCA plot of log transformed microRNA expression in NOF and OA groups. Red circles represent OA group patients and blue circles NOF group patients. Intra-patient samples were seen to cluster closely. The OA group demonstrated a greater distribution along both X and Y axes. A weak pattern of clustering was evident within the NOF group.

Of these dysregulated microRNAs the most increased and decreased, and their log fold change are displayed in Table 3-2 and Table 3-3.

Table 3-2 Top 20 microRNAs with increased expression in NOF group vs OA group, with log 2-fold change.

	microRNA	Log 2-Fold Change
1	hsa-miR-146a-3p	2.25
2	hsa-miR-4662a-5p	2.17
3	hsa-miR-1304-3p	2.13
4	hsa-miR-935	1.83
5	hsa-mir-2114	1.75
6	hsa-mir-3671	1.67
7	hsa-mir-549a	1.62
8	hsa-miR-4653-5p	1.35
9	hsa-miR-4286	1.11
10	hsa-miR-99a-5p	1.16
11	hsa-miR-100-5p	1.00
12	hsa-miR-3200-3p	0.92
13	hsa-miR-598-3p	0.84
14	hsa-miR-125b-2-3p	0.80
15	hsa-miR-212-5p	0.75
16	hsa-miR-31-5p	0.75
17	hsa-let-7a-2-3p	0.71
18	hsa-miR-500a-3p	0.69
19	hsa-mir-491	0.56
20	hsa-miR-29a-3p	0.53

Table 3-3 Top 20 microRNAs with decreased expression in NOF group vs OA group, with log 2-fold change.

	microRNA	Log 2-Fold Change
1	hsa-mir-4467	-2.42
2	hsa-miR-124-3p	-2.37
3	hsa-mir-124-2	-2.20
4	hsa-miR-133a-3p	-2.04
5	hsa-mir-1-2	-1.98
6	hsa-miR-16-1-3p	-1.69
7	hsa-mir-3167	-1.66
8	hsa-mir-150	-1.61
9	hsa-mir-6868	-1.53
10	hsa-miR-18a-5p	-1.12
11	hsa-miR-2355-3p	-1.11
12	hsa-miR-299-3p	-1.08
13	hsa-miR-143-5p	-1.07
14	hsa-mir-3182	-1.03
15	hsa-miR-106a-5p	-1.01
16	hsa-miR-455-5p	-0.99
17	hsa-miR-3529-3p	-0.97
18	hsa-miR-7-5p	-0.97
19	hsa-miR-7-2	-0.97
20	hsa-miR-20a-5p	-0.95

Several pathways were highlighted as being predicted to be altered due to this expression profile of microRNAs in the NOF group. Figure 3-14 demonstrates a network centred on AGO2, a member of the Argonaute family crucial to RNA silencing. This network was observed by IPA to be related to organismal injury.

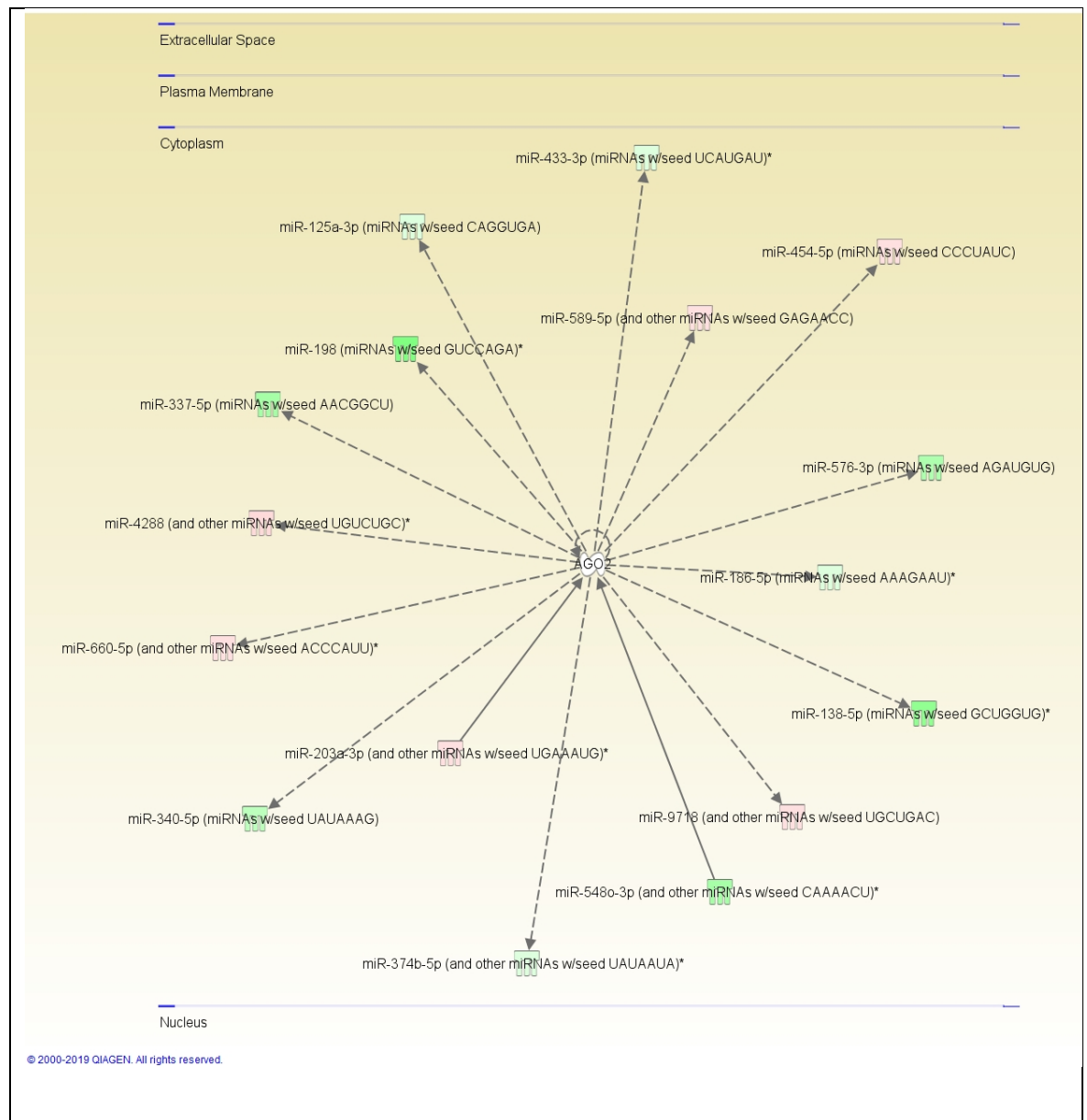


Figure 3-14 Network 1, demonstrating an abnormally regulated pathway in the NOF group relative to the OA group, centred upon the cytoplasmic actions of AGO2, generated via IPA software. Red represents predicted increased expression, and green decreased. N = 3 patient samples, with 3 technical replicates each. Solid line represents direct, and dotted line indirect, effect.

Figure 3-15 demonstrates another IPA generated network observed to be dysregulated in the NOF group. The main functions of the network were cellular movement, development, growth and proliferation. The down-regulation of miR-143 is observed to target Transgelin (TAGLN), observed to control differentiation via regulating cytoskeleton organization (Elsafadi *et al.*, 2016), B-cell lymphoma 2 (BCL2), known to promote cell survival and regulate mitochondrial activity (Pantschenko *et al.*, 2005) and smooth muscle actin, observed in active osteoblasts (Kinner and Spector, 2002). Furthermore, there is reduced

expression of miRNAs involved in the regulation of molecules related to osteogenesis such as Wingless-type MMTV integration site family, member 2 (Wnt2), Wingless-type MMTV integration site family, member 3A (Wnt3A) and bone morphogenic protein 2 (BMP2) (Liu *et al.*, 2013).

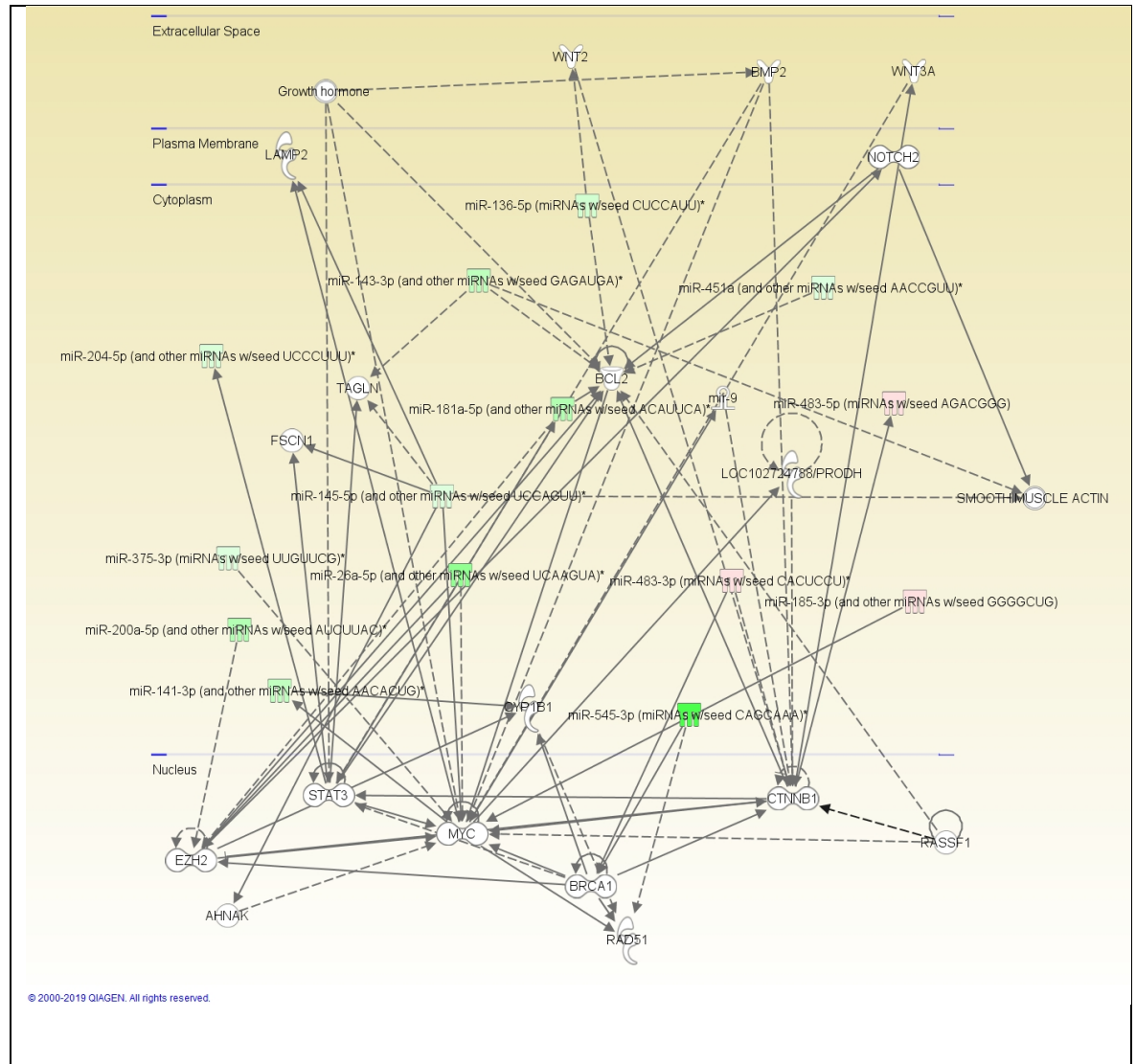


Figure 3-15 Network 2 demonstrating an abnormally regulated pathway in the NOF group, relative to the OA group, with effects on molecules related to cellular growth, proliferation and movement. Red represents predicted increased expression, and green decreased. N = 3 patient samples, with 3 technical replicates each. Solid line represents direct, and dotted line indirect, effect.

Figure 3-16 shows a third network IPA generated network, with dysregulation of cell death and survival and cell cycle regulation. Abnormalities in inflammatory response are observed in the NOF group. MiR-31-5p upregulation is noted. MiR-31-5p indirectly regulates CXCL5 and IL1B, known inflammatory regulators (Lange *et al.*, 2010; Sepuru, Poluri and Rajarathnam, 2014).

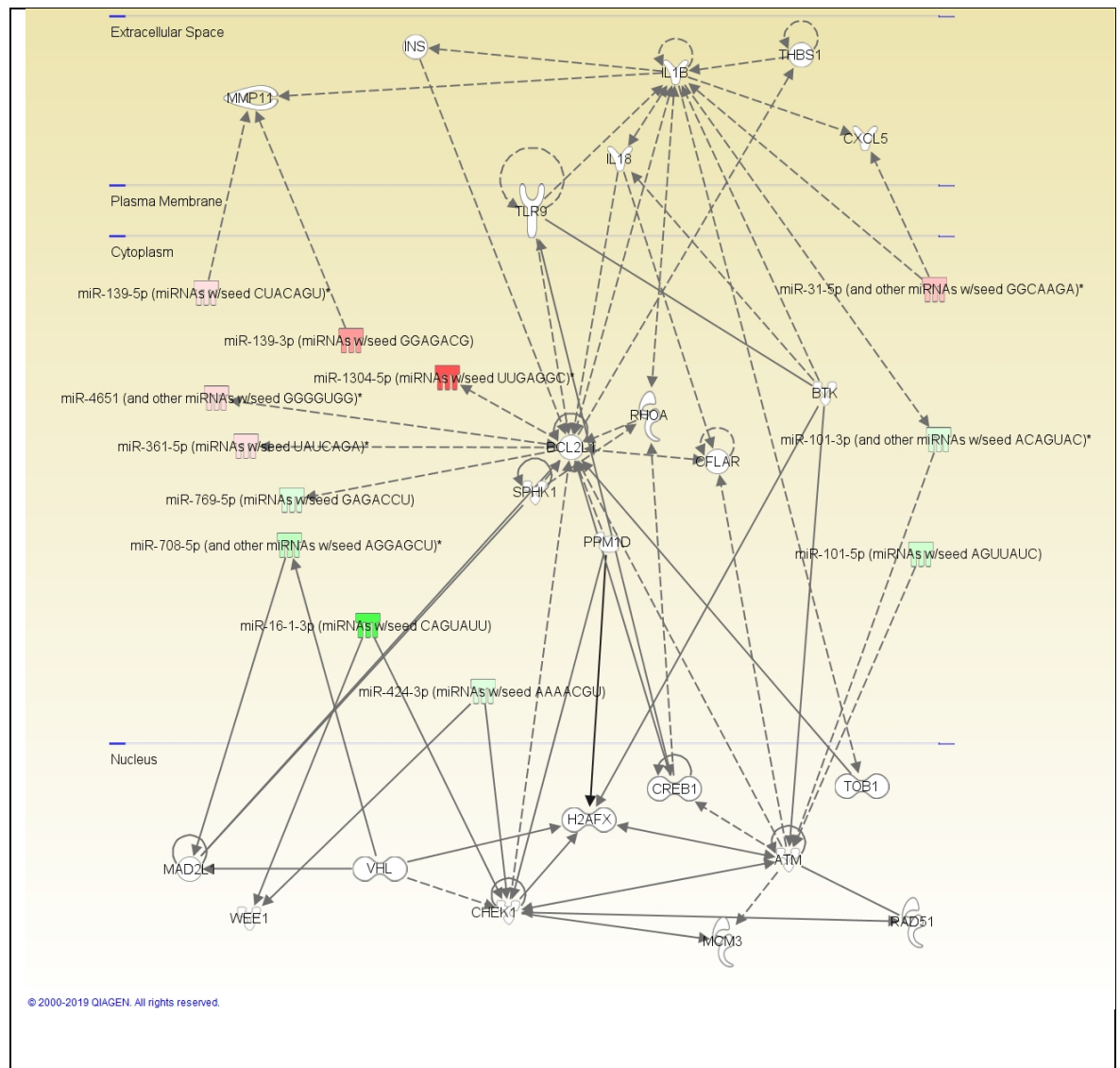


Figure 3-16 Network 3 Demonstrating a dysregulated miRNA network in the NOF group, relative to the OA group, with abnormalities of cell death and survival and cell cycle regulation predicted. Red represents predicted increased expression, and green decreased. N = 3 patient samples, with 3 technical replicates each. Solid line represents direct, and dotted line indirect, effect.

Figure 3-17 illustrates network 4 which was again identified by IPA to be abnormally regulated in the NOF group, with effects on cellular growth, organismal injury noted. Furthermore, notch signalling via the notch receptor protein was noted to be implicated, via NOTCH1 and NOTCH2. Both have been shown to have roles in osteoblast differentiation (Hilton *et al.*, 2008; Regan and Long, 2013).

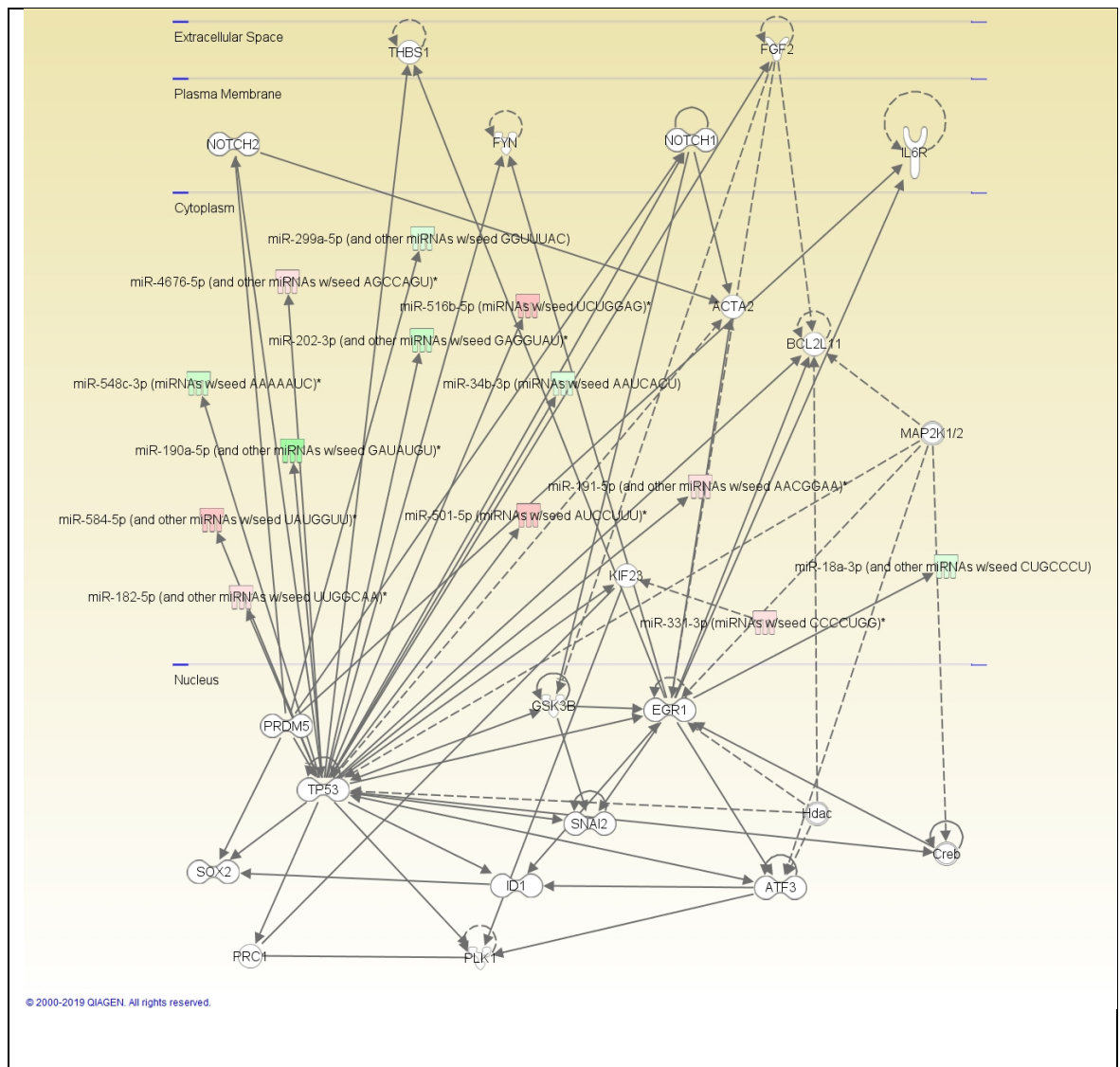


Figure 3-17 Network 4 displays predicted abnormalities in cell growth, organismal injury and cancer pathways in the NOF group, relative to the OA group. Red represents predicted increased expression, and green decreased. N = 3 patient samples, with 3 technical replicates each. Solid line represents direct, and dotted line indirect, effect.

3.3.4 MicroCT Characteristics of femoral head samples from NOF and OA

MicroCT scanning was performed to assess multiple bony characteristics of femoral head samples from both patient groups. Femoral heads were from the same patients as utilised in the microRNA expression analysis.

Seven volume of interests (VOI) were plotted within the femoral head. VOI 1 was determined from the mid axial scan image, the other VOIs were determined respective to its position, see Figure 3-2 for further description of the VOIs locations.

Multiple indices were assessed within the VOIs, to obtain a comprehensive overview of the microarchitecture of each sample. BV/TV was a key index that was assessed and is displayed by group, Figure 3-18, and by patient, Figure 3-19 and Figure 3-20. The highest BV/TV value was observed in VOI 1 in the NOF group. The lowest BV/TV value was seen in VOI 4 of the OA group. BV/TV was seen to be statistically significantly varied in the OA group when comparing VOI 1 vs VOI 4 only.

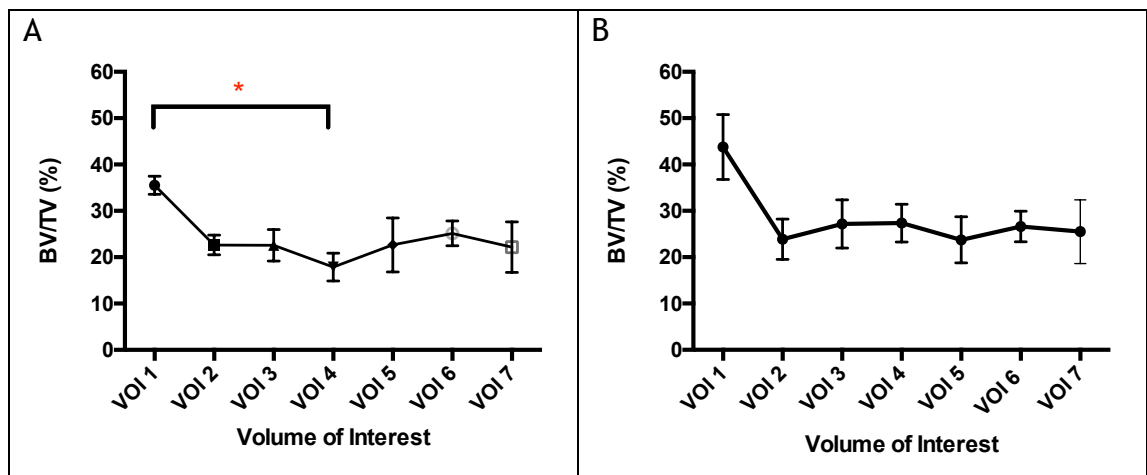


Figure 3-18 Mean BV/TV % with SD observed in each VOI, in group A (OA) and B (NOF). $N=3$. Statistical analysis by Kruskal Wallis test with Dunn's multiple comparison showed significant variation in VOI 1 vs VOI 4 in group A (OA) only.

Figure 3-19 and Figure 3-20 show the individual patient BV/TV values in each VOI. This demonstrates no uniform pattern of BV/TV throughout the femoral head, with individual trends observed in both patient groups.

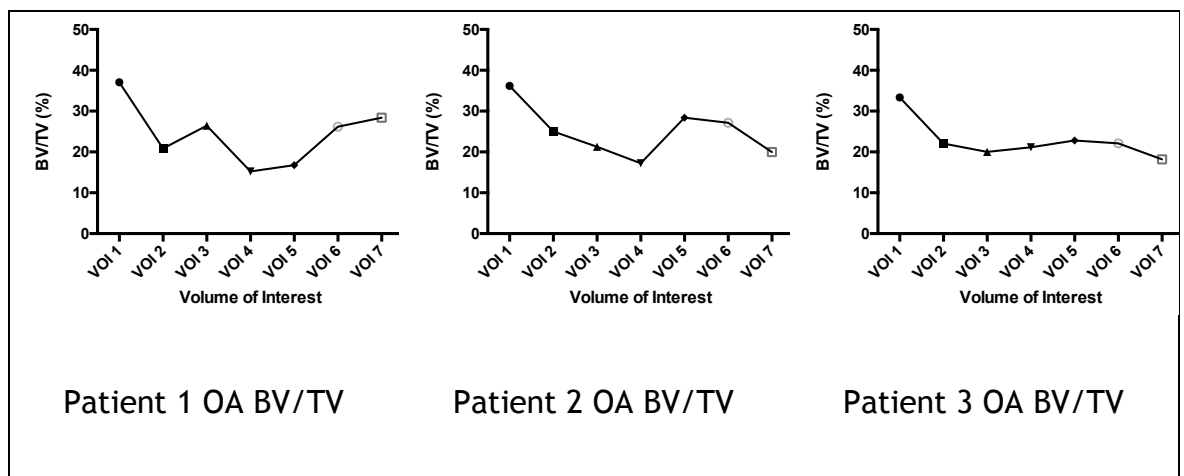


Figure 3-19 Range of BV/TV (%) observed in patient samples from OA group in each VOI.

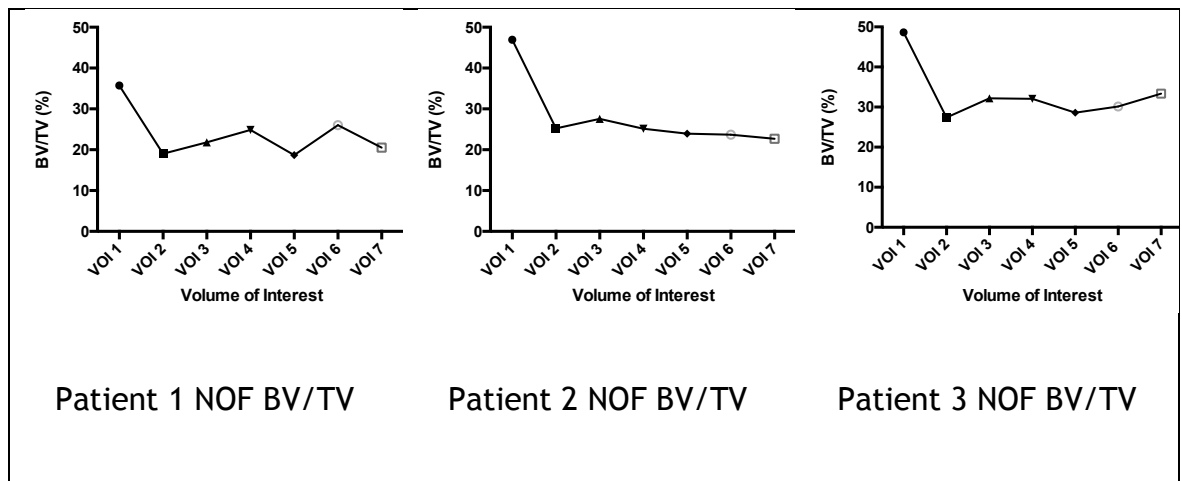


Figure 3-20 Range of BV/TV (%) observed in patient samples from NOF group in each VOI.

Trabecular thickness, Figure 3-21, was also assessed and demonstrated similar trends to BV/TV in both groups. In keeping with the BV/TV data, trabecular thickness was greatest in VOI 1 in both groups. Marked variation in the remaining VOIs was observed in NOF group in comparison to the OA group.

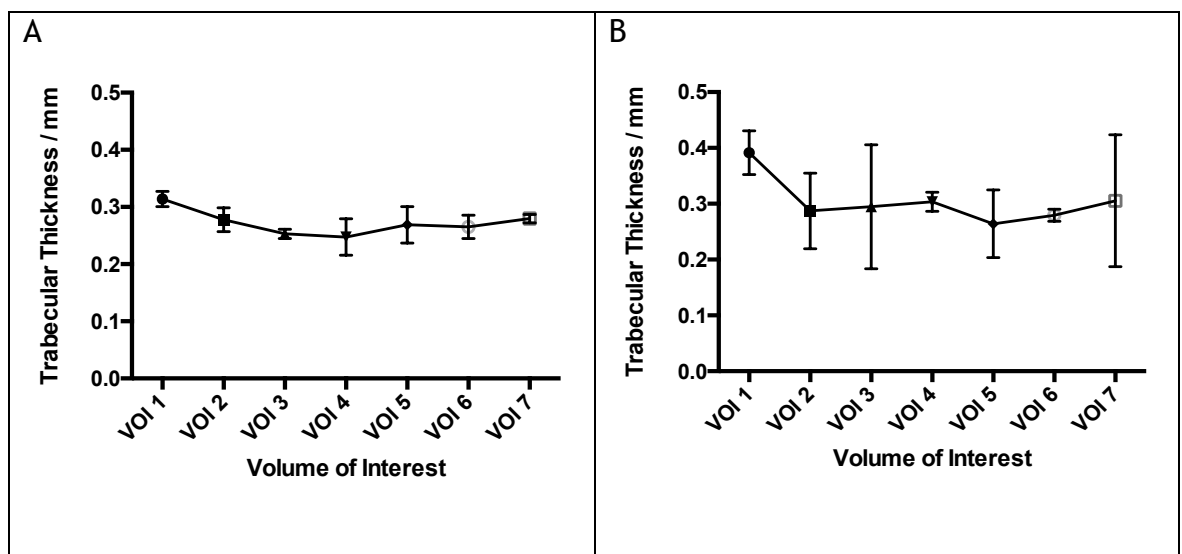


Figure 3-21 Mean trabecular thickness with standard deviation at the 7 Volume of Interest sites within the femoral heads of in group A (OA) and B (NOF). $n=3$

It is evident that a more uniform trabecular thickness is observed in the OA group with very large variation seen in the NOF group, Figure 3-21.

Similar mean values of trabecular separation were observed in the two groups, Figure 3-22, with VOI 1 showing the shortest distance between trabeculae. This was statistically significantly different in comparison to VOI 4 in the OA group. VOI 2 and 4 in both groups showed large separation of trabeculae. Little

difference is noted in VOI 6 and 7 in the NOF group, whereas a suggestion of more closely associated trabecular is observed in VOI 6 in the OA group.

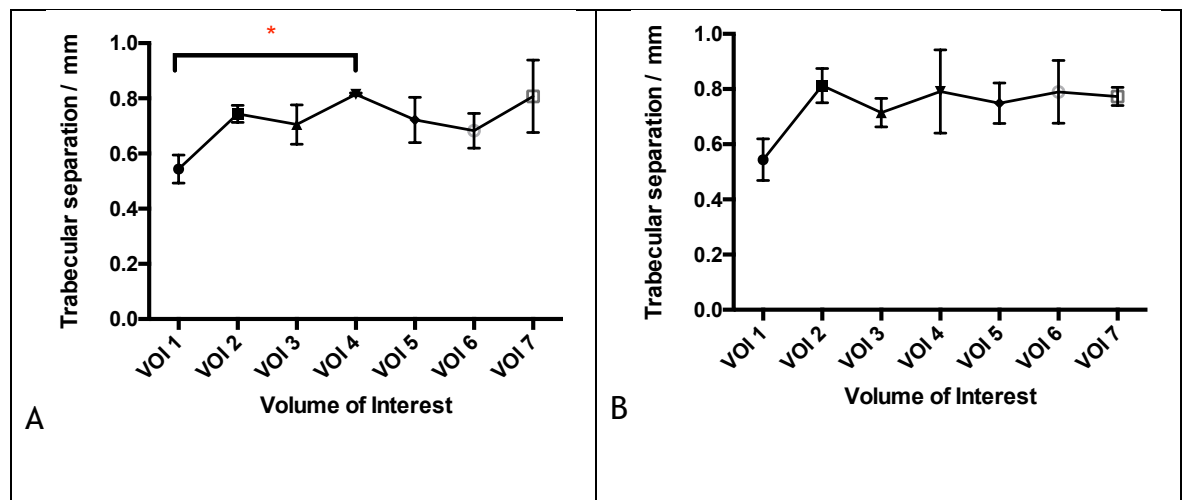


Figure 3-22 Mean trabecular separation/mm with SD observed in each VOI, in group A (OA) and B (NOF). $N=3$. Statistical analysis by Kruskal-Wallis test with Dunn's multiple comparison showed significant variation in VOI 1 vs VOI 4 in group A only, ($P=0.0467$).

Trabecular number, assessed in all seven VOIs, is demonstrated in Figure 3-23. The OA group showed a significant difference of mean trabecular number in VOI 1 in comparison to VOI 4, which were observed to have the highest and lowest trabeculae number respectively. Similar peak trabecular number was observed in the two groups in VOI 1, however little variation in mean trabecular number was demonstrated in the remaining VOIs in the NOF group. In both groups, VOI 7, the most inferior VOI in the femoral head showed a lower mean value than VOI 6.

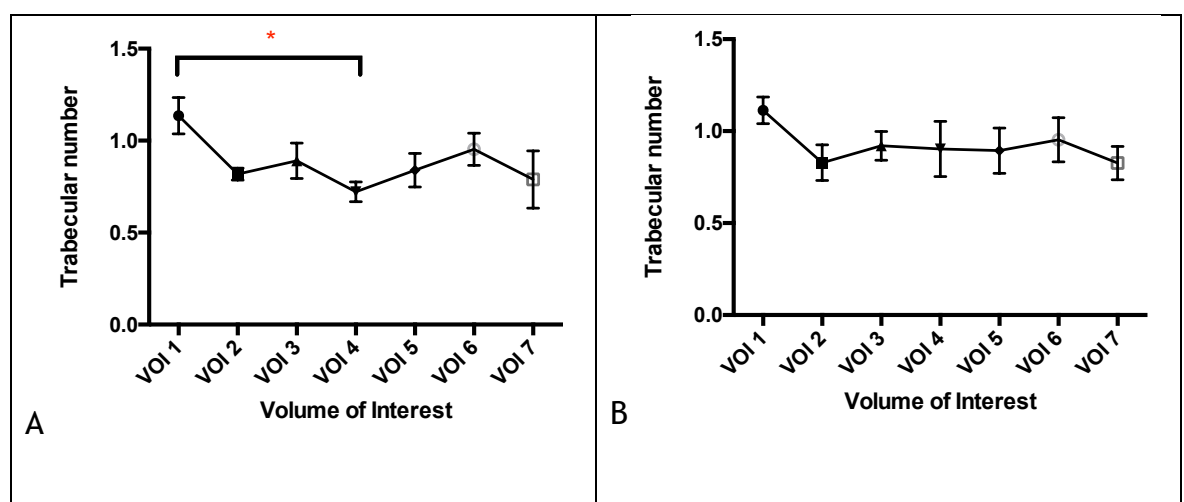


Figure 3-23 Mean trabecular number with SD observed in each VOI, in group A (OA) and B (NOF). $N=3$. Statistical analysis by Kruskal-Wallis test with Dunn's multiple comparison showed significant variation in VOI 1 vs VOI 4 in group A only, ($P=0.0339$).

The SMI values across the seven VOIs was observed to follow a similar pattern in the NOF and OA group, Figure 3-24. Large variation in the SMI values in each VOI was noted in the NOF in contrast to the OA group.

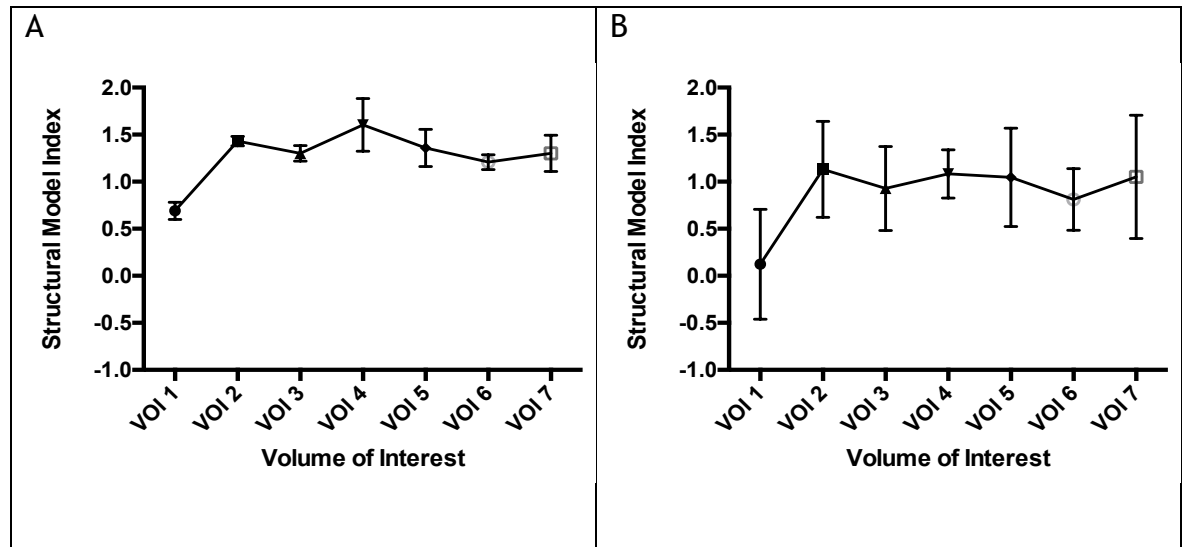


Figure 3-24 Mean structural model index with SD at the 7 VOIs sites within the femoral heads of in group A (OA) and B (NOF). $n=3$.

Variation in degree of anisotropy was seen throughout the femoral heads in both groups, Figure 3-25. This reached statistical significance in the OA group only. VOI 2 contained the lowest DA in the OA group, suggestive of containing the most plate like-trabeculae. VOI 4 in the NOF group contained the lowest DA value but this was not significant likely due to high variance in the NOF samples. Similar trends were observed in both groups.

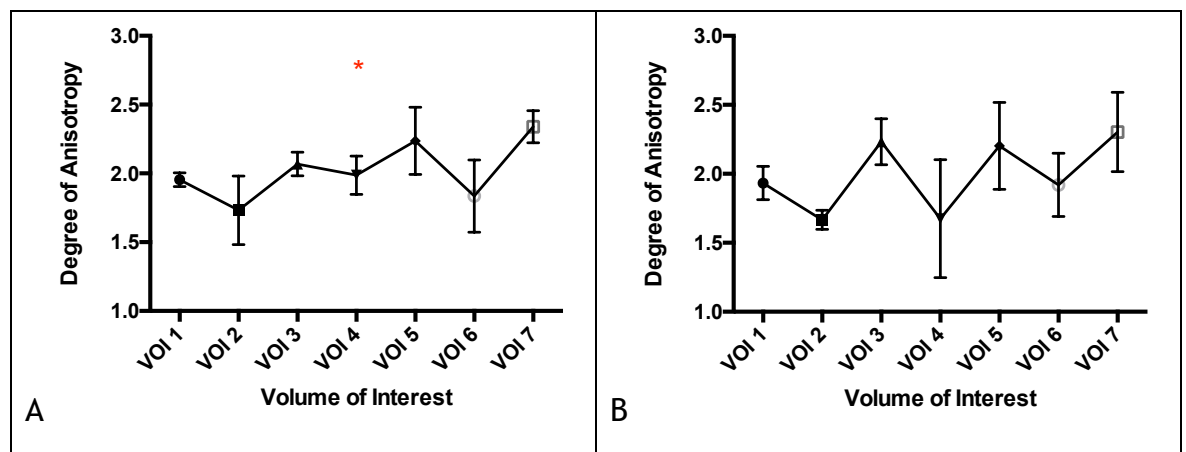


Figure 3-25 Mean degree of anisotropy with SD observed in each VOI, in group A (OA) and B (NOF). $N=3$. Statistical analysis by Kruskal-Wallis test showed significant variation in group A only, ($P=0.0380$).

Figure 3-26 demonstrates mean connectivity density, with a similar trend, but with lower values in the NOF group. Intra-VOI variability was greatest again in the NOF groups suggesting large patient-patient variability. A more uniform degree of connectivity density was noted in the OA group.

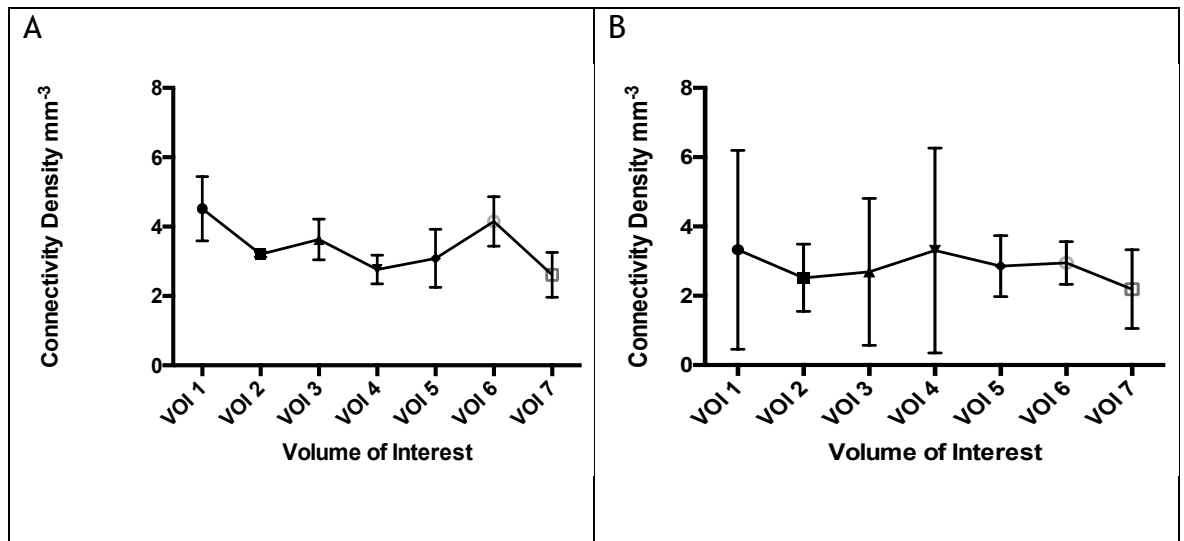


Figure 3-26 Mean Connectivity density with SD observed in each VOI, in group A (OA) and B (NOF). *N*=3.

3.4 Discussion

These experiments sought to rigorously assess the MSC characteristics of the two groups and also to identify any phenotypic differences from bone samples.

3.4.1 Flow cytometry confirms cell populations contain MSCs

MSCs have long held great hope for greater understanding of diseases and providing a therapeutic source. There are multiple tissue sources of MSCs and furthermore there are many different techniques used for their isolation. This variation causes difficulties when comparing research outcomes, and predicting future areas of investigation.

In order to minimise this heterogeneity criteria have been set for defining MSCs (Dominici *et al.*, 2006). In 2006 the International Society for Cellular Therapy proposed the following criteria to define the human MSC;

1. Adherence to plastic
2. Specific Antigen expression
 - a. Expression of CD 105, CD 73, CD 90
 - b. Lack of expression of CD45, CD34, C14, CD11b, CD79 α , CD19 and HLA-DR
3. Multipotent *in vitro* differentiation potential
 - a. Adipogenic
 - b. Osteogenic
 - c. Chondrogenic

Culturing MSCs from the adherent fraction of bone marrow aspirates has been used extensively. However, a comparison of extracellular markers between these two groups is relatively unexplored. It was important to assess the population of cells being utilised in experiments, to ensure the presence of MSCs and the absence of HSCs.

Results from the flow cytometric analysis confirmed the adherent fraction of the bone marrow samples was producing a cell population containing MSCs, which was consistent to both patient groups. Importantly both groups did not express surface antigens known to represent HSC populations, which would have been suggestive of co-culture conditions. The percentages of expression of these

extracellular markers was not calculated which could be performed, to fully comply with the above criteria, in future experiments.

Co-cultures have their role in MSK research, with a particular importance when assessing osteoclast/osteoblast interactions (Young *et al.*, 2015; Silverwood *et al.*, 2016). The focus of experiments in this project, however, was MSC differentiation and thus it was favourable to have populations not containing HSCs or their progeny.

3.4.2 MSCs from neck of femur fracture patients show reduced stemness

A trend of reduced expression of markers of MSC naivety and potency was observed in the NOF group. A reduction in the expression of CD90 was observed in the NOF group. CD90 is a cell surface protein originally discovered as a thymocyte antigen, and is also known as Thy-1 (Williams and Gagnon, 1982). CD90 has been used as a marker of many cell types, including mature neurons, it is notably utilised as one of the characteristic markers of MSCs (Dominici *et al.*, 2006; Rege and Hagood, 2006). CD90 has also been strongly linked to differentiation. Studies have assessed the osteogenic effect of increased or decreased expression of CD90 (Moraes *et al.*, 2016). Demonstrations of increased osteogenesis in both *in vitro* and *in vivo* experiments has been observed with high CD90 expression, which is in keeping with the flow cytometry results displayed in Figure 3-3, suggesting an impaired osteogenic capacity of MSCs from the NOF group (Chung *et al.*, 2012).

CD13 expression was also observed to be significantly downregulated in the NOF group. CD13 is well expressed by many cell types, but has been shown to have an important role in MSC function (Iaffaldano *et al.*, 2013). CD13 plays a significant role in MSC adhesion, migration and angiogenesis, CD13 knockout studies have shown impaired tissue repair (Rahman *et al.*, 2014). The reduced expression of CD13 within the NOF group is, again, suggestive of impaired MSC function. It can be postulated that this would contribute to impaired fracture healing *in vivo* and thus could be a significant barrier to successful management of fragility fractures occurring secondary to OP.

Activated leukocyte cell adhesion molecule (ALCAM), also known as CD166, is an immunoglobulin with important roles in cell adhesion, migration, haematopoiesis and tumour progression (Xu *et al.*, 2016). It is described to play an important role in osteoblastic support of HSC function and maintenance (Chitteti BR, Cheng Y-H, Kacena MA, 2014). The decreased expression observed in the NOF group, Figure 3-3, is suggestive of an impaired bone marrow niche environment. This could contribute to poorer osteoblast function and bone deposition.

3.4.3 Mesenchymal stem cells from NOF patients have impaired functionality

As discussed earlier part of Dominici *et al.*'s criteria of defining an MSC population is the ability to differentiate through osteogenic, adipogenic and chondrogenic lineages (Dominici *et al.*, 2006). I chose to focus on osteogenesis and adipogenesis as differential regulation of these processes have been associated with OP (Abdallah and Kassem, 2012; Bidwell *et al.*, 2013).

The differentiation capacity of MSCs from the two patient groups was assessed by culture in differentiation media. This was to assess the multipotency of each group, and to determine whether MSCs from the NOF group remained as active. It was hypothesised that the NOF group would be relatively more adept at differentiating to adipocytes, and have poorer osteogenic differentiating capacity.

Both patient groups were able to differentiate to osteoblasts and adipocytes in the presence of differentiation media. When compared to a basal control media both groups demonstrated a statistically significant increase in von Kossa staining, evidence of osteogenic differentiation. It was predicted that the NOF MSCs would show a reduced ability to form osteoblasts in comparison to the OA group, however this was not evident.

The impaired adipogenic activity from the NOF MSCs suggests more about the potency of the cells than it does explain a propensity to form osteoblasts in favour of adipocytes. The OA group showed a much greater ability to form mature adipocytes with positive Oil Red O staining, which was statistically significant. The inability of the OP group to produce a statistically significant

increase in Oil Red O staining even with induction suggests that the OP MSCs may be less reactive to differentiation stimuli.

The source of MSCs may have been implicated in the multipotency of the MSCs. This study utilised MSCs from bone marrow. It has been suggested that these have an osteogenic propensity in comparison to other sources, including adipose tissue derived MSCs (Xu *et al.*, 2017; Mohamed-Ahmed *et al.*, 2018).

As discussed in section 1.1.12 the literature remains in equipoise with regards to the ability of OP MSCs to form osteoblasts in comparison to control populations (Bidwell *et al.*, 2013). The previous hypothesis of ageing and osteoporotic MSCs being pro-adipogenic, at the expense of osteogenesis, was refuted by many studies (Stenderup *et al.*, 2001; Veronesi *et al.*, 2014). It appears more nuanced than to suggest that with age bone marrow MSCs have a propensity to the adipogenic lineage and thus the cause of OP MSC dysfunction is not directly in keeping with this simplistic view.

This is supported by Abdallah & Kassem, who disregard the simple notion of an inverse relationship between adipogenesis and osteogenesis in the bone marrow environment (Abdallah and Kassem, 2012). They state that secreted factors from different MSC populations within the bone marrow exert significant regulatory control of differentiation. Furthermore, with regards to osteogenic differentiation of OP MSCs, Prall *et al.* suggest that pre-induction these cells have a reduced osteogenic state, but maintain a sufficient upregulation of osteogenic differentiation on BMP-2 induction (Prall *et al.*, 2013). This group further identified reduced cellular migration and invasion of MSCs from OP patients (Haasters *et al.*, 2014).

The development of OP has many factors. However, determining to what extent the MSC or the local environment is responsible has not yet been addressed. These experiments show a trend of reduced potency of MSCs from patients at significant risk of OP. This identifies limitations of therapies, as a reduced differentiation effect will be exerted in MSCs from this population.

3.4.4 MicroRNA expression in NOF patients shows significant dysregulation

105 microRNAs were observed to be significantly dysregulated between the two patient groups as illustrated by Figure 3-12. Of the significantly dysregulated microRNAs in the NOF group, 63 were seen to be downregulated and 42 upregulated.

PCA is a method of identifying patterns from large datasets. The key data is depicted by principle components and are used to demonstrate the variation within the samples of an experiment. Figure 3-13 displays the PCA plot of the OA vs NOF group and identifies a weak pattern of differential expression between the two groups. It is evident that within each group there is variation, with the NOF samples grouping less tightly and showing the greater degree of variation.

3.4.4.1 Abnormal expression of known microRNAs related to bone fragility is observed in the NOF group

The microRNA expression profiles observed in the NOF group show overlap with known fracture related and OP profiles.

The miR-125 family is seen to be highly conserved in humans and be involved in multiple pathways (Sun, Lin and Chen, 2013). It has been extensively linked to OP and also highlighted as a potential biomarker of the disease (Kelch *et al.*, 2017). In keeping with this miR-125b-2-3p was seen to be significantly overexpressed in the NOF group.

MiR-29a was also seen to be significantly upregulated in the NOF group, and has been shown to be pro-osteogenic, and linked to low bone mass states, (Ko *et al.*, 2015; Materozzi *et al.*, 2018). Within this experimental context it appears to be upregulated to stimulate osteoblastogenesis, rather than suppressed as seen in OP linked states such as glucocorticoid therapy. Furthermore, miR-20a was significantly downregulated in the NOF group, with its known action of increasing osteoblast markers and regulators such as bone morphogenic protein-2 (BMP2), Runt-related transcription factor 2 (RUNX2), osterix (OSX), osteocalcin (OCN) and osteopontin (OPN) (Zhang *et al.*, 2011; Sun *et al.*, 2016).

Conversely miR-21 was significantly down-regulated in the NOF group. Previous research has shown elevated expression post fracture, but it is also known as a marker of OP (Nugent, 2017). MiR-21 has been shown to be down-regulated in both serum and bone samples of patients with OP and is observed to play an important role in osteoblast differentiation from MSCs (Zhao *et al.*, 2018).

Unexpectedly, miR-99a-5p and miR-100-5p were seen to be significantly upregulated within the NOF group. They have been documented in the literature previously to be significantly down-regulated in OP, and have been shown to be regulators of osteoclast activity (Mandourah *et al.*, 2018; Zhou *et al.*, 2019). The observed up-regulation in this experiment is in keeping with an expectant picture post fracture.

MiR-31 has been observed to have significance in the development of OP and potentially as a biomarker, (Materozzi *et al.*, 2018). It has been noted to be upregulated in the serum of female and male patients with OP in comparison to controls, as seen in this study. MiR-31 has been shown to have a pro-osteoclastic effect, by targeting RhoA (Mizoguchi *et al.*, 2013). Furthermore, inhibiting or antagonising miR-31 activity has been shown to be osteogenic (Weilner *et al.*, 2016).

MiR-143 is reported to be involved in several pathways which are of significance to OP. Firstly it was known as a positive regulator of adipogenesis, with increased expression shown in differentiating adipocytes, reported to act through ERK5 (Esau *et al.*, 2004). More recently a Finnish study has shown miR-143 to be down regulated in OP and has identified it as being key to a genetic form of the disease (Riikka Mäkitie *et al.*, 2018). Additionally, MiR-143 is seen to suppress osteogenesis through several pathways. MiR-143 is seen to inhibit the nuclear factor kappa B (NF- κ B) signalling pathway in dental pulp stem cells (Zhang *et al.*, 2018). MiR-143 has also been identified as a negative regulator of OSX, with its up-regulation resulting in decreased osteogenesis (E. Li *et al.*, 2014).

A comparison of the significantly dysregulated microRNA expression in the NOF group was made to the post fracture state. The literature was reviewed, with many studies published on microRNA expression post skeletal injury (Nugent,

2017). MiR-106a is known to inhibit osteoblast differentiation and promote adipogenesis. In keeping with the literature, it was observed to be down-regulated in the NOF group (Inose *et al.*, 2009; Li *et al.*, 2013). MiR-133 has been shown to inhibit RUNX2, and thus osteogenic activity, it has been observed in several studies, and within this experiment to be down-regulated, supporting a pro-osteogenic state (Huang *et al.*, 2010).

MicroRNAs often observed to be dysregulated in osteosarcoma were notably dysregulated in both the over and under expressed in the NOF group. No patient had a known diagnosis of a bone tumour, and these profiles are suggestive of the pro-osteogenic state occurring post fracture. MicroRNAs such as miR-3200 have been shown to be overexpressed in osteosarcoma (Li *et al.*, 2018).

However, low expression of miR-598 is associated with invasiveness and progression of osteosarcoma (Liu *et al.*, 2017), whereas an increased expression was observed in the NOF group. MiR-150 and miR-6868 were down regulated in this dataset and have been shown to be overexpressed in osteosarcomas (Lulla *et al.*, 2011; Xie *et al.*, 2017). In addition. miR-18a-5p was seen to be reduced in its expression, which similarly has been reported to be overexpressed in osteosarcoma (Lu *et al.*, 2018). Therefore, it appears a pro-osteogenic but not malignant state is being produced post fracture, with regulation occurring through different miRNAs.

The NOF group also contained dysregulation of microRNAs related to inflammation and injury, which corresponds well to the clinical situation in comparison to the OA group. The OA group had not suffered any trauma, so should not have had a pro-inflammatory response on culture of their MSCs. This is evident in the upregulation of miR-146a-3p, observed to be crucial to immune and inflammatory responses (Li, Chen and Li, 2010). Furthermore, miR-150 was significantly down-regulated in-keeping with a known inflammatory regulatory mechanism (Sang *et al.*, 2016).

3.4.4.2 Comparison of microRNA expression profile in the NOF group to previous OP research reveals a varied picture

A review of the literature regarding fragility fractures and the pathogenesis of OP was performed. The miRNAs previously noted to be of importance were cross-referenced with the expression data in the NOF and OA group. This is displayed in Table 3-4.

Table 3-4 Table showing previously identified abnormally regulated microRNAs related to OP and their action and the observed expression level in the NOF group within this study. LTFx- low trauma fracture, Fx- fracture, ↑- denotes increased expression, ↓ decreased expression and NS= not statistically significant.

microRNA	Source	Experimental setting	Effect	Action	This study
Let-7g-5p	Weilner (2015)	LTFx vs control	↓	Promotes osteogenic differentiation	↓ NS
miR-100-5p	Seeliger (2014)	OP Fx vs non-OP Fx	↑	Inhibits osteogenic differentiation	↑ * (1.0)
miR-10b-5p	Weilner (2015)	LTFx vs control	↑	Up-regulated during osteogenic differentiation	↑ NS
miR-122a	Seeliger (2014)	OP Fx vs non-OP Fx	↑	Mechanism unknown	↑ NS
miR-124a	Seeliger (2014)	OP Fx vs non-OP Fx	↑	Inhibits Osteoclast differentiation via NFATc1	↓ NS
miR-125b	Seeliger (2014)	OP Fx vs non-OP Fx	↑	Inhibits osteogenic differentiation	↑ NS
miR-133b	Li (2014), Weilner (2015),	LTFx vs control/Low BMD vs normal BMD	↓/↑	Inhibits osteogenic differentiation via RUNX2	↑ NS

miR-328-3p	Weilner (2015)	LTFx vs control	↓	Represses Wnt inhibitor SFRP-1	↑ NS
miR-148a-3p	Seeliger (2014)	OP Fx vs non-OP Fx	↑	Promotes osteoclast differentiation via MAFB	↓ NS
miR-21-5p	Li (2014), Seeliger (2014), Weilner, (2015)	OP Fx vs non-OP Fx, Low BMD vs normal BMD, LTFx vs control	↑/↓	Promotes osteogenic and impairs adipogenic differentiation	↓ NS
miR-22-3p	Weilner (2015)	LTFx vs control	↓	Up-regulated during osteogenic differentiation. Targets Wnt 1, Tcf7, Ep300.	↓ NS
miR-23a-3p	Seeliger (2014)	OP Fx vs non-OP Fx	↑	Inhibits osteogenic differentiation via SATB2	↑ NS
miR-24-3p	Seeliger (2014)	OP Fx vs non-OP Fx	↑	Inhibits osteogenic differentiation via SATB2	↑ NS
miR-93-5p	Seeliger (2014)	OP Fx vs non-OP Fx	↑	Attenuates osteoblast mineralization	↓ NS

Within the literature differing, and often, opposing profiles are observed. There are several factors which could attribute to this. Whilst all the studies aimed to research miRNA expression in patients with OP, the patients used from the samples often differed. For example, some studies had patients in the OP group diagnosed with a DXA scan (H. Li *et al.*, 2014; Seeliger *et al.*, 2014), whereas others had a clinical diagnosis with a low energy NOF (Weilner *et al.*, 2015). The tissue source used may also be of interest, as some studies assessed serum

samples (H. Li *et al.*, 2014), and Weilner *et al* utilising adipose tissue as a source of MSCs. These differences in patient samples and tissue source may account for the varied expression profiles observed, which would be in-keeping with this study using of patients without a formal diagnosis of OP.

Identifying miRNAs consistently dysregulated in both local, disease relevant tissue and serum samples is of importance to identify a diagnostic or biomarker miRNA, which could be of great clinical benefit. Providing a rapid, non-ionising diagnosis of OP would allow quicker initiation of therapy and an improved use of health care resources.

3.4.4.3 Dysregulated microRNA networks

The analysis software used for miRNA expression data predicted several networks to be dysregulated in the NOF group, Figure 3-14, Figure 3-15, Figure 3-16 and Figure 3-17. These pathways were often reported to be linked to organismal injury, in keeping with these patient samples coming from patients who had suffered a fall and fracture.

Figure 3-14 shows a dysregulated network centred upon Argonaute2 (AGO2). AGO2 is part of the argonaute family of proteins, which are essential components of miRNA and small interfering RNA mediated post transcriptional gene-silencing pathways. AGO2 is known to be crucial to the RNA-induced silencing complex (RISC) that endonucleolytically cleaves mRNA of complementary sequence (Martinez and Gregory, 2013). Multiple miRNAs are implicated in this network suggestive of the widespread differences in microRNA expression in the two groups.

Molecules intrinsic to bone physiology were also implicated, with reduced miR-143 and miR-145-5p having an indirect effect on Transgelin (TAGLN). *TAGLN* has been identified as being upregulated during osteoblastic and adipocytic differentiation of MSCs *in vitro*, and deficiency is also noted to lead to reduced cell motility (Elsafadi *et al.*, 2016). This is in keeping with the NOF group having poorer differentiation potential.

Furthermore, Figure 3-15 also shows the dysregulation of key osteogenic molecules in the NOF group. Wnt 2, Wnt 3A and bone morphogenic protein were all implicated within this network (Liu *et al.*, 2013).

Network 3, Figure 3-16, was implicated in the NOF group showing abnormalities in cell death and survival and cell cycle regulation. The upregulation of MiR-31-5p was predicted to indirectly effect CXCL5, and IL1B, which are known to be important pro-inflammatory chemokine and cytokines (Lange *et al.*, 2010; Sepuru, Poluri and Rajarathnam, 2014). This network was centred around BCL2L1 which acts as an apoptotic regulator by controlling outer mitochondrial membrane channels (VDAC). VDAC controls the production of reactive oxygen species and cytochrome C which induce apoptosis. BCL2 in bone has been observed to play an important role in bone strength, and its reduction has been observed to be related to glucocorticoid-induced bone loss (Pantschenko *et al.*, 2005). Furthermore, BCL2L1 was shown to be important in osteoblast differentiation and proliferation, with its overexpression leading to reduced osteoblast apoptosis (Moriishi *et al.*, 2016).

Figure 3-17 depicts network 4, which was predicted to have dysregulation of pathways related to cellular growth and organismal injury. Interestingly NOTCH 1 and NOTCH2 were identified, which are known regulators of osteoblast differentiation (Hilton *et al.*, 2008; Regan and Long, 2013).

The miRNA expression data identified dysregulation of key bone related miRNAs. There was correlation to miRNA profiles of previous OP and of post fracture studies, showing that this group was not specific to either. However, this provides key information for patients at risk of developing OP.

From the above miRNA expression data miR-31 and miR-143 were identified for further investigation into their roles in MSC differentiation and osteogenesis.

3.4.4.4 MicroCT data

The microCT analysis produced somewhat unexpected results upon comparisons of the two groups. The highest BV/TV and trabecular thickness values were observed in the NOF group, in patients at risk of, or suffering from OP. OP is

known as a quantitative bone condition, and it was hypothesised that the microCT data would demonstrate thinner, less dense trabecular bone within the femoral heads.

A similar, but not exact, trend of BV/TV was observed in the VOIs of both patient groups. VOI 1 corresponded to the area of greatest BV/TV in both patient groups. Corresponding to the centre of the femoral head, this result is in keeping with the expected higher areas of density.

VOI 4 was observed to have the lowest BV/TV in the OA group, corresponding to the most lateral area of the femoral head, at a transition point to the femoral neck. This was statistically significant in the OA group when comparing VOI 1 and VOI 4. When further analysing the groups, the more heterogeneous nature of the NOF group becomes apparent, Figure 3-20. A greater range of BV/TV is observed in the VOIs, with notable inter-patient variability. Large discrepancies are observed from the VOI with the highest BV/TV value to the VOI with the lowest. This is in contrast to the OA group, Figure 3-19, with a reduced range of BV/TV values within the VOIs in each sample.

In keeping with the BV/TV data the greatest trabecular thickness values were observed in the NOF group, again associated with large inter-sample variability in the NOF group. Neither group demonstrated significant variation in trabecular thickness throughout the femoral head.

Figure 3-22 demonstrates the trabecular separation observed within each VOI of the femoral head samples. The OA group was seen to have significant variation in distance between trabeculae, between VOI 1 and 4. A similar trend was observed in the NOF group. However, this did not reach statistical significance. As expected, the trabeculae were most widely spread in VOI 4, which corresponds to the most lateral portion of the femoral head. It is at this area where the femoral head blends with the femoral neck.

In both groups VOI 1 was seen to have the most closely associated trabeculae, in keeping with a dense area of bone. VOI 1 corresponds to the most central portion of the femoral head, and this data correlates well to macroscopic observations of the specimens. VOI 6 represents the upper central portion of

bone analysed in the femoral heads which is thought to represent a low-density region within the femoral head. Within the NOF group VOI 6 demonstrated greater trabecular separation in keeping with previous research (Jenkins *et al.*, 2013). This is of importance for surgical procedures, where metalwork is inserted to the femoral head, and areas of strong bone are sought to prevent failure of the implant (Baumgaertner *et al.*, 1995; Parmar *et al.*, 2005).

Figure 3-23 demonstrates the trabecular number observed in VOIs in both groups. In keeping with the separation analysis, VOI 1 contained the greatest number of trabeculae in both groups. In the OA group a statistically significant increase in trabecular number was observed when comparing VOI1 to VOI 4. The overall trend was similar in the two groups, however in the NOF group the lowest trabecular number was observed in VOI 2, and no significant variation was observed. The OA group demonstrated variation in trabecular number throughout the femoral head, whereas a more consistent level was observed in the NOF group, with the exception of VOI 1.

Variation in degree of anisotropy was seen throughout the femoral heads in both groups, Figure 3-25. This reached statistical significance in the OA group only. VOI 2 contained the lowest DA in the OA group, suggestive of containing the most plate like-trabeculae. Interestingly the lowest DA value in the NOF group was observed in VOI 4, the most lateral area assessed. Similar trends were observed in both groups, with a greater variability evident in the NOF group. This is in keeping with previous research into variation of DA in femoral heads of patients with OP (Jenkins *et al.*, 2013).

Structural model index (SMI) and connectivity density values failed to reach statistically significant variation throughout the VOIs. SMI values followed a similar pattern in the femoral head in both groups, with the OA group demonstrating predominantly higher values. VOI 1 in both groups showed the lowest value, indicative of dense, plate like orientation of bone in this region. Connectivity density values were lower in the NOF group, again with great inter-sample variability, which is in keeping with previous findings (Zupan *et al.*, 2013). This is suggestive of improved inter-connections between trabeculae in the OA group throughout the femoral heads, with the exception of VOI 4.

These results demonstrate a variability in micro-architectural characteristics throughout the adult femoral head. Despite the presence of disease, the OA group demonstrated more consistent results throughout the patient samples and demonstrated the only statistically significant results. It is interesting to note that when analysing trabecular characteristics in the NOF group a more uniform picture is observed across the VOIs. It was hypothesised that a variation in trabecular characteristics would be seen throughout the femoral head, as per Wolff's law (Wolff and Wolff, 1986), due to bone deposition being relative to the stress produced within that VOI. However, in the NOF group this was not observed. Osteoporosis is known to produce thinner and defective trabeculae and this data may suggest that patients at risk of the disease have globally impaired trabeculae within the femoral head.

A limitation of the microCT data was the restriction of the analyses to only trabecular bone within the femoral head. It is known that significant cortical thinning is present in patients with proximal femoral fractures (Bell *et al.*, 1999). This may be more responsible for the propensity to hip fractures which patients with OP suffer than changes in trabecular size and number. Unfortunately, samples within the NOF group only included the femoral head, and therefore analyses on the cortices of the femoral neck could not be performed.

The microCT data was not as hypothesised, with the NOF group having similar mean levels of micro-architectural indices, indicative of strength and density. However, these patients are at high risk of developing OP and by definition have already suffered a fragility fracture. This NOF group is still representative of this patient population, who after suffering such an injury are known to be at high risk of, or have undiagnosed, OP. Furthermore, the miRNA expression profiles of the NOF group, again, are associated with OP profiles observed in the literature, providing more evidence that this group is representative and relevant to patients at risk of OP.

Conclusion

A thorough assessment of the bone biology of both groups has been undertaken in this chapter. Flow cytometric analysis revealed the consistent MSC expression and lack of HSC expression in both patient groups. Furthermore, a reduction in expression of key MSC markers linked to cell mobility and differentiation was observed in the NOF group. In keeping with the flow data, the propensity of MSCs from the NOF group to differentiate in conditioned media was significantly reduced. These experiments highlight an impaired functionality of MSCs from patients at risk of OP.

The dysfunction of MSCs in the NOF group was further highlighted by multiple abnormally expressed miRNAs which have key roles in differentiation and osteogenesis. MicroCT analysis of the NOF group revealed large variations in bone indices within the group, in comparison to a more uniform picture within the OA group.

These results provide insight to the impaired bone health of patients at risk of OP and will help direct future research into therapeutic targets.

Chapter 4

4 An assessment of mesenchymal stromal cell differentiation following microRNA manipulation

4.1 Introduction

Increasingly miRNAs are being investigated for their therapeutic potential in many diseases (Hanna, Hossain and Kocerha, 2019). Clinical trials are underway for their use in many pathological conditions within several different organ sites, such as miR-16 for mesothelioma, miR-92 for heart failure and miR-29a in tendon injury (van Zandwijk *et al.*, 2017; Watts *et al.*, 2017; Bonneau *et al.*, 2019). There is great hope that they can be utilised in diseases such as OP.

In this chapter, the effect the miRNA mimic 143 has on adipogenesis with MSCs from two patient groups, OA and NOF, group will be assessed. AntagomiR-31 will be cultured with MSCs to assess if it can increase osteogenesis in both patient groups, and be a potential target for improving bone quality in patients at risk of fragility fractures.

MicroRNA-31 has been shown previously to significantly influence osteogenesis, and when impaired, can result in improved mineralisation (Weilner *et al.*, 2016). Furthermore, it is known to be upregulated in patients with OP (Materozzi *et al.*, 2018). Manipulating the function of MiR-31 has a potentially important role in developing new therapeutics for the treatment of impaired bone quality.

Previously published in the literature, and evident here in the miRNA array, MiR-143 is dysregulated in patients with OP and recent fragility fractures (Mäkitie *et al.*, 2018). Its role has previously been linked with adipogenesis (Esau *et al.*, 2004), more recently a negative regulatory role of osteogenesis has been described (E. Li *et al.*, 2014). As such it is of importance to understand more about its role in MSC function and bone fragility.

Differentiating cells have been shown to have heightened metabolic activity, while quiescent stem cells have relatively inactive metabolism (Chung *et al.*, 2007; Yanes *et al.*, 2010). The increase in metabolism has been previously reported to occur rapidly (Reyes *et al.*, 2006) and metabolomic studies are being

increasingly utilised in bioengineering research to gain greater insight into the effect on MSCs. Several key areas of metabolism are commonly assessed to determine a manipulation of differentiation (Tsimbouri *et al.*, 2012). Amino acid metabolism, with the presence of an increased abundance of amino acids correlated to differentiation (Sampath *et al.*, 2008), carbohydrate metabolism and respiration shown to be enhanced during MSC differentiation (Varum *et al.*, 2011) and lipid metabolism, with specific lipids observed to be depleted during osteogenesis (Alakpa *et al.*, 2016), are key metabolic pathways to be interrogated to understand differentiation induced by miRNA manipulation.

Due to the cost implications of performing metabolomic analysis only miR-31 will be investigated by this technique.

4.2 Objectives

This chapter has three main objectives

1. To manipulate adipogenesis via a miR-143 mimic and to determine the effect on differentiation at a gene and protein level
2. To manipulate osteogenesis via a miR-31 inhibitor and to determine the effect on differentiation at a gene and protein level
3. To identify the mechanism of miRNA manipulation on osteogenic differentiation at a metabolite level

4.3 Materials and Methods

4.3.1 Cell Culture

In this chapter bone marrow extraction was performed from the OA and NOF groups, and culture of MSCs in monolayer was as described in section 2.4.1. The cells were seeded from growing flasks at a concentration of 2000 cells per cm² and after allowing 24 hours of attachment the media was exchanged for the conditions described in Table 2-3. After 48 hours of incubation the media were exchanged and for the remaining time in culture did not include nanoparticles. Cells were cultured for 7 days.

4.3.2 Nanoparticles

MicroRNA-143 mimic and AntagomiR-31 (AmiR-31) were delivered on gold thiolated nanoparticles. Non-targeting nanoparticles were also utilised. See section 2.5.2 for further information.

4.3.3 Differentiation Media

In addition to basal media, differentiation media, to stimulate differentiation, was used to act as a positive control in both experiments, Section 2.4.3 describes their constituents.

4.3.4 Quantitative real-time (qRT)-PCR

qRT-PCR was utilised to quantitatively assess gene expression at day 7 with regards to osteogenesis and adipogenesis in the AmiR-31 and miR-143 mimic cultures respectively. Full details of the qRT-PCR process is described in sections 2.12 - 2.14.

4.3.5 In Cell Western™ (ICW)

Described in full in section 2.11, immunostaining and analysis by ICW was performed at day 7. Samples were scanned with detection in the 800 nm channel for the protein of interest, and in the 700 nm channel for the detection of CellTag fluorescence, which was indicative of observed cell number.

Fluorescence units in the 800 nm channel were divided by the 700 nm channel to determine levels of expression within each culture condition.

4.3.6 Metabolomic analysis

An IDEOM excel interface file was generated by the University of Glasgow Polyomics facility. Metabolites were identified from this IDEOM file in conjunction with the Kyoto Encyclopaedia of Genes and Genomes (KEGG) database (Kanehisa *et al.*, 2012). Data relating to specific metabolism areas, such as amino acid, carbohydrate and lipid, were exported from the IDEOM interface and further analysed using Metaboanalyst. Metaboanalyst was utilised to generate principal component analysis plots (PCA) and heatmaps (Xia *et al.*, 2015).

4.4 Results

4.4.1 MicroRNA-143 mimic culture

4.4.1.1 qRT-PCR analysis

MiR-143 mimic was cultured with MSCs from both patient groups, in basal and adipogenic media. At Day 7 the effect on PPAR γ expression was analysed by qRT-PCR. This is displayed in Figure 4-1, and demonstrates the positive effect of the adipogenic induction media. In both patient groups an increase in PPAR γ expression was evident with the positive control culture medium; however no statistically significant increase was observed in any condition. In the basal conditions, no appreciable difference in PPAR γ expression was observed.

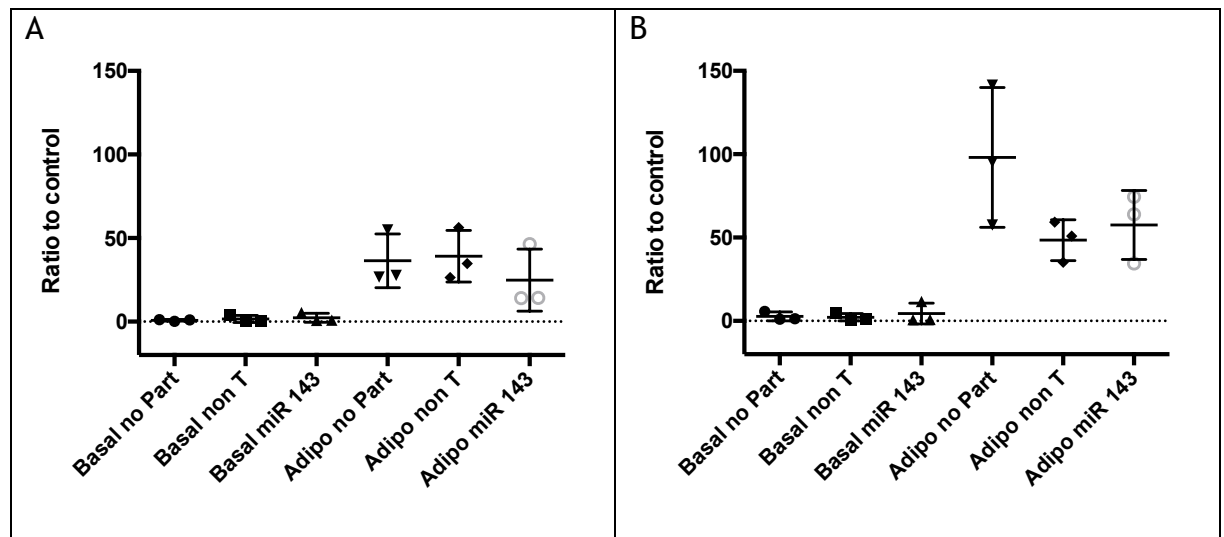


Figure 4-1 qRT-PCR analysis of PPAR γ at day 7 culture of OA and NOF MSCs in miR-143 experimentation. Ratio of expression in comparison to reference gene GAPDH. The addition of adipogenic media resulted in increase in PPAR γ expression in both patient groups, without responding to one condition specifically. A = OA group, B = NOF group. Basal no part = basal media; Basal non T = basal media and non targeting nanoparticles; Basal miR-143 = basal media and miR-143 mimic nanoparticles; Adipo no part = adipogenic induction media; Adipo non T = adipogenic induction media and non targeting nanoparticles; Adipo miR-143 = adipogenic induction media and miR-143 mimic nanoparticles. Each culture condition represents 3 patients with 2 technical replicates. Results are mean with standard deviation. No statistical significance reached upon Kruskal-Wallis analysis.

FABP was also assessed at day 7, and displayed in Figure 4-2. No statistically significant difference in FABP expression was noted in any condition in both patient groups. Intra-group variation within each condition was notable in both patient groups.

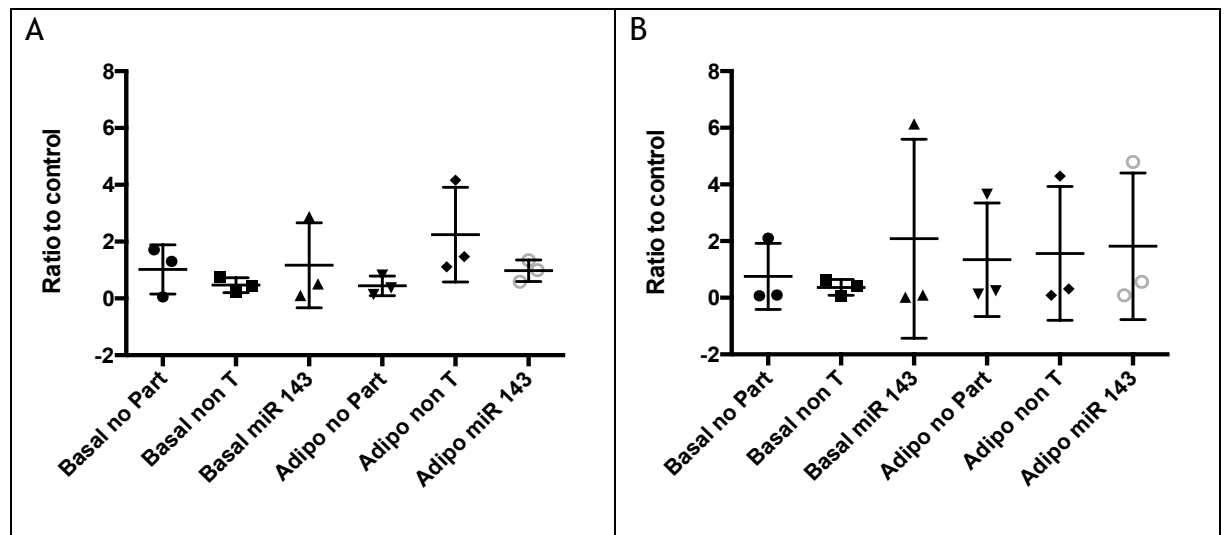


Figure 4-2 qRT-PCR analysis of FABP at day 7 culture of OA and NOF MSCs in miR-143 experimentation. Ratio of expression in comparison to reference gene GAPDH. No clear increase in FABP expression was noted upon addition of miR-143 mimic or adipogenic media in either patient group. A = OA group, B = NOF group. Basal no part = basal media; Basal non T = basal media and non targeting nanoparticles; Basal miR-143 = basal media and miR-143 mimic nanoparticles; Adipo no part = adipogenic induction media; Adipo non T = adipogenic induction media and non targeting nanoparticles; Adipo miR-143 = adipogenic induction media and miR-143 mimic nanoparticles. Each culture condition represents 3 patients with 2 technical replicates. Results are mean with standard deviation. No statistical significance reached upon Kruskal-Wallis analysis.

4.4.1.2 In Cell Western™ analysis miR-143

In Cell Western analysis was used to determine the protein expression of PPAR γ at day 7, Figure 4-3. The OA group demonstrated a positive adipogenic response to the induction media, with the highest expression observed in the Adipo-miR-143 group. No appreciable trend of increased PPAR γ expression in the NOF group was noted.

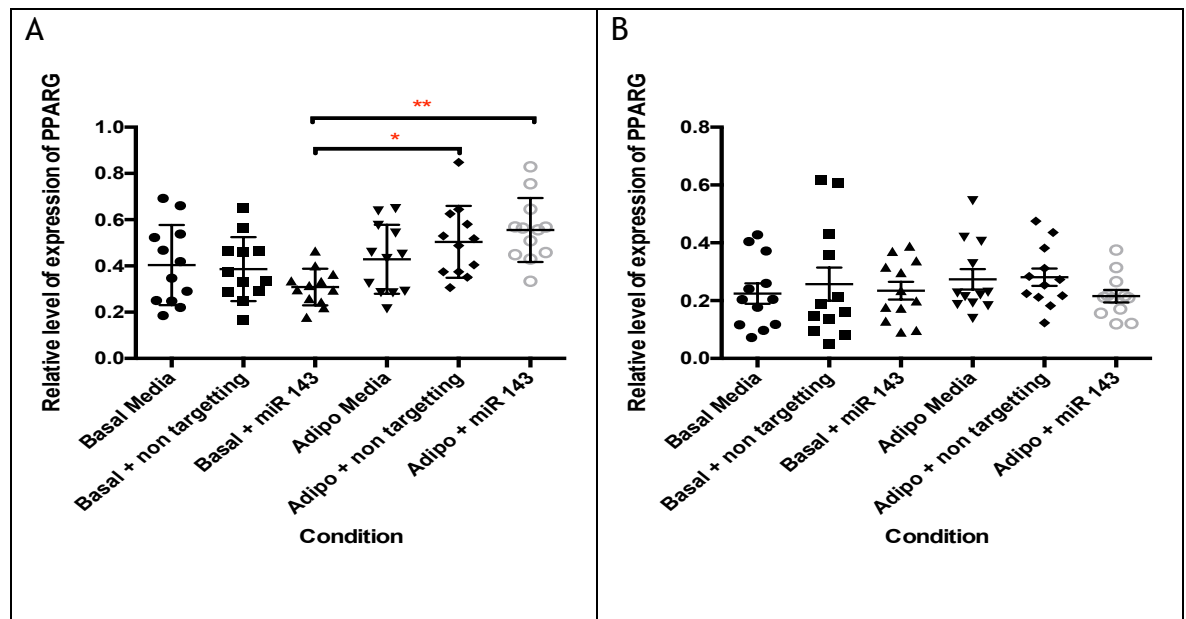


Figure 4-3 In Cell Western™ analysis of PPAR γ protein expression of OA and NOF MSCs in miR-143 experimentation. Within the OA group the addition of adipogenic media resulted in increased expression of PPAR γ most notably with the addition of miR-143 mimic. No appreciable trend of increased expression was noted in the NOF group. A = OA group, B = NOF group. Basal no part = basal media; Basal non T = basal media and non targeting nanoparticles; Basal miR-143 = basal media and miR-143 mimic nanoparticles; Adipo no part = adipogenic induction media; Adipo non T = adipogenic induction media and non targeting nanoparticles; Adipo miR-143 = adipogenic induction media and miR-143 mimic nanoparticles. Each culture condition represents 3 patients with 4 technical replicates. Results are mean with standard error of mean. Statistical analysis by Kruskal-Wallis, * $P \leq 0.05$, ** $P \leq 0.01$.

4.4.2 AntagomiR-31 culture

4.4.2.1 qRT-PCR analysis

AmiR-31 was cultured with MSCs from both patient groups, in basal and osteogenic media. At day 7, the effect on osteogenic differentiation was assessed by analysing Osterix and RUNX2 expression by qRT-PCR. This is displayed in Figure 4-4 and Figure 4-5.

At day 7 of culture no statistically significant increase in either gene were observed in either group or condition. RUNX2 expression in the NOF group demonstrated a trend of increased expression in the osteogenic media conditions.

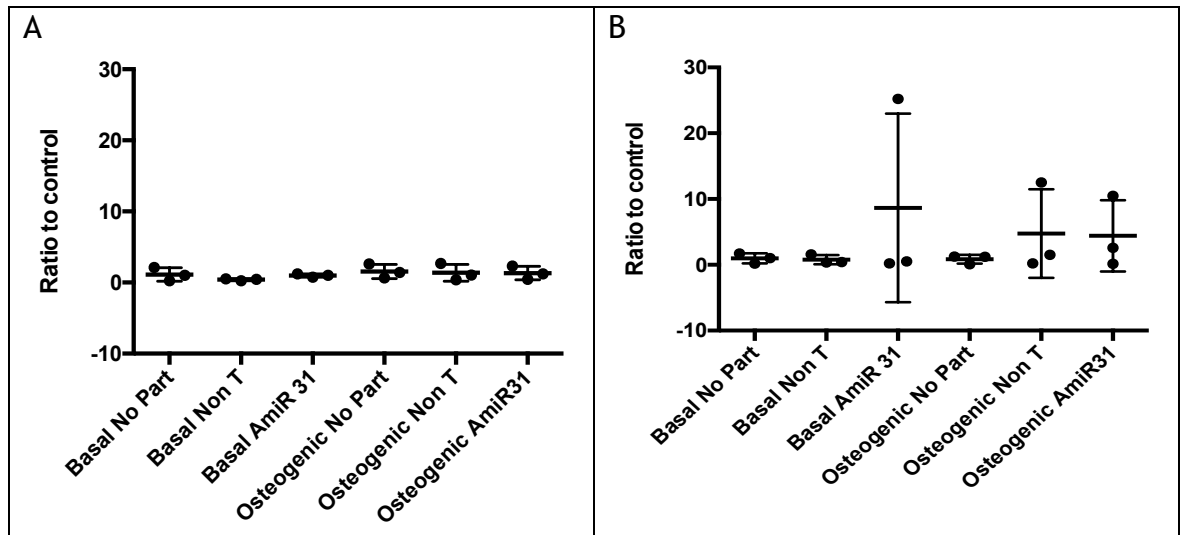


Figure 4-4 qRT-PCR analysis of Osterix at day 7 culture of OA and NOF MSCs in AntagomiR-31 experimentation. Ratio of expression in comparison to reference gene GAPDH. Minimal increase in Osterix expression was observed in the OA group within the osteogenic media conditions, with the NOF group showing no consistent trend. A= OA group, B = NOF group. Basal no part = basal media; Basal non T = basal media and non targeting nanoparticles; Basal AmiR-31 = basal media and AmiR-31 nanoparticles; Osteogenic no part = osteogenic induction media; Osteogenic non T = osteogenic induction media and non targeting nanoparticles; Osteogenic AmiR-31 = osteogenic induction media and AmiR-31 nanoparticles. Each culture condition represents 3 patients with 2 technical replicates. Results are mean with standard deviation. No statistical significance reached upon Kruskal-Wallis analysis.

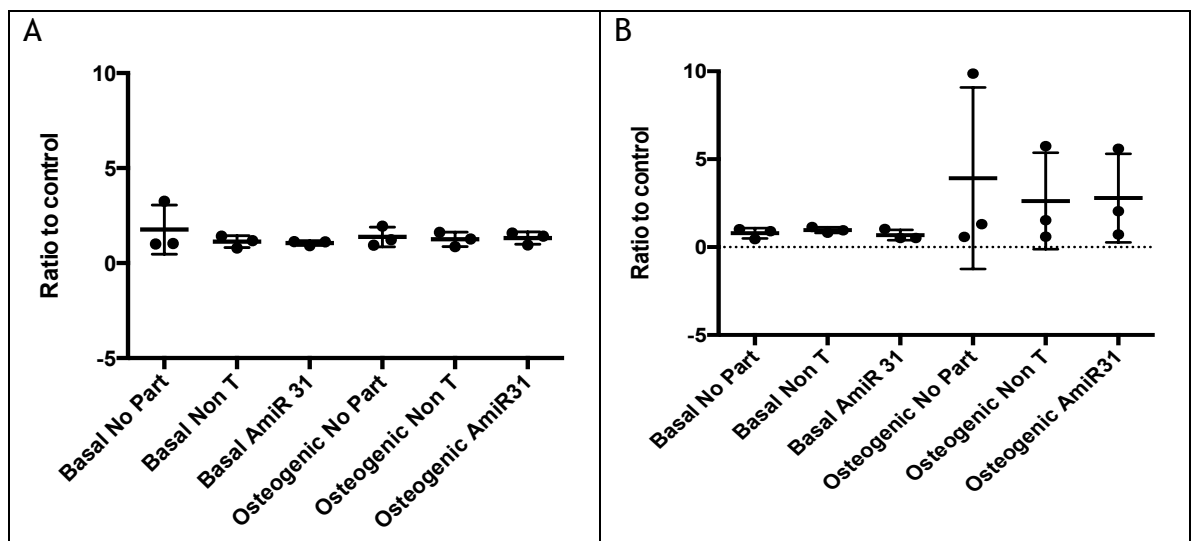


Figure 4-5 qRT-PCR analysis of RUNX2 expression at day 7 culture of OA and NOF MSCs in AntagomiR-31 experimentation. Ratio of expression in comparison to reference gene GAPDH. A trend to increased RUNX2 expression was observed in the NOF group. No change was evident in the OA group. A = OA group, B = NOF group. Basal no part = basal media; Basal non T = basal media and non targeting nanoparticles; Basal AmiR-31 = basal media and AmiR-31 nanoparticles; Osteogenic no part = osteogenic induction media; Osteogenic non T = osteogenic induction media and non targeting nanoparticles; Osteogenic AmiR-31 = osteogenic induction media and AmiR-31 nanoparticles. Each culture condition represents 3 patients with 2 technical replicates. Results are mean with standard deviation. No statistical significance reached upon Kruskal-Wallis analysis.

4.4.2.2 In Cell Western™ analysis AntagomiR-31

Figure 4-6 demonstrates the day 7 Osterix protein expression levels. A trend of increased osteogenic activity was observed in the OA group within the AmiR-31 conditions, reaching statistical significance in the Osteo + AmiR-31 condition in comparison to basal media alone. A similar trend is visible in the NOF group, but did not reach statistical significance.

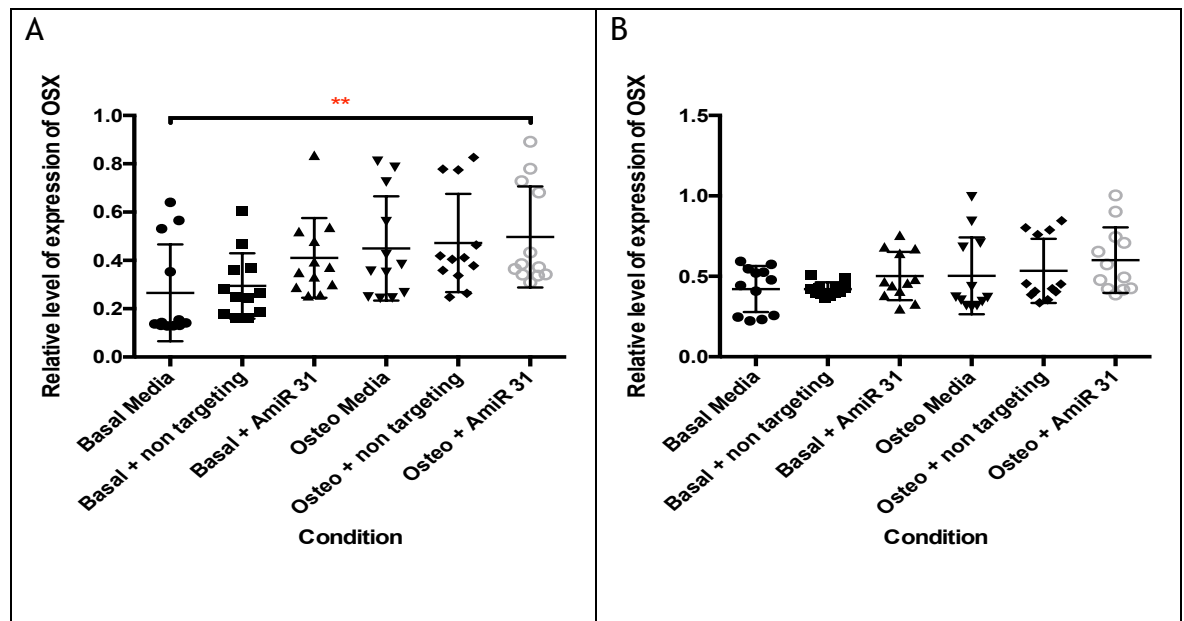


Figure 4-6 In Cell Western™ analysis of Osterix protein expression of OA and NOF MSCs in AntagomiR-31 experimentation. The addition of AmiR-31 to basal media resulted in increased Osterix expression, with an increased effect evident in the osteogenic media with AmiR-31. This was notable in both patient groups, but statistically significant only in the OA group. A = OA group, B = NOF group. Basal no part = basal media; Basal non T = basal media and non targeting nanoparticles; Basal AmiR-31 = basal media and AmiR-31 nanoparticles; Osteo media = osteogenic media; Osteo non targeting = osteogenic media and non targeting nanoparticles; Osteo + AmiR-31 = osteogenic media and AmiR-31 nanoparticles. Each culture condition represents 3 patients with 4 technical replicates. Results are mean with standard error of mean. Statistical analysis by Kruskal-Wallis, ** $P \leq 0.01$.

4.4.2.3 Metabolomics

The metabolomic effect on MSCs was assessed at Day 7 in the AmiR-31 culture experiment. All 6 culture conditions were assessed in 3 patients from the OA and NOF group.

Heatmaps are utilised in the following figures to allow easy recognition of fold changes in the abundance of metabolites present in each culture condition. The metabolites are ranked from hot (shown as dark red colours, indicating increased

abundance) to cold (shown as dark blue colours, indicating decreased abundance).

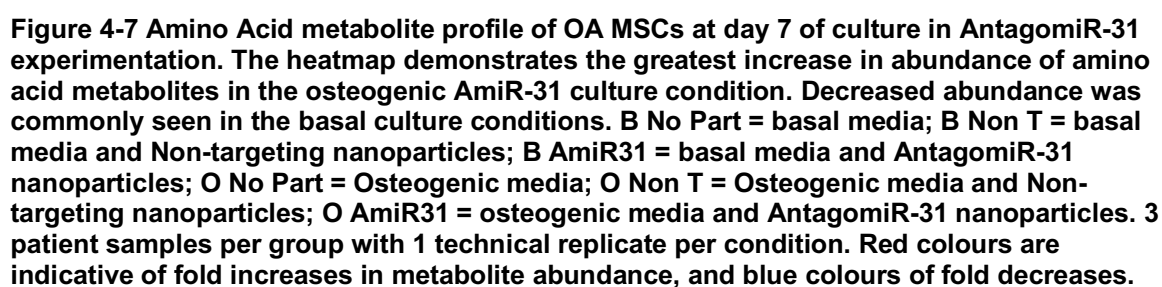
Principal component analysis (PCA) plots are also utilised in the following figures, which use scatter plots to demonstrate variance within data sets.

Finally, networks demonstrating the potential effect of the change in metabolites observed in the treatment conditions were generated through the use of IPA software.

4.4.2.4 Amino acid metabolism

The heat map in Figure 4-7 demonstrates the variation in amount of amino acid metabolites present in the specific culture conditions. Most notably a high abundance of amino acid metabolites were present in the AmiR-31 culture condition with the addition of osteogenic media. This was present both in the OA and NOF group, with 2 patients in each group showing a strong response.

Low levels, indicated by blue colouring in the heatmap, indicative of a more quiescent culture environment, were observed more frequently when the AmiR-31 nanoparticles and osteogenic media were not present.



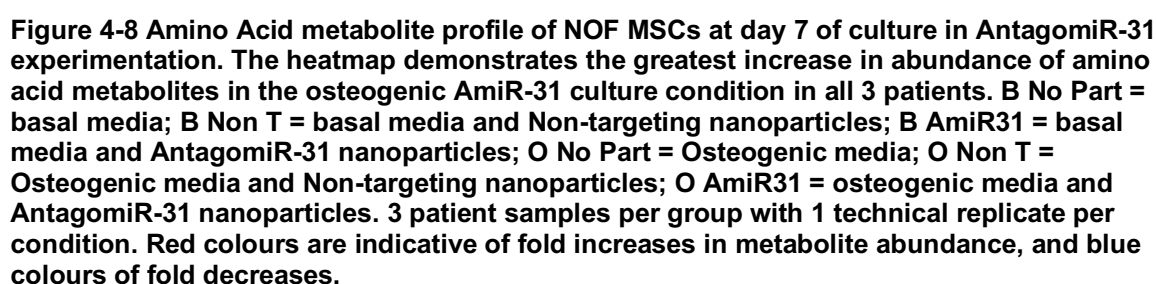


Figure 4-9 displays the PCA plot of amino acid metabolism and displays overlap between the conditions, evident in both patient groups. However, in both groups the osteogenic AmiR-31 group is seen to differ most in comparison to the other culture conditions, suggestive of a drive towards osteogenesis. The remaining conditions clustered closely in the NOF group.

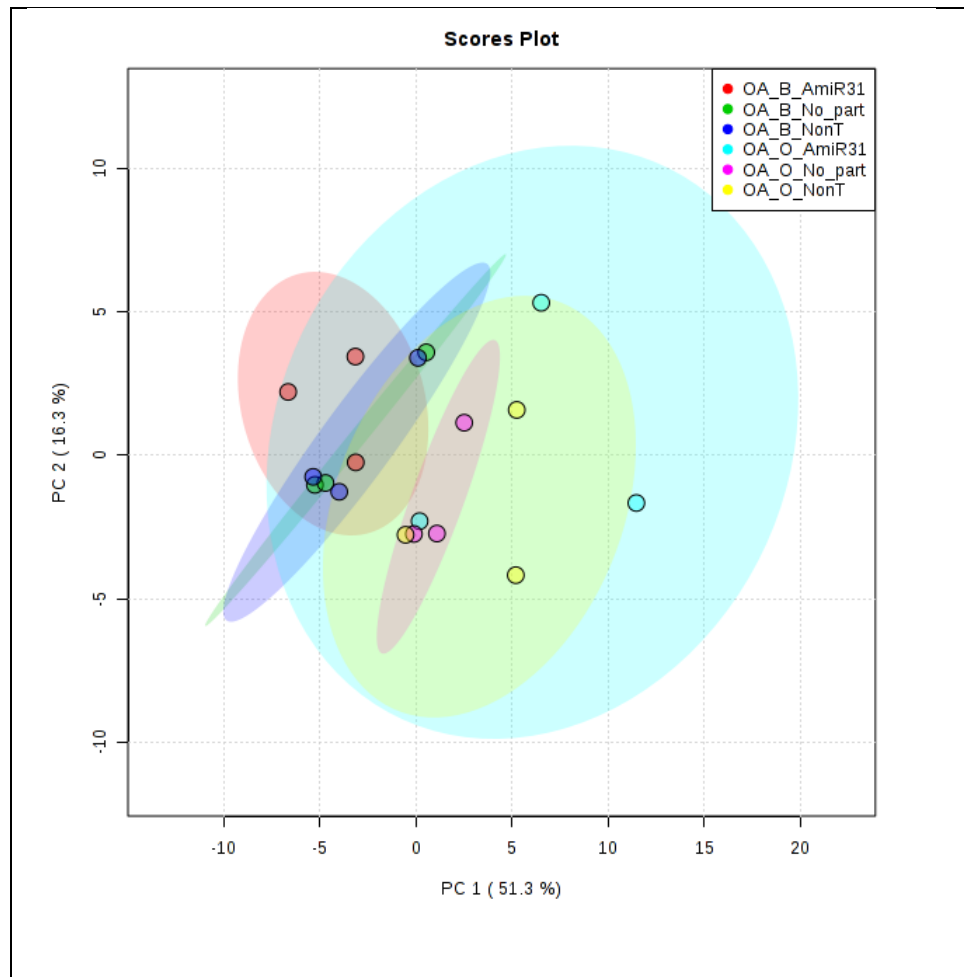


Figure 4-9 PCA plot of amino acid metabolites detected at day 7 of MSC culture in the OA group AntagomiR-31 experimentation. Within the OA group variation between basal and osteogenic conditions was noted with the Osteogenic media and AmiR-31 condition showing large differences. Data sets were derived from putative amino acid metabolites identified within the different culture conditions at day 7 of culture. B No Part = basal media; B Non T = basal media and Non-targeting nanoparticles; B AmiR31 = basal media and AntagomiR-31 nanoparticles; O No Part = Osteogenic media; O Non T = Osteogenic media and Non-targeting nanoparticles; O AmiR31 = osteogenic media and AntagomiR-31 nanoparticle. Points represent individual samples of each condition. 3 patient samples per group with 1 technical replicate per condition. The coloured ellipses represent the spatial borders associated with each condition, to a 95% confidence interval.

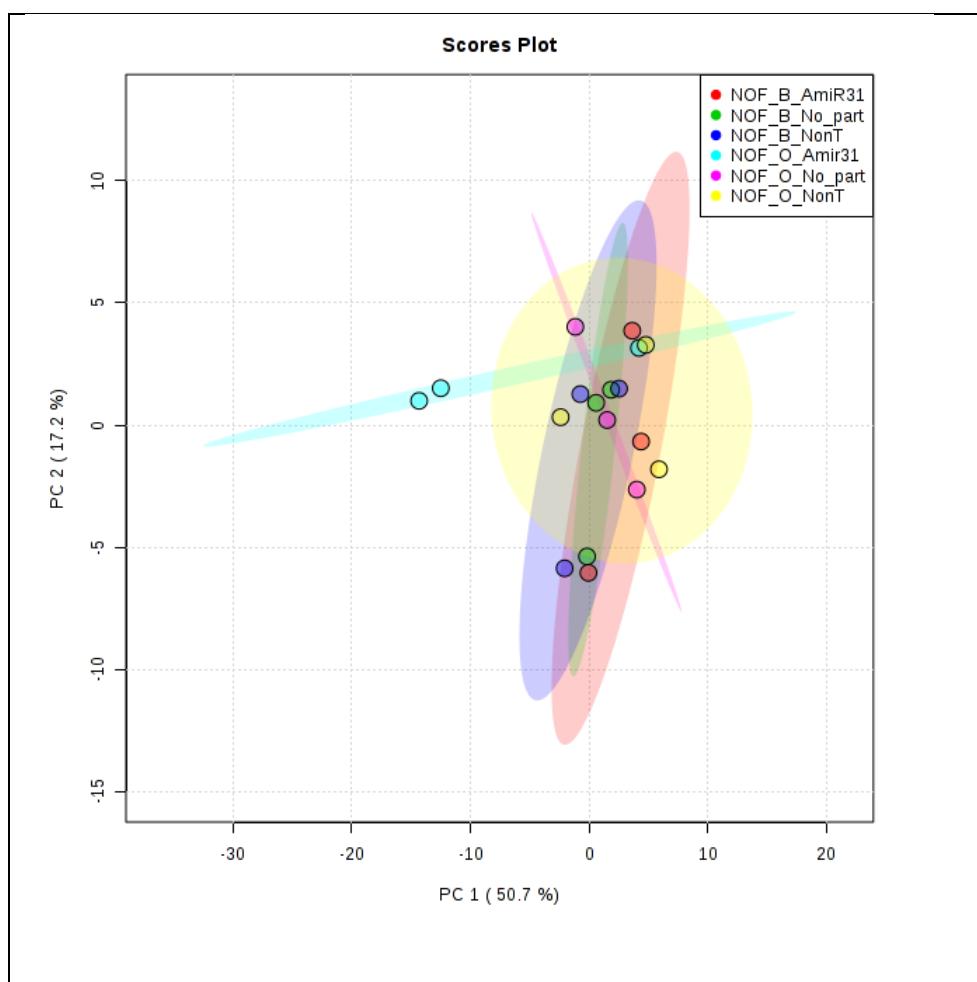


Figure 4-10 PCA plot of amino acid metabolites detected at day 7 of MSC culture in the NOF group AntagomiR-31 experimentation. Within the NOF group the Osteogenic media and AmiR-31 condition lead to the greatest variation, with clustering of the remaining conditions observed. Data sets were derived from putative amino acid metabolites identified within the different culture conditions at day 7 of culture. B No Part = basal media; B Non T = basal media and Non-targeting nanoparticles; B AmiR31 = basal media and AntagomiR-31 nanoparticles; O No Part = Osteogenic media; O Non T = Osteogenic media and Non-targeting nanoparticles; O AmiR31 = osteogenic media and AntagomiR-31 nanoparticles. Points represent individual samples of each condition. 3 patient samples per group with 1 technical replicate per condition. The coloured ellipses represent the spatial borders associated with each condition, to a 95% confidence interval.

4.4.2.5 Carbohydrate metabolism

Carbohydrate metabolism was observed to differ greatly in the OA group. This is striking in the PCA plot, Figure 4-11. The greatest decrease in both PC1 and PC2 was noted in the OA Osteogenic AmiR31 condition. No overlap is observed in the basal and osteogenic media PCA in the OA group. The NOF group showed closer groupings on PCA analysis, with the largest divergence between the NOF Basal AmiR31 and Osteogenic AmiR31.

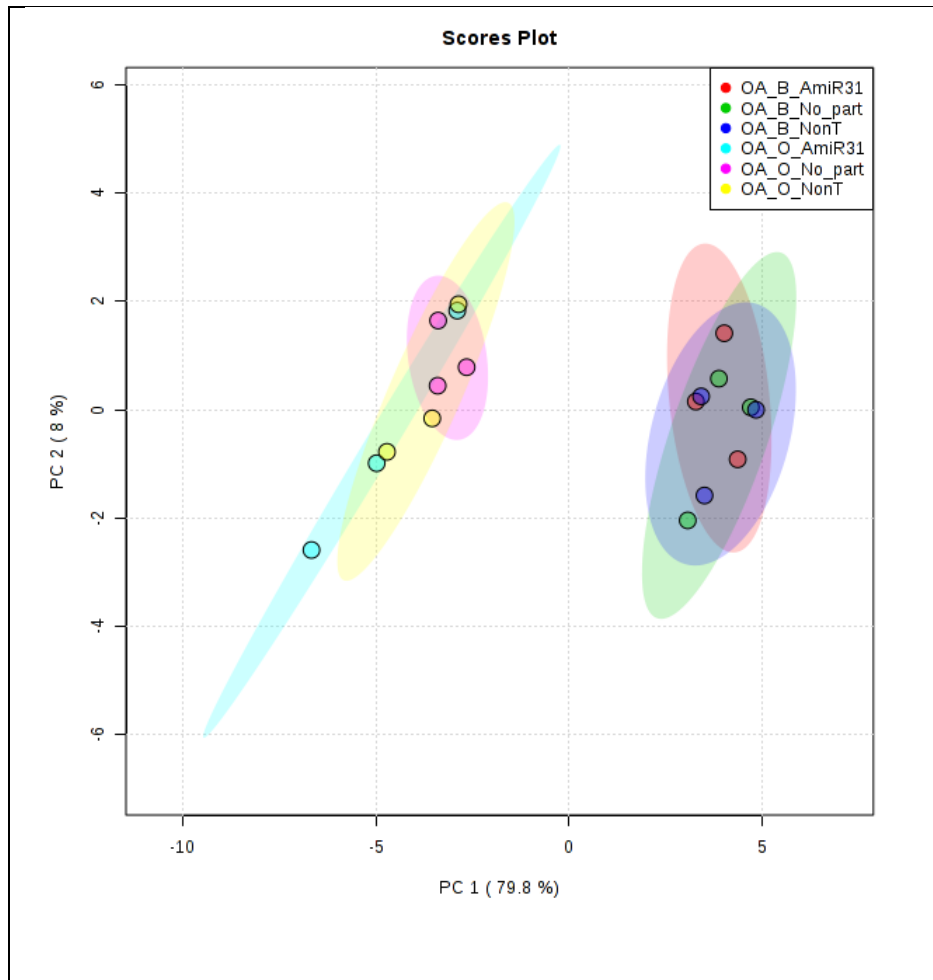


Figure 4-11 PCA plot of carbohydrate metabolites detected at day 7 of MSC culture in the OA group AntagomiR-31 experimentation. Large separation was observed in the osteogenic media conditions in the OA group. The osteogenic media and AmiR-31 condition differed most notably from the other conditions. Data sets were derived from putative carbohydrate metabolites identified within the different culture conditions at day 7 of culture. B No Part = basal media; B Non T = basal media and Non-targeting nanoparticles; B AmiR31 = basal media and AntagomiR-31 nanoparticles; O No Part = Osteogenic media; O Non T = Osteogenic media and Non-targeting nanoparticles; O AmiR31 = osteogenic media and AntagomiR-31 nanoparticles. Points represent individual samples of each condition. 3 patient samples per group with 1 technical replicate per condition. The coloured ellipses represent the spatial borders associated with each condition, to a 95% confidence interval.

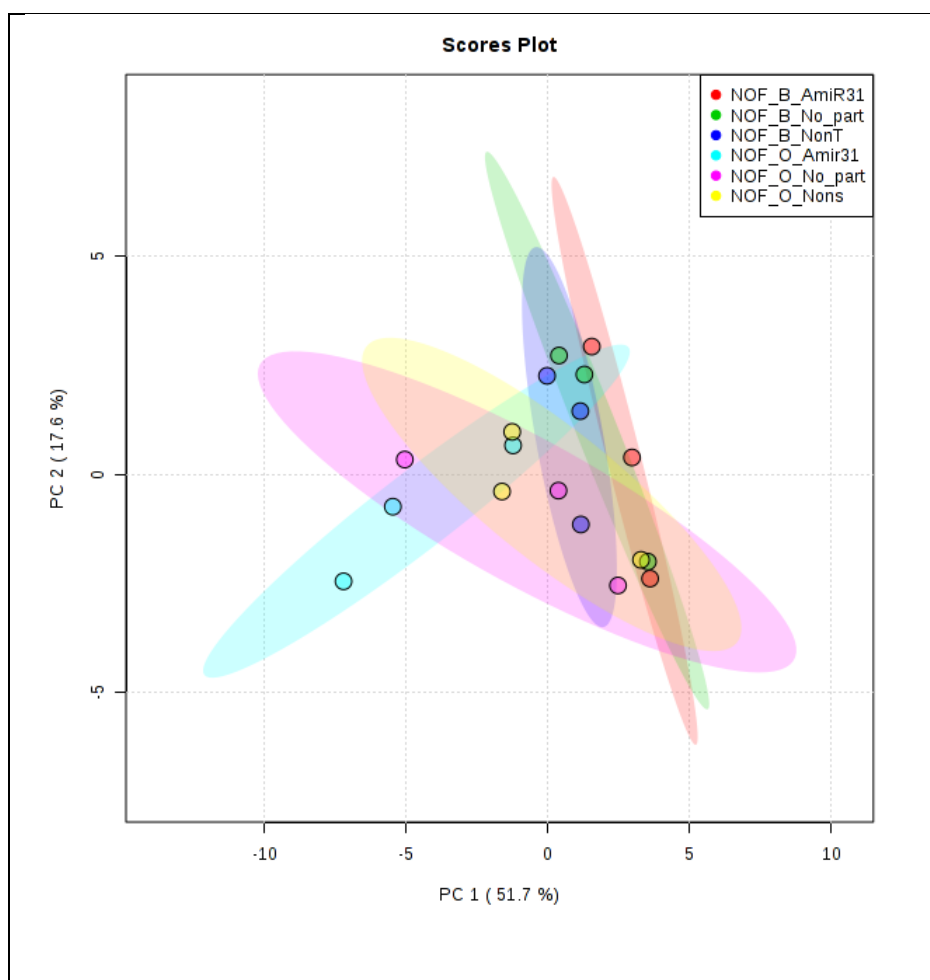


Figure 4-12 PCA plot of carbohydrate metabolites detected at day 7 of MSC culture in the NOF group AntagomiR-31 experimentation. A trend of separation is noted in the osteogenic media conditions in comparison to the basal. Data sets were derived from putative carbohydrate metabolites identified within the different culture conditions at day 7 of culture. B No Part = basal media; B Non T = basal media and Non-targeting nanoparticles; B AmiR31 = basal media and AntagomiR-31 nanoparticles; O No Part = Osteogenic media; O Non T = Osteogenic media and Non-targeting nanoparticles; O AmiR31 = osteogenic media and AntagomiR-31 nanoparticles. Points represent individual samples of each condition. 3 patient samples per group with 1 technical replicate per condition. The coloured ellipses represent the spatial borders associated with each condition, to a 95% confidence interval.

The above PCA findings are corroborated by the accompanying heatmap, shown in Figure 4-13. In both patient groups the greatest abundance of carbohydrate metabolites was observed in the osteogenic AmiR-31 condition. In the OA group a clear increase in carbohydrate metabolite presence was observed in all osteogenic conditions in comparison to basal media. These findings were also observed, but more subtly in the NOF group.

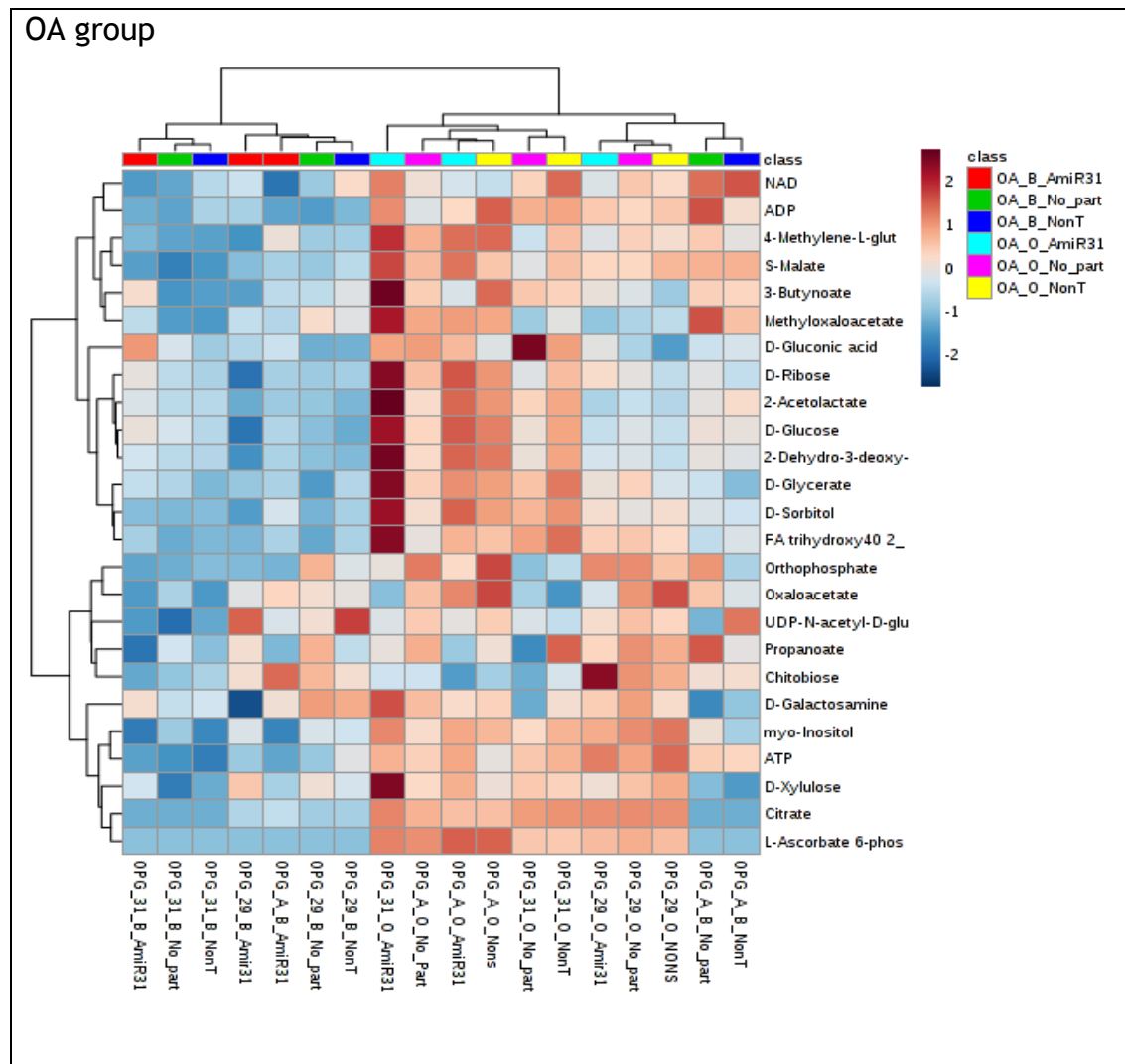


Figure 4-13 Carbohydrate metabolite profile of OA group MSCs at day 7 of culture in AntagomiR-31 experimentation. The heatmap demonstrates a trend to increased abundance of carbohydrate metabolites in the osteogenic conditions, the strongest observed in the osteogenic and AmiR-31 culture condition. B No Part = basal media; B Non T = basal media and Non-targeting nanoparticles; B AmiR31 = basal media and AntagomiR-31 nanoparticles; O No Part = Osteogenic media; O Non T = Osteogenic media and Non-targeting nanoparticles; O AmiR31 = osteogenic media and AntagomiR-31 nanoparticles. 3 patient samples per group with 1 technical replicate per condition. Red colours are indicative of fold increases in metabolite abundance, and blue colours of fold decreases.

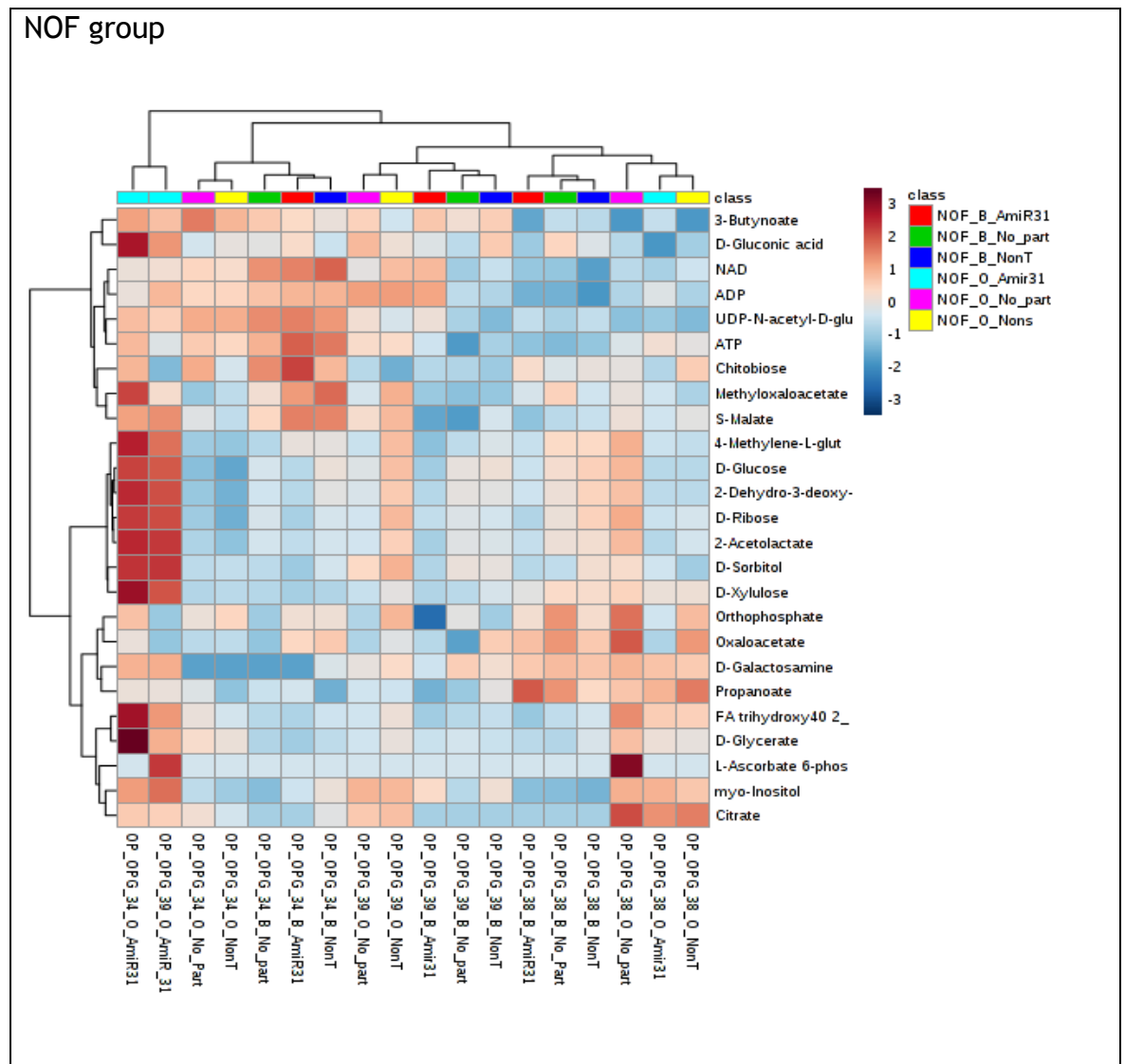


Figure 4-14 Carbohydrate metabolite profile of NOF MSCs at day 7 of culture in AntagomiR-31 experimentation. Increased abundance of carbohydrate metabolites in the osteogenic conditions is seen in all patients, with the strongest observed in the osteogenic and AmiR-31 culture condition demonstrated in 2 of the patient samples. B No Part = basal media; B Non T = basal media and Non-targeting nanoparticles; B AmiR31 = basal media and AntagomiR-31 nanoparticles; O No Part = Osteogenic media; O Non T = Osteogenic media and Non-targeting nanoparticles; O AmiR31 = osteogenic media and AntagomiR-31 nanoparticles. 3 patient samples per group with 1 technical replicate per condition. Red colours are indicative of fold increases in metabolite abundance, and blue colours of fold decreases.

4.4.2.6 Lipid metabolism

On assessing lipid metabolism, the culture conditions showed large overlap in all replicates in the OA and NOF group, Figure 4-15. The OA group showed more evidence of localising by media type, with some variation evident on comparing the basal to the osteogenic media. This was not present in the NOF group.

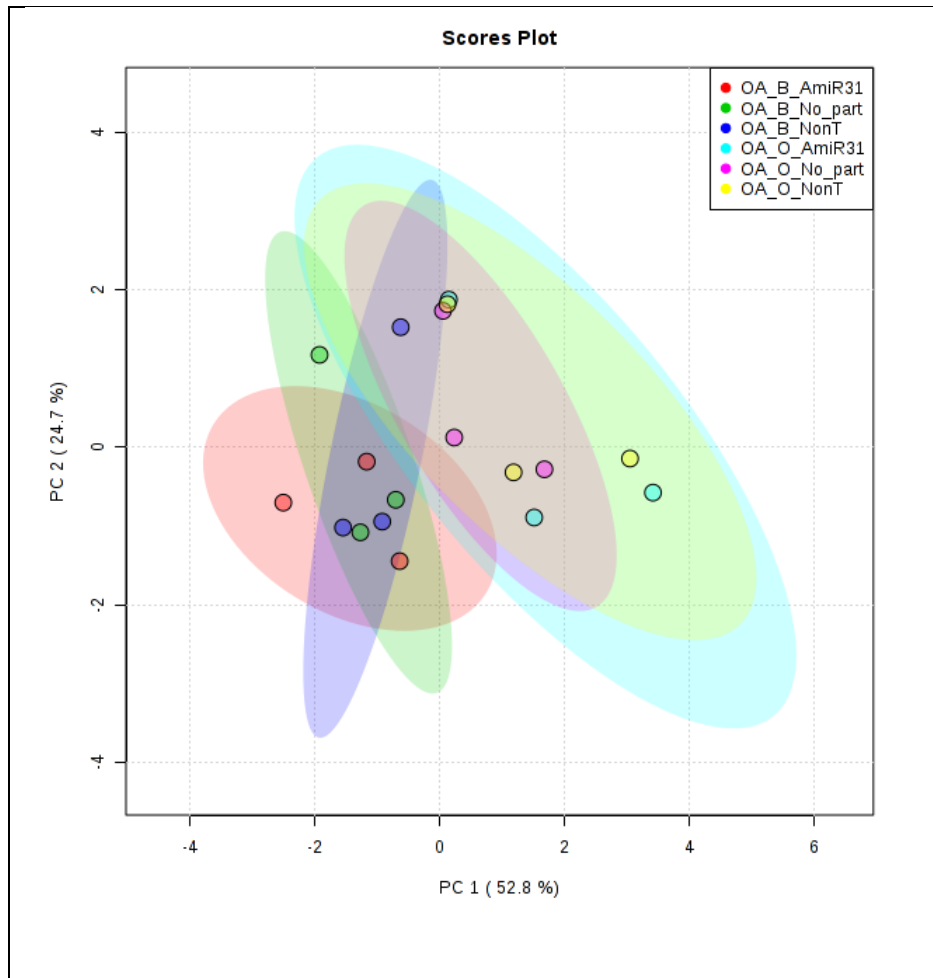


Figure 4-15 PCA plot of lipid metabolites detected at day 7 of MSC culture in the OA group AntagomiR-31 experimentation. Large overlap, with no clear clustering by condition was observed. Data sets were derived from putative lipid metabolites identified within the different culture conditions at day 7 of culture. B No Part = basal media; B Non T = basal media and Non-targeting nanoparticles; B AmiR31 = basal media and AntagomiR-31 nanoparticles; O No Part = Osteogenic media; O Non T = Osteogenic media and Non-targeting nanoparticles; O AmiR31 = osteogenic media and AntagomiR-31 nanoparticles. Points represent individual samples of each condition. 3 patient samples per group with 1 technical replicate per condition. The coloured ellipses represent the spatial borders associated with each condition, to a 95% confidence interval.

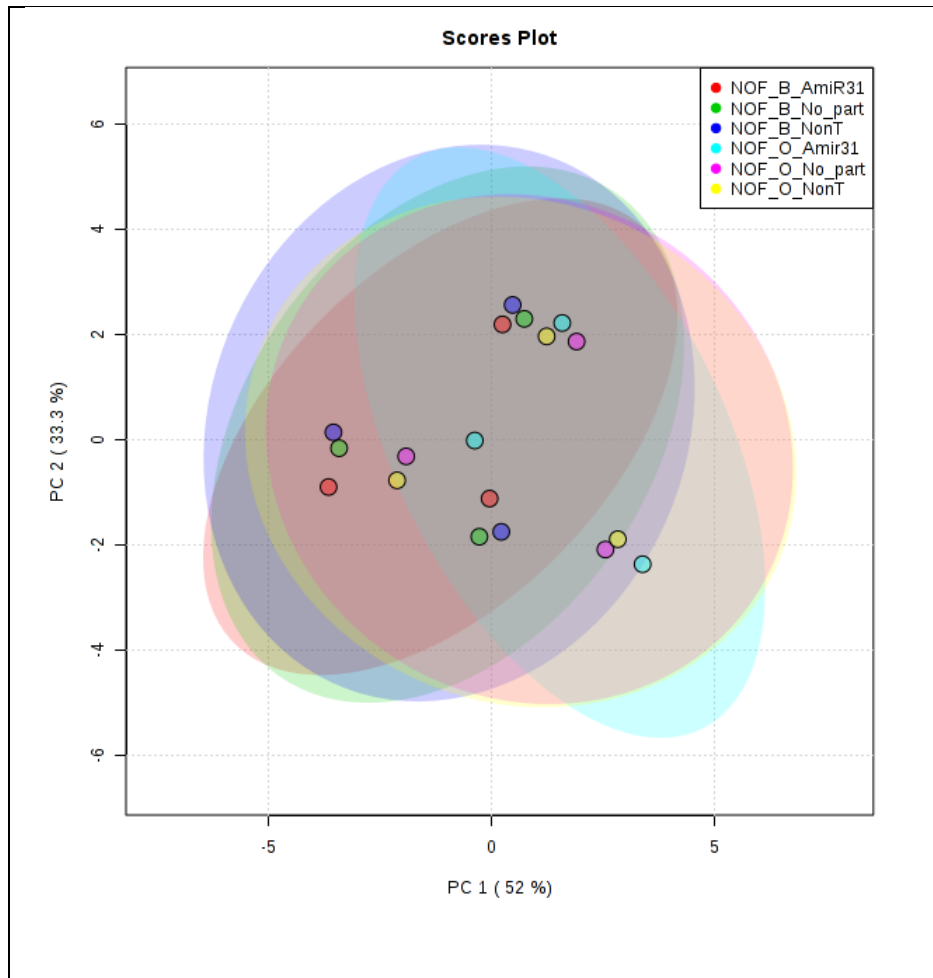


Figure 4-16 PCA plot of lipid metabolites detected at day 7 of MSC culture in the NOF group AntagomiR-31 experimentation. No clustering by condition was noted. Data sets were derived from putative lipid metabolites identified within the different culture conditions at day 7 of culture. B No Part = basal media; B Non T = basal media and Non-targeting nanoparticles; B AmiR31 = basal media and AntagomiR-31 nanoparticles; O No Part = Osteogenic media; O Non T = Osteogenic media and Non-targeting nanoparticles; O AmiR31 = osteogenic media and AntagomiR-31 nanoparticles. Points represent individual samples of each condition. 3 patient samples per group with 1 technical replicate per condition. The coloured ellipses represent the spatial borders associated with each condition, to a 95% confidence interval.

In keeping with the PCA data, the heatmaps demonstrate a slight trend of increased abundance of lipid metabolites in the osteogenic AmiR31 culture condition, Figure 4-17. However, this was not uniformly seen across all replicates, and was most pronounced in the OA group.

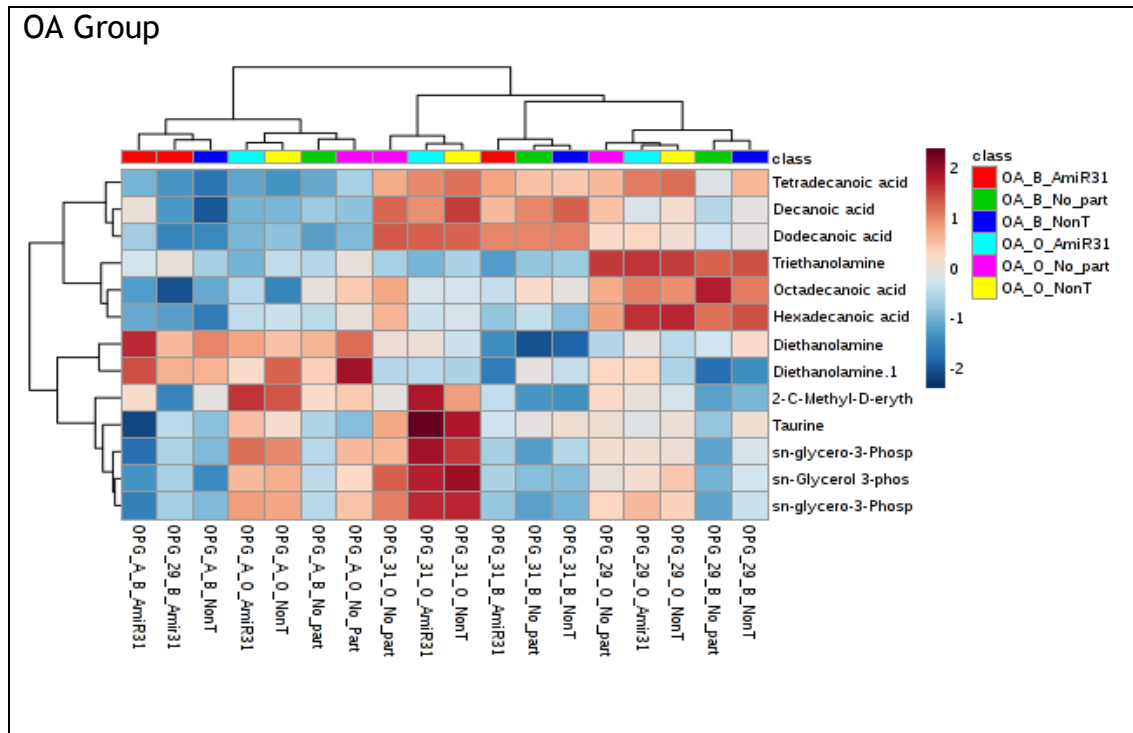


Figure 4-17 Lipid metabolite profile of OA MSCs at day 7 of culture in AntagomiR-31 experimentation. Increased abundance of metabolites was observed across the culture conditions, with the greatest increase noted in the osteogenic conditions. B No Part = basal media; B Non T = basal media and Non-targeting nanoparticles; B AmiR31 = basal media and AntagomiR-31 nanoparticles; O No Part = Osteogenic media; O Non T = Osteogenic media and Non-targeting nanoparticles; O AmiR31 = osteogenic media and AntagomiR-31 nanoparticles. 3 patient samples per group with 1 technical replicate per condition. Red colours are indicative of fold increases in metabolite abundance, and blue colours of fold decreases.

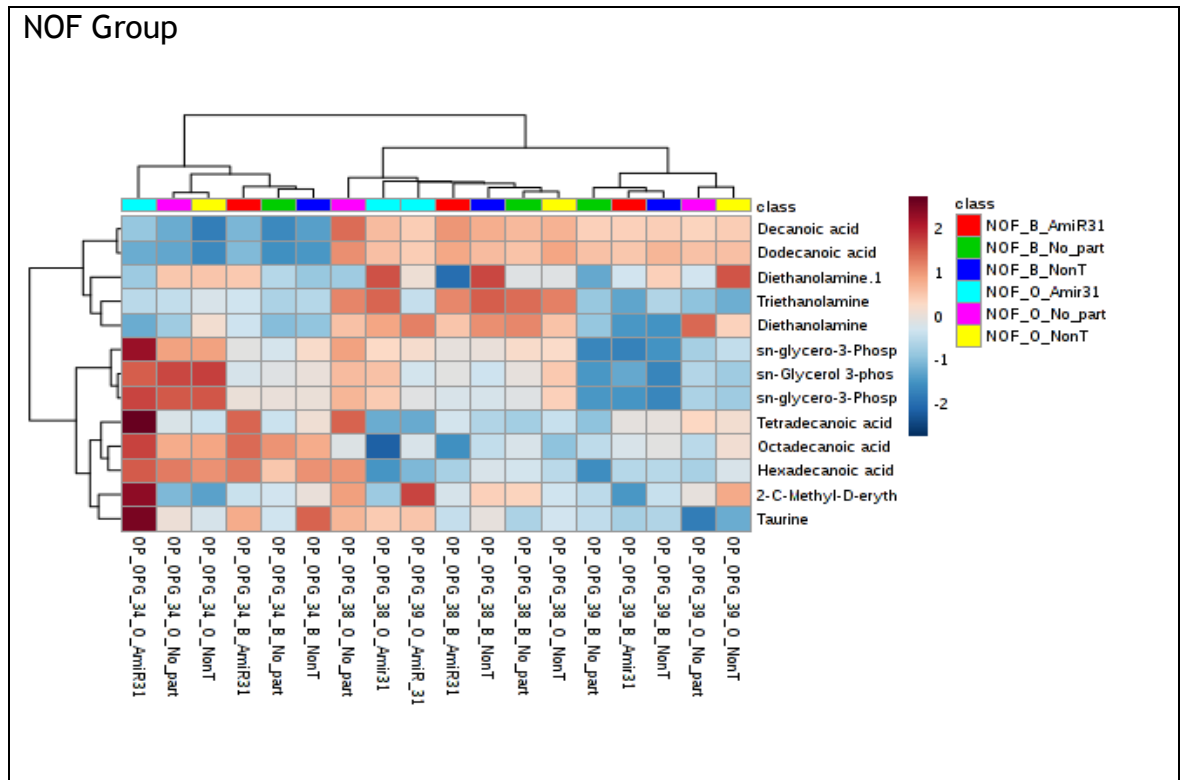


Figure 4-18 Lipid metabolite profile of NOF MSCs at day 7 of culture in AntagomiR-31 experimentation. Both basal and osteogenic media conditions resulted in an increased abundance of metabolites. B No Part = basal media; B Non T = basal media and Non-targeting nanoparticles; B AmiR31 = basal media and AntagomiR-31 nanoparticles; O No Part = Osteogenic media; O Non T = Osteogenic media and Non-targeting nanoparticles; O AmiR31 = osteogenic media and AntagomiR-31 nanoparticles. 3 patient samples per group with 1 technical replicate per condition. Red colours are indicative of fold increases in metabolite abundance, and blue colours of fold decreases.

4.4.2.7 Alteration in metabolic networks initiated by AntagomiR-31

An assessment on the effect the AmiR-31 nanoparticle had on metabolic networks was undertaken via the IPA software. The basal no particle condition was utilised as a control, with the remaining culture conditions compared to it.

IPA predicted alteration in many canonical pathways in both patient groups. Displayed in Figure 4-19 and Figure 4-20 are the top altered canonical pathways in conditions of basal media and AmiR-31, osteogenic media and AmiR-31 and osteogenic media with no particles. This consistently demonstrated the same canonical pathways as being the most altered. These canonical networks were transfer RNA charging, citrulline metabolism and arginine, citrulline and glutathione biosynthesis. Whilst the pathways were the same, differences occurred in the number of upregulated and downregulated molecules for each condition. Within the NOF group the Osteogenic media with AmiR-31 was

predicted to upregulate more molecules than the other two conditions. Within the OA group similar trends were predicted, however the basal media with AmiR-31 was predicted to have a greater number of downregulated molecules in comparison to the other conditions.

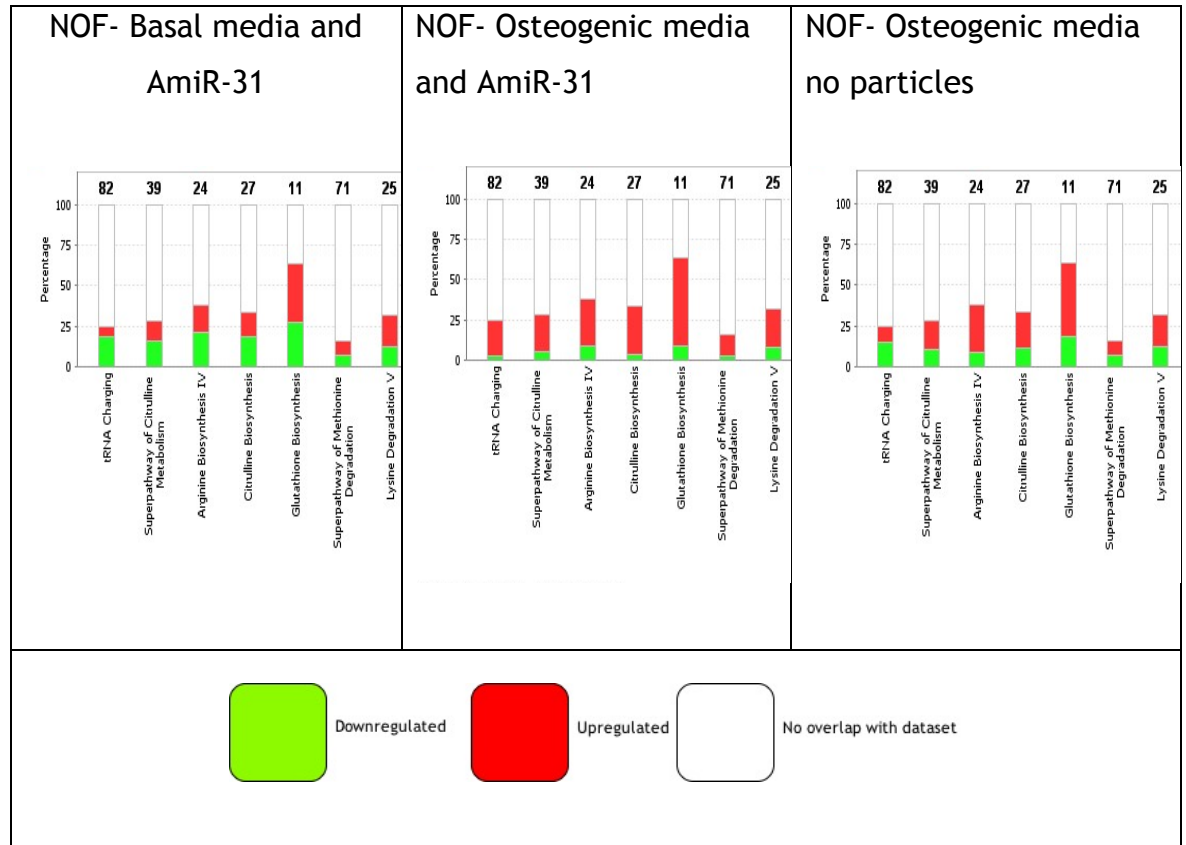


Figure 4-19 Predicted altered canonical pathways in the NOF group culture conditions in comparison to basal media. The osteogenic media with AmiR-31 is predicted to upregulate more molecules in each pathway with similar expression in the remaining two conditions. Top 7 pathways displayed with the number of molecules involved in each pathway noted above each bar. Green colour represents downregulation, red upregulation and clear no overlap within the dataset. 3 patient samples per group with 1 technical replicate per condition.

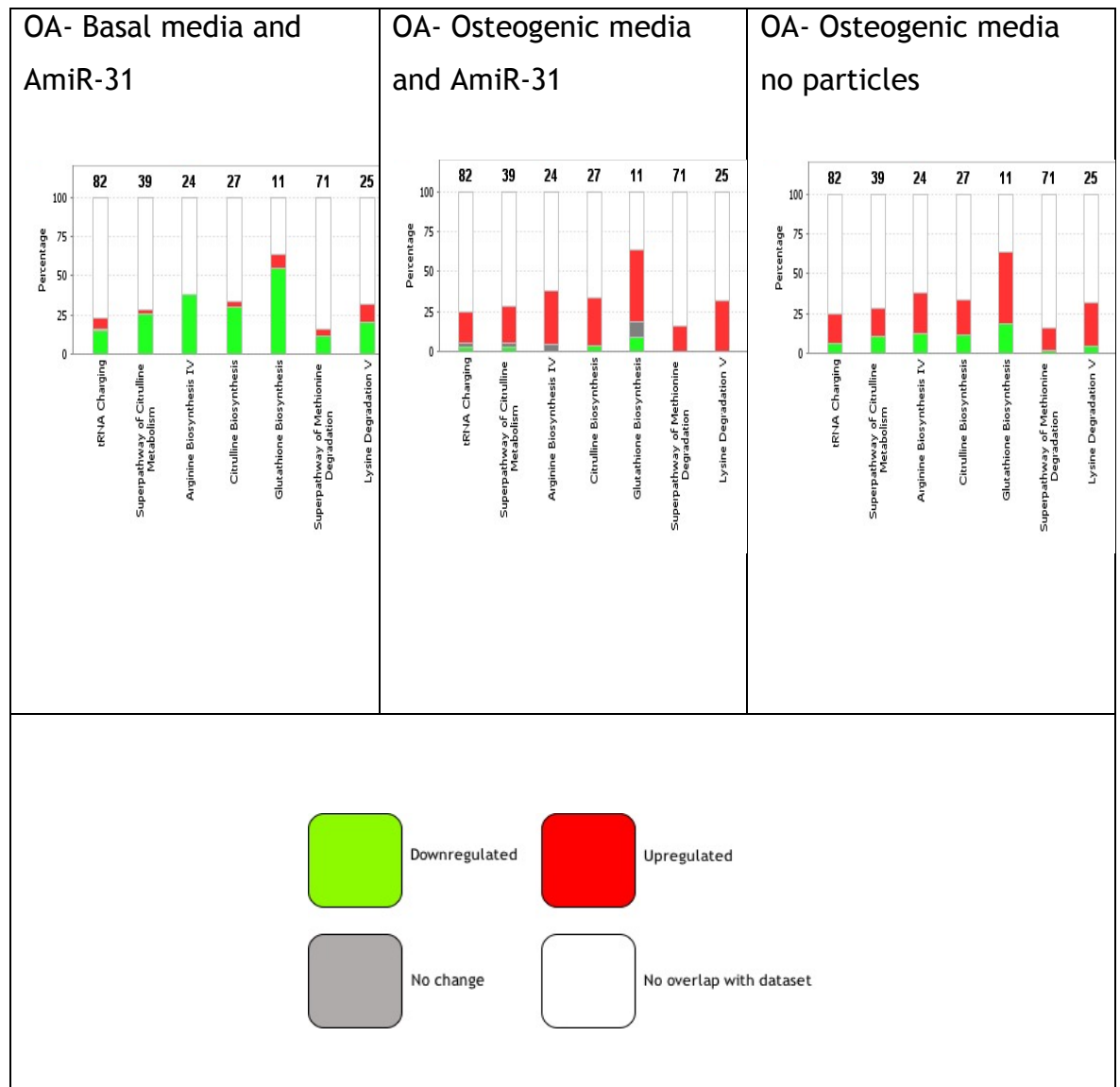
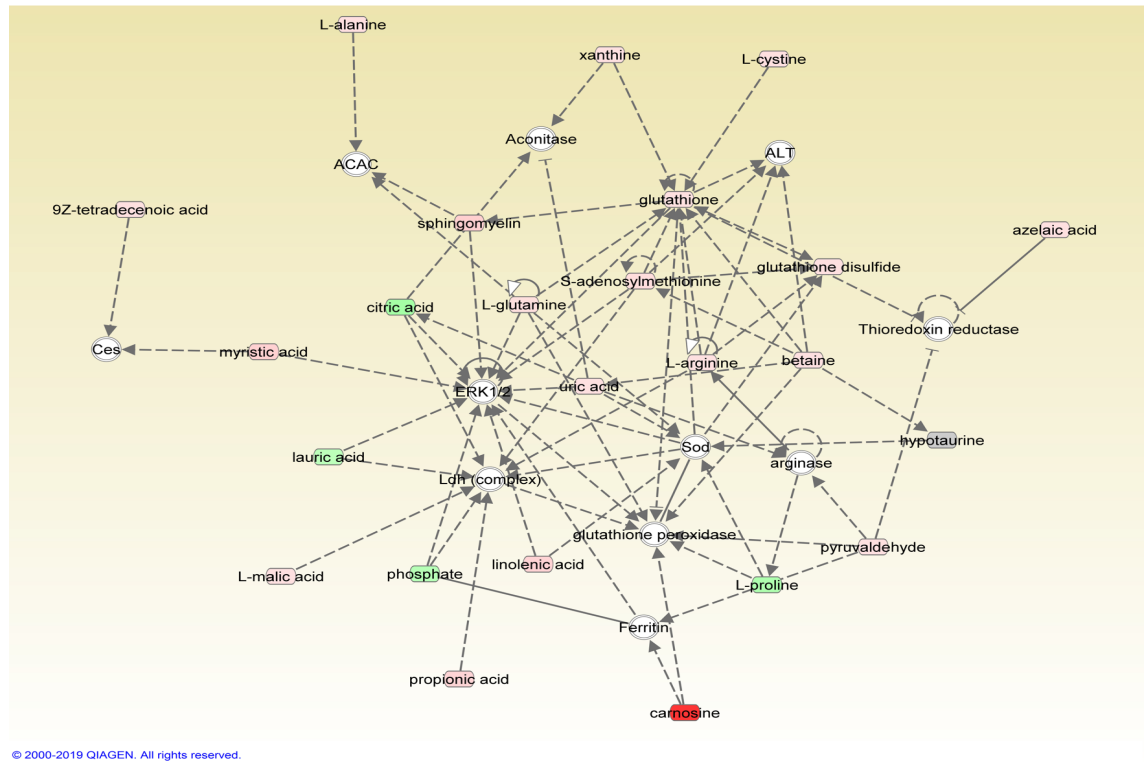


Figure 4-20 Predicted altered canonical pathways in the OA group in comparison to basal media. The osteogenic media with AmiR-31 is predicted to upregulate more molecules in each pathway in comparison to the other two conditions. The basal media and AmiR-31 condition led to a greater number of downregulated molecules within the pathways than the other two conditions. Top 7 pathways displayed with the number of molecules involved in each pathway noted above each bar. Green colour represents downregulation, red upregulation, grey no change and clear no overlap within the dataset. 3 patient samples per group with 1 technical replicate per condition.

Moving to network analysis, Figure 4-21 and Figure 4-22 display network 1, an IPA predicted network, centred upon extracellular signal-regulated kinases 1/2 (ERK 1/2) and glutathione of the NOF and OA groups in conditions of osteogenic media and basal media with AmiR-31 in comparison to basal no particles as a control. The addition of osteogenic media led to similar levels of molecule expression in both groups, Figure 4-21 .

A



B

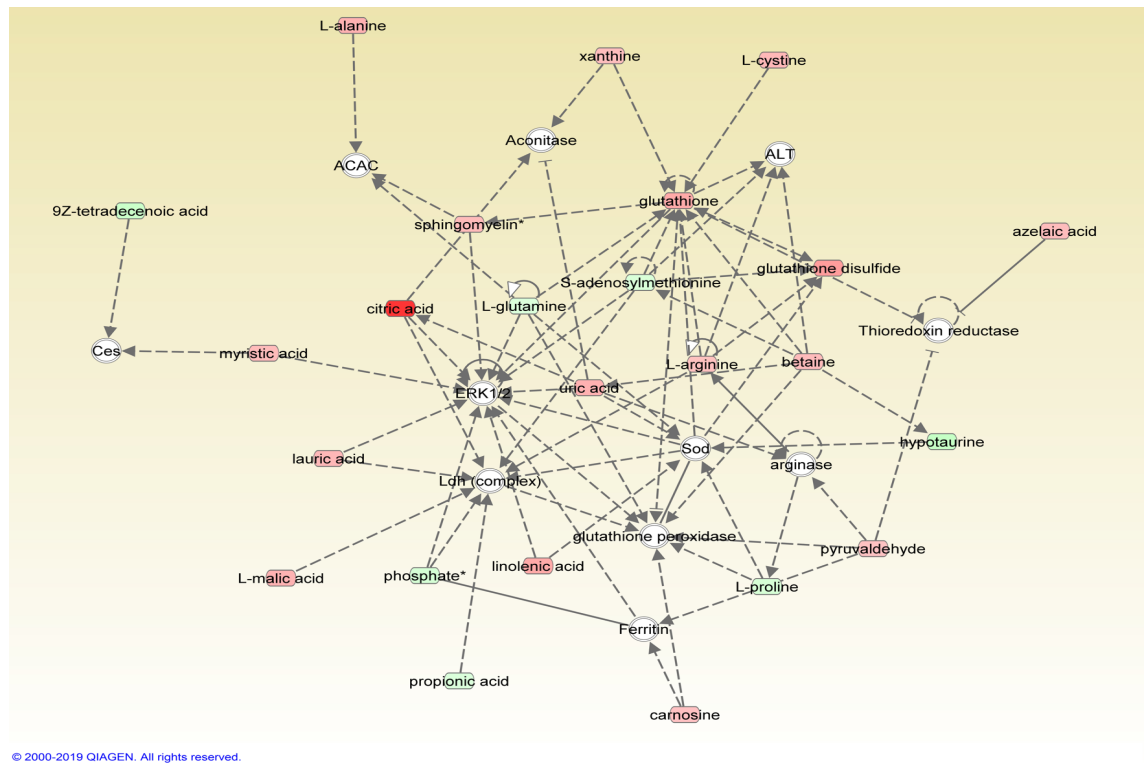
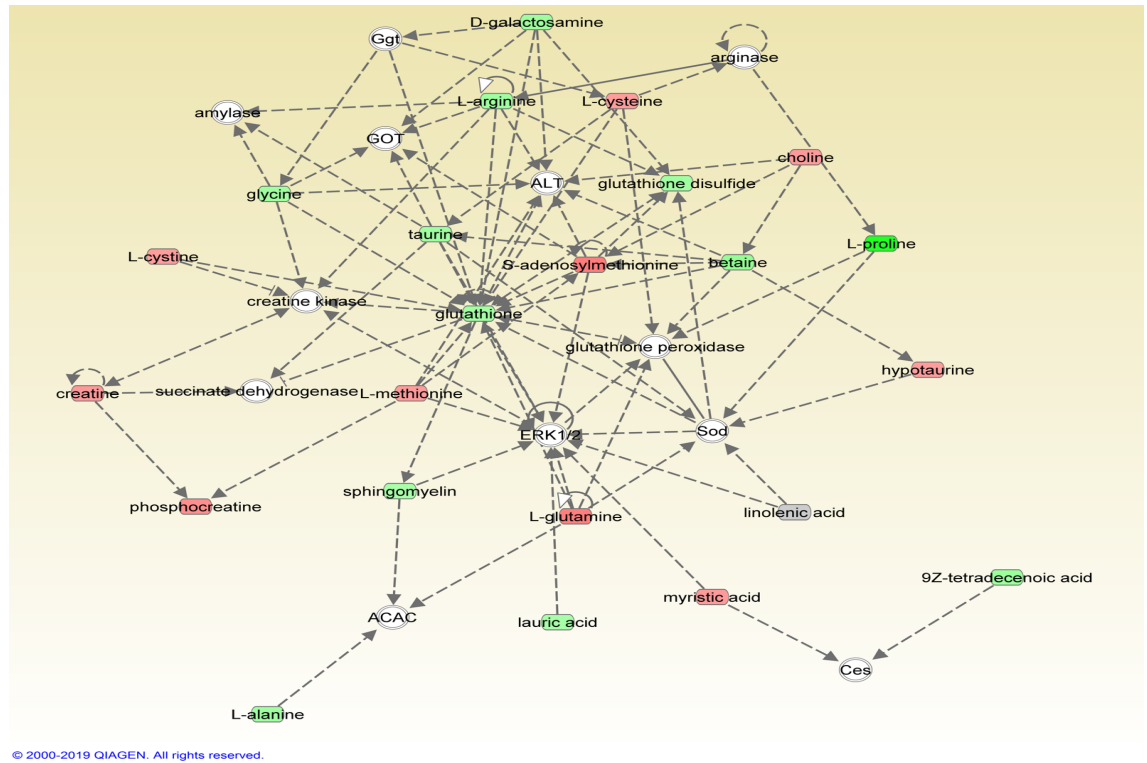


Figure 4-21 Metabolomic Network 1 at day 7 of culture in osteogenic media in comparison to basal media. The addition of osteogenic media leads to similar patterns of expression in both patient groups. A = OA group, B= NOF group. 3 patient samples per group with 1 technical replicate. Red = increased expression, Green = decreased expression.

Strong upregulation of glutathione continued in the NOF group in the basal media and AmiR-31 condition. In contrast, the addition of AmiR-31 to the OA group lead to a decrease in glutathione expression, Figure 4-22.

A



B

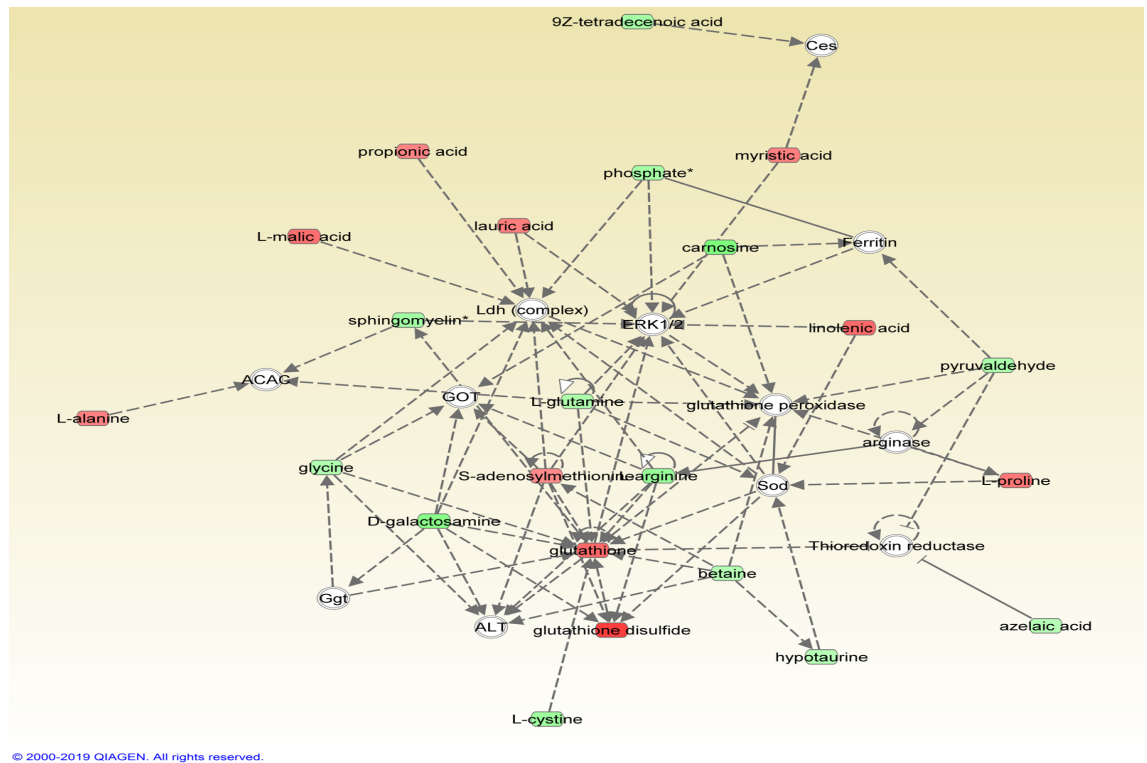
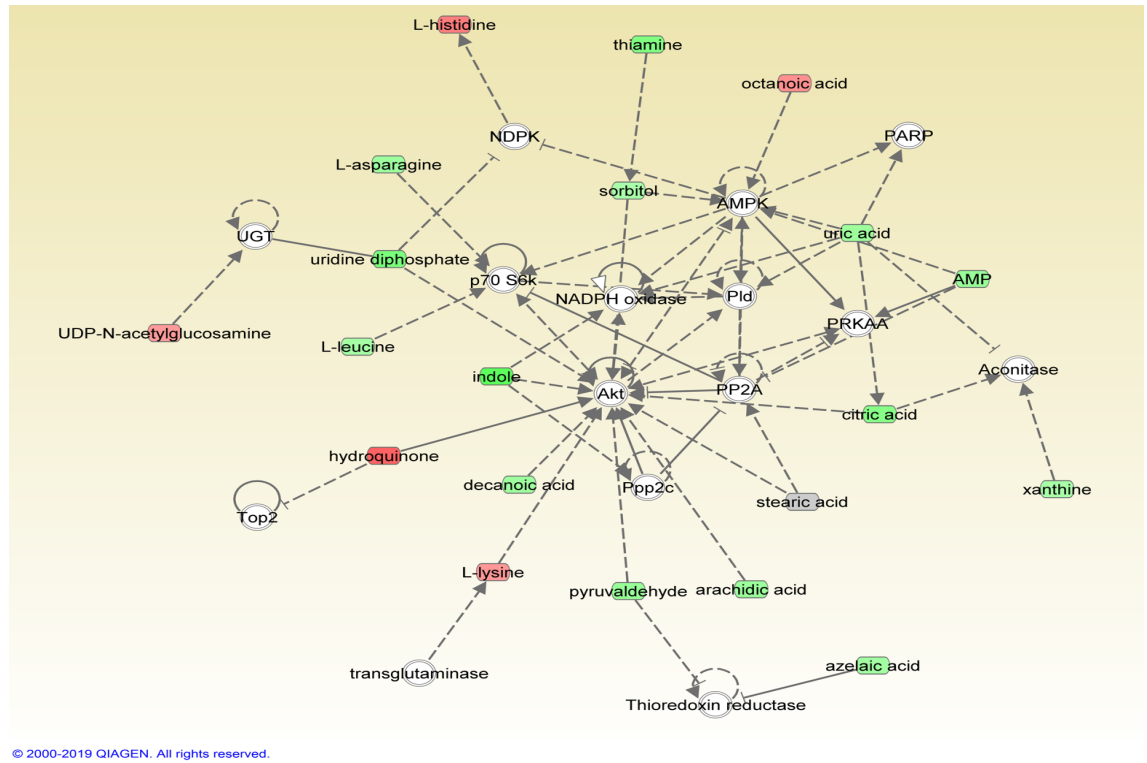


Figure 4-22 Metabolomic pathway Network 1 at day 7 of culture in basal media and AmiR-31 in comparison to basal media. Glutathione expression was decreased in the OA group and increased in the NOF group. A = OA group, B= NOF group. 3 patient samples per group with 1 technical replicate. Red = increased expression, Green = decreased expression.

Network 2 was centred upon protein kinase B (AKT), protein phosphatase 2 (PP2A) and AMP activated protein kinase Figure 4-23. Inverse expressions were again observed in the two patient groups upon addition of AmiR-31.

A



B

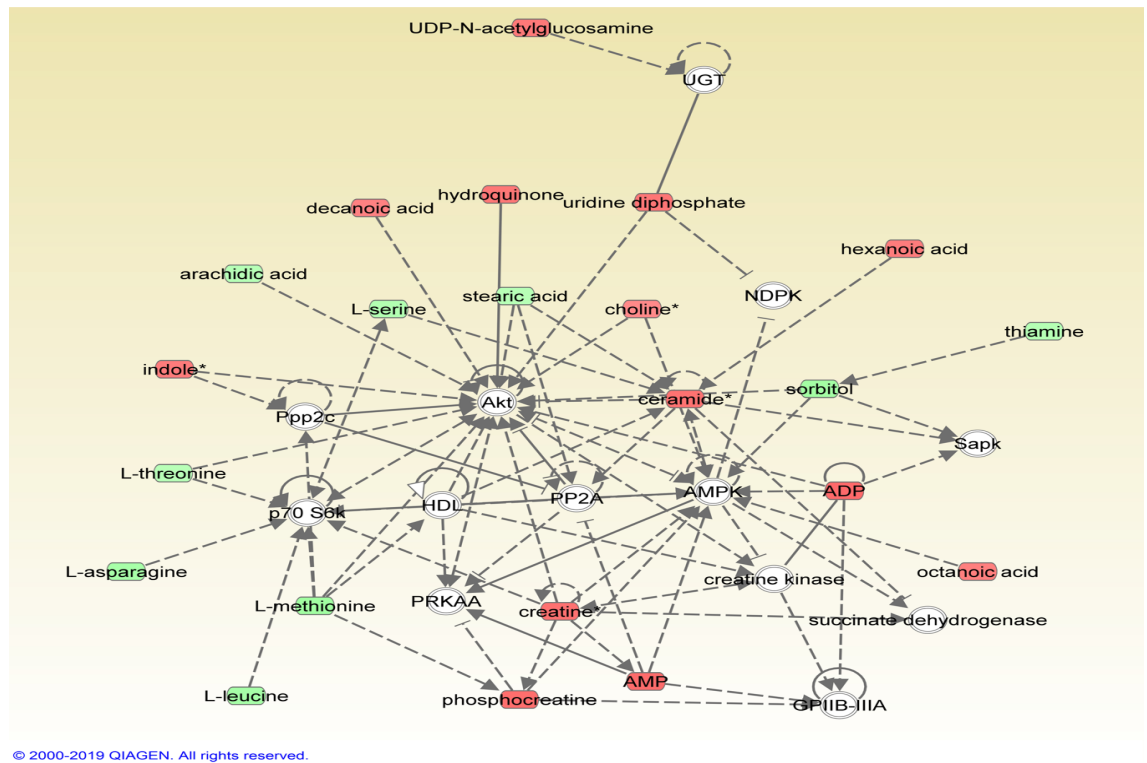
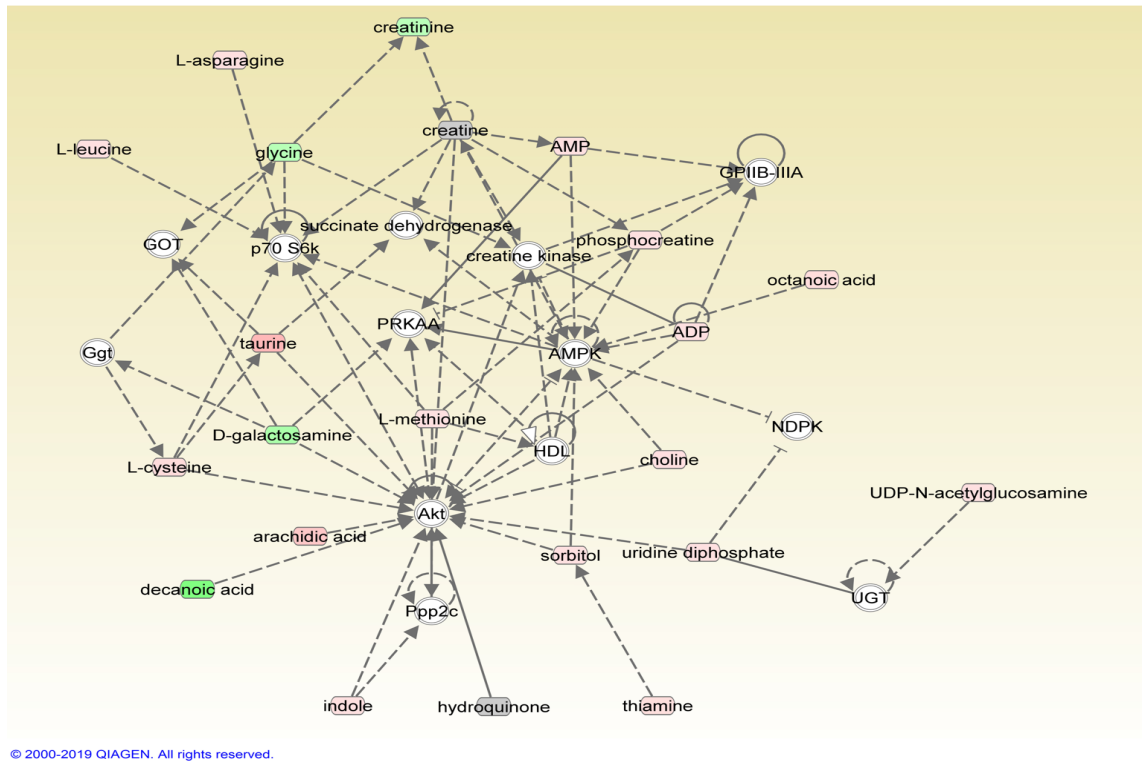


Figure 4-23 Metabolomic pathway Network 2 at day 7 of culture in basal media and AmiR-31 in comparison to basal media. Large increases in expression of regulators of this network were observed in the NOF group only. A = OA group, B= NOF group. 3 patient samples per group with 1 technical replicate. Red = increased expression, Green = decreased expression.

Upon analysis of Network 2 in the osteogenic media only, weaker change in regulation of molecules is predicted in both groups, Figure 4-24, in comparison to the basal media and AmiR-31 condition, Figure 4-23. However, the NOF group continues to have more molecules upregulated in comparison to the OA group, as observed in the AmiR-31 condition.

A



B

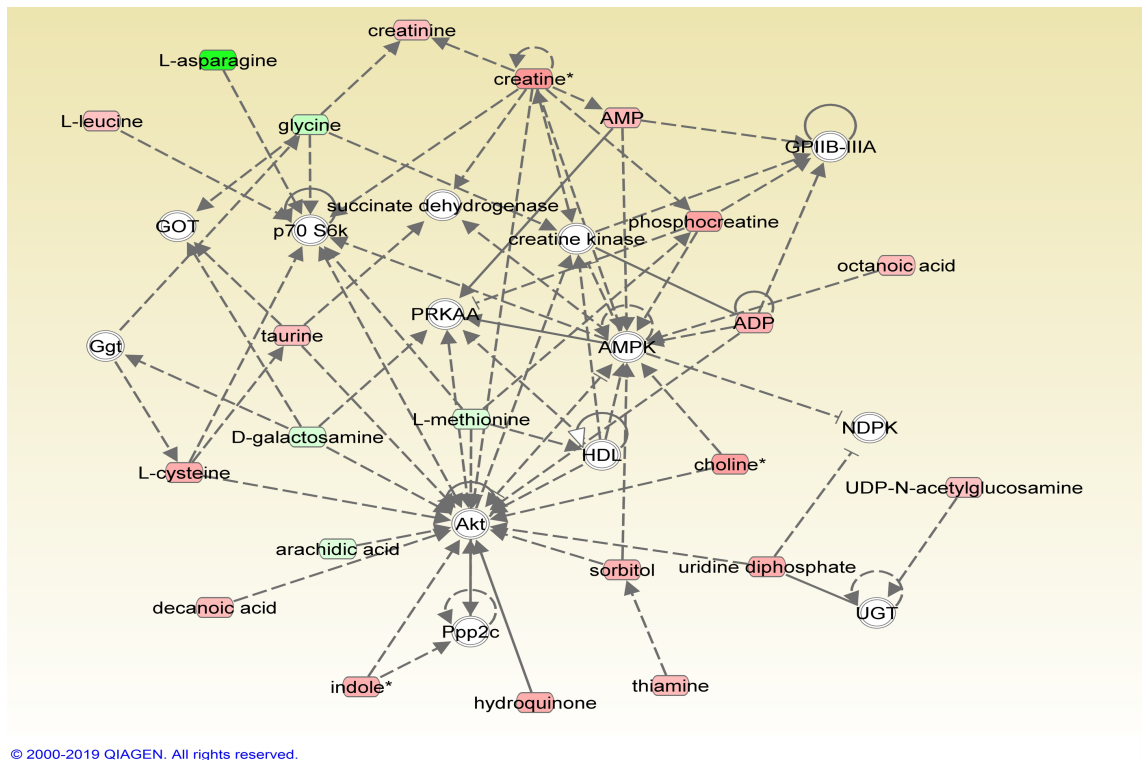


Figure 4-24 Metabolomic pathway Network 2 at day 7 of culture in osteogenic media in comparison to basal media. A greater number of molecules are predicted to be upregulated in the NOF group, without evidence of strong up or downregulation. A = OA group, B= NOF group. 3 patient samples per group with 1 technical replicate. Red = increased expression, Green = decreased expression.

Network 4, Figure 4-25, centred upon adenosine triphosphate, and involving nuclear factor Kappa-light-chain-enhancer of activated B cells (NF κ B), demonstrated variance between the two patient groups. Upon addition of AmiR-31 in the NOF group a large increase in the expression of adenosine triphosphate is observed. Conversely, a reduced expression of adenosine triphosphate was noted in the OA group.

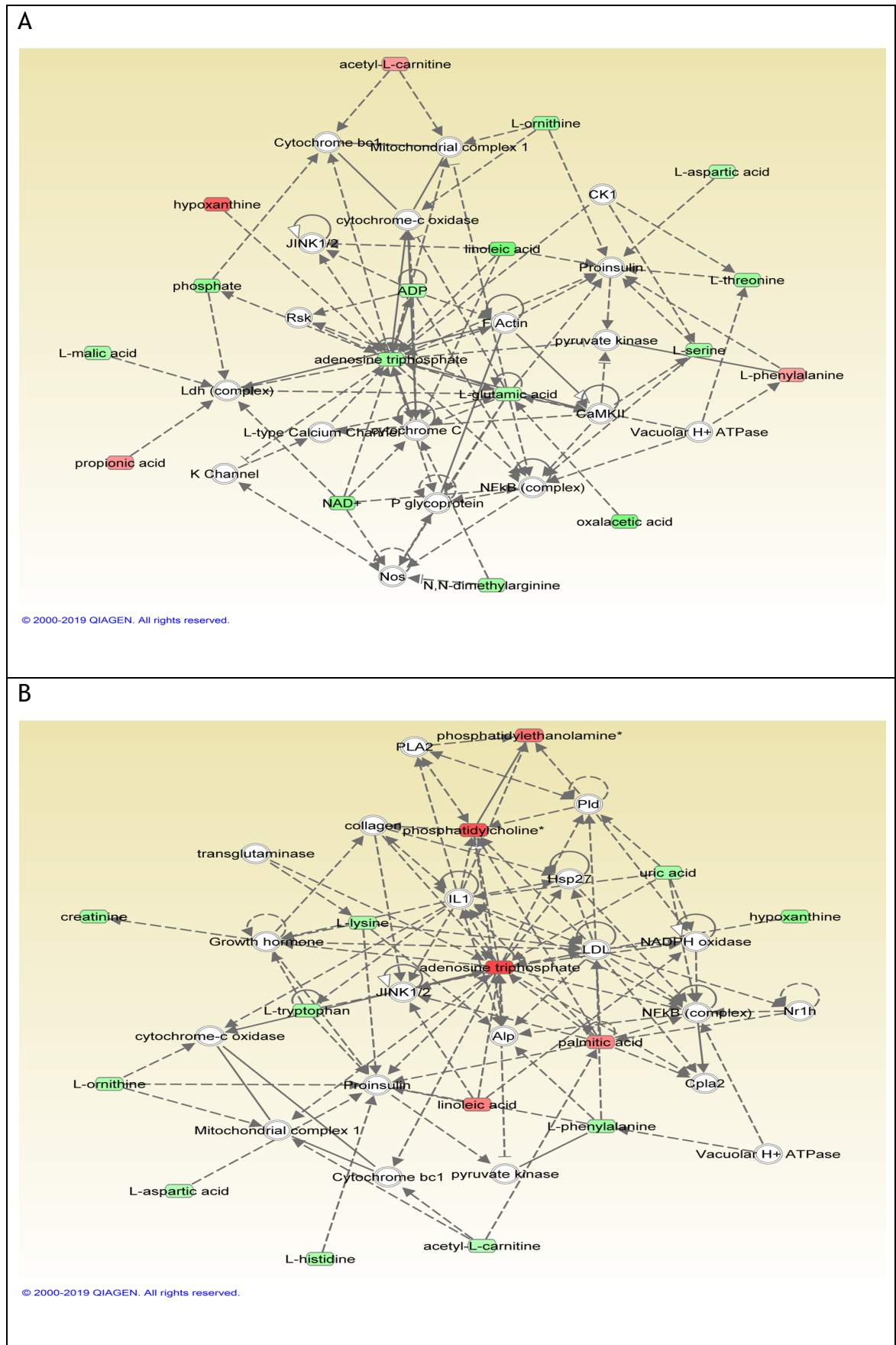


Figure 4-25 Metabolomic pathway Network 4 at day 7 of culture in basal media and AmiR-31 in comparison to basal media. Large increases in expression of adenosine triphosphate were predicted in the NOF group only, with reduced expression in the OA group. A = OA group, B = NOF group. 3 patient samples per group with 1 technical replicate. Red = increased expression, Green = decreased expression.

4.5 Discussion

4.5.1 MicroRNA manipulation influences differentiation

The *in vitro* monolayer culture results presented above show miRNA manipulation lead to trends of affect in both adipogenic and osteogenic differentiation. Whilst the qRT-PCR results did not show the hypothesised effects, the ICW and metabolomic data suggested that the miRNA mimic and inhibitor cultures were leading to change within the MSCs.

The miR-143 culture demonstrated that adipogenesis can be stimulated utilising the miR-143 nanoparticle mimic. This required the addition of adipogenic induction media, and was only evident on ICW protein analysis and within the OA group. This is in keeping with the impaired differentiation potential observed in this patient group in chapter 3. The NOF group was seen to be stimulated towards adipogenesis on qRT-PCR analysis, but not specifically increased by the addition of the miR-143 mimic. Several studies have demonstrated the adipogenic inductive nature of miR-143, interestingly Xie et al demonstrated in an *in vivo* experiment that although a potent driver of adipogenesis, in the obese state miR-143 expression is low (Esau *et al.*, 2004; Xie, Lim and Lodish, 2009).

MiR-143 was chosen due to its high level of dysregulation in the microRNA expression data and its observed role in inherited forms of OP (Mäkitie *et al.*, 2018). Furthermore, miR-143 has been more recently identified as an osterix expression regulator, and therefore osteogenesis. Li et al showed that the induction of osteogenesis in a mouse osteoblast cell line led to a reduced expression of miR-143, when cultured with a miR-143 mimic a significant decrease in alkaline phosphatase and osteocalcin expression was observed after 2 days of culture (E. Li *et al.*, 2014).

MiR-143 is evidently an important regulator of MSC differentiation. It has been described to play critical roles in both adipogenesis and osteogenesis. However, its role in bone formation is yet to be fully understood. By upregulating the expression of miR-143 this experiment attempted to restore the differentiation potential of the NOF group with regards to adipogenesis. MiR-143 was evidently a stimulator of adipogenesis in the OA group, where the MSCs are theorised to be

of improved stemness, but the mimic nanoparticle failed to return the differentiation level to comparable levels in the NOF group in comparison to OA. Performing further experimentation into the effects miR-143 mimic has on bone formation in the NOF group would be of significant interest.

Identifying methods to improve the activity of MSCs from patients at risk of OP is important. Improving the functionality of the MSCs would hopefully lead to an increase in bone quality and quantity.

MiR-31 was chosen due to its known role in osteogenesis and its dysregulation in the NOF group in the miRNA expression data. Previous research has shown that miR-31 targets key markers of osteogenesis, such as osteopontin, osteocalcin and osterix, furthermore reducing miR-31 expression results in increased osteogenesis (Deng *et al.*, 2013; McCully *et al.*, 2018). Although MiR-31 dysregulation in OP is well documented, little has been published with regards to its manipulation of bone marrow MSCs from at risk of fragility fractures (Weilner *et al.*, 2016; Mäkitie *et al.*, 2018).

An increase in osterix protein expression at day 7 was observed on ICW analysis in both OA and NOF patient groups, with the addition of differentiation media again leading to an additive effect with the miRNA nanoparticle (Figure 4-6). This increase in osteogenesis was not clearly evident on qRT-PCR, with a trend to increase expression in all osteogenic conditions in the NOF group the main finding (Figure 4-4).

The disappointing qRT-PCR results may have been impaired due to the timepoint of analysis, with day 7 representing an early timepoint for adipogenesis and osteogenesis. More clear results between the culture conditions would be expected at a later timepoint (Tsimbouri, 2015; Young *et al.*, 2015). With only having 3 patients per group, the results may have suffered due to variability between patients. Increasing the patient number, and replicate number analysed may also reduce the variability observed in the qRT-PCR data.

These experiments have examined the effect on one form of MSC differentiation after the manipulation of a single miRNA. Due to the non-specific binding of miRNAs viewing these results in isolation would be ill-advised. Both miRNAs have

been shown to be abnormally expressed in other diseases. Upregulation of miR-31 is observed in squamous cell cancers of the lung, head and neck and oesophagus, post myocardial infarction, with reduced expression in sepsis and cancers of breast, prostate, and ovarian cancers tissue (Van Der Heide *et al.*, 2016; Martinez *et al.*, 2017; T. Yu *et al.*, 2018). The wide ranging, multiple tissue type sites regulated by MiR-31 are due to it targeting genes related to cell proliferation, apoptosis and cell motility (Stepicheva and Song, 2016). With regards to miR-143 it has been implicated in cardiovascular disease, the development of type 2 diabetes mellitus and many malignancies such as colorectal and pancreatic cancer (B. Yu *et al.*, 2018; Li, Fan and Chen, 2018; Li *et al.*, 2019; Xie *et al.*, 2019).

Thus, the implications of delivering a systemic miRNA therapy, to induce osteogenesis and improve bone density, on other physiological systems may be far ranging. Analysis of the miRNA manipulation on other cell lines, or disease models would be imperative before upscaling to *in vivo* experimentation. Furthermore, the crossover between osteogenesis and adipogenesis in the function of miR-143 highlights that targeting a single miRNA in attempt to provide a therapeutic effect may be ineffective.

Developing our understanding of miRNAs in bone pathophysiology is of great therapeutic importance. This experiment provides insight to the potential role miR-31 and miR-143 could play in preventing or treating OP. These results have importance due to the limited published results of studies utilising bone marrow MSCs from patients with, or at risk of, OP.

4.5.2 Metabolomic analysis displays manipulation of differentiation

Metabolomic data shows interesting findings, providing a clearer insight into the mechanisms of osteogenic differentiation induced by AmiR-31. The conclusions are limited by the small-scale experiment, with only one technical replicate per biological replicate, i.e. 3 patients per condition. However, interesting summations can still be drawn.

4.5.2.1 Analysis of heatmaps and PCA plots

Metabolomic experiments generate vast amounts of data, which is a feature that is both lauded and criticised of this technique (Daviss, 2005). Therefore, key pathways are required to be selected, relevant to the research question.

Analysis within this experiment was focused on the metabolism of amino acids, carbohydrates and lipids.

On assessing the metabolic profile of the culture conditions during the AmiR-31 experiment, large differences were evident in several areas associated with MSC activity and osteogenesis.

Displayed in the heatmaps, Figure 4-7, Figure 4-13 and Figure 4-17, the osteogenic AmiR-31 condition frequently produced several fold-change in metabolite abundance, most notably in the amino acid and carbohydrate metabolite dataset. These metabolomic pathways have been linked to osteogenesis and MSC differentiation (Sampath *et al.*, 2008). A quiescent MSC state is associated with low abundance of metabolites in these pathways (Chung *et al.*, 2007), again indicative of both patient groups undergoing differentiation and proliferation. This effect was demonstrated in both the OA and NOF group, again showing the potential of MSCs from the NOF group to undergo differentiation upon the correct stimulus.

The heat maps and PCA plots of amino acid and carbohydrate metabolism in Figure 4-7, Figure 4-9, Figure 4-11 and Figure 4-13 demonstrate a low abundance of metabolites in the basal conditions. The addition of osteogenic media causes notable increases, however the strongest expression in both groups is observed upon addition of AmiR-31 to the osteogenic media. Encouragingly this effect was seen in the NOF group. This is suggestive that at an early time point to observe a large increase in osteogenic differentiation stimulated by AmiR-31 a positive control condition is required. The stark difference in effect may have lessened at a later time point, i.e. with longer culture the osteogenic effects of AmiR-31 may have become more apparent and less reliant on the osteoinductive conditioned media.

The lipid profile produced less clear results, the PCA plot in Figure 4-15 shows significant overlap in all conditions. The heatmaps in Figure 4-17 demonstrate mixed increased and decreased fold changes in lipid metabolites in the AmR-31 condition. Changes in lipid metabolism have been described in the process of osteogenic differentiation, however the effects in this experiment were not clearly in keeping with these (Alakpa *et al.*, 2016). It may be that a longer culture duration would provide greater insight to the effect AmiR-31 has on lipid metabolism and osteogenesis.

4.5.2.2 Network analysis

The IPA software predicted AmiR-31 to lead to up and downregulation of several pathways, with often opposing effects in the OA and NOF group.

The previous analysis in the heatmaps suggested the osteogenic media and AmiR-31 condition to be the most active, however the strongest levels of change of expression occurred in the NOF basal media and AmiR-31 condition. This is evident in Figure 4-22 of network 1. In network 1 the addition of osteogenic media produced similar changes to the pathway, but the extent of change in expression was less strong than in the basal media and AmiR-31 condition.

Glutathione was noted to be a crucial part of Network 1. Glutathione is known to be involved in osteogenic differentiation and its redox status also key to osteoclastogenesis (Romagnoli *et al.*, 2013). It is thought to be pivotal to bone remodelling. Glutathione expression was predicted to increase in both patient groups on culturing with osteogenic media, Figure 4-21. The addition of the AmiR-31 to basal media was predicted to produce an increase in glutathione expression in the NOF group but a decrease in the OA group, Figure 4-22. This difference is intriguing as supplementing levels of glutathione are associated with osteogenesis, however glutathione levels are known to decrease during osteogenesis induced by differentiation media (Romagnoli *et al.*, 2013). It is encouraging to see it highlighted in the IPA network, but intriguing to observe a strong difference between the patient groups.

Network 2, Figure 4-23, was centred upon AKT, PP2A and AMPK. This network is intrinsic to cell survival, and tissue growth, with AKT a regulator of apoptosis.

Furthermore, AKT is a known regulator of osteogenic differentiation, the inhibition of AKT function is seen to impair osteoblast differentiation and maturation (Mukherjee and Rotwein, 2009; Baker, Sohn and Tuan, 2015). Due to the regulation AKT plays in osteogenesis, it is of interest to note this pathway to be predicted to be upregulated in the NOF group, suggesting the positive differentiation stimulus provided by AmiR-31. This result was not replicated in the OA group, with molecules targeting AKT predicted to be decreased in expression.

The final network analysed in Figure 4-25, network 4 surprisingly predicted large differences in adenosine triphosphate (ATP) expression. ATP is a crucial metabolite which plays fundamental roles as an energy transfer molecule, a phosphate donor and in intracellular signalling (Tantama and Yellen, 2014). The NOF group was predicted to have high levels of expression of ATP on addition of AmiR-31. The OA group was observed to have predicted low expression of ATP. ATP function has also been linked to MSC differentiation, with pre-treatment of ATP during *in vitro* cultures leading to enhanced adipogenesis and osteogenesis (Ciciarello *et al.*, 2013), and its role in osteogenesis recently described to be dependent on intracellular calcium pathways (Stovall *et al.*, 2019). This network provides further confirmation of the positive differentiation stimuli provided by AmiR-31.

The above networks demonstrated intriguing results in the NOF group, suggestive of a pro-differentiation state induced by AmiR-31. The results in the OA group did not mirror these trends, despite in previous chapters showing improved differentiation capacity. The time point utilised of the metabolomic analysis thus may be questioned. The effect of the addition of Amir-31 could be temporal, and potentially delayed in the NOF group, with an earlier increase present in the OA group, not captured at this timepoint of day 7. It would be important to interrogate these findings further with future experiments.

It would be of interest to analyse the miR-143 mimic in similar metabolomic experiments to elucidate its role in MSC differentiation and osteogenesis further. Due to the financial constraints of this project it was unable to be performed within this study. These experiments will hopefully be conducted within the laboratory group in future research projects.

4.6 Conclusion

This chapter demonstrates the potential for miRNA targeting therapies. Utilising nanoparticles osteogenic and adipogenic differentiation was manipulated. This effect was scrutinised by several modalities, and adds new information to the scientific literature with a metabolomic assessment of miRNA-31 manipulation. The data displayed in this chapter also paves a clear path for future work into the development of targeted therapies for the prevention of fragility fractures.

Chapter 5

5 Optimising Bone Marrow Derived MSC Spheroid Formation

5.1 Introduction

Developing consistent and credible 3D *in vitro* techniques for bone research is crucial to producing future translational work. They will allow improved analysis of basic science and more clinically relevant platforms for drug screening. 3D cell culture is more physiologically relevant than traditional 2D monolayer culture due to the recreation of physiological features such as a supportive matrix, tissue gradients and cell-cell interactions (Saleh *et al.*, 2012). Such models therefore provide an improved approach for assessing drug therapies, and predicting their effect, prior to animal models and clinical trials. To this end, the utilisation of 3D models reduces the use of animal models, by bridging the gap between *in vitro* and *in vivo* conditions. In addition, the use of 3D human-physiologically relevant bioengineered models reduces the risk and cost of running clinical trials, thereby reducing financial waste in the Pharma sector (Saleh and Genever, 2011).

Culturing cells as spheroids, a method of 3D cell culture, has been practiced in non-musculoskeletal research for several decades. Multiple different techniques exist for the formation of spheroids, which all share the same goal of reproducing the *in vivo* environment as closely as possible (Metzger *et al.*, 2011; Saleh and Genever, 2011). The Hanging Drop technique (HD) has been successfully employed for several decades with multiple cell types (Han, Asano and Hsu, 2019). A small aliquot of a single cell suspension is utilised, after seeding the aliquots are converted to a droplet, which is kept in place due to surface tension. The cells accumulate at the tip of the droplet, at the liquid-air interface, and are prevented from monolayer formation. After proliferation the spheroid is transported for ongoing culture in a non-adherent well (Breslin and O'Driscoll, 2013).

A second reputable technique is the Ultra-Low Attachment (ULA) method, which utilises a non-adherent coating to round bottomed wells. This is a form of the liquid overlay technique, also known as forced floating, and can be achieved by various techniques which prevent the cells from attaching to a vessel, including coating the plates with a substance such as 0.5% poly-2-hydroxyethyl methacrylate or the addition of 1.5% agarose to the culture medium (Ivascu and

Kubbies, 2006; Friedrich *et al.*, 2009). This technique prevents cells from adhering to the tissue culture plastic and promotes cell-cell contacts, resulting in cell aggregation and spheroid formation. Multiple different cell types have been utilised for this techniques, with extensive use in cancer research due to its ability to allow high throughput screening and large scale production of spheroids (Costa *et al.*, 2018).

Finally, there is the magnetic nanoparticle (MNP) method (Souza *et al.*, 2010; Lewis *et al.*, 2015). Here, cells are loaded with super paramagnetic iron oxide nanoparticles, prior to being detached, and the resultant cell suspension pipetted into a well below a magnet. This causes cell levitation towards the magnet, encouraging aggregation of the cells, resulting in spheroid formation. This technique has also been applied to several cell types, and benefits from the ability of functionalisation of the nanoparticles. However, the success of the MNP technique in an unselected adherent fraction of BM MSCs has not been thoroughly investigated. Previous work in our group has used STRO-1 selected mesenchymal stromal cells and proprietary mesenchymal stromal cells, namely PromoCell human mesenchymal stem cells (PromoCell GmbH, Germany).

Scaffold free techniques of spheroid formation were chosen for further analysis in this chapter. Scaffold techniques utilise a non-adhesive matrix, produced from substances such as collagen or hyaluronic acid, within the culture setting to promote spheroid formation. However, the use of scaffolds for spheroid based research has been criticised for its poor reproducibility, impaired analysis by optical techniques due to the scaffold size or transparency and finally therapeutics may be adsorbed by the scaffold instead of the cells, thus confounding the therapeutic effect (Gurski *et al.*, 2009; Rimann and Graf-Hausner, 2012).

Due to the multiple options available for spheroid culture, with varying degrees of complexity and cost, it is important to identify and optimise a technique. This will facilitate, and enhance, future *in vitro* research of musculoskeletal conditions utilising BM MSCs.

5.2 Objectives

This chapter aims to thoroughly assess three established spheroid-forming techniques when used with BM MSCs. The hanging drop, ultra-low attachment and magnetic nanoparticle techniques will be assessed with BM MSCs from osteoarthritic donors and the spheroids produced will be assessed as follows.

1. Assessment of spheroid size and effect on increasing seeding density.
2. Determination of cell viability over time in 3D spheroid culture.
3. Spheroid and cell morphological analysis via electron microscopy

Materials and Methods

5.2.1 Cells and Spheroid forming techniques

MSCs were cultured from BM samples from patients with OA, undergoing hip arthroplasty, as described in section 2.4.1. Three spheroid forming techniques were assessed:

1. Hanging drop

As described in section 2.6.1 MSCs were detached from a T75 flask and cell suspensions were prepared at concentrations of 5×10^3 , 1×10^4 , 2×10^4 cells per 40 μ l. A GravityPLUS™ (Perkin Elmer, Waltham, MA, USA) 96 well plate was used. After 24 or 72 hours of culture, the spheroid was transferred to a non-adherent plate placed below, GravityTRAP™ (Perkin Elmer, Waltham, MA, USA) for long term culture. Day 0 was on pipetting the cell suspension to the GravityPLUS™ 96 well plate.

2. Ultra-Low Attachment

Described in 2.6.2 MSC cell suspensions were prepared at concentrations of 5×10^3 , 1×10^4 , 2×10^4 cells per 100 μ l. CellCarrier Spheroid ULA 96-well microplates (Perkin Elmer, Waltham, MA, USA) were used, which have round-bottomed wells and a non-adherent coating. Day 0 was on pipetting the cell suspension into the ULA 96-well microplate.

3. Magnetic nanoparticle levitation

Described in detail in section 2.6.4, MSCs were seeded at concentrations of 5×10^3 , 1×10^4 , 2×10^4 cells in a 24 well plate. The media was exchanged for basal media containing 0.1mg/ml 200nm diameter magnetic nanoparticles (mNPs) (Chemicell, GmbH, Berlin, Germany), followed by an incubation period in the presence of a magnetic field of 350mT. After this incubation period the cells were washed, detached and re-suspended in 4ml of media within a 6 well plate, with a magnet placed above; this was taken as day 0 in spheroid culture.

5.2.2 Light microscopy

Spheroids were imaged at defined time points, days 3 and 21, to quantify their diameter. A minimum of 3 spheroids were imaged at each timepoint. The maximal diameter was measured and the mean diameter was utilised for each cell seeding concentration and technique.

5.2.3 Viability staining

Cell viability within the spheroid was determined at time points of day 7 and 21, using an ethidium homodimer/calcein AM viability kit (Life Technologies, Carlsbad, CA, USA). This technique is described in full in section 2.16. Fluorescent microscopy was then performed, utilising a Zeiss Axiovert 200M fluorescent microscope.

A representative cross-section of the spheroid was assessed to evaluate the presence of necrosis, utilising ImageJ software. FITC and TRITC signals from the cross-section were then plotted. The FITC channel represented live cells and the TRITC dead cells, indicative of necrosis.

5.2.4 Electron Microscopy

As fully described in 2.15 at 24 hours of spheroid formation, samples were prepared for scanning electron microscopy (SEM) and transmission electron microscopy (TEM). SEM samples were mounted on to stubs and sputter coated in gold prior to microscopy. TEM samples were embedded in resin and sectioned prior to imaging.

5.2.5 Statistical analysis

To determine the presence of a statistically significant difference in spheroid size produced, spheroid diameters from differing seeding densities were compared with the Kruskal-Wallis test with Dunn's multiple comparison.

Results

5.2.6 Hanging Drop (HD) Technique

5.2.6.1 Cell number and spheroid size

The effect of spheroid seeding density was assessed in the HD method and significant differences were observed, Figure 5-1. At day 3, a defined, stable structure morphology was observed, with a significant increase in size with increasing cell number. At day 21 of culture the diameter size had reduced in all seeding densities. A statistically significant increase in spheroid diameter was maintained when comparing the lowest and highest seeding density groups.

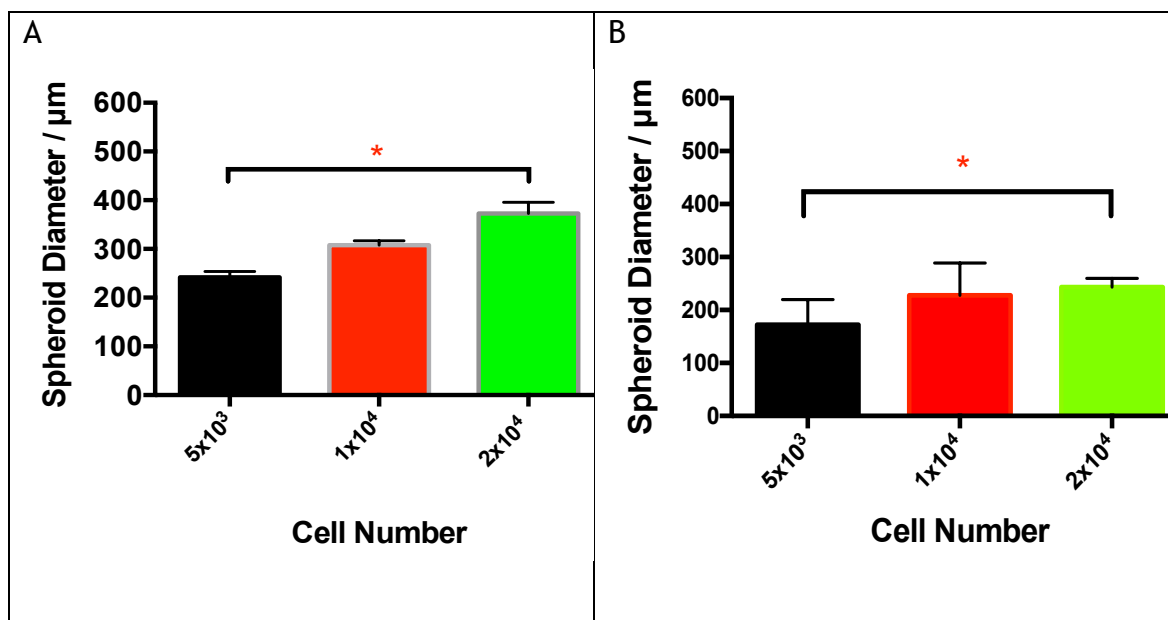


Figure 5-1 Mean spheroid diameter measured at day 3 (A) and day 21 (B) by the HD technique with different cell seeding densities. A: $N=3$ for all seeding densities. $p = 0.0036$. B: 5×10^3 $N=10$, 1×10^4 $N=8$, and 2×10^4 $N=6$. $p = 0.0249$.

5.2.6.2 Hanging Drop Spheroid Viability

High levels of cell viability were noted for HD spheroids at day 7, Figure 5-2. Where irregular shaped spheroids were observed at 24 hours with SEM (Figure 5-4), by day 7, spheroids demonstrated improved morphology, generating spherical and robust spheroids. At day 21, there was evidence of dead cells, particularly at the higher seeding density, but the spheroids remained mainly viable, Figure 5-3. A round morphology was maintained, but the spheroid size was greatly decreased, supporting the measurement graphs (day 3 and day 21).

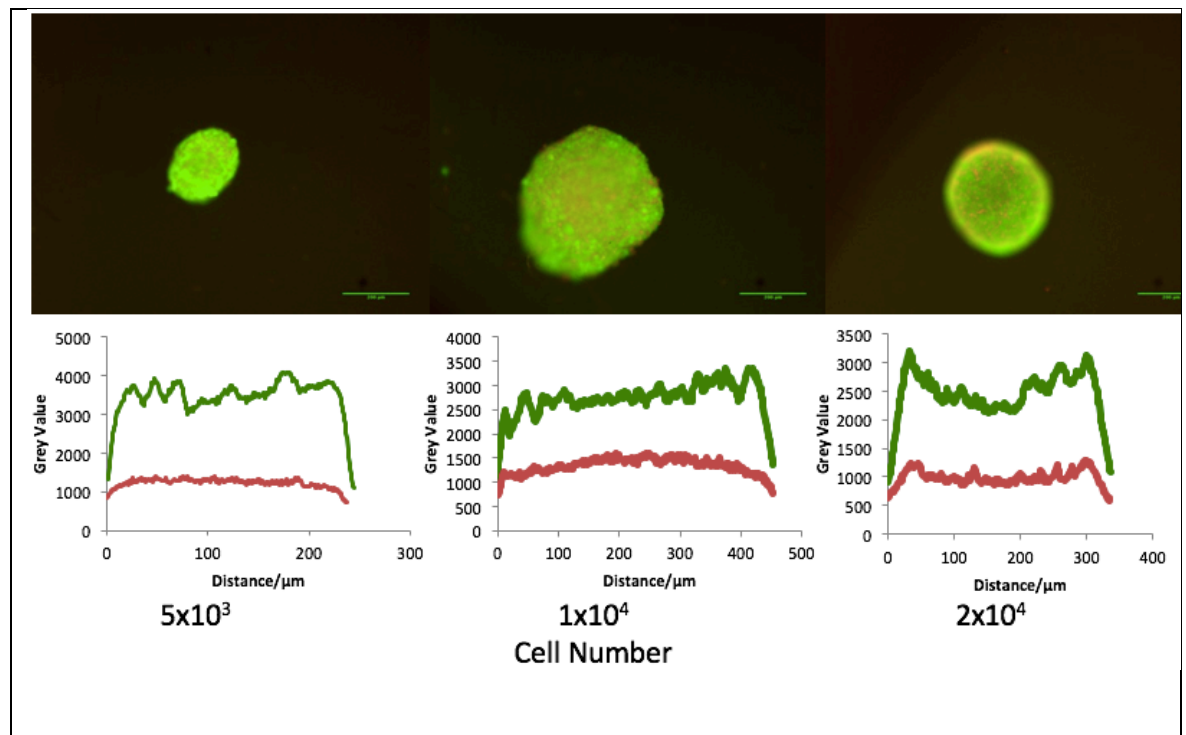


Figure 5-2. Day 7 viability staining- the cross-sectional viable (green; FITC) and dead (red; TRITC) fluorescent signal after calcein/ethidium staining in HD spheroids with different cell seeding densities. Peaks in the graph represent increasing signal. Scale bar 200 μm .

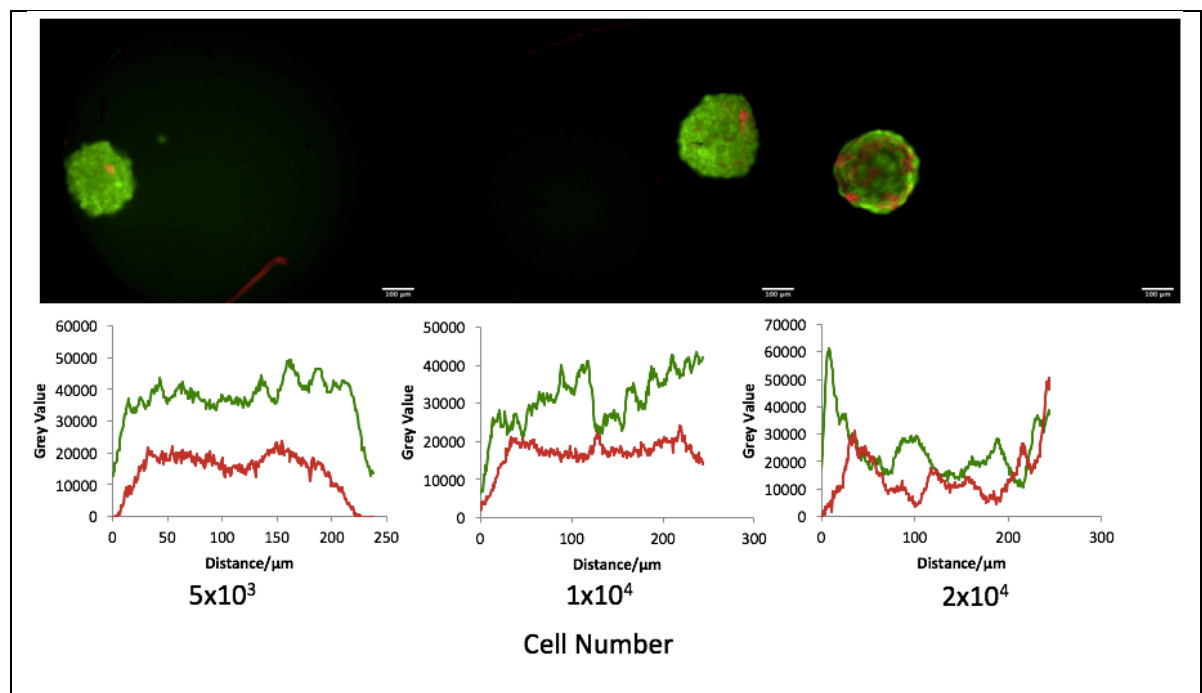


Figure 5-3 Day 21 viability- the cross-sectional viable (green; FITC) and dead (red; TRITC) fluorescent signal after calcein/ethidium staining in HD spheroids with different cell seeding densities. Peaks in the graph represent increasing signal. Scale bar 100 μm .

5.2.6.3 Electron microscopy

Electron microscopy was performed at 24 hours. Figure 5-4 represents the SEM, whilst Figure 5-5 the TEM images obtained. SEM images showed the multicellular aggregate formation of MSCs at 24 hours, with true spheroid formation not yet

visible. Increasing the cell number at seeding was shown to increase the spheroid size, Figure 5-4. In addition, an irregular border and shape of the spheroid was observed via SEM.

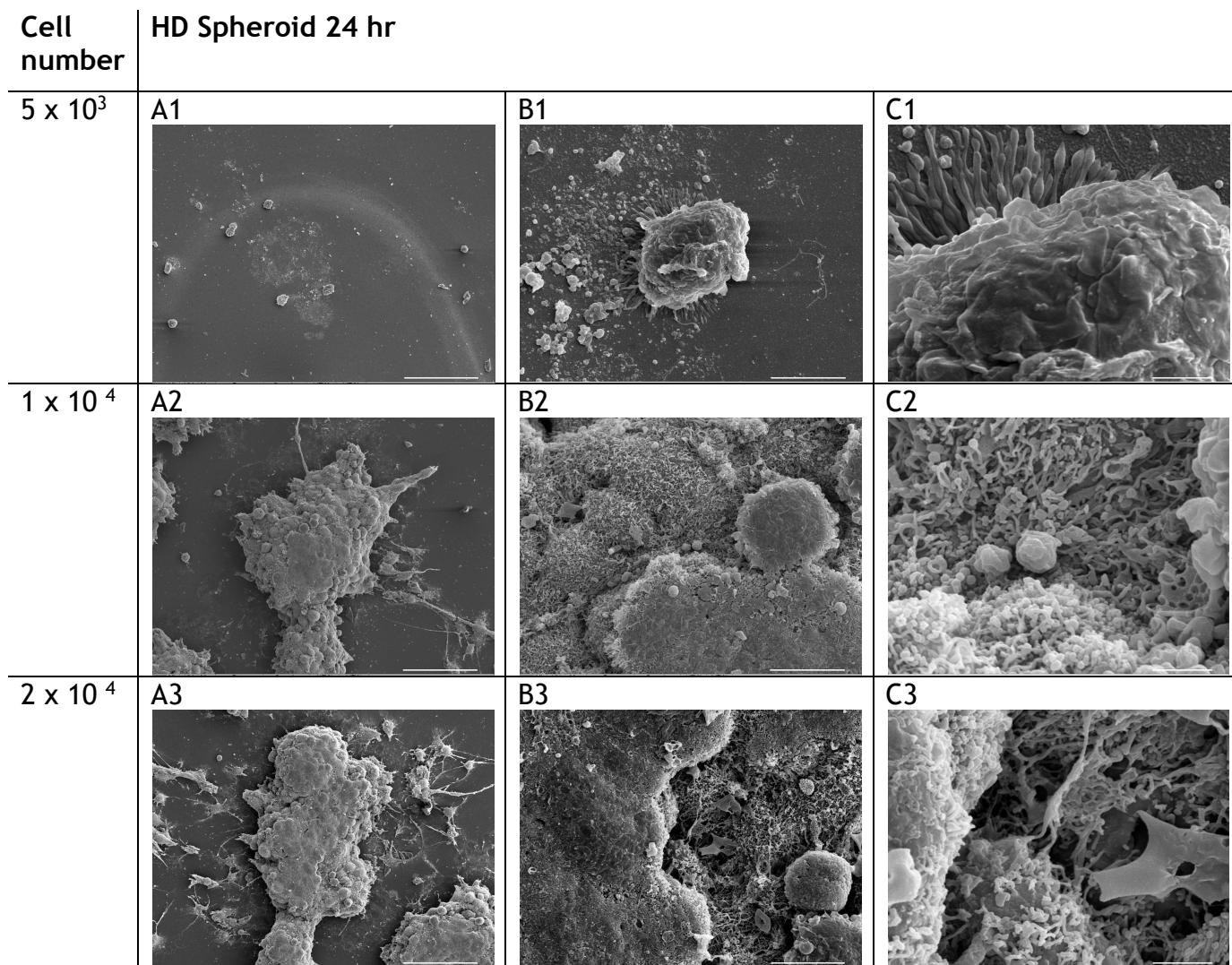


Figure 5-4 Scanning electron microscopy of spheroids formed by the HD technique at 24 hours with different cell seeding densities. A1-A3 scale bar 100 μm , B1-B3 10 μm and C1-C3 2 μm .

TEM allowed the observation of individual cells within the spheroids at all seeding densities. Cell-cell gap junctions were noted at all seeding densities. Organelles were also visible with the presence of the nuclear membrane evident in all seeding densities, Figure 5-5.

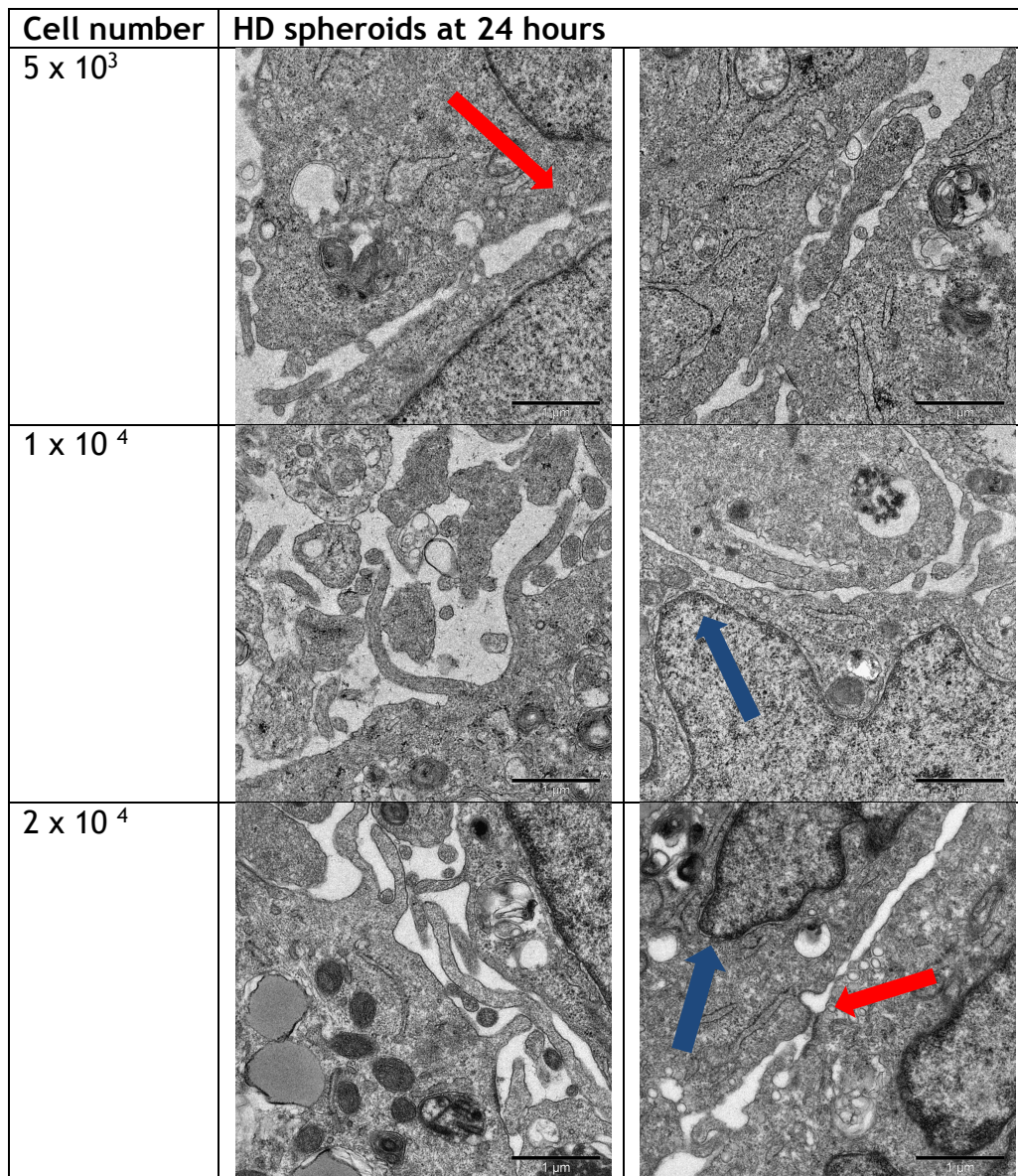


Figure 5-5 Transmission electron micrographs of HD spheroids at 24 hours, with different cell seeding densities. Blue arrows demonstrate nuclear membranes and red arrows inter-cellular connections. Scale bar 1 μ m.

5.2.7 Ultra-Low Attachment Technique

5.2.7.1 Cell number and spheroid size

Adjusting the spheroid seeding number significantly increased the spheroid diameter using the ULA technique, Figure 5-6. At both days 3 and 21, the size of spheroid produced was consistent, with a small range of diameters observed in each of the seeding groups. However, a reduction in spheroid size was noted with time in culture.

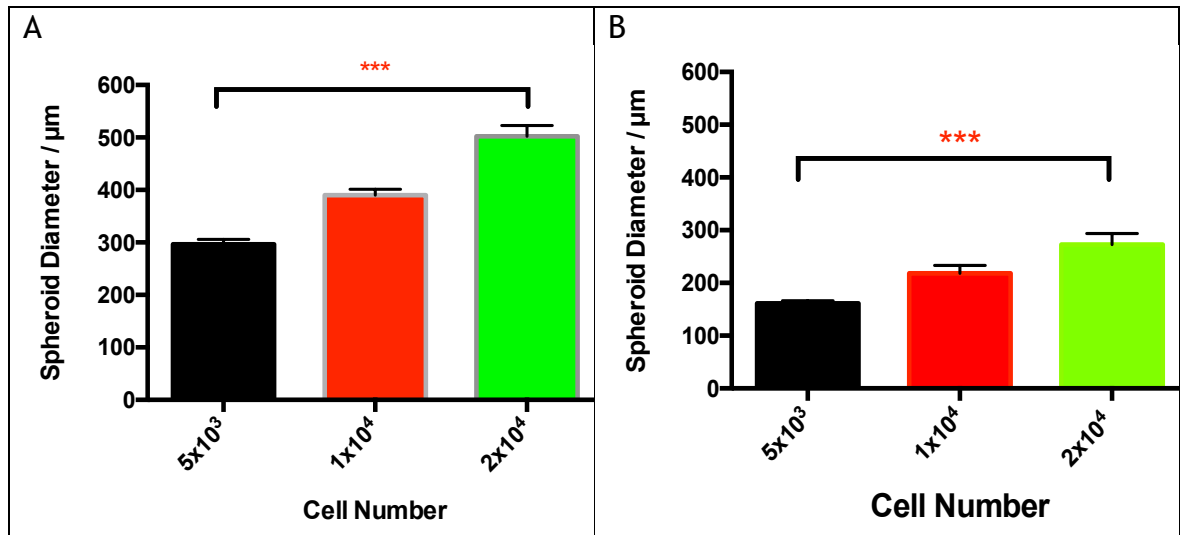


Figure 5-6 Mean spheroid diameter measured at day 3 (A) and day 21 (B) by the ULA technique with different cell seeding densities. N = 6. $p < 0.0001$.

5.2.7.2 Ultra-Low Attachment Spheroid Viability staining

ULA generated highly viable spheroids at day 7 across the seeding densities, Figure 5-7. A uniform, round morphology was observed. At day 21 of culture the lowest seeding density spheroids remained mainly viable, however dead cells were evident at higher seeding density, Figure 5-8. A robust, round morphology was maintained at day 21.

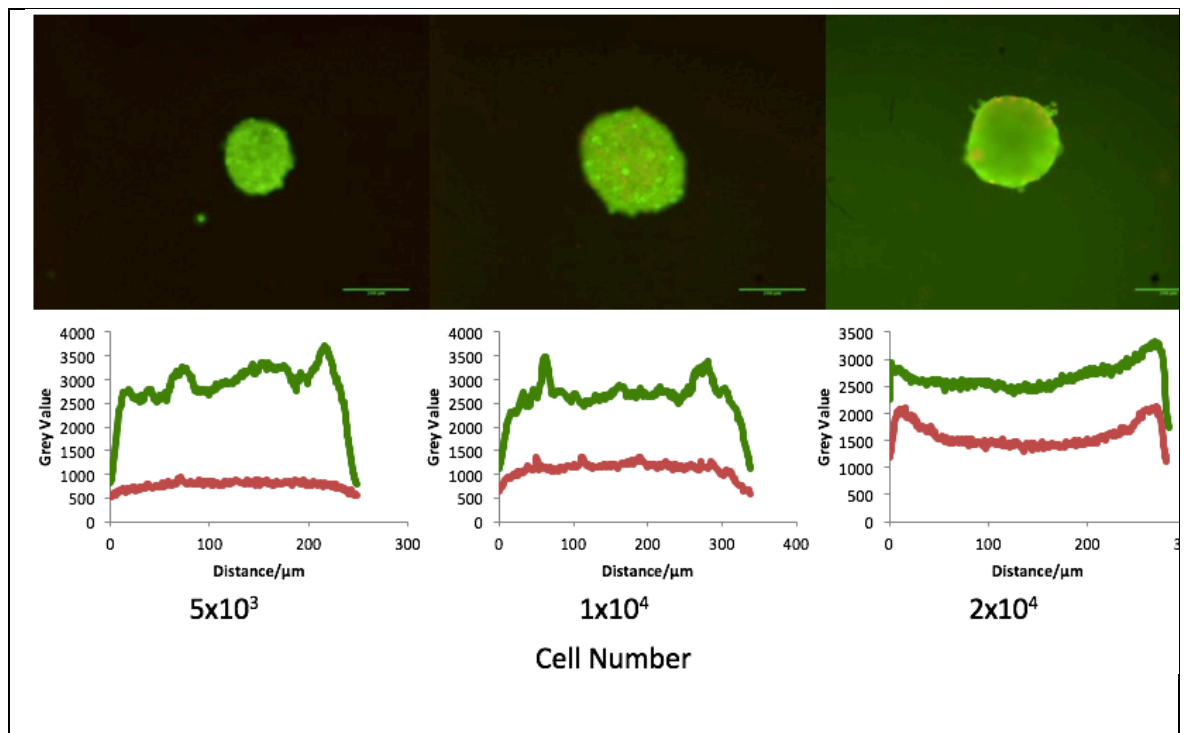


Figure 5-7 Day 7 viability staining-the cross-sectional viable (green; FITC) and dead (red; TRITC) fluorescent signal after calcein/ethidium staining in ULA spheroids, with different cell seeding densities. Peaks in the graph represent increasing signal. Scale bar 200 μm .

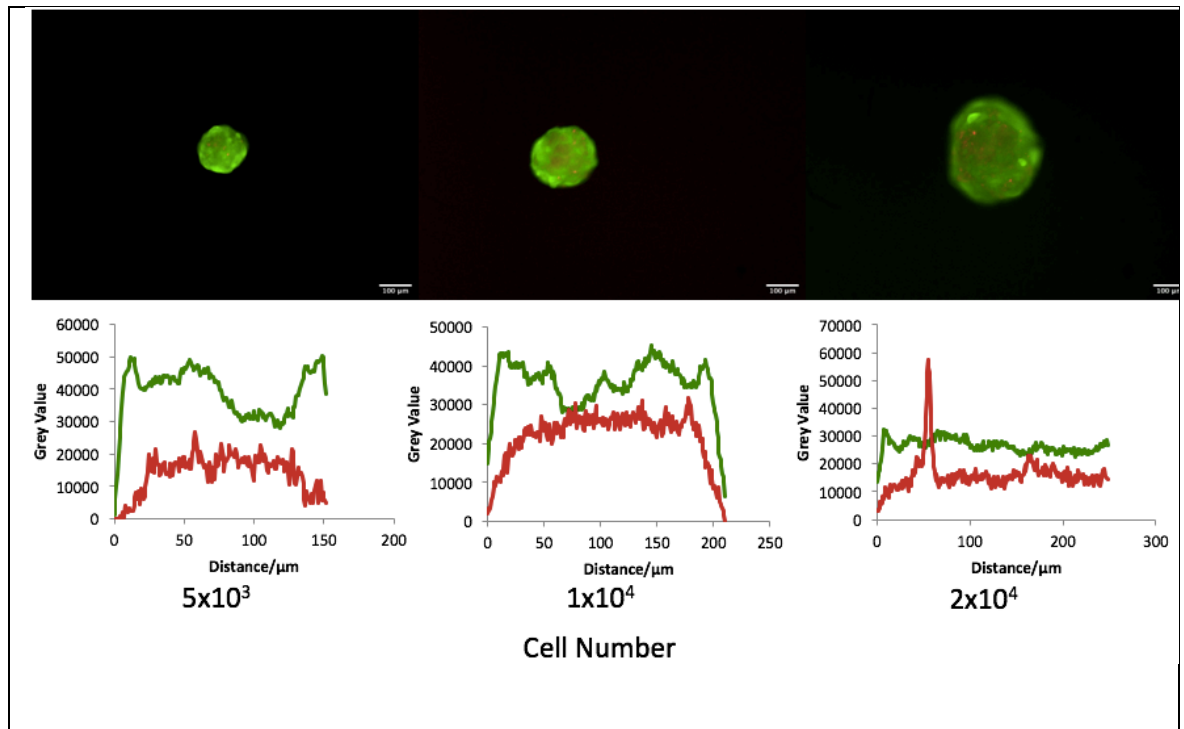


Figure 5-8 Day 21 viability staining- the cross-sectional viable (green; FITC) and dead (red; TRITC) fluorescent signal after calcein/ethidium staining in ULA spheroids, with different cell seeding densities. Peaks in the graph represent increasing signal. Scale bar 100 μm.

5.2.7.3 Electron microscopy

SEM supported the diameter values recorded, indicating large, highly regular spheroids are produced when using the ULA technique, Figure 5-9. This was evident at the early time point of 24 hours and was consistent across all 3 seeding densities.

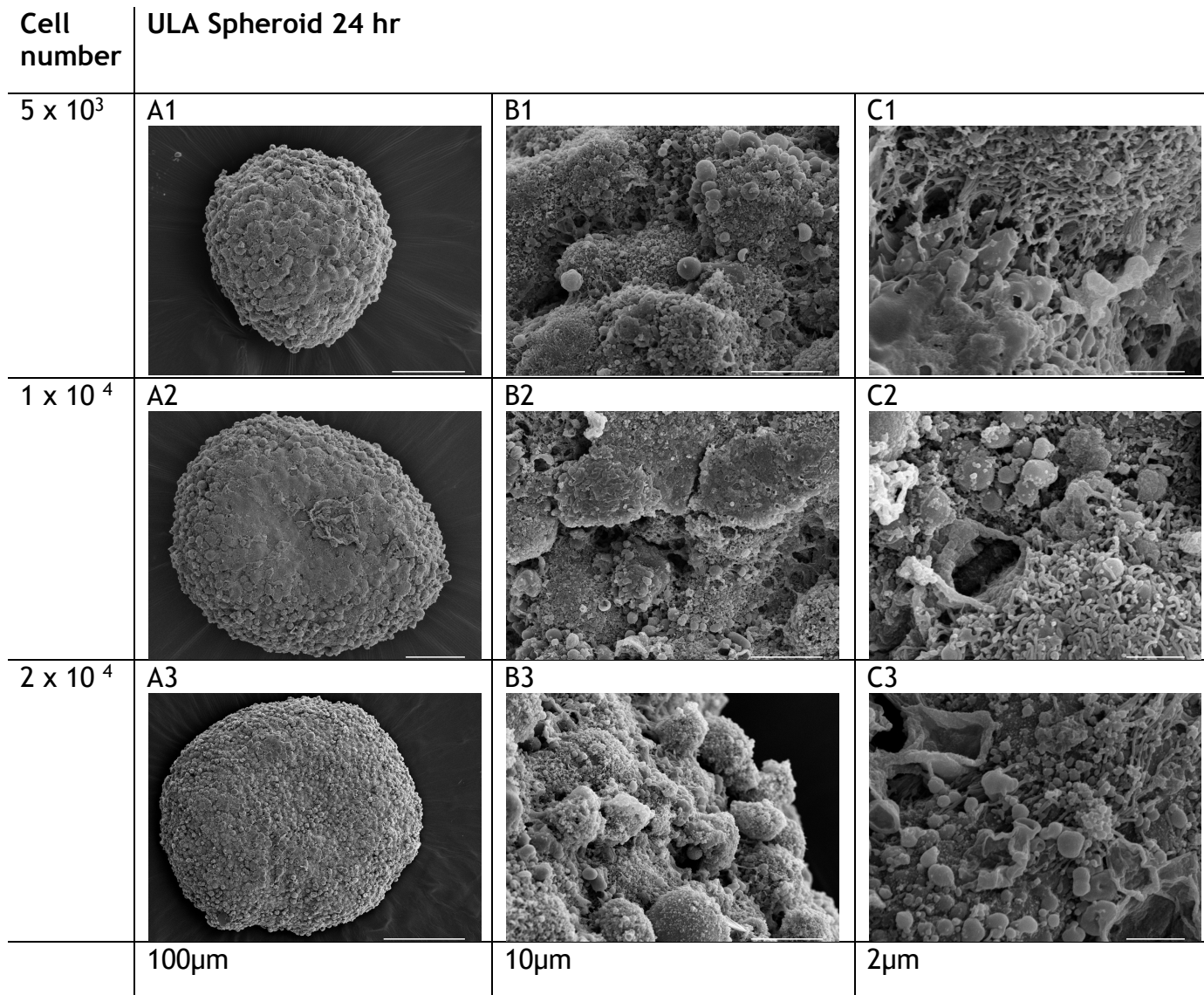


Figure 5-9 Scanning electron microscopy of spheroids formed by the ULA technique at 24 hours with different cell seeding densities. Scale bars A1-A2 100 μm, A3 200 μm, B1-B3 10 μm and C1-C3 2 μm.

TEM demonstrated many intercellular connections between neighbouring cells, supporting the formation of a regular spheroid at 24 hours, rather than a multicellular aggregate, Figure 5-10. The imaged spheroids appeared healthy with multiple organelles, including mitochondria visible.

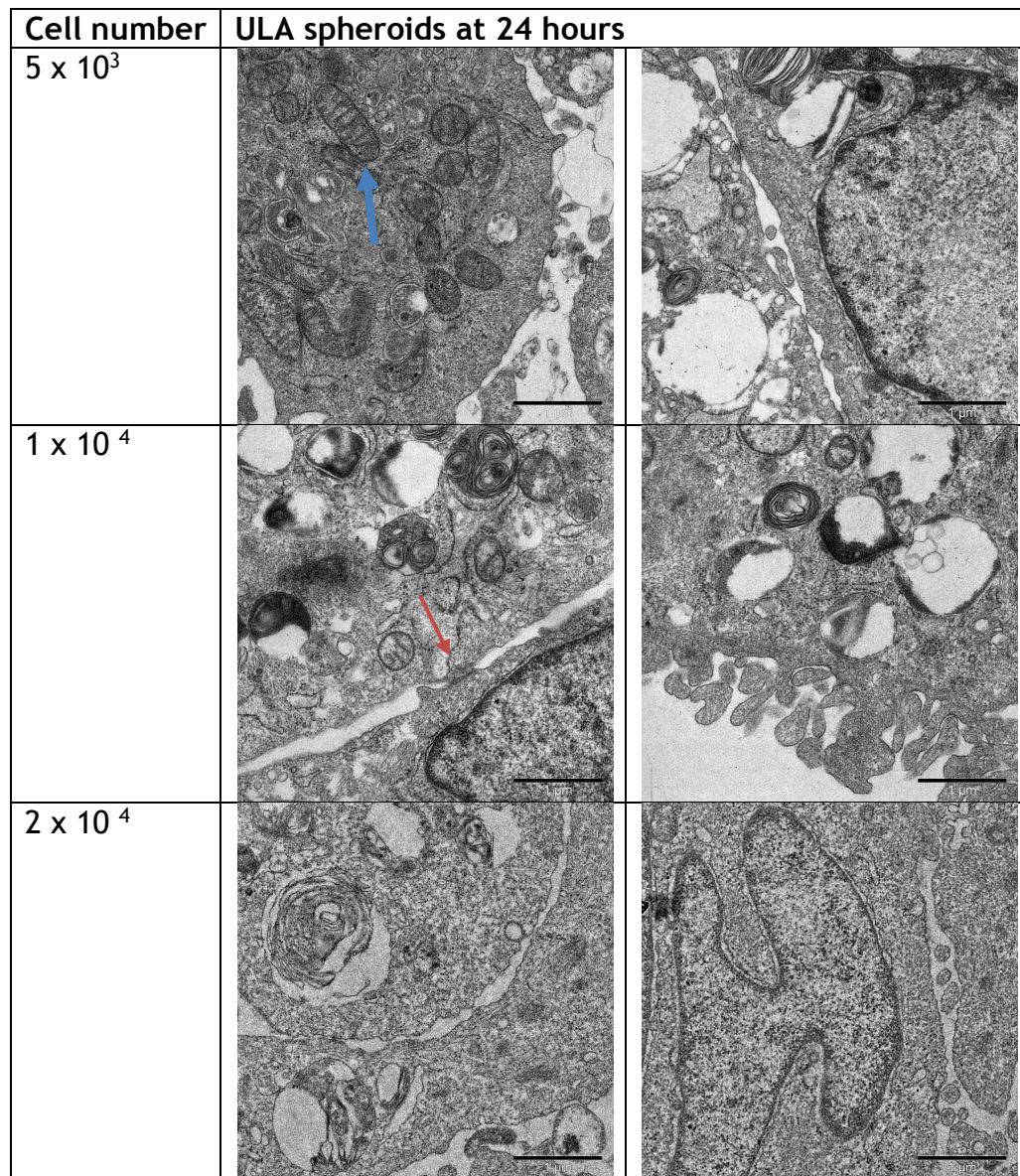


Figure 5-10 Transmission electron micrographs of ULA spheroids at 24 hours, with different cell seeding densities. Blue arrow demonstrating mitochondria, red arrow inter-cellular connections. Scale bar 1 μ m.

5.2.8 Magnetic Nanoparticle Technique

5.2.8.1 Cell Number and spheroid size

Spheroids were generated and diameters were assessed by light microscopy, using 3 different cell seeding densities, Figure 5-11. Surprisingly, an increase in diameter was not observed with increasing cell seeding density. The two lower seeding densities were seen to produce larger spheroids, however, there was no significant difference in diameter between the 3 seeding densities. At day 21 of culture the two smaller seeding density spheroids appear to have condensed in diameter, Figure 5-11-B. However, the largest seeding density remained relatively

similar to the early culture time point. No statistically significant difference in diameter was observed. Large variability in spheroid diameter was noted at both timepoints.

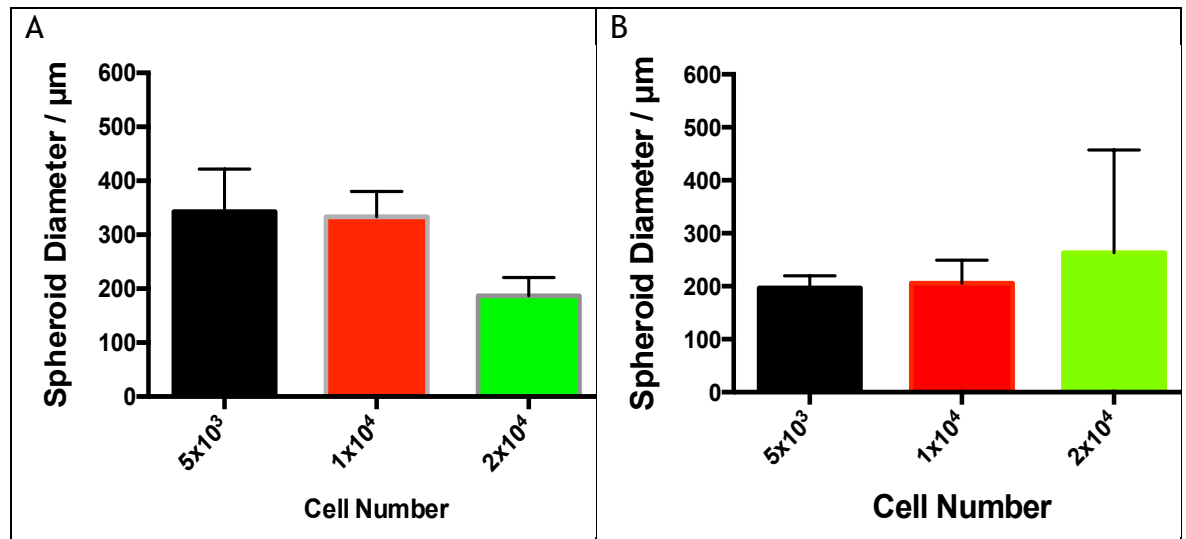


Figure 5-11 Mean spheroid diameter with SD produced at day 3 (A) and day 21 (B) by the MNP technique with three different cell seeding densities. A- $N=3$, B- 5×10^3 and 1×10^4 $N=3$, 2×10^4 $N=4$. No statistically significant difference was recorded.

5.2.8.2 Magnetic Nanoparticle Spheroid Viability

Viability staining was performed at day 7 and day 21 of culture, Figure 5-12 and Figure 5-13. High levels of ethidium were observed in all spheroid seeding densities at both time points. This suggests necrosis within the spheroid at day 7 of culture. Small healthy spheroids were also present, noted by the calcein staining. At day 21 there was also evidence of cell escape from the spheroid mass in the 2×10^4 seeding density, with the formation of a monolayer on the well.

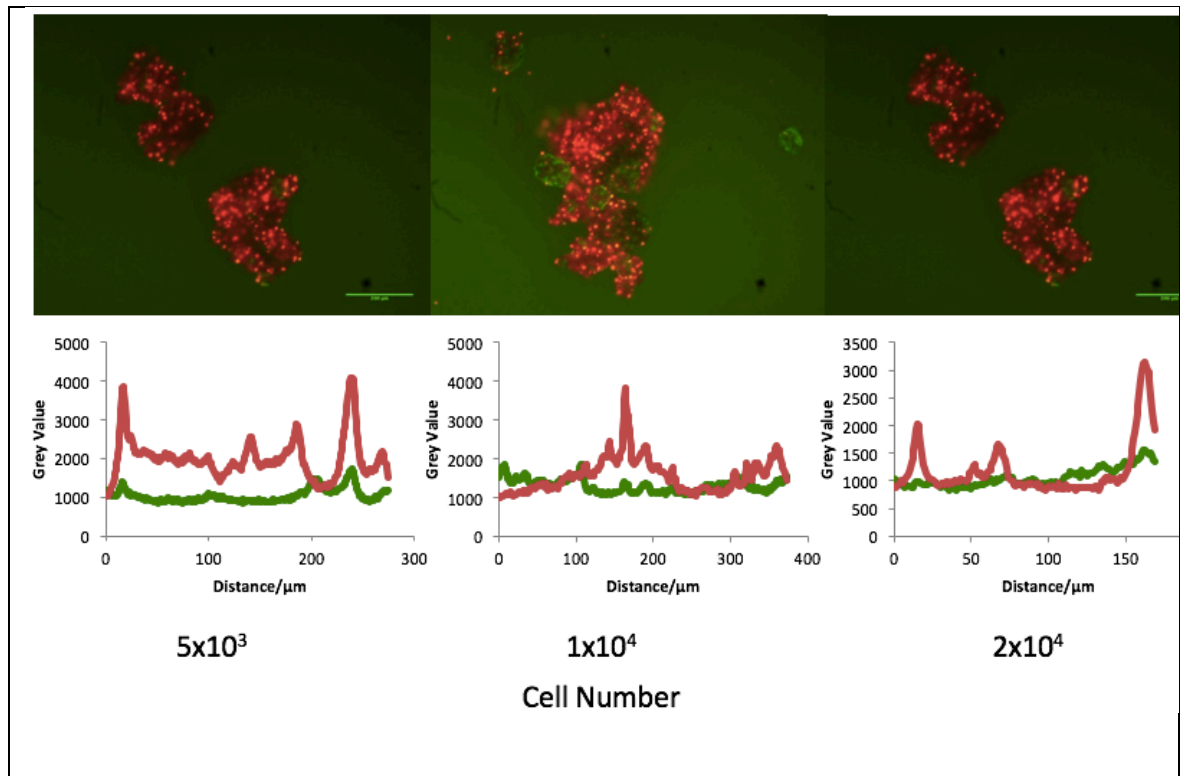


Figure 5-12 Day 7 viability staining - cross-sectional viable (green; FITC) and dead (red; TRITC) fluorescent signal after calcein/ethidium staining in MNP spheroids with different cell seeding densities. Peaks in the graph represent increasing signal. Scale bar 200 μm .

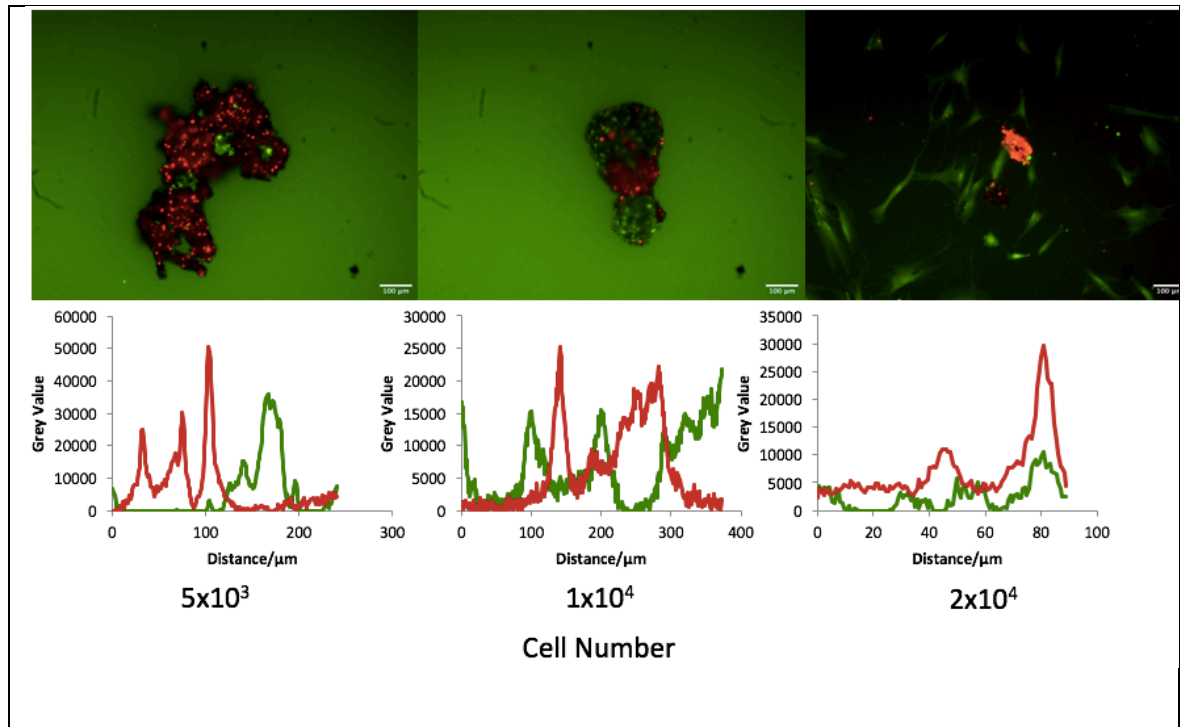


Figure 5-13 Day 21 viability staining- the cross-sectional viable (green; FITC) and dead (red; TRITC) fluorescent signal after calcein/ethidium staining in MNP spheroids with different cell seeding densities. Cell escape and monolayer formation is evident in the 2×10^4 seeding density. Peaks in the graph represent increasing signal. Scale bar 100 μm .

5.2.8.3 Electron Microscopy

Figure 5-14 demonstrates the SEM images of the MNP generated spheroids. Multiple spheroids were produced with varying size for each seeding density, as illustrated in Figure 5-14 image A2. The presence of the MNPs on the outside of the spheroid were noted, whilst cellular projections were also visible on the spheroid surface. Non-circular morphology was produced by this method, in all seeding densities.

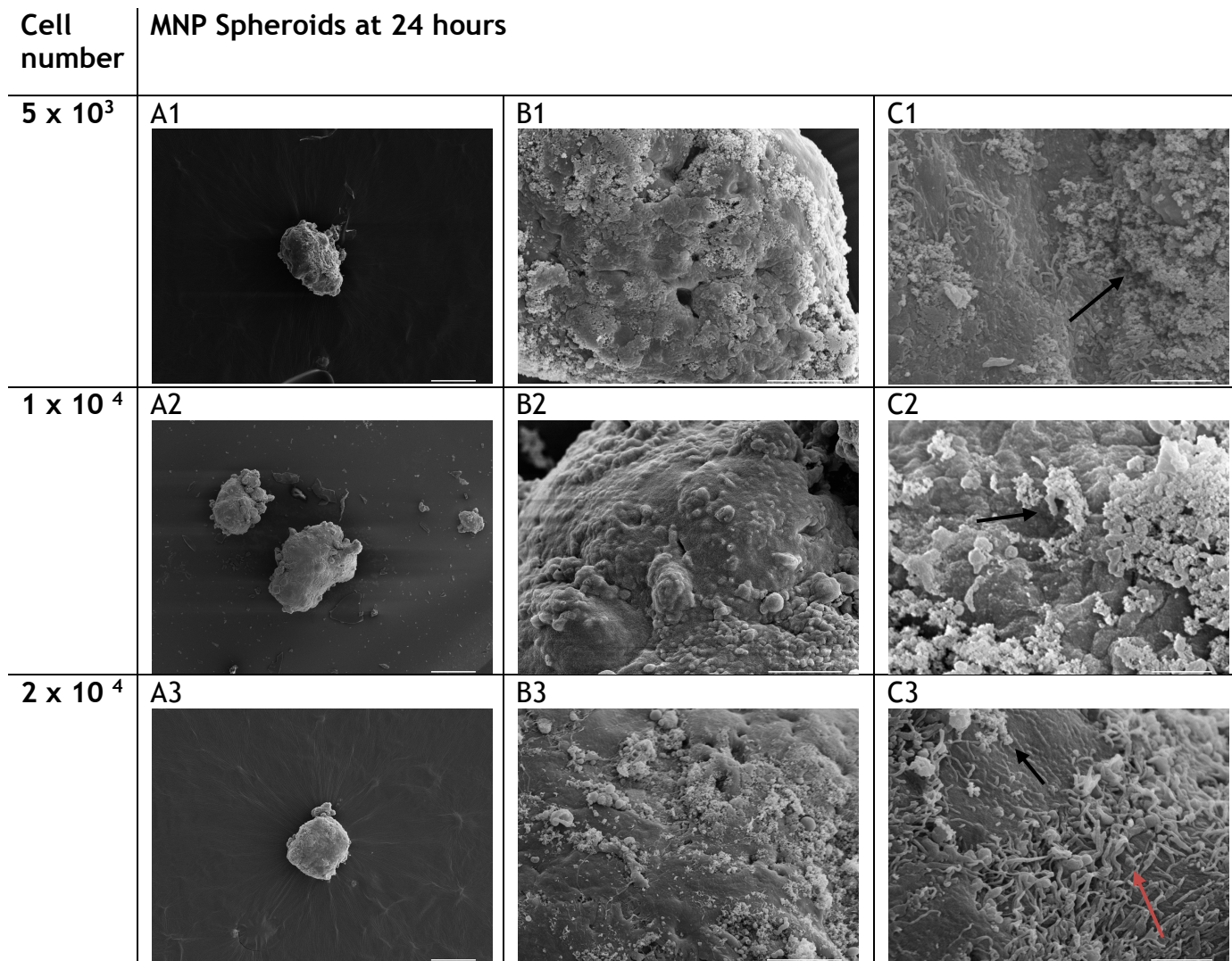


Figure 5-14 Scanning electron microscopy of spheroids formed by the MNP technique at 24 hours with different cell seeding densities. Black arrows demonstrate MNPs on the surface of the spheroids. Red arrows depict cellular projections. A1-A3 scale bar 100 μ m, B1-B3 10 μ m and C1-C3 2 μ m.

Transmission electron microscopy (TEM) allowed visualisation of MNPs internalisation into MSCs and subsequent intracellular localisation, Figure 5-15. MNPs were clearly present on the cell surface, within vesicles and free within the

cytoplasm, demonstrating their effective uptake into the MSCs. TEM also highlighted the cell-cell interactions, with the presence of gap junctions notable.

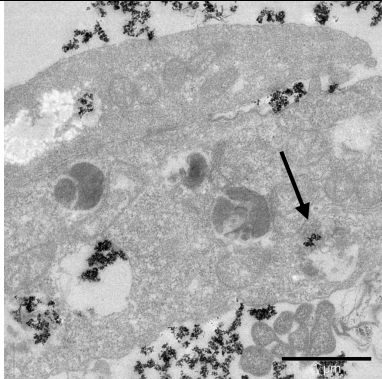
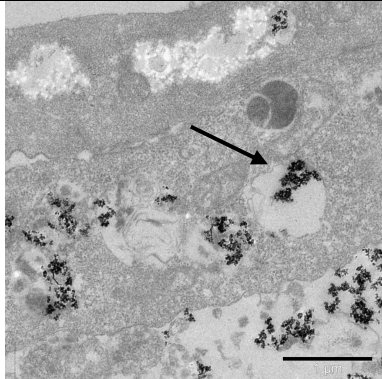
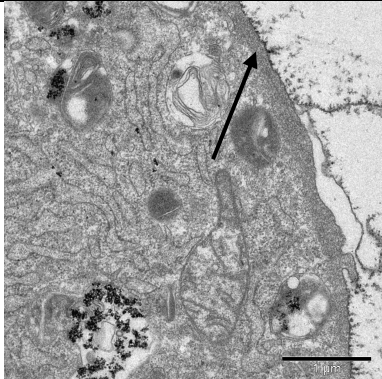
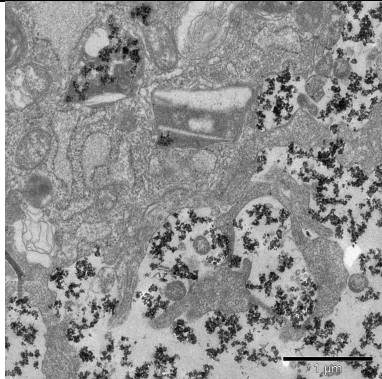
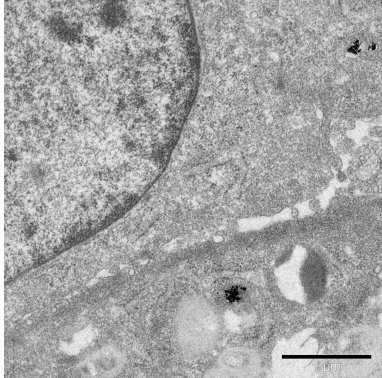
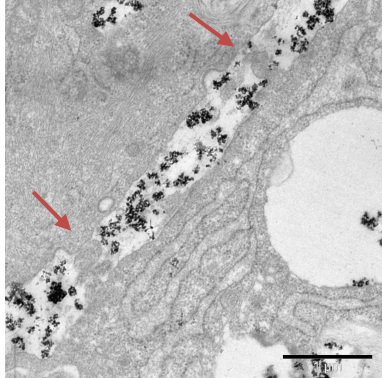
Cell number	MNP Spheroids at 24 hours	
5×10^3		
1×10^4		
2×10^4		

Figure 5-15 Transmission electron micrographs of MNP spheroids at 24 hours, with different cell seeding densities. Black arrows depict MNPs present on the cell surface and intracellularly- within vesicles and free in the cytoplasm. Red arrows depict inter-cellular connections. Scale bar 1 μ m.

5.3 Discussion

This chapter has investigated the suitability of three different spheroid forming techniques in the culture of BM MSCs. All three techniques are well established and have been utilised thoroughly in other areas of *in vitro* research. A summary of the results generated is shown in Table 5-1.

Table 5-1 Summary of results for 3 spheroid forming techniques.

Technique	Spheroid size- with seeding density	Spheroid size- with time	Viable culture	Electron microscopy
HD	Increases	Decreases	Yes	Aggregate & non-circular
ULA	Increases	Decreases	Yes	Circular
MNP	No change	Decreases	No	Non-circular

5.3.1 Hanging Drop technique generates stable spheroids over 72 hours

The HD technique is a well-established method of 3D culture *in vitro*. It has been utilised for many different cell types (Kelm *et al.*, 2003). Its advantages include its ability to produce easily accessible spheroids and its potential for low cost culture if using a standard 96-well plate (Breslin and O'Driscoll, 2013).

The HD method took noticeably longer to form spheroids than the ULA technique. At 24 hours multicellular aggregates were visible, however the morphology was greatly improved by day 7. Although slow to form, in comparison to the other techniques analysed, the viability was uniformly high across all seeding densities. This is comparable with other studies utilising the HD technique (Rimann and Graf-Hausner, 2012). This method also potentially allows scale up, for producing multiple spheroids or drug testing platforms, with the use of multiwell plates (Tung *et al.*, 2011).

Electron microscopy at 24 hours further supported the longer time needed to form spheroids with the HD technique. SEM demonstrated an irregular morphology with

all seeding densities at 24 hours. However, TEM demonstrated healthy cells with evidence of inter-cellular connections forming. As shown in Figure 5-16, spheroid formation occurs over three stages; (1) dispersed cells are drawn closer together to form loose aggregates; (2) this direct cell-cell contact encourages increased cadherin expression, which is accumulated at the cell membranes, and (3) the cells are finally compacted into aggregates to form spheroids (Cui, Hartanto and Zhang, 2017). Whilst cell-cell contacts are forming within 24 hours, utilising BM MSCs with the HD technique, requires more time for the stages of spheroid formation to progress.

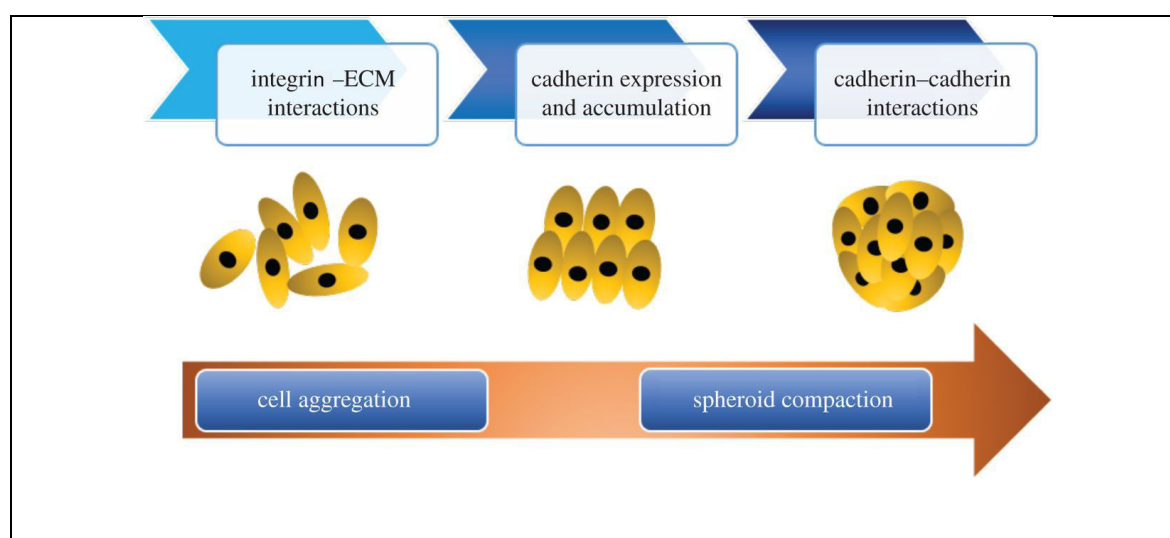


Figure 5-16 The three stages of multicellular spheroid formation. Initial loose cell aggregates encourage direct cell-cell contact, which enable cadherin accumulation and spheroid compaction (Cui, Hartanto and Zhang, 2017).

For long-term culture of spheroids, the HD method requires transfer of the samples to a non-adherent plate. This allows medium exchange and easier visualisation. The step required to transfer can be technically challenging and can result in dissociation of the spheroid. It also incurs the extra cost of an additional plate. When performing large scale studies, this extra technical step, and cost, has the potential to become prohibitive. Furthermore, spheroid size was observed to decrease with time in the HD group, from day 3 to day 21 in all seeding densities, Figure 5-1, which contributes to the technical challenge described above, and has been reinforced previously in the literature (Breslin and O'Driscoll, 2013).

5.3.2 Ultra-Low Attachment technique rapidly produces spheroids with consistent morphology and viability

The ULA method appears to be the quickest to form spheroids, and furthermore the least labour and material intensive. Spheroids were observed in the ULA wells within 24 hours, with a significant increase in size with increasing cell density. This is in keeping with previous research utilising this technique (Metzger *et al.*, 2011). However, with time, a notable reduction in size occurred, from a mean diameter of 502 μm to 272 μm in the 2×10^4 seeding density, Figure 5-6. Change in spheroid size with long term culture has been reported previously, and may be due to the development of a central necrotic core (Ivascu and Kubbies, 2006; Mehta *et al.*, 2012). Thus, handling of the spheroids became more difficult with time, as there was a greater risk of pipetting and damaging the spheroid. Macroscopic spheroids are less likely to be aspirated or dissociated when exchanging media and thus a lower stress and more consistent culture is achievable (Grässer *et al.*, 2018).

The morphology of the spheroid produced in the ULA technique was consistently the most geometrically circular, when observed by light microscopy and EM. This was observed across all cell seeding densities. The low attachment technique is well established and has been previously reported to generate reproducible, stable spheroids within 24 hours (Raghavan *et al.*, 2016).

Furthermore, the ULA method produced spheroids which were highly viable at both day 7 and 21 of culture, in keeping with literature published utilising other cell types, such as fibroblasts and endothelial cells, with the liquid-overlay technique (Metzger *et al.*, 2011).

5.3.3 Magnetic Nanoparticle technique generates spheroids of varied size with compromised viability

The MNP method requires 2 overnight culture steps, therefore additional time to generate the spheroids is required using this technique. However, the MNP technique of spheroid formation has several unique advantages. As visualised in the TEM imaging, the MNPs freely enter the cells. Utilising the MNPs allows for cell labelling, either fluorescently or via electron microscopy. Additionally, the MNPs can serve as vehicles to allow the delivery of therapeutic substances. For

example, MNPs have been functionalised for use in gene silencing and provide great potential in regenerative medicine (Conde *et al.*, 2015). GNPs have been functionalised with small interfering RNAs to silence protooncogenes (Conde *et al.*, 2012), and MNPs have been shown to be able to be guided to the tumour site to initiate gene silencing through their delivery of silencing RNA, in a gastric cancer mouse model (Namiki *et al.*, 2009).

Surprisingly, the spheroid size produced by this technique did not increase with the cell seeding density. A maximum spheroid diameter was produced using the lower cell suspension of 1×10^4 cells; this was supported by the SEM images, Figure 5-14. The inability for this technique to produce single, larger spheroids may be a disadvantage when performing a longer-term culture, where robust, large spheroids are practically easier. This is further compounded by the presence of multiple spheroids in one well, as opposed to other 3D culture techniques which typically result in one spheroid per well.

It could be argued that the cell seeding densities used in the MNP technique were responsible for the failure to form one spheroid as observed in the other techniques. Each cell seeding density was pipetted into a large well, with a comparatively much greater volume of culture medium. However, this technique has been reproduced successfully within the laboratory group (Lewis *et al.*, 2015, 2017). It would be of interest to vary the well size and culture medium volume to observe if an improved morphology was produced.

Viability staining demonstrated a large presence of dead cells within the spheroid. Cell escape from the spheroid and into monolayer formation, was also observed (Figure 5-13). This appeared to increase with culture duration and suggests cells may be migrating away from areas of cell necrosis. The cause of the necrosis was not obvious. At 24 hours viable cells were present within the spheroid, however with increasing time their numbers decreased. Research from our laboratory group has previously reported on the good viability achieved with this technique, (Lewis *et al.*, 2017). However, they used STRO-1 selected or proprietary MSCs, and utilised a type 1 collagen gel, for the culture of their spheroid. It is postulated that these cell populations may possess improved cellular functions of viability, motility and proliferation in comparison to the unselected group.

Aggregates and spheroids were formed rapidly once the cells were detached and suspended by a magnetic charge. This step, whilst time efficient, may cause cell death due to the abnormally close, and fast forming, interactions between the cells. The other two techniques saw improved viability, and shared in a common lack of external coercing force.

The presence of necrosis within spheroid culture is common, and it offers benefits to cancer research as it may recreate the *in vivo* necrotic core of a tumour (Ivascu and Kubbies, 2006; Mehta *et al.*, 2012). However, overall viability of the spheroid should persist in long term culture. The utilisation of the unselected BM MSCs and the MNP technique did not produce an optimal model for spheroid culture.

5.4 Conclusion

In this chapter, the ULA method has been identified as being optimal for spheroid culture of BM MSCs. Spheroids from this technique were notably healthier and also increased in size on increasing cell density. The hanging drop method similarly produced healthy spheroids, but was slower to form, and required and required additional time and cost for set up. After encouraging results within the department, the MNP technique produced disappointing results with abundant necrosis and poor morphology.

Chapter 6

6 Discussion

6.1 Relevance of results

Fragility fractures, secondary to OP, represent an enormous burden to healthcare services worldwide (Compston, McClung and Leslie, 2019). It is evident, due to changing demographics, that our current therapies have proven insufficient (Khosla and Shane, 2016; Khosla and Hofbauer, 2017). Furthermore, side effects such as atypical femoral fractures and jaw osteonecrosis cause serious morbidity and pose great challenges to a patient's clinician (Shane *et al.*, 2014). Improvements in therapies for OP would lead to great benefits to society and importantly to reduce suffering of millions of patients.

The results of these experiments have demonstrated several important findings, which will hopefully add to the knowledge required to develop targeted therapies for OP.

6.1.1 The functionality of mesenchymal stromal cells from patients with neck of femur fractures is impaired

The literature has many conflicting studies on the capacity and propensity of differentiation of MSCs from patients with OP. It is clear that a confounding matter in many of these studies is the age of donor used (Sethe, Scutt and Stolzing, 2006).

The results of this study show that even in a small group of patients either suffering from OA or a NOF fracture, the functional capacity of MSCs differs. It may seem intuitive that MSCs from the NOF group would have decreased potency however their capability to commit to the osteogenic lineage was not compromised. The theory of adipogenic switch was again, not evident, in agreement with previous research of Abdallah & Kassem suggestive of local environmental factors playing a crucial role in the bone marrow niche, controlling MSC fate and ultimately bone marrow adiposity and strength (Abdallah and Kassem, 2012).

Along with a reduction in differentiation capacity it is of great interest to observe significantly different extracellular markers of MSCs in the NOF group.

Additionally, these markers are known to signify MSC potency and differentiation potential and therefore adds further weight to the argument that dysfunction of MSCs plays a role in the development of OP (Rahman *et al.*, 2014; Xu *et al.*, 2016). Little has been reported in the literature on this topic, and this data should provide impetus for further research, and to consider patients who have suffered a fragility fracture as potentially having impaired MSC functionality, and thus limiting expected treatment benefits.

6.1.2 microRNA expression of mesenchymal stromal cells is dysregulated post neck of femur fracture

Developing a more sensitive test for the diagnosis of OP is essential in the improvement of the management of the disease. Importantly, utilising a biomarker which is sensitive to increases in bone health and density would allow accurate treatment durations. This is currently not possible and results in often many years of drug therapy, with no strong evidence on when to stop, and what risk that poses to a patient (Compston, McClung and Leslie, 2019).

The first utilisation of miRNAs in the management of OP may be their application as a biomarker, they will hopefully be applied as a blood sample to diagnose OP and identify patients at risk of developing the disease. Currently companies are developing this strategy, and panels for the investigation of samples for miRNA sample related to bone diseases have been made commercially available (TAmiRNA, Austria). A recent cost-utility model simulated the outcomes of utilising this method, via TAmiRNA's osteomiR™ product, in the screening and management of OP in women, with favourable outcomes in comparison to DXA and the FRAX tool (Walter *et al.*, 2018).

Corelating miRNA expression to BMD will further our understanding of the role miRNAs can play in the current management of OP. This would hopefully allow for earlier diagnosis. Kelch *et al* found 5 miRNAs upregulated in a cohort of OP patients showed linear correlation with BMD values. Furthermore, levels of miR-21-5p expression allowed identified of BMD levels correlating to osteopaenia or OP (Kelch *et al.*, 2017).

The results of the miRNA expression in the NOF group in chapter 3 show that even in a small patient group there is significant dysregulation which cannot be solely attributed to the post fracture state (Nugent, 2017). The overlap of dysregulated miRNAs with known miRNAs associated with OP indicates their high-risk status for developing OP (Materozzi *et al.*, 2018). This data, in a patient group without a diagnosis of OP, further highlights the potential utility of miRNAs in targeted therapies.

It will be important for future research assessing miRNA expression in OP to be expanded upon to include a diverse range of patients. The main focus has been of Caucasian and Asian post-menopausal women (H. Li *et al.*, 2014; Seeliger *et al.*, 2014; Panach *et al.*, 2015; Heilmeier *et al.*, 2016). To provide a holistic view of the benefits of utilising miRNA expression in the management of OP future studies should be expanded to include male patients, multiple ethnicities and larger age ranges.

6.1.3 microRNA manipulation represents an important method of differentiation control

MiRNAs therapies are becoming increasingly close to clinical use, with multiple human trials in progress (Bonneau *et al.*, 2019). They hold great promise for regenerative medicine, and as stated above, for the management of OP.

The focus of miRNA research has often been on cancer (T. Yu *et al.*, 2018). As such the osteogenic effect of inhibiting miR-31 has not been thoroughly investigated, with studies not yet utilising MSCs from the target patient group, or tissue source (Deng *et al.*, 2013; Mizoguchi *et al.*, 2013; McCully *et al.*, 2018). This is a distinct benefit of the research presented in this thesis, as utilising the NOF group allows for the potential of miR-31 inhibition to be put into context.

The osteogenic benefit of inhibiting miR-31 function has been previously described, and miR-31 is recognised as a regulator of osteogenic transcription factors osteopontin, osterix and osteocalcin (Deng *et al.*, 2013). It was encouraging to see an increase in expression of osterix at day 7 of culture in response to the AmiR-31 and osteogenic media condition within the OA group. Assessing the effect of miR-31 inhibition has not been reported in the literature

in an OP patient group, as such this experiment, whilst ultimately not resulting in statistically significant upregulation in osteogenesis at day 7 in the NOF group on qRT-PCR or ICW analysis, provides a direction for future research.

It was of great interest to observe the metabolomic effect of AmiR-31 on MSCs, a further area yet to be reported upon in the literature. Utilising metabolomic studies has become an increasingly important technique to gain a greater understanding of differentiation effects in bioengineering studies (McNamara *et al.*, 2012; Tsimbouri *et al.*, 2012).

The addition of AmiR-31, in comparison to the control basal media condition, was predicted to lead to significant increase in molecules and networks related to differentiation and osteogenesis, namely glutathione, adenosine triphosphate and AKT, section 4.4.2.7 (Mukherjee and Rotwein, 2009; Ciciarello *et al.*, 2013; Romagnoli *et al.*, 2013). It was intriguing to note the difference between the two patient groups in these networks, with the AmiR-31 seemingly producing a stronger pro-differentiation effect in the NOF group. This is perhaps not in keeping with the results of the differentiation studies in chapter 1 or ICW analysis of osterix expression. It raises questions as to why this metabolomic effect is not resultant in a phenotypic change in the NOF group. The time point of the metabolomic study may also have importance, with glutathione levels noted to decrease after the induction of osteogenesis (Romagnoli *et al.*, 2013).

MiR-143 has wide ranging physiological roles, and is linked to many diseases, from colorectal cancer, type 2 diabetes mellitus and OP (Panach *et al.*, 2015; Li, Fan and Chen, 2018; Li *et al.*, 2019). It has been described as both an adipogenic and osteogenic differentiation regulator (Xie, Lim and Lodish, 2009; E. Li *et al.*, 2014). It represents an intriguing miRNA with regards to OP, due to the diseases association with increased bone marrow adiposity and reduced BMD (Abdallah and Kassem, 2012). MiR-143 expression was observed to be reduced in chapter 3, which correlates to published research concerning a genetic form of OP, and patients from who had an OP hip fracture (Panach *et al.*, 2015; Mäkitie *et al.*, 2018).

The results in chapter 4 demonstrated that miR-143 was pro-adipogenic on assessment by ICW, in the OA group only. It was not noted to significantly

stimulate differentiation in the NOF group as hypothesised. Adipogenesis was chosen to assess the restorative effects of the miR-143 mimic on differentiation. Due to its known role in osteoblast differentiation it will be important to assess miR-143 manipulation in osteogenic experiments within the NOF group also (E. Li *et al.*, 2014).

6.1.4 ULA technique identified as optimal method for spheroid formation in bone marrow derived MSCs

To improve upon the clinical relativity of the miRNA cultures displayed in chapter 4, performing them in a 3D *in vitro* model would represent a significant advancement. Chapter 5 demonstrated the outcomes of three commonly used spheroid forming techniques. The importance of 3D culture has become increasingly recognised, and reduces the gap between *in vitro* research and human trials (Saleh and Genever, 2011). Utilising MSCs from the OA group it was evident that the ULA technique produced spheroids rapidly, with little technical difficulty. Furthermore, viability was satisfactory at all time points.

The ULA technique is a form of liquid overlay spheroid formation, and has been utilised successfully for several decades (Carlsson and Yuhas, 1984). It has remained a popular method for spheroid culture due to its low cost, low shear stress environment, non-requirement of specialized equipment and its ability to be upscaled being advantageous for high throughput screening (Costa *et al.*, 2018).

The HD technique produced spheroids of good morphology, but is a less attractive method for larger, future studies and application to NOF MSCs due to its labour intensiveness, cost and difficulties in scaling up the spheroid size. These are common criticisms of the HD technique (Breslin and O'Driscoll, 2013; Costa *et al.*, 2018).

The MNP technique benefits from the ability to utilise the nanoparticles to deliver bioactive substances, a significant benefit over the other two techniques. This functionalisation of nanoparticles, and the ability to deliver small interfering RNA accurately to a tissue, provides great interest for regenerative medicine (Conde *et al.*, 2015). The ultimate aim of RNA

interference (RNAi) is to modulate the phenotype of the tissue affected by the disease, whilst minimizing off target and systemic side effects (Conde *et al.*, 2015). The addition of nanoparticles was previously shown to not compromise cell viability or function (Lewis *et al.*, 2015; McCully *et al.*, 2018). Unfortunately, in this experiment poor spheroid shape and viability was produced in the MNP group. Differing from previous studies utilising this technique in our research group, the MSCs were from bone marrow aspirates, and were not proprietary MSCs (Lewis *et al.*, 2017).

The experimentations in this chapter determined the ULA technique to be the optimal method for spheroid formation in MSCs from a bone marrow source, and provide a platform to be utilised for future studies in the NOF group.

6.2 Limitations

The applicability of the results from this research are limited by the small sample size. To improve the confidence of these results, performing larger experiments with more strict and controlled inclusion criteria would be required. Furthermore, increasing the number of technical replicates utilised in the metabolomic experiments would provide greater validity.

To ensure the patients were truly OP a DXA scan would need to be performed. Furthermore, using a control group which was not afflicted by a bone disease, such as OA would be a significant improvement. This would potentially provide clearer distinctions in bone microarchitectural indices on microCT scanning.

Bone marrow MSCs from patients suffering from OA were utilised as a control group, largely to provide an easy source of cells. However, OA is known to produce its own dysregulation of miRNA expression and result in changes in the microscopic characteristics of cortical and trabecular bone (Jenkins *et al.*, 2013; Nugent, 2016). However, the utilisation of bone samples from healthy donors would not be without its difficulties, with regards to access to these samples and/or cost.

The ICW and qRT-PCR analysis of miRNA manipulation at day 7 provided a basis for understanding the effect on differentiation this has. Utilising further

timepoints and more markers of adipogenic and osteogenic differentiation would have allowed for improved conclusions to be drawn to the effectiveness of the miR-143 mimic and AmiR-31. Performing an analysis of osteogenic differentiation in the miR-143 mimic study would also have been an improvement.

6.3 Future work

6.3.1 Further interrogation of mesenchymal stromal cell biology in patients who have suffered fragility fractures

As discussed above, the properties and functional capacity of MSCs from OP patients requires significant further research. The apparent differences on flow cytometry of extracellular markers warrant further interrogation. Expanding this experiment would provide further insight to the significance of this finding and provide clarity to the extent of its usefulness.

Conducting a more controlled study with age matched groups would reduce the effect on ageing on MSCs. Ideally groups would be: OP, NOF, healthy with a pre-operative DXA scan to identify their bone status. It is idealistic to have a healthy group, with no bone disease, however in practice this would be difficult to achieve. Thus, continuing to use an OA group as a control would be the most practical option. The experiment would aim to explore differences in extracellular markers of MSCs in OP, and determine if patients at high risk of the disease, who have suffered a fragility fracture, express similar profiles.

The MSCs from the above study would also be used in further differentiation studies and in immune suppression assays to determine their functionality.

6.3.2 Longer culture and assessment of effect of microRNA-31 in mesenchymal stromal cells

The short term metabolomic effect of AmiR-31 was identified with the 7-day culture. However, to gain a fuller understanding of the potential usefulness of miR-31 as a therapeutic target to increase osteogenesis it would be important to scale up this experiment, with a multiple timepoints, both earlier and later, greater number of biological and technical replicates. This would be in conjunction with further protein and gene level of analysis of differentiation.

These conditions would then be applied to a 3D culture. An assessment of differentiation would be undertaken via sectioning the spheroids and performing immunofluorescent staining. Furthermore, the spheroids could be disaggregated and the RNA extracted, to allow qRT-PCR analysis.

Utilising these conditions, in both monolayer and 3D techniques, could allow for the assessment of other miRNAs with potential therapeutic activity. As demonstrated with the miR-143 culture, it would not need to be limited to osteogenesis. Focussing on local bone marrow niche regulators could provide other methods to increase the activity and vitality of MSCs in patients who have suffered a fragility fracture.

6.3.3 Assessing the impact of current osteoporosis therapies on microRNA expression

It is clear that miRNAs provide a potential biomarker and therapeutic targets to manipulate osteogenesis (Weilner *et al.*, 2015; Heilmeier *et al.*, 2016; Sun *et al.*, 2016), however the effect on their expression from current therapies is yet to be fully explored. A recent study has assessed this topic in a rat *in vivo* model of postmenopausal OP, with zoledronate and teriparatide have been observed to revert miRNA changes associated with the disease (Kocijan *et al.*, 2020).

Conducting a culture of human BM MSCs with commonly used drug therapies for OP, such as bisphosphonates, would be followed by an assessment of miRNA expression. This would ascertain the extent of non-specific targeting already occurring with first line therapies. Not only would this provide useful data on miRNA expression but would prevent replicating current inappropriate therapeutic strategies.

6.3.4 Application of three-dimensional culture method to osteoporotic mesenchymal stromal cells

The ULA spheroid forming method was proven successful in the OA patient group, and is required to be applied to the NOF patient group. This would ideally be extended to patient samples who have a pre-operative diagnosis of OP, via DXA scanning. The OA group would be utilised as a control for comparison. Furthermore, an assessment of differentiation through culture in differentiation

media would be performed. At the end of culture an assessment of osteogenesis and adipogenesis would be made, to ensure the model remains applicable to differentiation experimentation. This would be performed via fixing and sectioning the spheroids, prior to performing immunofluorescent staining.

6.4 Thesis conclusion

This thesis achieved the aims outlined in Chapter 1. MSCs from patients who have suffered a NOF have demonstrated abnormal expression of extracellular markers in comparison to OA patients, and decreased differentiation capabilities suggestive of impaired MSC function. Furthermore, miRNA expression in this group, without a known diagnosis of OP, shows significant dysregulation. By targeting two key miRNAs, linked to the pathogenesis of OP, differentiation of MSCs was manipulated adding further evidence to the promise of utilising miRNAs in the management and treatment of OP. Finally, an optimal technique was identified for the 3D culture of MSCs from a bone marrow source, and has been prepared for future experiments.

These results provide further insight into the impaired MSC function in patients who have suffered a fragility fracture, and will hopefully help in the future development of targeted therapies.

Bibliography

- Abdallah, B. M. and Kassem, M. (2012) 'New factors controlling the balance between osteoblastogenesis and adipogenesis', *Bone*. Elsevier Inc., 50(2), pp. 540-545. doi: 10.1016/j.bone.2011.06.030.
- Aggarwal, S. and Pittenger, M. F. (2005) 'Human mesenchymal stem cells modulate allogeneic immune cell responses', *Blood*. doi: 10.1182/blood-2004-04-1559.
- Alakpa, E. V. *et al.* (2016) 'Tunable Supramolecular Hydrogels for Selection of Lineage-Guiding Metabolites in Stem Cell Cultures', *Chem*. doi: 10.1016/j.chempr.2016.07.001.
- Alakpa, E. V. *et al.* (2018) 'The Prismatic Topography of *Pinctada maxima* Shell Retains Stem Cell Multipotency and Plasticity In Vitro', *Advanced Biosystems*, 2(6). doi: 10.1002/adbi.201800012.
- De Albornoz, P. M. *et al.* (2018) 'Cell therapies in tendon, ligament, and musculoskeletal system repair', *Sports Medicine and Arthroscopy Review*. doi: 10.1097/JSA.0000000000000192.
- Ammann, P. and Rizzoli, R. (2003) 'Bone strength and its determinants.', *Osteoporosis international : a journal established as result of cooperation between the European Foundation for Osteoporosis and the National Osteoporosis Foundation of the USA*.
- Baker, N., Sohn, J. and Tuan, R. S. (2015) 'Promotion of human mesenchymal stem cell osteogenesis by PI3-kinase/Akt signaling, and the influence of caveolin-1/cholesterol homeostasis', *Stem Cell Research and Therapy*. Stem Cell Research & Therapy, 6(1), pp. 1-11. doi: 10.1186/s13287-015-0225-8.
- Ball, L. M. *et al.* (2007) 'Cotransplantation of ex vivo-expanded mesenchymal stem cells accelerates lymphocyte recovery and may reduce the risk of graft failure in haploidentical hematopoietic stem-cell transplantation', *Blood*. doi: 10.1182/blood-2007-04-087056.

Baumgaertner, M. R. *et al.* (1995) 'The value of the tip-apex distance in predicting failure of fixation of peritrochanteric fractures of the hip', *Journal of Bone and Joint Surgery - Series A*. doi: 10.2106/00004623-199507000-00012.

Bell, K. L. *et al.* (1999) 'Structure of the femoral neck in hip fracture: Cortical bone loss in the inferoanterior to superoposterior axis', *Journal of Bone and Mineral Research*, 14(1), pp. 111-119. doi: 10.1359/jbmr.1999.14.1.111.

Bidwell, J. P. *et al.* (2013) 'Functional impairment of bone formation in the pathogenesis of osteoporosis: The bone marrow regenerative competence', *Current Osteoporosis Reports*, 11(2), pp. 117-125. doi: 10.1007/s11914-013-0139-2.

Blain, H. *et al.* (2008) 'Cortical and trabecular bone distribution in the femoral neck in osteoporosis and osteoarthritis', *Bone*. Elsevier Inc., 43(5), pp. 862-868. doi: 10.1016/j.bone.2008.07.236.

Bolland, M. J. and Grey, A. (2016) 'Ten years too long: Strontium ranelate, cardiac events, and the European Medicines Agency', *BMJ (Online)*, 354(September), pp. 1-8. doi: 10.1136/bmj.i5109.

Bonneau, E. *et al.* (2019) 'How close are miRNAs from clinical practice? A perspective on the diagnostic and therapeutic market', *Electronic Journal of the International Federation of Clinical Chemistry and Laboratory Medicine*.

Boskey, A. L. and Imbert, L. (2017) 'Bone quality changes associated with aging and disease: a review', *Annals of the New York Academy of Sciences*. doi: 10.1111/nyas.13572.

Brandi, M. L. (2009) 'Microarchitecture, the key to bone quality', *Rheumatology (United Kingdom)*. doi: 10.1093/rheumatology/kep273.

Breslin, S. and O'Driscoll, L. (2013) 'Three-dimensional cell culture: The missing link in drug discovery', *Drug Discovery Today*. doi: 10.1016/j.drudis.2012.10.003.

Cann, C. E. *et al.* (2014) 'CTXA hip - An extension of classical DXA measurements using Quantitative CT', *PLoS ONE*, 9(3). doi: 10.1371/journal.pone.0091904.

Carlsson, J. and Yuhas, J. M. (1984) 'Liquid-overlay culture of cellular spheroids.', *Recent results in cancer research. Fortschritte der Krebsforschung. Progres dans les recherches sur le cancer*. doi: 10.1007/978-3-642-82340-4_1.

Cauley, J. A. *et al.* (2003) 'Effects of Estrogen Plus Progestin on Risk of Fracture and Bone Mineral Density: The Women's Health Initiative Randomized Trial', *Journal of the American Medical Association*. doi: 10.1001/jama.290.13.1729.

Cesarz, Z. and Tamama, K. (2016) 'Spheroid Culture of Mesenchymal Stem Cells', *Stem Cells International*. doi: 10.1155/2016/9176357.

Cheng, V. K.-F. *et al.* (2019) 'MicroRNA and Human Bone Health', *JBMR Plus*, 3(1), pp. 2-13. doi: 10.1002/jbm4.10115.

Chevalier, Y. *et al.* (2007) 'Validation of a voxel-based FE method for prediction of the uniaxial apparent modulus of human trabecular bone using macroscopic mechanical tests and nanoindentation', *Journal of Biomechanics*. doi: 10.1016/j.jbiomech.2007.05.004.

Chew, E., Prakash, R. and Khan, W. (2017) 'Mesenchymal stem cells in human meniscal regeneration: A systematic review', *Annals of Medicine and Surgery*. doi: 10.1016/j.amsu.2017.09.018.

Chitteti BR, Cheng Y-H, Kacena MA, S. E. (2014) 'THE SIGNIFICANT ROLE OF CD166 IN HEMATOPOIETIC STEM', *Bone*, 54(1), pp. 58-67. doi: 10.1016/j.bone.2013.01.038.HIERARCHICAL.

Chung, M. T. *et al.* (2012) 'CD90 (Thy-1)-Positive Selection Enhances Osteogenic Capacity of Human Adipose-Derived Stromal Cells', *Tissue Engineering Part A*, 19(7-8), pp. 989-997. doi: 10.1089/ten.tea.2012.0370.

Chung, S. *et al.* (2007) 'Mitochondrial oxidative metabolism is required for the cardiac differentiation of stem cells', *Nature Clinical Practice Cardiovascular*

Medicine. doi: 10.1038/ncpcardio0766.

Ciciarello, M. *et al.* (2013) 'Extracellular purines promote the differentiation of human bone marrow-derived mesenchymal stem cells to the osteogenic and adipogenic lineages', *Stem Cells and Development*. doi: 10.1089/scd.2012.0432.

Compston, J. *et al.* (2017) 'UK clinical guideline for the prevention and treatment of osteoporosis', *Archives of Osteoporosis*. *Archives of Osteoporosis*, 12(1). doi: 10.1007/s11657-017-0324-5.

Compston, J. E., McClung, M. R. and Leslie, W. D. (2019) 'Osteoporosis', *The Lancet*. doi: 10.1016/S0140-6736(18)32112-3.

Conde, J. *et al.* (2012) 'Design of multifunctional gold nanoparticles for in vitro and in vivo gene silencing', *ACS Nano*. doi: 10.1021/nn3030223.

Conde, J. *et al.* (2015) '15 years on siRNA delivery: Beyond the State-of-the-Art on inorganic nanoparticles for RNAi therapeutics', *Nano Today*. Elsevier Ltd, 10(4), pp. 421-450. doi: 10.1016/j.nantod.2015.06.008.

Costa, A. G. *et al.* (2011) 'Cathepsin K: Its skeletal actions and role as a therapeutic target in osteoporosis', *Nature Reviews Rheumatology*. doi: 10.1038/nrrheum.2011.77.

Costa, E. C. *et al.* (2018) 'Spheroids Formation on Non-Adhesive Surfaces by Liquid Overlay Technique: Considerations and Practical Approaches', *Biotechnology Journal*. doi: 10.1002/biot.201700417.

Cotter, M. M. *et al.* (2009) 'Trabecular microarchitecture of hominoid thoracic vertebrae', *Anatomical Record*. doi: 10.1002/ar.20932.

Cui, X., Hartanto, Y. and Zhang, H. (2017) 'Advances in multicellular spheroids formation', *Journal of the Royal Society Interface*. doi: 10.1098/rsif.2016.0877.

Daviss, B. (2005) 'Growing pains for metabolomics: the newest 'omic science is producing results--and more data than researchers know what to do with', *The Scientist*.

- Delmas, P. D. and Seeman, E. (2004) 'Changes in bone mineral density explain little of the reduction in vertebral or nonvertebral fracture risk with anti-resorptive therapy', *Bone*. doi: 10.1016/j.bone.2003.12.022.
- Deng, Y. *et al.* (2013) 'Effects of a miR-31, Runx2, and Satb2 regulatory loop on the osteogenic differentiation of bone mesenchymal stem cells', *Stem Cells and Development*. doi: 10.1089/scd.2012.0686.
- Dominici, M. *et al.* (2006) 'Minimal criteria for defining multipotent mesenchymal stromal cells. The International Society for Cellular Therapy position statement', *Cytotherapy*. Elsevier, 8(4), pp. 315-317. doi: 10.1080/14653240600855905.
- Duguay, D., Foty, R. A. and Steinberg, M. S. (2003) 'Cadherin-mediated cell adhesion and tissue segregation: Qualitative and quantitative determinants', *Developmental Biology*. doi: 10.1016/S0012-1606(02)00016-7.
- Dweep, H., Sticht, C. and Pandey, P. (2011) 'miRWalk-database: prediction of possible miRNA binding sites by', *Journal of biomedical informatics*.
- Elsafadi, M. *et al.* (2016) 'Transgelin is a TGF β -inducible gene that regulates osteoblastic and adipogenic differentiation of human skeletal stem cells through actin cytoskeleton organization', *Cell Death and Disease*. doi: 10.1038/cddis.2016.196.
- Esau, C. *et al.* (2004) 'MicroRNA-143 Regulates Adipocyte Differentiation', *Journal of Biological Chemistry*. American Society for Biochemistry and Molecular Biology, 279(50), pp. 52361-52365. doi: 10.1074/JBC.C400438200.
- Fajardo, R. J. and Müller, R. (2001) 'Three-dimensional analysis of nonhuman primate trabecular architecture using micro-computed tomography', *American Journal of Physical Anthropology*. doi: 10.1002/ajpa.1089.
- Farr, J. N. and Khosla, S. (2015) 'Skeletal changes through the lifespan - From growth to senescence', *Nature Reviews Endocrinology*. doi: 10.1038/nrendo.2015.89.

Feldkamp, L. A., Davis, L. C. and Kress, J. W. (1984) 'Practical cone-beam algorithm', *Journal of the Optical Society of America A*. doi: 10.1364/josaa.1.000612.

Florio, M. *et al.* (2016) 'A bispecific antibody targeting sclerostin and DKK-1 promotes bone mass accrual and fracture repair', *Nature Communications*. doi: 10.1038/ncomms11505.

Foessler, I., Kotzbeck, P. and Obermayer-Pietsch, B. (2019) 'miRNAs as novel biomarkers for bone related diseases', *Journal of Laboratory and Precision Medicine*. doi: 10.21037/jlpm.2018.12.06.

Foty, R. A. and Steinberg, M. S. (2005) 'The differential adhesion hypothesis: A direct evaluation', *Developmental Biology*. doi: 10.1016/j.ydbio.2004.11.012.

Freitag, L. *et al.* (2019) 'Relative effects of age on implant integration in a rat model: A longitudinal in vivo microCT study', *Journal of Orthopaedic Research*. doi: 10.1002/jor.24210.

Friedrich, J. *et al.* (2009) 'Spheroid-based drug screen: Considerations and practical approach', *Nature Protocols*. doi: 10.1038/nprot.2008.226.

Frost, H. M. (1958) 'Preparation of thin undecalcified bone sections by rapid manual method', *Biotechnic and Histochemistry*. doi: 10.3109/10520295809111862.

Gielkens, P. F. M. *et al.* (2008) 'A comparison of micro-CT, microradiography and histomorphometry in bone research', *Archives of Oral Biology*. doi: 10.1016/j.archoralbio.2007.11.011.

Goldstein, S. A., Goulet, R. and McCubbrey, D. (1993) 'Measurement and significance of three-dimensional architecture to the mechanical integrity of trabecular bone', *Calcified Tissue International*. doi: 10.1007/BF01673421.

Grässer, U. *et al.* (2018) 'Dissociation of mono- and co-culture spheroids into single cells for subsequent flow cytometric analysis', *Annals of Anatomy*. doi:

10.1016/j.aanat.2017.10.002.

Gurski, L. A. *et al.* (2009) 'Hyaluronic acid-based hydrogels as 3D matrices for in vitro evaluation of chemotherapeutic drugs using poorly adherent prostate cancer cells', *Biomaterials*. doi: 10.1016/j.biomaterials.2009.07.054.

Gurski, L. A. *et al.* (2010) '3D Matrices for Anti-Cancer Drug Testing and Development', *Oncology Issues*. doi: 10.1080/10463356.2010.11883480.

Haasters, F. *et al.* (2014) 'Mesenchymal stem cells from osteoporotic patients reveal reduced migration and invasion upon stimulation with BMP-2 or BMP-7', *Biochemical and Biophysical Research Communications*, 452(1), pp. 118-123. doi: 10.1016/j.bbrc.2014.08.055.

Hamersma, H., Gardner, J. and Beighton, P. (2003) 'The natural history of sclerosteosis', *Clinical Genetics*. doi: 10.1034/j.1399-0004.2003.00036.x.

Han, H. W., Asano, S. and Hsu, S. H. (2019) 'Cellular spheroids of mesenchymal stem cells and their perspectives in future healthcare', *Applied Sciences (Switzerland)*. doi: 10.3390/app9040627.

Hanna, J., Hossain, G. S. and Kocerha, J. (2019) 'The potential for microRNA therapeutics and clinical research', *Frontiers in Genetics*. doi: 10.3389/fgene.2019.00478.

Hannah, S. D. *et al.* (2017) 'The changing case-mix of hip fractures in Scotland - Evidence from the Scottish hip fracture audit', *Scottish Medical Journal*. doi: 10.1177/0036933017741057.

Hassan, M. Q. *et al.* (2010) 'A network connecting Runx2, SATB2, and the miR-23a~27a~24-2 cluster regulates the osteoblast differentiation program', *Proceedings of the National Academy of Sciences of the United States of America*. doi: 10.1073/pnas.1007698107.

Van Der Heide, V. *et al.* (2016) 'Down-regulation of MicroRNA-31 in CD4⁺ T cells contributes to immunosuppression in human sepsis by promoting TH2skewing',

Anesthesiology. doi: 10.1097/ALN.0000000000001031.

Heilmeier, U. *et al.* (2016) 'Serum miRNA Signatures Are Indicative of Skeletal Fractures in Postmenopausal Women With and Without Type 2 Diabetes and Influence Osteogenic and Adipogenic Differentiation of Adipose Tissue-Derived Mesenchymal Stem Cells In Vitro', *Journal of Bone and Mineral Research*, 31(12), pp. 2173-2192. doi: 10.1002/jbmr.2897.

Hildebrand, T. and Rüegsegger, P. (1997) 'Quantification of bone microarchitecture with the structure model index', *Computer Methods in Biomechanics and Biomedical Engineering*. doi: 10.1080/01495739708936692.

Hilton, M. J. *et al.* (2008) 'Notch signaling maintains bone marrow mesenchymal progenitors by suppressing osteoblast differentiation', *Nature Medicine*. doi: 10.1038/nm1716.

Hong, J. K. *et al.* (2015) 'Three-dimensional culture of mesenchymal stem cells', *Tissue Engineering and Regenerative Medicine*. doi: 10.1007/s13770-015-0005-7.

Hounsfield, G. N. (1973) 'Computerized transverse axial scanning (tomography): I. Description of system', *British Journal of Radiology*. doi: 10.1259/0007-1285-46-552-1016.

Huang, J. *et al.* (2010) 'MicroRNA-204 regulates Runx2 protein expression and mesenchymal progenitor cell differentiation', *Stem Cells*. doi: 10.1002/stem.288.

Iaffaldano, L. *et al.* (2013) 'High Aminopeptidase N/CD13 Levels Characterize Human Amniotic Mesenchymal Stem Cells and Drive Their Increased Adipogenic Potential in Obese Women', *Stem Cells and Development*, 22(16), pp. 2287-2297. doi: 10.1089/scd.2012.0499.

Inose, H. *et al.* (2009) 'A microRNA regulatory mechanism of osteoblast differentiation', *Proceedings of the National Academy of Sciences*. doi: 10.1073/pnas.0909311106.

Ivascu, A. and Kubbies, M. (2006) 'Rapid generation of single-tumor spheroids for high-throughput cell function and toxicity analysis', *Journal of Biomolecular Screening*. doi: 10.1177/1087057106292763.

Jackson, R. D. *et al.* (2006) 'Calcium plus vitamin D supplementation and the risk of fractures: Commentary', *Obstetrical and Gynecological Survey*. doi: 10.1097/01.ogx.0000219470.83259.8d.

Jenkins, P. J. *et al.* (2013) 'A micro-architectural evaluation of osteoporotic human femoral heads to guide implant placement in proximal femoral fractures', *Acta Orthopaedica*, 84(5), pp. 453-459. doi: 10.3109/17453674.2013.842432.

Jones, O. (2019) 'Proximal', pp. 1-7. Available at: <https://teachmeanatomy.info/lower-limb/bones/femur/>.

Kanehisa, M. *et al.* (2012) 'KEGG for integration and interpretation of large-scale molecular data sets', *Nucleic Acids Research*. doi: 10.1093/nar/gkr988.

Kanis, J. A. *et al.* (2003) 'The components of excess mortality after hip fracture.', *Bone*.

Kelch, S. *et al.* (2017) 'MiRNAs in bone tissue correlate to bone mineral density and circulating miRNAs are gender independent in osteoporotic patients', *Scientific Reports*. doi: 10.1038/s41598-017-16113-x.

Kelm, J. M. *et al.* (2003) 'Method for generation of homogeneous multicellular tumor spheroids applicable to a wide variety of cell types', *Biotechnology and Bioengineering*. doi: 10.1002/bit.10655.

Khosla, S. and Hofbauer, L. C. (2017) 'Osteoporosis treatment: recent developments and ongoing challenges', *The Lancet Diabetes and Endocrinology*, 5(11), pp. 898-907. doi: 10.1016/S2213-8587(17)30188-2.

Khosla, S. and Shane, E. (2016) 'A Crisis in the Treatment of Osteoporosis', *Journal of Bone and Mineral Research*. doi: 10.1002/jbmr.2888.

- Kim, K. M. and Lim, S. K. (2014) 'Role of miRNAs in bone and their potential as therapeutic targets', *Current Opinion in Pharmacology*, 16(1), pp. 133-141. doi: 10.1016/j.coph.2014.05.001.
- Kinner, B. and Spector, M. (2002) 'Expression of smooth muscle actin in osteoblasts in human bone', *Journal of Orthopaedic Research*. doi: 10.1016/S0736-0266(01)00145-0.
- Ko, J. Y. *et al.* (2015) 'MicroRNA-29a mitigates glucocorticoid induction of bone loss and fatty marrow by rescuing Runx2 acetylation', *Bone*. doi: 10.1016/j.bone.2015.06.022.
- Kocijan, R. *et al.* (2020) 'MicroRNA levels in bone and blood change during bisphosphonate and teriparatide therapy in an animal model of postmenopausal osteoporosis', *Bone*. doi: 10.1016/j.bone.2019.115104.
- Kunz-Schughart, L. A. *et al.* (2004) 'The use of 3-D cultures for high-throughput screening: The multicellular spheroid model', *Journal of Biomolecular Screening*. doi: 10.1177/1087057104265040.
- Lane, N. E. *et al.* (2006) 'Glucocorticoid-treated mice have localized changes in trabecular bone material properties and osteocyte lacunar size that are not observed in placebo-treated or estrogen-deficient mice', *Journal of Bone and Mineral Research*. doi: 10.1359/JBMR.051103.
- Lange, J. *et al.* (2010) 'Action of IL-1 β during fracture healing', *Journal of Orthopaedic Research*. doi: 10.1002/jor.21061.
- Larrea, E. *et al.* (2016) 'New concepts in cancer biomarkers: Circulating miRNAs in liquid biopsies', *International Journal of Molecular Sciences*. doi: 10.3390/ijms17050627.
- Lee, R. C., Feinbaum, R. L. and Ambros, V. (1993) 'The *C. elegans* heterochronic gene *lin-4* encodes small RNAs with antisense complementarity to *lin-14*', *Cell*. doi: 10.1016/0092-8674(93)90529-Y.

Legrand, E. *et al.* (2000) 'Trabecular bone microarchitecture, bone mineral density, and vertebral fractures in male osteoporosis', *Journal of Bone and Mineral Research*. doi: 10.1359/jbmr.2000.15.1.13.

Lewis, B. P. *et al.* (2003) 'Prediction of Mammalian MicroRNA Targets', *Cell*. doi: 10.1016/S0092-8674(03)01018-3.

Lewis, E. E. L. *et al.* (2015) 'The influence of particle size and static magnetic fields on the uptake of magnetic nanoparticles into three dimensional cell-seeded collagen gel cultures', *Journal of Biomedical Materials Research - Part B Applied Biomaterials*. doi: 10.1002/jbm.b.33302.

Lewis, E. E. L. *et al.* (2016) 'A Quiescent, Regeneration-Responsive Tissue Engineered Mesenchymal Stem Cell Bone Marrow Niche Model via Magnetic Levitation', *ACS Nano*. doi: 10.1021/acsnano.6b02841.

Lewis, N. S. *et al.* (2017) 'Magnetically levitated mesenchymal stem cell spheroids cultured with a collagen gel maintain phenotype and quiescence', *Journal of Tissue Engineering*. doi: 10.1177/2041731417704428.

Li, B., Fan, J. and Chen, N. (2018) 'A Novel Regulator of Type II Diabetes: MicroRNA-143', *Trends in Endocrinology and Metabolism*. doi: 10.1016/j.tem.2018.03.019.

Li, Chenyao *et al.* (2019) 'Prognostic roles of microRNA 143 and microRNA 145 in colorectal cancer: A meta-analysis', *International Journal of Biological Markers*. doi: 10.1177/1724600818807492.

Li, E. *et al.* (2014) 'MiR-143 suppresses osteogenic differentiation by targeting Osterix', *Molecular and Cellular Biochemistry*, 390(1-2), pp. 69-74. doi: 10.1007/s11010-013-1957-3.

Li, G. *et al.* (2018) 'MicroRNA-3200-5p Promotes Osteosarcoma Cell Invasion via Suppression of BRMS1', *Molecules and cells*, 41(6), pp. 523-531. doi: 10.14348/molcells.2018.2200.

- Li, H. *et al.* (2009) 'A novel microRNA targeting HDAC5 regulates osteoblast differentiation in mice and contributes to primary osteoporosis in humans', *Journal of Clinical Investigation*. doi: 10.1172/JCI39832.
- Li, H. *et al.* (2013) 'MiR-17-5p and miR-106a are involved in the balance between osteogenic and adipogenic differentiation of adipose-derived mesenchymal stem cells', *Stem Cell Research*. doi: 10.1016/j.scr.2012.11.007.
- Li, H. *et al.* (2014) 'Plasma miRNA levels correlate with sensitivity to bone mineral density in postmenopausal osteoporosis patients', *Biomarkers*. doi: 10.3109/1354750X.2014.935957.
- Li, L., Chen, X. P. and Li, Y. J. (2010) 'MicroRNA-146a and human disease', *Scandinavian Journal of Immunology*, 71(4), pp. 227-231. doi: 10.1111/j.1365-3083.2010.02383.x.
- Van Lierop, A. H. *et al.* (2013) 'Van Buchem disease: Clinical, biochemical, and densitometric features of patients and disease carriers', *Journal of Bone and Mineral Research*. doi: 10.1002/jbmr.1794.
- Liu, K. *et al.* (2017) 'MiR-598: A tumor suppressor with biomarker significance in osteosarcoma', *Life Sciences*. Elsevier, 188(September), pp. 141-148. doi: 10.1016/j.lfs.2017.09.003.
- Liu, X. *et al.* (2013) 'Wnt signaling in bone formation and its therapeutic potential for bone diseases', *Therapeutic Advances in Musculoskeletal Disease*. doi: 10.1177/1759720X12466608.
- Liu, X. *et al.* (2019) 'Circulating microRNA-23b as a new biomarker for rheumatoid arthritis', *Gene*. doi: 10.1016/j.gene.2019.06.001.
- Lu, C. *et al.* (2018) 'MiR-18a-5p promotes cell invasion and migration of osteosarcoma by directly targeting IRF2', *Oncology Letters*, 16(3), pp. 3150-3156. doi: 10.3892/ol.2018.9032.
- Lu, J. *et al.* (2017) 'MicroRNA-218-5p as a Potential Target for the Treatment of

Human Osteoarthritis', *Molecular Therapy*. doi: 10.1016/j.ymthe.2017.08.009.

Lulla, R. R. *et al.* (2011) 'Identification of differentially expressed microRNAs in osteosarcoma', *Sarcoma*, 2011. doi: 10.1155/2011/732690.

Mäkitie, R. E. *et al.* (2018) 'Altered MicroRNA Profile in Osteoporosis Caused by Impaired WNT Signaling', *Journal of Clinical Endocrinology and Metabolism*, 103(5), pp. 1985-1996. doi: 10.1210/jc.2017-02585.

Mandourah, A. Y. *et al.* (2018) 'Circulating microRNAs as potential diagnostic biomarkers for osteoporosis', *Scientific Reports*. doi: 10.1038/s41598-018-26525-y.

Martinez, E. C. *et al.* (2017) 'MicroRNA-31 promotes adverse cardiac remodeling and dysfunction in ischemic heart disease', *Journal of Molecular and Cellular Cardiology*. doi: 10.1016/j.yjmcc.2017.08.013.

Martinez, N. J. and Gregory, R. I. (2013) 'Argonaute2 expression is post-transcriptionally coupled to microRNA abundance', *RNA*. doi: 10.1261/rna.036434.112.

Materozzi, M. *et al.* (2018) 'The Potential Role of miRNAs as New Biomarkers for Osteoporosis', *International Journal of Endocrinology*. Hindawi, 2018. doi: 10.1155/2018/2342860.

McCalden, R. W., McGeough, J. A. and Court-Brown, C. M. (1997) 'Age-related changes in the compressive strength of cancellous bone. The relative importance of changes in density and trabecular architecture', *Journal of Bone and Joint Surgery - Series A*.

McClung, M., Baron, R. and Bouxsein, M. (2017) 'An update on osteoporosis pathogenesis, diagnosis, and treatment', *Bone*. Elsevier Inc., 98, p. 37. doi: 10.1016/j.bone.2017.02.013.

McCully, M. *et al.* (2018) 'Nanoparticle-AntagoMIR based targeting of MIR-31 to induce osterix and osteocalcin expression in mesenchymal stem cells', *PLoS ONE*,

13(2). doi: 10.1371/journal.pone.0192562.

McNamara, L. E. *et al.* (2012) 'Metabolomics: A valuable tool for stem cell monitoring in regenerative medicine', *Journal of the Royal Society Interface*. doi: 10.1098/rsif.2012.0169.

Mehta, G. *et al.* (2012) 'Opportunities and challenges for use of tumor spheroids as models to test drug delivery and efficacy', *Journal of Controlled Release*. doi: 10.1016/j.jconrel.2012.04.045.

Metzger, W. *et al.* (2011) 'The liquid overlay technique is the key to formation of co-culture spheroids consisting of primary osteoblasts, fibroblasts and endothelial cells', *Cytotherapy*, 13(8), pp. 1000-1012. doi: 10.3109/14653249.2011.583233.

Meunier, P. *et al.* (1971) 'Osteoporosis and the replacement of cell populations of the marrow by adipose tissue. A quantitative study of 84 iliac bone biopsies.', *Clinical orthopaedics and related research*. doi: 10.1097/00003086-197110000-00021.

Miller, M. and Thompson, S. (2016) *Miller's review of Orthopaedics*. 7th edn. Elsevier.

Mizoguchi, F. *et al.* (2013) 'MiR-31 controls osteoclast formation and bone resorption by targeting RhoA', *Arthritis Research and Therapy*. BioMed Central Ltd, 15(5), p. R102. doi: 10.1186/ar4282.

Moerman, E. J. *et al.* (2004) 'Aging activates adipogenic and suppresses osteogenic programs in mesenchymal marrow stroma/stem cells: The role of PPAR- γ 2 transcription factor and TGF- β /BMP signaling pathways', *Aging Cell*. doi: 10.1111/j.1474-9728.2004.00127.x.

Mohamed-Ahmed, S. *et al.* (2018) 'Adipose-derived and bone marrow mesenchymal stem cells: A donor-matched comparison', *Stem Cell Research and Therapy*. doi: 10.1186/s13287-018-0914-1.

Montoya, M. J. *et al.* (2014) 'Microstructural trabecular bone from patients with osteoporotic hip fracture or osteoarthritis: Its relationship with bone mineral density and bone remodelling markers', *Maturitas*, 79(3), pp. 299-305. doi: 10.1016/j.maturitas.2014.07.006.

Moraes, D. A. *et al.* (2016) 'A reduction in CD90 (THY-1) expression results in increased differentiation of mesenchymal stromal cells', *Stem Cell Research and Therapy*. *Stem Cell Research & Therapy*, 7(1), pp. 1-14. doi: 10.1186/s13287-016-0359-3.

Moriishi, T. *et al.* (2016) 'Overexpression of BCLXL in Osteoblasts Inhibits Osteoblast Apoptosis and Increases Bone Volume and Strength', *Journal of Bone and Mineral Research*. doi: 10.1002/jbmr.2808.

Mukherjee, A. and Rotwein, P. (2009) 'Akt promotes BMP2-mediated osteoblast differentiation and bone development', *Journal of Cell Science*, 122(5), pp. 716-726. doi: 10.1242/jcs.042770.

Murata, K. *et al.* (2013) 'Comprehensive microRNA Analysis Identifies miR-24 and miR-125a-5p as Plasma Biomarkers for Rheumatoid Arthritis', *PLoS ONE*. doi: 10.1371/journal.pone.0069118.

Namiki, Y. *et al.* (2009) 'A novel magnetic crystal-lipid nanostructure for magnetically guided in vivo gene delivery', *Nature Nanotechnology*. doi: 10.1038/nnano.2009.202.

National Institute for Health and Care Excellence (2016) *Osteoporosis - prevention of fragility fractures - NICE CKS, Clinical Knowledge Summaries*. doi: 10.1145/342001.339689.

'NOGG 2017 : Clinical guideline for the prevention and treatment of osteoporosis' (2017), (March). Available at: [https://www.sheffield.ac.uk/NOGG/NOGG Guideline 2017.pdf](https://www.sheffield.ac.uk/NOGG/NOGG%20Guideline%202017.pdf).

Nugent, M. (2016) 'MicroRNAs: Exploring new horizons in osteoarthritis', *Osteoarthritis and Cartilage*. doi: 10.1016/j.joca.2015.10.018.

Nugent, M. (2017) 'MicroRNAs and Fracture Healing', *Calcified Tissue International*. Springer US, 101(4), pp. 355-361. doi: 10.1007/s00223-017-0296-x.

Oreffo, Andrea Bennett, Andrew Carr, R. (2002) 'Patients with Primary Osteoarthritis Show No Change with Ageing in the Number of Osteogenic Precursors', *Scandinavian Journal of Rheumatology*. doi: 10.1080/030097498442235.

Panach, L. *et al.* (2015) 'Serum Circulating MicroRNAs as Biomarkers of Osteoporotic Fracture', *Calcified Tissue International*. doi: 10.1007/s00223-015-0036-z.

Pantschenko, A. G. *et al.* (2005) 'Effect of osteoblast-targeted expression of Bcl-2 in bone: Differential response in male and female mice', *Journal of Bone and Mineral Research*. doi: 10.1359/JBMR.050315.

Parmar, V. *et al.* (2005) 'Review of methods to quantify lag screw placement in hip fracture fixation', *Acta Orthopaedica Belgica*.

Prall, W. C. *et al.* (2013) 'Mesenchymal stem cells from osteoporotic patients feature impaired signal transduction but sustained osteoinduction in response to BMP-2 stimulation', *Biochemical and Biophysical Research Communications*, 440(4), pp. 617-622. doi: 10.1016/j.bbrc.2013.09.114.

Qadan, M. A. *et al.* (2018) 'Variation in primary and culture-expanded cells derived from connective tissue progenitors in human bone marrow space, bone trabecular surface and adipose tissue', *Cytotherapy*. doi: 10.1016/j.jcyt.2017.11.013.

Qin, Y. X. and Hu, M. (2014) 'Mechanotransduction in musculoskeletal tissue regeneration: Effects of fluid flow, loading, and cellular-molecular pathways', *BioMed Research International*. doi: 10.1155/2014/863421.

Rachner, T. D., Khosla, S. and Hofbauer, L. C. (2011) 'Osteoporosis: Now and the future', *The Lancet*. doi: 10.1016/S0140-6736(10)62349-5.

Raghavan, S. *et al.* (2016) 'Comparative analysis of tumor spheroid generation techniques for differential in vitro drug toxicity', *Oncotarget*. doi: 10.18632/oncotarget.7659.

Rahman, M. M. *et al.* (2014) 'CD13 promotes mesenchymal stem cell-mediated regeneration of ischemic muscle', *Frontiers in Physiology*, 4 JAN(January), pp. 1-12. doi: 10.3389/fphys.2013.00402.

Ramachandran, M. and Nunn, T. (2018) *Basic Orthopaedic Sciences, Basic Orthopaedic Sciences*. doi: 10.1201/9781315117294.

Regan, J. and Long, F. (2013) 'Notch signaling and bone remodeling', *Current Osteoporosis Reports*. doi: 10.1007/s11914-013-0145-4.

Rege, T. A. and Hagood, J. S. (2006) 'Thy-1 as a regulator of cell-cell and cell-matrix interactions in axon regeneration, apoptosis, adhesion, migration, cancer, and fibrosis', *FASEB Journal*. doi: 10.1096/fj.05-5460rev.

Reyes, J. M. G. *et al.* (2006) 'Metabolic Changes in Mesenchymal Stem Cells in Osteogenic Medium Measured by Autofluorescence Spectroscopy', *Stem Cells*. doi: 10.1634/stemcells.2004-0324.

Riggs, B. L. *et al.* (2004) 'Population-based study of age and sex differences in bone volumetric density, size, geometry, and structure at different skeletal sites', *Journal of Bone and Mineral Research*. doi: 10.1359/JBMR.040916.

Riikka Mäkitie *et al.* (2018) 'Altered MicroRNA Profile in Osteoporosis Caused by Impaired WNT Signaling', *Jcem*, (March). doi: 10.1210/jc.2017-02585.

Rimann, M. and Graf-Hausner, U. (2012) 'Synthetic 3D multicellular systems for drug development', *Current Opinion in Biotechnology*. doi: 10.1016/j.copbio.2012.01.011.

Rodeo, S. A. (2019) 'Cell therapy in orthopaedics', *The Bone & Joint Journal*. doi: 10.1302/0301-620x.101b4.bjj-2019-0013.r1.

Romagnoli, C. *et al.* (2013) 'Role of GSH/GSSG redox couple in osteogenic

activity and osteoclastogenic markers of human osteoblast-like SaOS-2 cells', *FEBS Journal*, 280(3), pp. 867-879. doi: 10.1111/febs.12075.

Rozental, T. D. *et al.* (2013) 'Premenopausal women with a distal radial fracture have deteriorated trabecular bone density and morphology compared with controls without a fracture', *Journal of Bone and Joint Surgery - Series A*. doi: 10.2106/JBJS.L.00588.

Saleh, F. A. *et al.* (2012) 'Three-dimensional in vitro culture techniques for mesenchymal stem cells', *Methods in Molecular Biology*. doi: 10.1007/978-1-61779-980-8-4.

Saleh, F. A. and Genever, P. G. (2011) 'Turning round: Multipotent stromal cells, a three-dimensional revolution?', *Cytotherapy*. Elsevier, 13(8), pp. 903-912. doi: 10.3109/14653249.2011.586998.

Samanta, S. *et al.* (2016) 'MicroRNA: A new therapeutic strategy for cardiovascular diseases', *Trends in Cardiovascular Medicine*. doi: 10.1016/j.tcm.2016.02.004.

Sampath, P. *et al.* (2008) 'A Hierarchical Network Controls Protein Translation during Murine Embryonic Stem Cell Self-Renewal and Differentiation', *Cell Stem Cell*. doi: 10.1016/j.stem.2008.03.013.

Sang, W. *et al.* (2016) 'MiR-150 impairs inflammatory cytokine production by targeting ARRB-after blocking CD28/B7 costimulatory pathway', *Immunology Letters*. doi: 10.1016/j.imlet.2015.11.001.

Scottish Hip Fracture Audit (2019) 'Scottish Hip Fracture Care Pathway Report 2017', pp. 1-44. Available at: www.shfa.scot.nhs.uk.

Scottish Intercollegiate Guidelines Network (2009) 'Management of hip fracture in older people: A national clinical guide', *Scottish Intercollegiate Guidelines Network*, (June), p. 49.

Seeliger, C. *et al.* (2014) 'Five freely circulating miRNAs and bone tissue miRNAs

are associated with osteoporotic fractures', *Journal of Bone and Mineral Research*. doi: 10.1002/jbmr.2175.

Seeman, E. (2002) 'Pathogenesis of bone fragility in women and men', *Lancet*. doi: 10.1016/S0140-6736(02)08706-8.

Sepuru, K. M., Poluri, K. M. and Rajarathnam, K. (2014) 'Solution structure of CXCL5 - A novel chemokine and adipokine implicated in inflammation and obesity', *PLoS ONE*. doi: 10.1371/journal.pone.0093228.

Sethe, S., Scutt, A. and Stolzing, A. (2006) 'Aging of mesenchymal stem cells', *Ageing Research Reviews*. doi: 10.1016/j.arr.2005.10.001.

Shane, E. *et al.* (2014) 'Atypical subtrochanteric and diaphyseal femoral fractures: Second report of a task force of the American society for bone and mineral research', *Journal of Bone and Mineral Research*. doi: 10.1002/jbmr.1998.

Shea, L. D. *et al.* (2000) 'Engineered bone development from a pre-osteoblast cell line on three-dimensional scaffolds', in *Tissue Engineering*. doi: 10.1089/10763270050199550.

Silverwood, R. K. *et al.* (2016) 'Analysis of Osteoclastogenesis/Osteoblastogenesis on Nanotopographical Titania Surfaces', *Advanced Healthcare Materials*, 5(8). doi: 10.1002/adhm.201500664.

Solomon, D. H. *et al.* (2014) 'Osteoporosis medication use after hip fracture in U.S. patients between 2002 and 2011', *Journal of Bone and Mineral Research*. doi: 10.1002/jbmr.2202.

Souza, G. R. *et al.* (2010) 'Three-dimensional Tissue Culture Based on Magnetic Cell Levitation', *Nature Nanotechnology*, 5(4), pp. 291-296. doi: 10.1038/nnano.2010.23.Three-dimensional.

Stenderup, K. *et al.* (2001) 'Number and proliferative capacity of osteogenic stem cells are maintained during aging and in patients with osteoporosis',

Journal of Bone and Mineral Research. doi: 10.1359/jbmr.2001.16.6.1120.

Stenderup, K. *et al.* (2003) 'Aging is associated with decreased maximal life span and accelerated senescence of bone marrow stromal cells.', *Bone*.

Stepicheva, N. A. and Song, J. L. (2016) 'Function and regulation of microRNA-31 in development and disease', *Molecular Reproduction and Development*. doi: 10.1002/mrd.22678.

Stolzing, A. *et al.* (2008) 'Age-related changes in human bone marrow-derived mesenchymal stem cells: Consequences for cell therapies', *Mechanisms of Ageing and Development*. doi: 10.1016/j.mad.2007.12.002.

Stovall, K. E. *et al.* (2019) ' Adenosine triphosphate enhances osteoblast differentiation of rat dental pulp stem cells via the PLC-IP 3 pathway and intracellular Ca²⁺ signaling ', *Journal of Cellular Physiology*. doi: 10.1002/jcp.29091.

Ström, O. *et al.* (2011) 'Osteoporosis: Burden, health care provision and opportunities in the EU', *Archives of Osteoporosis*. doi: 10.1007/s11657-011-0060-1.

Sun, M. *et al.* (2016) 'The Regulatory Roles of MicroRNAs in Bone Remodeling and Perspectives as Biomarkers in Osteoporosis', *BioMed Research International*. Hindawi Publishing Corporation, 2016. doi: 10.1155/2016/1652417.

Sun, Y. M., Lin, K. Y. and Chen, Y. Q. (2013) 'Diverse functions of miR-125 family in different cell contexts', *Journal of Hematology and Oncology*, 6(1), pp. 1-8. doi: 10.1186/1756-8722-6-6.

Svedbom, A. *et al.* (2013) 'Osteoporosis in the European Union: A compendium of country-specific reports', *Archives of Osteoporosis*. doi: 10.1007/s11657-013-0137-0.

Szulc, P., Kaufman, J. M. and Delmas, P. D. (2007) 'Biochemical assessment of bone turnover and bone fragility in men', *Osteoporosis International*. doi:

10.1007/s00198-007-0407-z.

Tanck, E. *et al.* (2009) 'Predictive value of femoral head heterogeneity for fracture risk', *Bone*. doi: 10.1016/j.bone.2008.12.022.

Tantama, M. and Yellen, G. (2014) 'Imaging changes in the cytosolic ATP-to-ADP ratio', in *Methods in Enzymology*. doi: 10.1016/B978-0-12-801415-8.00017-5.

Tibbitt, M. W. and Anseth, K. S. (2009) 'Hydrogels as extracellular matrix mimics for 3D cell culture', *Biotechnology and Bioengineering*. doi: 10.1002/bit.22361.

Tsimbouri, P. (2015) 'Adult Stem Cell Responses to Nanostimuli', *Journal of Functional Biomaterials*. doi: 10.3390/jfb6030598.

Tsimbouri, P. M. *et al.* (2012) 'Using nanotopography and metabolomics to identify biochemical effectors of multipotency', *ACS Nano*. doi: 10.1021/nn304046m.

Tucker, A. *et al.* (2017) 'The changing face of fractures of the hip in Northern Ireland', *Bone and Joint Journal*, 99B(9), pp. 1223-1231. doi: 10.1302/0301-620X.99B9.BJJ-2016-1284.R1.

Tung, Y. C. *et al.* (2011) 'High-throughput 3D spheroid culture and drug testing using a 384 hanging drop array', *Analyst*. doi: 10.1039/c0an00609b.

Ulrich, D. *et al.* (1997) 'The quality of trabecular bone evaluated with micro-computed tomography, FEA and mechanical testing', in *Studies in Health Technology and Informatics*. doi: 10.3233/978-1-60750-884-7-97.

Valenti, M. T. *et al.* (2011) 'Role of Ox-PAPCs in the differentiation of mesenchymal stem cells (MSCs) and Runx2 and PPAR γ 2 expression in MSCs-like of osteoporotic patients', *PLoS ONE*. doi: 10.1371/journal.pone.0020363.

Varum, S. *et al.* (2011) 'Energy metabolism in human pluripotent stem cells and their differentiated counterparts', *PLoS ONE*. doi: 10.1371/journal.pone.0020914.

- Veronesi, F. *et al.* (2014) 'Estrogen deficiency does not decrease the in vitro osteogenic potential of rat adipose-derived mesenchymal stem cells', *Age*, 36(3), pp. 1225-1238. doi: 10.1007/s11357-014-9647-y.
- Walter, E. *et al.* (2018) 'Cost-utility analysis of fracture risk assessment using microRNAs compared with standard tools and no monitoring in the Austrian female population', *Bone*. doi: 10.1016/j.bone.2017.12.017.
- Watts, A. E. *et al.* (2017) 'MicroRNA29a Treatment Improves Early Tendon Injury', *Molecular Therapy*. doi: 10.1016/j.ymthe.2017.07.015.
- Watts, N. B. *et al.* (2005) 'Relationship between changes in BMD and nonvertebral fracture incidence associated with risedronate: Reduction in risk of nonvertebral fracture is not related to change in BMD', *Journal of Bone and Mineral Research*. doi: 10.1359/JBMR.050814.
- Weilner, S. *et al.* (2015) 'Differentially circulating miRNAs after recent osteoporotic fractures can influence osteogenic differentiation', *Bone*, 79, pp. 43-51. doi: 10.1016/j.bone.2015.05.027.
- Weilner, S. *et al.* (2016) 'Secreted microvesicular miR-31 inhibits osteogenic differentiation of mesenchymal stem cells', *Aging Cell*, 15(4), pp. 744-754. doi: 10.1111/accel.12484.
- Williams, A. F. and Gagnon, J. (1982) 'Neuronal cell thy-1 glycoprotein: Homology with immunoglobulin', *Science*. doi: 10.1126/science.6177036.
- Wolff, J. and Wolff, J. (1986) 'Concept of the Law of Bone Remodelling', in *The Law of Bone Remodelling*. doi: 10.1007/978-3-642-71031-5_1.
- World Health Organization (2007) 'Who Scientific Group on the Assessment of Osteoporosis At Primary Health', *World Health*, May(May 2004), pp. 1-13. doi: 10.1016/S0140-6736(02)08761-5.
- Xia, J. *et al.* (2015) 'MetaboAnalyst 3.0-making metabolomics more meaningful', *Nucleic Acids Research*. doi: 10.1093/nar/gkv380.

- Xie, F. *et al.* (2019) 'MiR-143-3p suppresses tumorigenesis in pancreatic ductal adenocarcinoma by targeting KRAS', *Biomedicine and Pharmacotherapy*. doi: 10.1016/j.biopha.2019.109424.
- Xie, H., Lim, B. and Lodish, H. F. (2009) 'MicroRNAs induced during adipogenesis that accelerate fat cell development are downregulated in obesity', *Diabetes*. doi: 10.2337/db08-1299.
- Xie, L. *et al.* (2017) 'Identification of the miRNA-mRNA regulatory network of small cell osteosarcoma based on RNA-seq', *Oncotarget*, 8(26), pp. 42525-42536. doi: 10.18632/oncotarget.17208.
- Xu, L. *et al.* (2016) 'Cell adhesion molecule CD166 drives malignant progression and osteolytic disease in multiple myeloma', *Cancer Research*, 76(23), pp. 6901-6910. doi: 10.1158/0008-5472.CAN-16-0517.
- Xu, L. *et al.* (2017) 'Tissue source determines the differentiation potentials of mesenchymal stem cells: A comparative study of human mesenchymal stem cells from bone marrow and adipose tissue', *Stem Cell Research and Therapy*. doi: 10.1186/s13287-017-0716-x.
- Yamada, K. M. and Cukierman, E. (2007) 'Modeling Tissue Morphogenesis and Cancer in 3D', *Cell*. doi: 10.1016/j.cell.2007.08.006.
- Yanes, O. *et al.* (2010) 'Metabolic oxidation regulates embryonic stem cell differentiation', *Nature Chemical Biology*. doi: 10.1038/nchembio.364.
- Young, P. S. *et al.* (2015) 'Osteoclastogenesis/osteoblastogenesis using human bone marrow-derived cocultures on nanotopographical polymer surfaces', *Nanomedicine*. doi: 10.2217/nnm.14.146.
- Yu, B. *et al.* (2018) 'Inhibition of microRNA-143-3p attenuates myocardial hypertrophy by inhibiting inflammatory response', *Cell Biology International*. doi: 10.1002/cbin.11053.
- Yu, T. *et al.* (2018) 'Functions and mechanisms of microRNA-31 in human

cancers', *Biomedicine and Pharmacotherapy*. doi: 10.1016/j.biopha.2018.09.132.

van Zandwijk, N. *et al.* (2017) 'Safety and activity of microRNA-loaded minicells in patients with recurrent malignant pleural mesothelioma: a first-in-man, phase 1, open-label, dose-escalation study', *The Lancet Oncology*. doi: 10.1016/S1470-2045(17)30621-6.

Zhang, J. F. *et al.* (2011) 'MiRNA-20a promotes osteogenic differentiation of human mesenchymal stem cells by co-regulating BMP signaling', *RNA Biology*. doi: 10.4161/rna.8.5.16043.

Zhang, P. *et al.* (2018) 'miR-143 suppresses the osteogenic differentiation of dental pulp stem cells by inactivation of NF- κ B signaling pathway via targeting TNF- α ', *Archives of Oral Biology*. doi: 10.1016/j.archoralbio.2017.12.031.

Zhao, J. G. *et al.* (2017) 'Association between calcium or Vitamin D supplementation and fracture incidence in community-dwelling older adults a systematic review and meta-analysis', *JAMA - Journal of the American Medical Association*. doi: 10.1001/jama.2017.19344.

Zhao, Z. *et al.* (2018) 'Expression of microRNA-21 in osteoporotic patients and its involvement in the regulation of osteogenic differentiation', *Experimental and Therapeutic Medicine*, pp. 709-714. doi: 10.3892/etm.2018.6998.

Zhou, L. *et al.* (2019) 'MicroRNA-100-5p inhibits osteoclastogenesis and bone resorption by regulating fibroblast growth factor 21', *International Journal of Molecular Medicine*. doi: 10.3892/ijmm.2018.4017.

Zupan, J. *et al.* (2013) 'Osteoarthritic versus osteoporotic bone and intra-skeletal variations in normal bone: Evaluation with μ CT and bone histomorphometry', *Journal of Orthopaedic Research*, 31(7), pp. 1059-1066. doi: 10.1002/jor.22318.